UNIVERSITAT POLITÈCNICA DE VALÈNCIA

Departamento de Máquinas y Motores Térmicos

DOCTORAL THESIS

Development of an altitude simulator and analysis of the performance and emissions of turbocharged Diesel engines at different altitudes

Presented by: D. JAVIER GÓMEZ GIL

Supervised by: DR. D. JOSÉ RAMÓN SERRANO CRUZ

in fulfillment of the requisites for the degree of

Doctor of Philosophy

Valencia, March 23th, 2018

PhD Thesis

"Development of an altitude simulator and analysis of the performance and emissions of turbocharged Diesel engines at different altitudes"

AUTHORS

Presented by: D. Javier Gómez Gil

Supervised by: Dr. D. José Ramón Serrano

THESIS EVALUATORS

Dra. D. María de los Reyes García Contreras

Dr. D. Andrew Williams

Dr. D. Colin Douglas Copeland

DEFENSE COMMITTEE

Chairman: Dr. D. José María Desantes Fernández

Secretary: Dr. D. Octavio Armas Vergel

Member: Dr. D. Colin Douglas Copeland

Valencia, March 23th, 2018

Abstract

In the last decades, internal combustion engine research has been focused on the reduction of fuel consumption and emissions while maintaining performance. In recent years, there is increasing pressure on the engine manufacturers to close the gap between rig and road emissions. Homologation is a big challenge, mainly because of the introduction of real driving emissions cycles, which are more dynamic and have an extended range of ambient conditions. The ambient altitude can reach up to 1300 meters above sea level.

Manufacturers have different ways to test the engines and cars in conditions representing different altitudes. Real altitude tests, where the car, engineers and testing systems have to be displaced to an altitude require long periods of time. Another solution is to test the car in a hypobaric chamber, where the pressure can be controlled. However, these chambers are expensive, difficult to operate and intensive in use of space and resources.

In the present thesis, an altitude simulator is developed, which will introduce an alternative to testing engines at altitude. In this altitude simulator, the engine or car is at room pressure and only its intake and exhaust pipes are at the tested altitude conditions. The thesis describes the altitude simulator operation principle, its different elements and their effect on the altitude simulator performance, as well as the control strategies applied.

A turbocharged diesel engine is tested at different altitudes and its performance and emissions results are compared with those obtained in a hypobaric chamber to validate the method. The engine is tested at the different altitudes in dynamic cycles and its performance and emissions are analyzed, showing that the engine control strategy when it is operating at altitude is focused on the protection of the different elements, for example avoiding the turbocharger going into over speed or overheating, without taking into account the emissions. For these reason, it is important to study different strategies to reduce engine emissions in altitude.

Finally, parametric studies determining the effect of engine valves geometry and exhaust manifold geometry on the aftertreatment inlet temperature and the specific fuel consumption, show ways to reduce the time that it takes for the aftertreatment system to reach its target conversion efficiency.

Resumen

En las últimas décadas, la investigación de motores de combustión interna alternativos se ha centrado en la reducción del consumo de combustible y las emisiones, al tiempo que se mantenía constante el rendimiento. En los últimos años, existe una presión creciente sobre los fabricantes de motores para disminuir las diferencias entre las emisiones en el laboratorio y la carretera. La homologación de nuevos motores es un gran desafío, principalmente debido a la introducción de ciclos de homologación de emisiones más similares a la conducción real, que son más dinámicos y tienen un rango extendido de condiciones ambientales. La altitud ambiente puede alcanzar hasta 1300 metros sobre el nivel del mar.

Los fabricantes tienen diferentes formas de probar los motores y los automóviles a diferentes altitudes. Por un lado, ensayos de altitud real, donde el automóvil, los ingenieros y los sistemas de ensayo se desplazan a una altitud. Sin embargo, éstos requieren largos períodos de tiempo y elevados costes. Otra solución es ensayar el automóvil en una cámara hipobárica, donde se puede controlar la presión. Sin embargo, estas cámaras son muy caras de construir, difíciles de operar e intensivas en el uso de espacio y recursos.

En la presente tesis, se desarrolla un simulador de altitud, que presentará una alternativa para ensayar motores en altitud. En este simulador de altitud, el motor o el automóvil está a la presión de la sala y solo sus tubos de admisión y escape están en las condiciones de altitud a ensayar. La tesis describe el principio de operación del simulador de altitud, sus diferentes elementos y su efecto sobre el rendimiento del simulador de altitud, así como las estrategias de control aplicadas.

A continuación, un motor diésel turboalimentado se ha ensayado a diferentes altitudes y sus resultados de rendimiento y emisiones se comparan con los obtenidos en una cámara hipobárica para validar el método. El motor se ensaya en diferentes altitudes en ciclos dinámicos y se analizan su rendimiento y emisiones, lo que demuestra que la estrategia de control del motor cuando está operando en altitud se centra en la protección de los diferentes elementos, por ejemplo, evitando que el turbocompresor opere en sobre régimen o se sobrecaliente, sin tener en cuenta las emisiones. Por esta razón, es importante estudiar diferentes estrategias para reducir las emisiones de los motores en altitud.

Finalmente, los estudios paramétricos que determinan el efecto de la geometría de las válvulas del motor y la geometría del colector de escape

sobre la temperatura de entrada del tratamiento posterior y el consumo específico de combustible muestran formas de reducir el tiempo que tarda el sistema de postratamiento en alcanzar la eficiencia de conversión deseada.

Resum

En les últimes dècades, la investigació de motors de combustió interna alternatius s'ha centrat en la reducció del consum de combustible i les emissions, alhora que es mantenia constant el rendiment. En els últims anys, hi ha una pressió creixent sobre els fabricants de motors per a disminuir les diferències entre les emissions en el laboratori i la carretera. L'homologació de nous motors és un gran desafiament, principalment a causa de la introducció de cicles d'homologació d'emissions més similars a la conducció real, que són més dinàmics i tenen un rang estès de condicions ambientals. L'altitud ambient pot arribar fins a 1300 metres sobre el nivell del mar.

Els fabricants tenen diferents formes de provar els motors i els automòbils a diferents altituds. D'una banda, assajos d'altitud real, on l'automòbil, els enginyers i els sistemes d'assaig es desplacen a una altitud. No obstant això, aquests requereixen llargs períodes de temps i elevats costos. Una altra solució és assajar l'automòbil en una cambra hipobàrica, on es pot controlar la pressió. No obstant això, aquestes càmeres són molt cares de construir, difícils d'operar i intensives en l'ús d'espai i recursos.

En la present tesi, es desenvolupa un simulador d'altitud, que presentarà una alternativa per assajar motors a altitud. En aquest simulador d'altitud, el motor o l'automòbil està a la pressió de la sala i només els seus tubs d'admissió i escapament estan en les condicions d'altitud a assajar. La tesi descriu el principi d'operació del simulador d'altitud, els seus diferents elements i el seu efecte sobre el rendiment del simulador d'altitud, així com les estratègies de control aplicades.

A continuació, un motor dièsel turboalimentat s'ha assajat a diferents altituds i els seus resultats de rendiment i emissions es comparen amb els obtinguts en una cambra hipobàrica per validar el mètode. El motor s'assaja en diferents altituds en cicles dinàmics i s'analitzen seu rendiment i emissions, el que demostra que l'estratègia de control del motor quan està operant en altitud se centra en la protecció dels diferents elements, per exemple, evitant que el turbocompressor operi en sobre règim o es sobreescalfi, sense tenir en compte les emissions. Per aquesta raó, és important estudiar diferents estratègies per reduir les emissions dels motors en altitud.

Finalment, els estudis paramètrics que determinen l'efecte de la geometria de les vàlvules del motor i la geometria del col·lector d'escapament sobre la

temperatura d'entrada del tractament posterior i el consum específic de combustible mostren formes de reduir el temps que es pren el sistema de posttractament a aconseguir l'eficiència de conversió desitjada.

Acknowledgements

It is impossible to summarize in just a few lines the acknowledgements to all the people that have helped me in this work and during these years.

First of all, my most sincere acknowledgement to the whole CMT – Motores Térmicos team for giving me the opportunity of being part of it. Especially to Pedro Piqueras and José Galindo, who gave me the opportunity to join the CMT in 2013 to do my final degree project. Also, my most sincere thanks to my thesis supervisor, José Ramón Serrano, for being a great director, guiding me during these years with good advice.

Special mention to all the CMT members who have being working very close to me in the development of the altitude simulator. Alí Abbad for the endless discussions about the control, Miguel Ortíz for being always there to solve the mechanical problems and support with good advices (even if it sometimes leaded him to a "Copa Pistón") and Sergi Soro for his fast and good support. And to the technicians that helped me with the tests and experimental facilities during these four years: Valentín and Vicentón; but also to the others less involved with my work, but that have been close colleges (also in the after work beers in La Bodega Fila): Vicente Bermúdez, José "Torner, Toni "Horiba", Bernardo, Figo, Fito, Juanan, and many others.

To all the students that have helped me during their final degree or final master projects: Esther, Nico, Fabián, Sergio, Severiano, Ángel, José and Roberto. You have been also a key element in this thesis. And to the friends that a have made in the department during this time and that I will never forget: Emanuele, Dani, Álvaro, Ricardo "Richie", Lukas, Ricardo "Reinona", Enrique, Dani "Paisa", Julián, and many others, for being as good colleges as beers mates.

Also to my friends outside the department, too many too say their names. You are always a good company to share experiences, beers and travels.

To Silvia, for being the best company I could imagine. Thank you for putting up with me in my bad days. I really enjoy philosophizing about life with you, with beers, dancing or laying down.

And finally, to my family, because what I am today is because of them: for their support, their understanding, their good guide and big effort in finding always the balance.

"This is the real secret of life –
to be completely engaged with
what you are doing in the here
and now. And instead of calling
it work, realize it is play"

Alan W. Watts

Contents

List of Figures

List of Tables

Nomenclature

APE	Average Percentage Error
AQE	Average Quadratic Error
bfsc	break specific fuel consumption
bmep	brake mean effective pressure
c_p	Specific heat
C_s	Sutherland's constant
CAHU	Combustion Air Handling Unit
CO	Carbon monoxide
CO_2	Carbon dioxide
DOC	Diesel Oxidation Catalyst
DPF	Diesel Particle Filter
EGR	Exhaust Gas Recirculation
HC	Hydrocarbons
K	Turbulent losses coefficient
K_v	Flow coefficient
LNT	Lean NO_x Trap
MEDAS	Movable Efficient and Dynamic Altitude Simulator
MPE	Mean Percentage Error
NEDC	New European Driving Cycle
NO_x	Nitrogen Oxides
OPEx1	Overpressure valve in the altitude simulator for fine pressure control (guillotine model)
OPEx2	Overpressure valve in the altitude simulator for rough pressure control (butterfly model)
P	Power
p	Pressure
PEMS	Portable Emission Measurement System
PF	Particle Filter
PM	Particle Matter
PMR	Power-to-Mass Ratio

RDE	Real Driving Emissions
RMS	Root Mean Square
SCR	Selective Catalyst Reduction
T	Temperature
VGT	Variable Geometry Turbine
VGTb	Variable Geometry Turbine blades in the altitude simulator
VGTv	Variable Geometry Turbine valve in the altitude simulator
V_VGT_Ro	On-off valve connecting the VGT with the mechanical compressor in the altitude simulator
V_Coo_Sep	On-off valve connecting the water-to-air cooler with the cyclonic separator in the altitude simulator
V_Ro_Ex	On-off valve connecting the mechanical compressor with the outlet of the altitude simulator
V_Ro_Coo	On-off valve connecting the mechanical compressor with the water-to-air cooler in the altitude simulator
WG	Waste-Gate valve in the altitude simulator
WLTC	World-wide harmonized Light duty Test Cycle
WLTP	World-wide harmonized Light duty Test Procedure
Π	Pressure ratio
$\dot{m}$	Mass flow
η	Efficiency
μ	Dynamic viscosity
λ	Constant for a given gas

Units:

ºC	Celsius degrees
bar	bar
g	Gram
h	hour
K	Kelvin
kg	Kilograms per second

m	meters
mol	mol
Nm	Newton meter
s	second
V	Volts

Subindex:

*****	Corrected
0x	Total variable
1	Compressor inlet
2	Compressor outlet
3	Turbine inlet
4	Turbine outlet
C	Compressor
atm	Atmosphere
EI	Engine intake
ext	external
in	internal
max	Maximum
min	Minimum
n	n^{th} layer of the earth atmosphere
RI	Rotrex Inlet, mechanical compressor of the altitude simulator inlet
SP	Setpoint
st	Stoichiometric
ref	Reference
T	Turbine
v	Volumetric

CHAPTER 1

Introduction

Contents

Figures

1.1 Background

The Internal Combustion Engine (ICE) is the most common power source for land and water vehicle. This includes automobiles, motorcycles, ships and some locomotives [1]. Its origin can be dated about year 1876, when Nicolaus Otto and Eugen Langen invented the spark ignition internal combustion engine that compressed the fuel mixture prior to a premixed combustion [2]. Some years later, in 1892, Rudolf Diesel invented another kind of internal combustion engine in which ignition is due to compression of a non-homogeneous mixture and with a further diffusive combustion [3,4].

The large increase in the number of vehicles currently in circulation [5] has led to an exponential increase in the use of fossil fuels derived from oil and, consequently, a very significant increase in the polluting emissions produced. The effects of the ICE emissions have global and local effects. On one side, the CO_2 emitted by the ICE has about a 10% impact in the global warming, one of the main causes of the climate change and a major social problem [6]. On the other side, other pollutants such NO_x, soot and particulate matter (PM), has a local effect that increases the risk of lung and respiratory problems and diseases, especially relevant in the big urban areas [7].

Despite the fact that new technologies offer alternative propulsion systems, such as hybrid and electric cars, they present some problems coming from an immature technology, as for example the low power density in the batteries [8] – which leads to low autonomy – or long charging time [9]. Besides, the electric system in most of the countries is not ready to feed from one day to another to all the fleet of means of transport that operate with ICE [10,11]. In the meantime, most of the automotive companies are developing mild and full hybrid-electric vehicles using ICE as the prime energy converter with gasoline or diesel as fuels. These solutions reduce the emissions, but they still use an ICE inside and the emissions problem is not fully solved [12].

Governments are aware of these problems, mainly due to the increase of the social pressure, and are intensifying the efforts to reduce the emissions with new regulations [13]. However, up to now, no regulation has modified the boundary conditions in which homologation tests should be carried out. This is, the pressure and temperature of the ambient conditions where the different vehicles and ICE are homologated [14].

The new regulation Euro 6d that is already being applied since September 2017 [15] will go one step beyond and will extend the ambient conditions where an engine or a car has to be homologated and fulfill the emissions standards. Euro 6d changes the homologation cycle by replacing the NEDC with the new World-wide harmonized Light vehicles Test Cycle (WLTC) [16,17]. As a complement to the test cell tests, the Euro 6d also introduces the Real Driving Emissions (RDE). This is a new and additional vehicle test procedure under real life conditions using Portable Emission Measurement System (PEMS). Under these real conditions, the emissions have to be limited, with a certain margin coming from the PEMS measurement error or conformity factors [18]. The conformity factor only applies for one RDE test, not for the averaged values of many different RDE tests. This means, that the emissions in an individual RDE test cannot exceed 2.1 times the homologation, because the conformity factor is applied. However, the averaged emissions in all the RDE tests cannot exceed the norm, in this case the conformity factor does not apply [19]. Initially, only NOx and particulate number emissions are included in binding limits. RDE will also extend the ambient conditions under which the emissions will be regulated, known as extended conditions. The altitude can reach 1300 meters above sea level and the temperature can range from -7 ºC up to 35 ºC [14].

These new procedures will force the optimization of engine performance and emissions under these operating conditions, as the emissions have shown to be much higher under real driving conditions than in the controlled conditions of the homologation procedures [20].

1.2 Motivation of the thesis

For the reasons exposed in the previous section, it is important to have useful experimental tools able to carry out tests in such low-pressure and low-temperature operating conditions. For example, Sierra Nevada in Granada (Spain) has roads over 2500 m with noticeable temperature variations ranging from 0 to 35 ºC during the year [21]. The available tools the engine manufacturers have nowadays for the altitude tests are limited. The two most extended ways to perform altitude tests are the hypobaric chambers and in situ real altitude tests. However, both systems present some drawbacks that limit their use.

On the one hand, the total number of hypobaric chambers in the current test centers is reduced, as the old legislation did not limit the emissions in altitude. Already built atmospheric test cells cannot be easily converted to

hypobaric chambers; the extra room to build new hypobaric ones is limited and the price is extraordinary high.

On the other hand, the in situ test campaigns are very expensive, mainly caused by the big amount of people and technical equipment that has to be moved for long periods of time [22]. Moreover, they do not guarantee stable and repetitive conditions, as the temperature, pressure or humidity can change in day to day. Also the altitude roads usually are not flat and present some slope, which makes even more difficult the correlation and analysis of test results.

The research institute CMT-Motores Térmicos, in collaboration with HORIBA Europe, has developed within this thesis an altitude simulator that tries to solve the drawbacks of the hypobaric chambers, providing a powerful tool for the research and development tasks that have to be carried out with the new RDE.

The CMT-Motores Térmicos patented the idea of an altitude simulator connected only to the engine intake and exhaust pipes, while the rest of the test cell remains at ambient conditions [23]. This way, any existing test cell can be used to altitude testing. That patent was the trigger for this doctoral thesis.

1.3 Objectives

The objectives of this work are three fold: to provide a tool to investigate engines at altitude conditions, a contribution to the understanding of the effect of the altitude in the engine emissions, and to explore different strategies to reduce them. To achieve them, a longer list of partial objectives is presented in the following paragraphs.

- First of all it is important to get an overview of the current situation. Thus, a bibliographic review of the actual solutions to reproduce altitude conditions for the engine tests has been performed, as well as the effect of the altitude in the engine emissions and performance that has been observed in previous researches.
- The first objective is to develop an altitude simulator taking as the starting point the idea described in the first patent by CMT-Motores Térmicos department [23]. This prototype will be used to analyze the viability of the system and its performance.

- The second objective is to create a computer model of the altitude simulator for a deeper study on the system physics, analyzing how the design of the different elements of the altitude simulator affects its performance.
- The third objective is to design the final layout of the altitude simulator and its control. Based on the results of the previous model the aim is creating a product with an industrial objective: easy to use; easy to install in a test cell and able to be converted into a product useful for the automotive industry.
- The fourth objective is to validate the emissions measurements obtained from an engine when it is operating with the altitude simulator in comparison with a hypobaric chamber.
- The fifth objective is to analyze the effect of the altitude in a turbocharged diesel engine by using the developed experimental tool (altitude simulator).
- Finally, the last objective is to study different alternatives to reduce emissions in altitude conditions. It has been focused mainly in increasing the aftertreatment inlet temperature; since it will have a blind or positive effect in conventional sea level performance while will improve engine performance and help to reduce emissions in altitude operation.

1.4 Methodology

A work methodology has to be followed in order to achieve the proposed objectives. Figure 1.1 shows the followed methodology in the present doctoral thesis. The different chapters of the present documents can be found in independent boxes in Figure 1.1.

The present chapter, Chapter 1, is dedicated to the definition of the problem and objectives to be fulfilled in this doctoral thesis.

In Chapter 2 is presented a detailed bibliographic review of the different topics that will be the basis of the present doctoral thesis. The different technics to perform engine or car tests in altitude conditions, the effect of the altitude on the engine performance and emissions and the effect of the exhaust temperature in the aftertreatment performance and how to increase it.

In Chapter 3 is detailed the first phases of the altitude simulator development: the design and construction of the first prototype, its tests and performance maps analysis, the development description of the computer model of the altitude simulator, the effect of the different elements design in the performance of the altitude simulator and, taking all of this into account, the description and analysis of the final design of the altitude simulator.

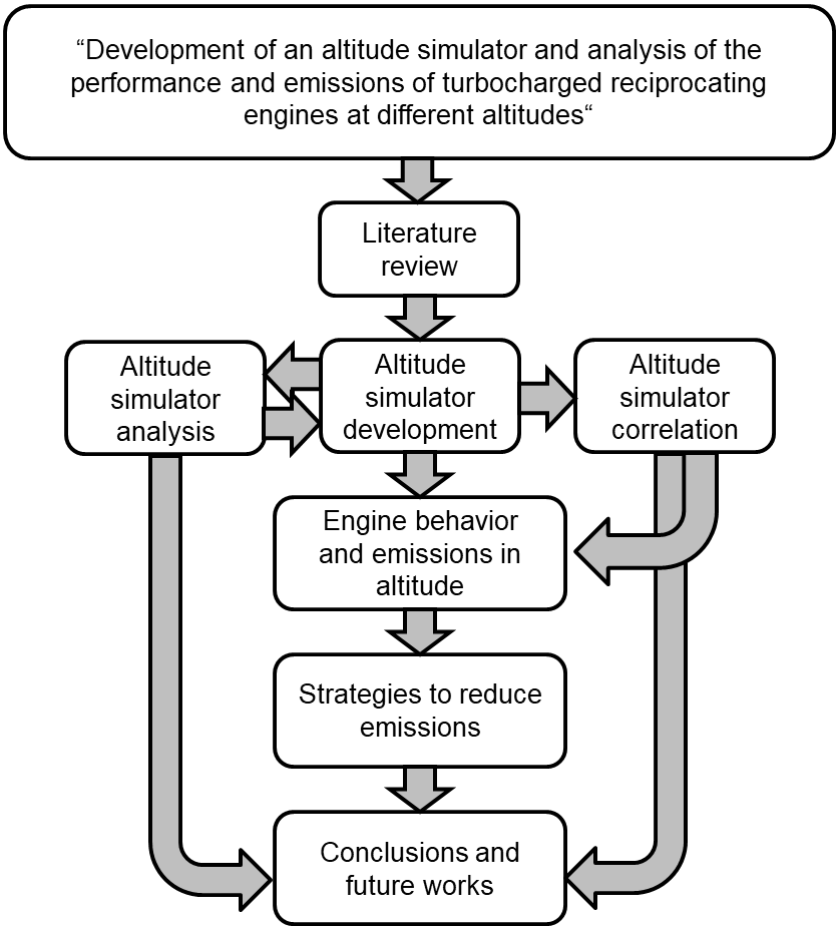

Figure 1.1 – Altitude simulator operation principle

In Chapter 4, a further analysis of the altitude simulator is performed. An analogy between the altitude simulator map and the mechanical compressor map is proposed and analyzed in detail. The control strategies

are also explained in this chapter, as well as the altitude simulator operation in the test cell.

Chapter 5 details the comparison tests between the altitude simulator and a hypobaric chamber. It is done at two different altitudes and for different steady state operation points of the engine, covering a wide range of its operation map.

In Chapter 6, the tests results of an E4 turbocharged diesel engine operating at four different altitudes is analyzed, considering different performance parameters and emissions, during steady state operating and during NEDC dynamic cycles.

In Chapter 7, different strategies to increase aftertreatment inlet temperature for cleaning engine emissions are proposed and analyzed with different parametric studies in an engine software model. It has been, taken into account both the effect in the aftertreatment inlet temperature and in engine bsfc.

Finally, Chapter 8 summarizes the main conclusions obtained in the present thesis and proposes a list of potential future works to give continuity to the works done.

1.5 References

[1] Global Internal Combustion Engine Market 2017-2021, (2017).

[2] H. Zhao, Overview of gasoline direct injection engines, in: H. Zhao (Ed.), Adv. Direct Inject. Combust. Engine Technol. Dev., Woodhead Publishing, 2010: pp. 1–19. doi:https://doi.org/10.1533/9781845697327.1.

[3] U. Shrinivasa, The evolution of diesel engines, Resonance. 17 (2012) 365–377. doi:10.1007/s12045-012-0038-3.

[4] F. Payri, J.M. Desantes, Motores de combustión interna alternativos, Editor. Reverté. (2015).

[5] Number of passenger cars and commercial vehicles in use worldwide from 2006 to 2015 in (1,000 units), (2015). https://www.statista.com/statistics/281134/number-of-vehicles-in-use-worldwide/.

[6] M. Desai, R.P. Harvey, Inventory of U.S. Greenhouse Gas Emissions and Sinks: 1990-2015, Fed. Regist. 82 (2017) 10767. doi:EPA 430-R-13-001.

[7] P. Handsford, S. Birkett, J. Bullied, T. Caccavone, N. Earnshaw, R.

Goldney, P. Gregory, P. Kumar, F. Medda, S. Moroney, H. Pantelidou, K. Simmonds, M. Sugarman, J. Venables, Engineering Cleaner Air, (2017).

[8] K. Young, C. Wang, L.Y. Wang, K. Strunz, Electric Vehicle Battery Technologies, 2013. doi:10.1007/978-1-4614-0134-6.

[9] Z.A. Needell, J. McNerney, M.T. Chang, J.E. Trancik, Potential for widespread electrification of personal vehicle travel in the United States, Nat. Energy. 1 (2016). doi:10.1038/nenergy.2016.112.

[10] J. García-Villalobos, I. Zamora, J.I. San Martín, F.J. Asensio, V. Aperribay, Plug-in electric vehicles in electric distribution networks: A review of smart charging approaches, Renew. Sustain. Energy Rev. 38 (2014) 717–731. doi:10.1016/j.rser.2014.07.040.

[11] F.O. Igbinovia, G. Fandi, R. Mahmoud, J. Tlustý, A Review of Electric Vehicles Emissions and its Smart Charging Techniques Influence on Power Distribution Grid, J. Eng. Sci. Technol. Rev. 9 (2016) 80–85.

[12] J.C.G. Palencia, Y. Otsuka, M. Araki, S. Shiga, Impact of new vehicle market composition on the light-duty vehicle fleet CO2 emissions and cost, Energy Procedia. 105 (2017) 3862–3867. doi:10.1016/j.egypro.2017.03.790.

[13] M. Tutuianu, P. Bonnel, B. Ciuffo, T. Haniu, N. Ichikawa, A. Marotta, J. Pavlovic, H. Steven, Development of the World-wide harmonized Light duty Test Cycle (WLTC) and a possible pathway for its introduction in the European legislation, Transp. Res. Part D Transp. Environ. 40 (2015) 61–75. doi:10.1016/j.trd.2015.07.011.

[14] European Commission, EU legislation on passenger car type approval and emissions standards, (2016). http://europa.eu/rapid/press-release_MEMO-16-4269_en.htm.

[15] Commission Regulations (EU) 2016/646, Euratom. (n.d.). doi:http://eur-lex.europa.eu/pri/en/oj/dat/2003/l_285/l_28520031101en00330037.pdf.

[16] DieselNet. Emission Test Cycles - Worldwide Harmonized Light Vehicles Test Cycle (WLTC), (n.d.). https://www.dieselnet.com/standards/cycles/wltp.php.

[17] M. André, The ARTEMIS European driving cycles for measuring car pollutant emissions, Sci. Total Environ. 334–335 (2004) 73–84. doi:10.1016/j.scitotenv.2004.04.070.

[18] J. Pielecha, J. Merkisz, J. Markowski, R. Jasiński, Analysis of Passenger Car Emission Factors in RDE Tests, 73 (2016) 1–7. doi:10.1051/e3sconf/20161000073.

[19] E. Commission, EU action to curb air pollution by cars : Questions and Answers, (2017).

[20] B. Degraeuwe, M. Weiss, Does the New European Driving Cycle (NEDC) really fail to capture the NOXemissions of diesel cars in Europe?, Environ. Pollut. 222 (2017) 234–241. doi:10.1016/j.envpol.2016.12.050.

[21] Weather statistics for Sierra Nevada, Andalucía (Spain), (n.d.). https://www.yr.no/place/Spain/Andalucía/Sierra_Nevada/statistics.html.

[22] A. Ashtari, E. Bibeau, S. Shahidinejad, Using Large Driving Record Samples and a Stochastic Approach for Real-World Driving Cycle Construction: Winnipeg Driving Cycle, Transp. Sci. 48 (2014) 170–183. doi:10.1287/trsc.1120.0447.

[23] F. Payri, J.M. Desantes, J. Galindo, J.R. Serrano, P. Piqueras, Unit for simulating the pressure and temperature conditions of the air drawn in by a reciprocating internal combustion engine, ES2398095B1 Spanish Pat. Date 20/01/2014. PCT/ES2012/070010. USA Pat. Nº 9038578. Japan Pat. Nº 5788025. Eur. Pat. Appl. No. 12742066.9 - EP2672248. Chinese Pat. Appl. Nº 201280007012.6. (2011).

CHAPTER 2

Literature review

Contents

Figures

Tables

2.1 Introduction

Nowadays, the emissions of the ICE have become an issue of great concern in the population, specially that affecting the big cities. The scandal of the emissions manipulation affecting Volkswagen engines, popularly known as *"Dieselgate"*, has affected the credibility and image of the big automotive groups, not only Volkswagen [1–3]. This scandal has boosted the previous incipient demands of new homologation procedures that reflect more precisely the emissions during real driving conditions, as the NEDC procedure has proven to be too far from the real driving [4].

To solve this concern, a new homologation procedure known as WLTC has been introduced in September 2017, and will be gradually implemented in all the new automobiles and engines until September 2020 [5]. This new homologation will have two different homologation procedures: a new homologation cycle in the test cell known as WLTC, more dynamic and closer to the real driving conditions than the NEDC, and the RDE, which will force to fulfill the emission standards under real driving conditions on the road, measured with On-Board Diagnosis systems (OBD) [6].

During the RDE, the ambient temperature and pressure can change in a wider range than during the NEDC, as reflected in Table 2.1. The temperature can vary from 0 °C to 30 °C, known as moderate conditions, and up to -7 °C and 35 °C under extended conditions. With respect to the altitude, this can change from sea level to 700 m in the moderate conditions, and up to 1300 m in the extended conditions.

Table 2.1. RDE ambient conditions.

Conditions	Temperature [°C]	Altitude [m]
Moderate	From 0 to 30	From 0 to 700
Extended	From -7 to 0 and from 30 to 35	From 700 to 1300

Therefore, the efforts in the altitude tests that the automotive companies will have to do will increase. Thus, new tools to enable altitude tests in the current test cells, reducing the tests campaigns in real altitude environments or hypobaric chambers, present big potential in the current situation.

In this chapter, a literature review in the different methods to perform altitude test is presented, focusing on the altitude simulators whose operation principle is similar to the one developed in the present thesis.

The state of the art of the engine behavior when operating in altitude is also presented. Finally, a literature review of the different research studying the impact of different engine parameters in the aftertreatment inlet temperature and emissions is also presented.

2.2 Objectives

The objectives pursued in the review of the state of the art are:

- Carry out an analysis of the current methods and technologies to perform altitude test in ICE, the effect of the altitude on the engine emissions and the different strategies to increase the inlet aftertreatment temperature, its impact on the emissions and in the specific fuel consumption.
- Collect and synthesize all the relevant information related to the content of the present doctoral thesis, trying to cover all the available information and knowledge that can be a reference for the different studies and works done in the present document.

2.3 International Standard Atmosphere

Due to the importance of having standard properties of the atmosphere at different altitudes, the International Civil Aviation Organization (ICAO) established the International Standard Atmosphere (ISA) [7]. ISA is an atmospheric model of how pressure, temperature, density and viscosity of the air changes with the altitude. It was established to assign a common reference for these variables and consists of a series of tables with their values at various altitudes, in addition to the formulas through which these values have been obtained [8].

The most recent definition of such variations is the United States Standard Atmosphere of 1976 developed jointly by NOAA, NASA and the USAF [9]. It consists of an idealized representation of the steady state of the Earth's atmosphere from the surface to a height of 1000 km, and assumes the existence of a period of moderate solar activity. This atmosphere is equal to the ISA for the first 86 km.

The ISA assume some physics simplifications:

- The atmosphere is divided in layers with linear temperature distribution, avoiding the necessity to integrate to obtain the value of the different properties.

- Gravity is constant with the altitude and its value is 9.80665 m/s², which is approximately the value of the gravity acceleration in latitude 45°.
- The air is dry, without vapor content.
- The air follows the perfect gases equation (Equation (2.1)).

$$pV = mRT \tag{2.1}$$

- The air follows the hydrostatic equation (Equation (2.2)).

$$\frac{dp}{dh} = -g\rho \tag{2.2}$$

All these simplifications link the temperature, pressure and density with the geopotential altitude instead with the geometrical. The relation between both altitudes is given by Equation (2.3). The difference between both altitudes is small when the altitude is small, for example, at 5000 m above sea level, the error between them is 0.08%.

$$h_{geometrical} = h_{geopotential}\frac{r_{earth}}{r_{earth} - h_{geopotential}} \tag{2.3}$$

2.3.1. ISA constants

The needed constants to define the ISA are the following.

- Fundamental constants:
  - Absolute zero temperature: $T_{absolute\ zero}$ = -273.15 °C.
- Earth constants:
  - Earth radius: $r_{earth = 6356.766}$ km.
  - Gravity acceleration at sea level: g_{sl} = 9.80665 m/s².
- Air properties:
  - Universal constant of the ideal gases: R = 287.053 J/kg/K.
  - Air molecular weight: MW_{air} = 0.0289644 kg/mol.
  - Adiabatic dilatation coefficient: γ = 1.4.
- Viscosity:
  - Sutherland Constant: C_s = 110.4 K.

- ß = $1.458 \cdot 10^{-6}$ kg/s/m/$R^{1/2}$.

- Sea level conditions:
  - T_{sl} = 15 °C.
  - P_{sl} = 101325 N/m².

2.3.2. Atmospheric layers

As has been already mentioned, the ISA model divides the atmosphere in different layers with linear temperature distribution. Table 2.2 describes the characteristics of each layer.

Table 2.2. Atmospheric layers and their characteristics.

LAYER	NAME	INITIAL GEOPOTENTIAL ALTITUDE [KM]	TEMP. VARIATION [°C/KM]	INITIAL TEMP. [°C]	INITIAL PRESS. [PA]
0	Troposphere	0	-6,5	15	101325
1	Tropopause	11	0	-56,5	22632
2	Estratosphere	20	1	-56,5	5474,9
3	Estratosphere	32	2,8	-44,5	868,02
4	Estratopause	47	0	-2,5	110,91
5	Mesosphere	51	-2,8	-2,5	67
6	Mesosphere	71	-2	-58,5	4
7	Mesopause	84,852	-	-86,28	0,3734

2.3.3. Physical laws and model equations

The physical laws that the model follows are Equation (2.1) and Equation (2.2), previously described, and Equation (2.4), which defines the viscosity model and it is only dependent on the temperature at any altitude.

$$\mu = \frac{\lambda T^{1.5}}{T + C_s} \tag{2.4}$$

Where:

$$\lambda = \frac{\mu_{ref}(T_{ref} + C_s)}{T_{ref}^{1.5}} \tag{2.5}$$

Finally, from the physical laws defined in these equations and the constants defined in Section 3.2.1, the behavior of the different variables with the altitude can be deducted.

On the one side, simplifying the density from the hydrostatic equilibrium law (Equation (2.2)), and substituting it in the perfect gas equation (Equation (2.1)), Equation (2.6) is obtained:

$$\frac{dp}{p} = -\frac{g}{R}\frac{dh}{T} \tag{2.6}$$

On the other side, for a linear temperature variation, as is assumed in the model for each layer, Equation (2.7) is obtained.

$$T = T_n + (h - h_n)\lambda_n \tag{2.7}$$

Where sub index n refers to the value of the variable at the beginning of the n^{th} layer. Then, it can be deducted Equation (2.8).

$$\frac{dT}{dh} = \lambda_n \tag{2.8}$$

That substituting in Equation (2.6), Equation (2.9) is obtained, that links the pressure variation with the altitude. Figure 2.1 shows the pressure and temperature variation with the altitude for the troposphere, which is the interest region in the present work studies.

$$\frac{p}{p_n} = \left(1 + (h - h_n)\frac{\lambda_n}{T_n}\right)^{-\frac{g}{\lambda_n R}} \tag{2.9}$$

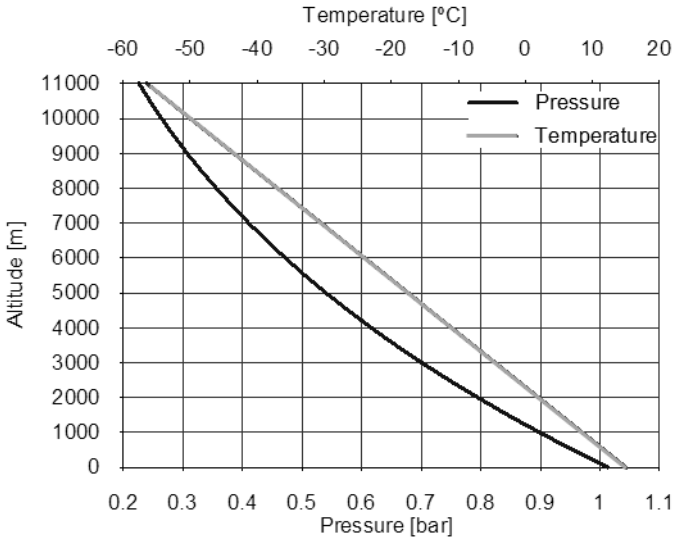

Figure 2.1 – Pressure and temperature variation with the altitude according to ISA

2.4 Altitude testing

In order to reproduce altitude conditions in an engine or a car, the automotive companies use different techniques that can be divided in three main groups: real altitude tests, hypobaric chambers and altitude simulators for the intake and exhaust air conditioning. The three groups will be detailed in the following paragraphs, explaining the differences between them and their advantages with respect to the others techniques.

2.4.1. Real altitude tests

The first and more direct way to perform altitude tests in engines is in a real altitude environment. This is a round robin test, that means: moving the engine or car to be tested, the measurement systems and all the technicians and research team to the desired altitude for a period of time in order to perform the testing campaign in that area.

Despite the fact that real altitude tests are the most accurate way to simulate altitude, this method presents some disadvantages:

Repetitiveness

Testing under real world conditions means that the environmental variables can change from one day to another and they cannot be modified.

For example, one day can be sunny and the next day can rain, i.e. the ambient pressure, temperature and humidity have changed and the results obtained each day cannot be easily compared [10].

Ambient restrictions

Other disadvantage is also related by the imposed ambient conditions. In order to ensure that the engine will operate as expected under all the possible situations, in some moment it should be tested under any given extreme ambient condition, such as high altitude and high ambient temperature or very low temperature. However, the ambient conditions are imposed depending on the location and the season of the year, and testing at different locations that fulfills the extreme conditions required is very expensive and difficult.

Economical costs

To solve the first two disadvantages, the tests can be performed in a movable test bench, similar to the one used by Xin et. al. [11], which consist in a test cell inside a truck. This way, the truck can be located in an altitude place and the tests can be performed in the engine dyno or chassis dyno inside the truck.

However, this solution still does not solve the economic costs disadvantage (minimum of 35 k€/week at 2017 prices cost). Moving the human team and measurement systems to a given location for the period of time needed to perform the test campaign [12] is always very expensive [13]. Moreover, in case of any trouble or failure with the vehicle or measurement system during the real altitude test campaign, the means to repair it are more limited. This increases the duration of the test campaign and the costs.

For these reasons, real altitude tests can be part of the testing campaign as a final part in the engine or car setup, but it cannot be the main tool to calibrate and test an engine under altitude conditions for the exposed reasons.

2.4.2. Hypobaric chambers

In order to shorter the number and lengths of the real altitude tests, other tools have been developed. The hypobaric chambers are one of these tools [14].

A hypobaric chamber consist on a test cell where the pressure inside can be controlled in order to simulate a given altitude. Then, the engine or car to be tested is placed inside it and it can be tested at that given altitude.

The results obtained from the hypobaric chambers can be directly compared with the results obtained in real altitude conditions, if the temperature, pressure and humidity are the same in both cases [15]. Therefore, they can be used in the first stages of the engine calibration, before real altitude tests.

However, hypobaric chambers present also some disadvantages.

Required space

A hypobaric chamber is a special designed test cell where the pressure inside can change up to high altitude [16]. To support the pressure difference between the ambient and the pressure inside the hypobaric chamber, the walls and the structure of the hypobaric chamber has to be specially designed, with reinforced supports and avoiding any leak through the windows or doors. Therefore, hypobaric chambers are bigger than normal test cells for the same useful space.

Besides, as the structural requirements are more restrictive than in normal test cells, it has to be planned during the construction phase of the building. However, as the altitude tests requirements will increase with the new homologation, automotive companies has a lack of hypobaric chambers to perform all the tests that will be needed to fulfill the emission limits.

Human risks

On one hand, in the hypobaric chambers with a chassis-dyno, the driver changes from ambient pressure to altitude conditions in short periods of time and many often. This has some risks on the human health as the human body cannot withstand repeated pressure changes [17–20]. This limits the number of hours and tests that can be performed in a hypobaric chamber with a chassis dyno.

On the other hand, in case of problems inside the test cell, it is more complex to repair or solve the problem, as not only the engine has to be stopped, also the pressure has to be increased up to ambient conditions before the operator can go inside the test cell. This increases the time needed to repair anything inside the test cell.

Economical costs

For all the reasons given above, a hypobaric chamber is also an expensive (about 10 M€ at 2017 prices cost) way to perform altitude tests [21].

2.4.3. Altitude simulators

The third way to perform altitude tests in engine or vehicles are altitude simulators. An altitude simulator is similar to a hypobaric chamber, but instead of changing the pressure of the complete test cell, only modifies the pressure inside the engine pipes, from the engine intake to the tailpipe, including the engine sump and other elements affected by the pressure.

In the literature, different systems and devices can be found that work as altitude simulators. Most of them have the same operation principle. Figure 2.2 shows the flow diagram that fulfills the altitude simulators that will be analyzed in detail in the following paragraphs.

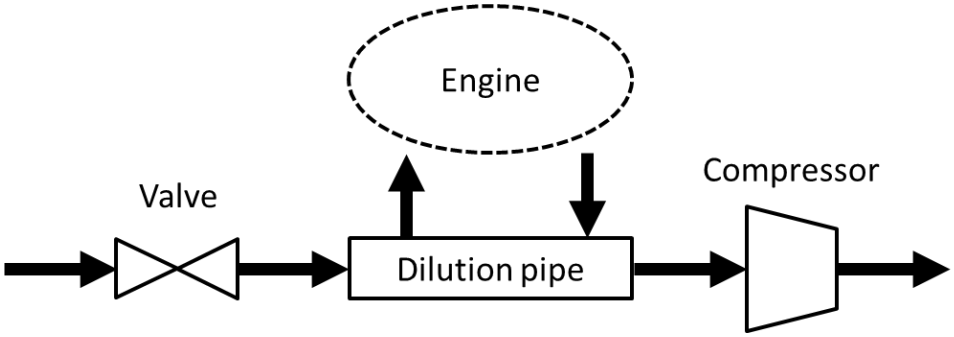

Figure 2.2 – Flow diagram of altitude simulators

- A blower or a compressor that sucks the air from inside the altitude simulator.
- A valve that generates the pressure losses between the ambient pressure and the simulated altitude.
- A dilution pipe that connects that connects the engine intake and exhaust and ensures the same pressure in both.

For example, Daniele Testa et al. [22] presents an installation that can reproduce altitude conditions. This installation can change pressure of the atmospheric air by means of two roots compressors, one upstream of the engine connection and other downstream. Additionally an independent air conditioning unit for temperature and humidity control is installed at the

inlet of the system. In vacuum mode, the compressor downstream the engine connection turns moved by an electric motor and the other compressor generates the pressure losses, operating like a valve. In overpressure mode, they exchange their functions.

Other similar system is presented by Simperl et al. [23], which uses two valves and two volumetric compressors to control the pressure, one of them upstream and the other downstream of the engine connection. In this case, the independent air conditioning unit to control the temperature and humidity is installed between the first valve and the engine intake. The operation mode is similar to the system described in [22], but now the pressure losses are generated by the valves instead of by the root compressors. Also an important difference with [22] is that Simperl et al. [23] proposes and additional blower and a check valve installed in the dilution channel to avoid back flows and to compensate pressure losses between intake and exhaust line. Both systems are unnecessary, as will be discussed later, and were avoided in Testa et al. [22] description.

In both systems the engine intake and exhaust connection are connected by a dilution pipe.

However, there are some differences between the altitude simulator developed in this doctoral thesis and the altitude simulators described in [22] and [23].

The main difference is that the altitude simulator developed in this doctoral thesis uses a turbine instead of an expansion valve or a pump to generate the pressure losses upstream the engine. An expansion valve or a pump generating pressure losses forces to use an air conditioning unit to reduce flow temperature in any case, increasing energy consumption and installation costs. With the use of a turbine, the pressure is decreased and at the same time the temperature can be controlled, as the expansion in the turbine cools down the atmospheric air [24].

Other important difference is that both systems used big flow machines to generate vacuum or overpressure (root compressor in [22] and blowers in [23]). These compressors show a number of disadvantages when compared with a radial compressor, as the one used in the altitude simulator developed in the present work. For the same mass flow, volumetric compressors are much bigger and blowers provide much lower pressure ratio. This increases the size needed in the altitude simulator or reduce the altitude range able to be simulated, making it more difficult to be installed in a test cell or useful less for extended range of new regulations. In spite of radial compressors advantages, they had the drawback of a big surge area

to be coping with. The surge issue will require special attention in present thesis in order to be able to keep radial compressors advantages for the developed altitude simulator.

Human et al. [25] also developed an altitude simulator and tested two different diesel engines, a natural aspiration 10.4 liters engine and a turbocharged 14 liters engine, at two different altitudes, analyzing its performance and emissions. Focusing on the altitude simulator used, as the emissions results will be analyzed in detail in Section 2.7, it is installed in the test cell and uses a volumetric pump to generate the vacuum in the engine exhaust and intake, as both are connected by a dilution pipe. However, the type of pump, its control and operation principle of the whole system is not fully explained and the system is installed in the test cell with a civil work and cannot be moved.

He et al. [26] followed a different approach to develop an altitude simulator. The system they used has not any dilution pipe. The intake throttle valve generates the pressure losses to simulate the desired altitude in the engine intake and the pump at the exhaust generates the same altitude at the engine exhaust. This system is only useful to test steady state engine points, as the system has to adjust the valve position and the compressor speed depending on the engine operation point. The absence of the extra flow contained in the dilution pipe will require that the altitude simulator will follow the fast engine transient response to keep a stable emulated atmosphere. Due to the fast accelerations and decelerations of reciprocating engines during normal operation this follow up is almost impossible to be achieved.

Advantages with respect to hypobaric chambers

Altitude simulators solve the main problems seen by the hypobaric chambers.

Required space

The required space is much smaller, as only is required the needed room to install the different components of the altitude simulator.

The combustion air handling units (CAHU) that are sold commercially can be installed in two different ways in the test cell. On the one hand, the elements can be installed in the test cell [27], where they are distributed adjusting it to the space in the test cell. They cannot be moved as are part of the test cell. On the other hand, some combustion air handling units (CAHU) are built in a structure with wheels [28]. This allows them to be

moved to different test cells, as any structural change in the test cell is not required. Nevertheless, none of the available movable systems are able to condition altitude (vacuum).

Therefore, an altitude simulator that could be installed in any test cell would be desirable. In that way testing centers can upgrade any test cell already built in a hypobaric chamber, increasing their capability to perform altitude tests in their current installations without the need to build new and expensive test cells.

Human risks

As the test cell pressure is not modified when an altitude simulator is operating, the driver of the car to be tested in the altitude tests does not suffer pressure changes. From the point of view of the driver, running a test with an altitude simulator is like running a test in ambient conditions, as he is not feeling any pressure change in his body.

Economical costs

The last problem that solves the altitude simulators is the economic costs, as they are much cheaper than building a complete hypobaric chamber.

Disadvantages with respect to hypobaric chambers

Despite the fact that altitude simulators show several advantages with respect to the hypobaric chambers, their use is not yet spread among the automotive industry. The reasons that explain that are listed below.

Correlation between altitude simulators and hypobaric chambers

As the homologation did not push to increase the number of altitude tests, the manufacturers had enough with the hypobaric chambers tests, whose results were very similar to the results obtained with the real altitude tests. The correlation between the results obtained with an altitude simulator and those obtained in real altitude tests is not so evident, as the ambient pressure might have some effect on the engine overall behavior (some flexible pipes must to be rigidized in order to avoid collapse, crank shaft seals may not be enough to withstand vacuum inside crank case). In fact, in the literature there are some tests with altitude simulators, as this one [25], that was performed with an altitude simulator installed in the test cell, but there are not any comparison test between hypobaric chambers and altitude simulators. The results and trends shown in [25] are similar to the trends shown in real altitude tests, as will be analyzed in Section 2.7;

but it cannot be said that the values shown are the same between the altitude simulator and the real altitude tests.

For the automotive companies, this information would be a key point to integrate of this new technology in their development process of new engines or control strategies. For this reason, in the present thesis, in Chapter 5, a correlation test campaign between the altitude simulator developed and a hypobaric chamber is performed.

Movable altitude simulators that does not require civil works

If civil work is required some of altitude simulators advantages with respect to hypobaric chamber vanish. Once again, a movable device that allows using it in several conventional-atmospheric cells would be desirable.

2.5 Homologation cycles

Worldwide harmonized Light Test Cycles (WLTC) are chassis dynamometer tests for the determination of emissions and fuel consumption from light-duty vehicles [5,29]. There are several WLTC cycles depending on the power-to-mass ratio (PMR) of the vehicle, which is defined as the ratio between the rated power (W) and the curb mass (kg).

The WLTC is part of the Worldwide harmonized Light vehicles Test Procedures (WLTP). The WLTP defines a number of other procedures that are needed to type approve a vehicle, in addition to the WLTC test cycles. The New European Driving Cycle (NEDC) is being replaced progressively by the WLTP. In September 2017 for the new vehicles and in September 2018 for all the vehicles sold [5].

The main WLTC cycle in Europe and Japan is Class 3 Cycle of the WLTC, because the vehicles sold there have a high power-to-mass ratio (PMR). Figure 2.3 shows the vehicle speed during the Class 3b cycle.

Table 2.3 shows the emissions limits imposed by the different European legislations.

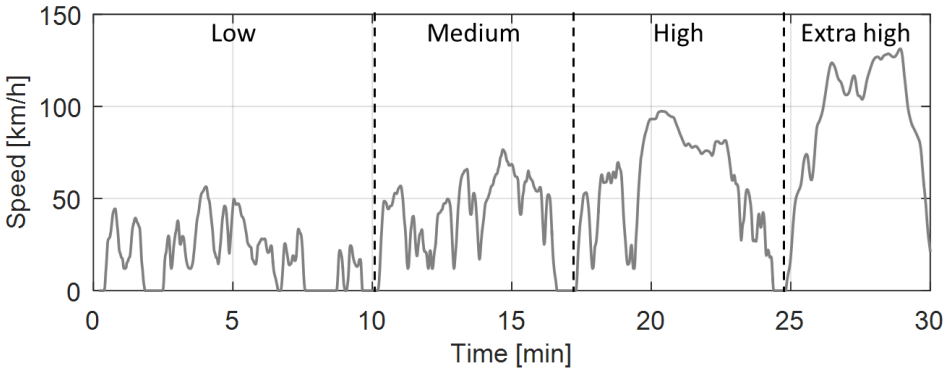

Figure 2.3 – Vehicle speed during WLTC class 3b [5,30]

Table 2.3. Emissions limits imposed by the different European legislations [31].

Stage	*Date*	*CO*	*HC*	*HC+NOx*	*NOx*	*PM*	*PN*
		g/km					#/km
	Positive Ignition (Gasoline)						
Euro 1	07.1992	2.72	-	0.97	-	-	-
Euro 2	01.1996	2.2	-	0.5	-	-	-
Euro 3	01.2000	2.30	0.2	-	0.15	-	-
Euro 4	01.2005	1	0.1	-	0.08	-	-
Euro 5	09.2009	1	0.1	-	0.06	0.005	-
Euro 6	09.2014	1	0.1	-	0.06	0.005	6.0×10^{11}
	Compression Ignition (Diesel)						
Euro 1	07.1992	2.72	-	0.97	-	0.14	-
Euro 2	01.1996	1	-	0.7	-	0.08	-
Euro 3	01.2000	0.64	-	0.56	0.5	0.05	-
Euro 4	01.2005	0.5	-	0.3	0.25	0.025	-
Euro 5a	09.2009	0.5	-	0.23	0.18	0.005	-
Euro 5b	09.2011	0.5	-	0.23	0.18	0.005	6.0×10^{11}
Euro 6	09.2014	0.5	-	0.17	0.08	0.005	6.0×10^{11}

The difference in the emissions homologated by the vehicles and the emissions emitted in real driving conditions has been progressively

increasing, especially in diesel engines [32]. This is, despite the fact that the limits stablished by the NEDC have been drastically reduced with each new homologation, the emissions measured during real driving conditions has been almost constant over the past 15 years [33–37].

For this reason, the other big novelty introduced by the WLTP is the Real Driving Emissions (RDE), which complements the WLTC. RDE limits the NOx and PM emissions under real driving conditions, measured with a Portable Emissions Measurement System (PEMS) [38].

RDE is being applied since September 2017 for new vehicles with a conformity factor of 2.1 with respect to WLTC. This means that NOx and PM emitted during a RDE can be 2.1 higher than the limit value for the WLTC. The conformity factor is a parameter taking into account additional measurement uncertainties of PEMS equipment, and is subjected to annual review. It is planned in 2020 to reduce the conformity factor to 1.5 [39].

The ambient conditions where the RDE can be performed are also wider than in the WLTC, being the maximum temperature range from -7 °C up to 35 °C and the altitude range from sea level up to 1300 m.

2.6 ICE emissions

Before going into detail with the engine emissions under altitude conditions, it is going to be exposed a short overview about how the different engine emissions are produced [40]. This will help for the latter understanding of the effect of the altitude in the emissions. Even this short overview is made general in the sake of completeness the scope of this thesis and the engines studied are restricted to the turbocharged compression ignition engines (Diesel engines).

An internal combustion engine emits different combustion products, but only a part of them are undesirable or pollutants and have to be reduced as much as possible.

- Non-pollutant products: CO_2 and Water vapor (H_2O), coming mostly from the fuel combustion; oxygen (O_2) and nitrogen (N_2), coming directly from the air. Even though water vapor and CO_2 are non-pollutant gases, they contribute to global warming. Being CO_2 the most undesired and non-pollutant gaseous emission, due to their longer life time in the atmosphere.
- Pollutant products: CO and hydrocarbons (HC) coming from an incomplete combustion. NO_x coming from the air nitrogen oxidation.

SO_x coming from the sulfur present in the fuel. Finally, the particle matter (PM) formed during and after the combustion.

In the following paragraphs, the main undesirable and pollutant gases formed during the combustion process will be analyzed.

2.6.1. Carbon dioxide

Equation (2.10) shows the general form of a simplified combustion reaction. The fuel, when burns with the air, forms carbon dioxide as an intrinsic combustion component, as the carbon in the fuel oxides to CO_2 during the combustion.

$$C_m H_n O_p + n_{air,st}\left(X_{O_2,a} O_2 + X_{N_2,a} N_2\right) \rightarrow 0.79 n_{air,st} N_2 + m CO_2 + \frac{n}{2} H_2 O \qquad (2.10)$$

In the following paragraphs it will be discussed how the pollutants can be reduced by different methods, but CO_2 emissions are directly related with the combustion process and cannot be avoided: producing energy from diesel or gasoline combustion leads to a production of CO_2 [41].

In the past, CO_2 has been reduced by reducing the heat and mechanical losses from the combustion to the wheels, i.e. increasing the indicated efficiency and the mechanical efficiency [42–45], as well as using biofuels [46–48] and reducing the energy expelled through the exhaust without being converted into useful work [49].

Nowadays, an additional way the automotive industry can increase deposit-to-wheel efficiency and reduce CO_2 emissions is increasing the electrification of the cars [50]. Despite the fact that pure electric cars, and/or using hydrogen to produce the energy in the car [51,52], still present big challenges to solve [53–55]; mild-hybrid cars are becoming an affordable way to fight against CO_2 emissions while having most of the advantages of the ICE [56].

2.6.2. Carbon monoxide

The carbon monoxide (CO) is a combustion product formed in an intermediate step during the oxidation process of the hydrocarbons of the fuel [57]. However, when the oxygen available during the combustion is limited, as happens in a rich mixture, the CO is not oxidized into CO_2 and it is emitted through engine tailpipe.

CO is a colorless, tasteless, odorless, and non-irritating gas. However, it is absorbed into the bloodstream through the lung cells and forms a product

derived from hemoglobin (Hb), known as carboxyhemoglobin (COHb), which produces hypoxia. Thus, sufficient high levels of CO can even cause death [58,59].

The main technique to reduce CO emissions is the Diesel Oxidation Catalyst (DOC) in Diesels. DOCs convert CO into CO_2 and water, helped by different precious metals as palladium (Pd) and platinum (Pt) [60].

2.6.3. Nitrogen oxides

The nitrogen present in the air is combined with the oxygen, also present in the air, and creates NO_x (nitric oxide – NO – and nitric dioxide – NO_2) during the combustion process of lean mixtures at high temperatures [61], as those achieved during the combustion process inside the combustion chamber of ICE. As high temperature combustion is the standard nowadays, NO_x are mainly produced by diffusion combustion in Diesels with stratified lean mixtures [62], being therefore an important problem of the big cities around the world, where the concentration of cars with this type of engines is higher [63].

NO_x contribute to the formation of smog and acid rain that impact on respiratory conditions causing inflammation of the airways, emphysema and bronchitis [64]. The acid rain also affects the ecosystems and causes biological death on lakes and rivers [65].

The main method applied in the modern ICEs to reduce NO_x emissions in lean combustion is Exhaust Gas Recirculation (EGR) technique. EGR consists in sending back to the intake manifold some amount of exhaust gases and mix them with fresh air, before supplying it to the cylinders for combustion. This way, the oxygen concentration is reduced (inert gasses concentration is increased) in the air inside the cylinders, what reduces the maximum temperature during the combustion process and therefore the NO_x formation [66].

The other main technique for the NO_x reduction is Selective Catalyst Reduction (SCR) and Lean NO_x Trap (LNT) after-treatment systems, which are focused on the reduction of the NO_x emissions (in an oxidizing atmosphere) after its formation in the combustion chamber [67]. Despite the fact that both systems objective is the same, their operation is different.

LNT works absorbing the NO_x formed in lean mixture combustion in a substrate, which is generally made of barium nitrate. When this substrate becomes saturated, it is regenerated oxidizing the NO_x trapped in solid nitrate in milliseconds [68].

In SCR, the exhaust gas is mixed with a water solution of urea and then it passes through the SCR, where both components react in a chemical reaction that converts nitrogen oxides into nitrogen, water and small amounts of carbon dioxide (CO_2) [69].

In premixed combustion with stoichiometric mixtures the TWC is the main aftertreatment method applied for NO_x cleaning from the exhaust gases [70].

2.6.4. Unburned hydrocarbons

Similarly to the CO, unburned hydrocarbons (HC) are a combustion product formed in an intermediate step during the oxidation process of the hydrocarbons of the fuel [57]. However, in an engine HC are produced mainly by three mechanisms: jet-to-wall impingements (also known as misfiring) [71], poor fuel evaporation [72] and extreme air-to-fuel ratios [73].

Unburned hydrocarbons, through chemical reactions in the troposphere, play an important role in forming NO_2 and O_3 which are health and environmental hazards. For example, benzene has been found to deplete red blood cells, cause cancer and damage bone marrow [74,75].

DOC and TWC after-treatment is also used to control HC emissions in compression and spark ignition engines respectively. Similarly than with the CO process, DOC and TWC oxides HC into CO_2 and water.

2.6.5. Particle matter

Finally, the other important pollutant emitted by the ICE during the combustion is the particle matters (PMs). PMs are formed from the agglomeration of very small carbonic material produced during the combustion process, as unburned fuel, burned lube oil, and ash content of fuel oil and cylinder lube oil [76].

PM size is a key parameter to determine some factors as the period of time they remain in suspension in the atmosphere before deposition, the probability of being absorbed by plants or inhaled by living beings or the degree of penetration in the pulmonary alveoli. Diesel PMs are typically spheres about 15 to 40 nm in diameter and approximately more than 90% of PM is smaller than 1 μm diameter [77].

The size of PM is also linked to its health risk on humans [78]. On the one hand, as explained before, the smaller particles penetrate further down in

the respiratory tract and in the extra pulmonary organs, including the central nervous system [79]. On the other hand, big PMs are associated to greater potential for adverse health impacts [80].

PM can be removed from the exhaust gas by means of Particle Filter (PF). PF reduces the emitted PM to the atmosphere by capturing it. PFs are made by a porous material forming small channels that are sealed alternatively in each extreme, forcing the exhaust gas to pass through the channel wall to reach the tailpipe [81,82].

2.7 Compression Ignition Engines performance and emissions in altitude conditions

When an engine is operating in altitude conditions, its overall behavior is affected by the ambient pressure reduction. As explained before, with the altitude the pressure decreases, and hence the oxygen content in the air also decreases. Therefore, if the engine ECU does not modify its operation with the altitude, immediately the vehicle will experiment a reduction in torque and power [83].

Manufacturers have been developing a series of control strategies to mitigate the power and torque reduction with the altitude, taking also into account the integrity of the different elements of the engine. However, the control of the emissions in altitude has not been a priority in the applied control strategies [84,85].

In the following paragraphs, a literature review is performed, focusing on the effect of the altitude in the combustion process and in the different elements of the engine, such as the turbocompressor, paying attention to the control strategies to mitigate this effect and its effect on emissions.

2.7.1. Altitude effect on the combustion chamber

With the altitude increase, the pressure and the oxygen content in the engine intake air decreases; this affects several parameters in the combustion process.

With higher altitudes, the ignition delay in compression ignition engines slightly increases, resulting in a longer premixed-phase combustion duration and longer total combustion duration due to reduced molecular concentration of oxygen (mol/m^3) at high altitudes [86].

On the one hand, the lower pressure also leads to a decrease of the maximum in cylinder pressure and mean effective pressure, that decreases the thermal efficiency [87,88]. On the other hand, as the combustion duration increases and the peak of the heat release delays, the temperature of the exhaust gases in the exhaust manifold increases [83], what can limit the engine performance [89]. Despite the fact that the exhaust manifold temperature increases, as the outlet turbine pressure decreases with the altitude, the expansion ratio in the turbine increases. This leads to a lower inlet aftertreatment temperature with the altitude.

All these effects reduce the engine bmep, but this reduction is lower than the pressure reduction, because it is compensated by the control strategies applied by the engine [90–92], as will be detailed later.

2.7.2. Altitude effect on the ICE elements

The changes in the pressure and combustion process leads to a change in the operation conditions of the different engine elements.

Turbine

For example, the turbine power experiments two positive effects. On the one hand, the increase of the exhaust gases temperature in the exhaust manifold leads to an increase of the available energy to produce work. On the other hand, the decrease of the ambient pressure also decreases outlet turbine pressure, and therefore increases its expansion capability.

The negative effect on turbine power comes from a decrease of the boosting pressure at a given altitude due to the decrease of the ambient pressure; and therefore on the turbine inlet pressure, what should reduce its expansion capability.

Compressor

With respect to the compressor performance, the altitude effect leads to several negative effects. The lower inlet pressure leads to lower outlet pressure, what decreases the amount of air trapped by the cylinders and therefore its power [90].

However, if the turbine has enough energy to keep the boosting pressure constant, the compressor has overspeed risk [93]. The explanation is as follows: on the one hand, as the outlet pressure is kept constant and the inlet pressure is decreasing, the pressure ratio in the compressor increases; on the other hand, as the outlet pressure is kept constant, the real mass

flow to the cylinders and through the compressor is kept constant, but the decrease of the inlet pressure, leads to an increase of the corrected mass flow. These two effects moves the operation point of the compressor to higher speed, being therefore risk of reaching the overspeed area. It is worth noting that overspeed is linked with high temperatures of the air at compressor outlet. Whatever the limit is reached first will limit the maximum pressure ratio.

In addition, there is a risk of getting compressor into surge at a given low engine speed. This will happen if the surge-limit line in compressor map is crossed by previous described trajectory of increasing pressure ratio and reduced mass flow (high positive slope line in compressor map) [94].

2.7.3. ICE control strategies in altitude

In order to mitigate the effect of the altitude, the ECU applies some control strategies, different than those applied at sea level.

In order to compensate the effect of the altitude, one possible solution is to keep the boosting pressure constant, by increasing the pressure ratio in the compressor, as proposed by Zhang et al. [94]. This can be achieved by closing the VGT blades, but with the corresponding increment of the pumping losses.

However, at a certain altitude, the VGT cannot compensate the pressure reduction and the boosting pressure starts to decrease, what leads to a reduction in the output power and torque [90,95], even with two-stage turbochargers, the altitude effect on the engine power cannot be compensated in all the operation conditions, being more evident at low and medium loads [96].

With respect to the EGR, as the old Euro V legislation did not limit emissions in altitude, the easiest control strategy for the EGR in altitude is closing it, what also increases the fresh air through the compressor, mitigating the effect of the pressure decrease with the altitude [97]. But of course, this solution increases NOx emissions, as will be detailed in Section 2.7.4.

Some other studies are focused in the impact of the altitude in the cylinder, and propose solutions to mitigate it, such as modifying the valves opening to control exhaust back-flows and volumetric efficiency, or changing the injection timing.

As explained before, the start of the combustion delays and the total combustion duration increases with the altitude. Therefore, some authors as Zhu et at. [98] have found that advancing the injection timing with the altitude improves the engine efficiency.

2.7.4. Compression ignition ICE emissions in altitude

All the changes in the control strategies shown above lead to a variation in the engine emissions.

NO_x

The effect of the altitude in the NO_x emissions is affected by different variables.

On the one hand, with the increase of the altitude, the maximum temperature in the cylinders decreases, because the maximum in cylinder pressure also decreases caused by the decrease of the atmospheric air with the altitude. This would lead to a decrease in the NO_x emissions, as has been pointed in several studies [25,26,90,99].

On the other hand, the two main control strategies to mitigate the altitude effect in the engine performance have a big impact in the NO_x emissions. Closing the EGR with the altitude increases drastically the adiabatic flame temperature [100] and closing the VGT in order to keep the boosting pressure constant keeps the maximum in cylinder pressure also constant [101].

Therefore, depending on the engine control and technologies applied, the NO_x emissions can present a different trend with the altitude, as can be seen in different studies where the NO_x trend is different depending on the control strategies of the engine tested and the altitude [102–104].

CO and HC

With respect to the CO and HC emissions with the altitude, all the studies have shown a big increment in their values with the altitude increase. The CO and HC emissions are very affected by the in-cylinder pressure and the DOC performance. With the increase of the altitude, the in-cylinder pressure decreases, and this leads to an increase of the jet-to-wall impingements [105], what has been pointed that increases the CO and HC emissions [106].

The negative effect of the increase of the jet-to-wall impingements is more relevant on the engine emissions in altitude, because all the studies show an increment of the CO and HC emissions [88,107].

With respect to the DOC performance, it is very dependent on the temperature and dwell time. With the altitude both effects are opposed. On the one hand, the inlet aftertreatment temperature increases [108], mainly caused by the increase of the maximum in-cylinder temperature and the delay of the combustion start. On the other hand, the dwell time decreases if boost pressure is kept constant, due to the higher gas velocities caused by the lower gas density, or somehow compensates if mass flow is reduced.

In addition, VGT control strategies [90,95] or other turbine control strategies (WG, 2-stage, …) which increase engine back-pressure to keep constant engine boost pressure, can lead to an unexpected level of backflows to the combustion chamber during the exhaust process and valves overlap periods. This uncontrolled 'internal EGR' can lead to further unexpected emissions of CO and HC.

PM

The PM emissions with the altitude also increases, mainly caused by the increase of the autoignition delay with the altitude, which reduces the late combustion phase and soot burnout process deteriorates [109]. Also, previous described mechanism of back-flows generation contributes to increase PM emissions, when turbine control strategies are used.

CO_2 and BSFC

The CO_2 emissions increase (BSFC increases) with the altitude, but this increment is not as big as the increment of the pollutants [26]. The main reason of the increment of the BSFC and CO_2 emissions is the increase of the pumping losses caused by the back pressure increment (turbine control strategies) with the altitude [94].

2.8 Strategies to compensate altitude effects

In the previous section, the altitude has been pointed to have an important role in the engine performance and emissions. The most spread strategies that are currently applied to withstand the altitude negative effects on the engine performances are EGR closing and back pressure increment due to turbine control (VGT & WG closing), both oriented to increase the amount of fresh air that goes into the cylinder. However, they have shown also big increases in the exhaust emissions, increasing drastically CO, HC and soot

emissions. For this reason, other strategies have been studied by different authors to mitigate the effect of the altitude in the engine performance and emissions.

The use of different fuels and additives has been the most researched tool to improve engine performance and emissions in altitude. For example, the use of enriched oxygen fuel shows interesting results as the oxygen reduction with the altitude is compensated with the oxygen increase present in the fuel [99,103,110]. Also the use of biofuels leads to shorter ignition delay and premixed stage duration, what is a very desirable effect to compensate the opposite effect with the altitude increase [86].

Wang et al. [87] tested a turbocharged diesel engine at different altitudes in two different operation points without modifying the engine control. Results showed that the peak heat release rate of biodiesel operations in premixed combustion duration was a little earlier but the lower than of diesel operations. Besides, the BSFC increased with the use of biodiesel.

Benjumea et al. [86] also tested an engine fueled with a palm biodiesel at different altitudes and found that the thermal efficiency was higher with the biofuel and its reduction with the altitude was lower in comparison with the conventional diesel fuel. Besides, they found that the premixed combustion duration was shortened and the transition between the premixed combustion and diffusion combustion was smoother.

With respect to the emissions, Yu et al. [111] found a similar increase of the BSFC with the altitude with the diesel and biodiesel fuels, but the start of the combustion delay was lower with the use of biodiesel, while the CO, THC and PM emissions increase with the altitude for both fuels. However, found that the benefits of biodiesel with respect to THC and PM emissions declined at higher altitudes, perhaps due to poorer atomization of biodiesel under these conditions. With respect to the NO_x emissions, the use of biofuel does not show differences with respect to regular fuel at different altitudes [97].

Tan et al. [108], using an altitude simulator, tested also a turbocharged diesel engine with different blending ratios of biodiesel. The results showed that for a given altitude, the BSFC increases 4.32% and the output power decreases 4.38% when a bend with 30% of biodiesel with respect to standard diesel. However, the smoke decreases more than 50%.

Another way to reduce emissions in altitude is reducing the aftertreatment heating time, it is, the time that takes to the aftertreatment systems to reach the target conversion temperature, what improves its performance

and reduces the emissions during the cold start [112]. In altitude, despite the fact that the exhaust temperature is higher than at sea level, the air mass flow decreases caused by the pressure reduction, therefore, the energy of the exhaust gases reduces and therefore the activation time of the DOC and DPF increases. Also an important effect of the lower energy of the exhaust gases is caused by the increase of the exergy destruction with the altitude, caused by the greater irreversibility resulting in lower energy quality of the exhaust gases [113].

2.9 References

[1] L. Bovens, The Ethics of Dieselgate, Midwest Stud. Philos. 40 (2016) 262–283. doi:10.1111/misp.12060.

[2] C. Brand, Beyond "Dieselgate": Implications of unaccounted and future air pollutant emissions and energy use for cars in the United Kingdom, Energy Policy. 97 (2016) 1–12. doi:10.1016/j.enpol.2016.06.036.

[3] F.R. Jacur, The environmental dimension of the dieselgate: A European and international legal perspective, in: Dieselgate A Leg. Perspect., 2017: pp. 171–178. doi:10.1007/978-3-319-48323-8_10.

[4] L. Yang, V. Franco, P. Mock, R. Kolke, S. Zhang, Y. Wu, J. German, Experimental Assessment of NOxEmissions from 73 Euro 6 Diesel Passenger Cars, Environ. Sci. Technol. 49 (2015) 14409–14415. doi:10.1021/acs.est.5b04242.

[5] M. Tutuianu, P. Bonnel, B. Ciuffo, T. Haniu, N. Ichikawa, A. Marotta, J. Pavlovic, H. Steven, Development of the World-wide harmonized Light duty Test Cycle (WLTC) and a possible pathway for its introduction in the European legislation, Transp. Res. Part D Transp. Environ. 40 (2015) 61–75. doi:10.1016/j.trd.2015.07.011.

[6] M. Weiss, P. Bonnel, R. Hummel, N. Steininger, A complementary emissions test for light-duty vehicles: Assessing the technical feasibility of candidate procedures, 2013. doi:10.2790/65654.

[7] ISO, Standard Atmosphere, ISO 2533:1975, Int. Stand. Organ. 2533 (1975).

[8] ESDU International PLC, Equations for calculation of International Standard Atmosphere and associated off-standard atmospheres, 1986.

[9] National Geophysical Data Center, U.S. standard atmosphere (1976), Planet. Space Sci. 40 (1992) 553–554. doi:10.1016/0032-0633(92)90203-Z.

[10] V. Betageri, R. Mahesh, Effects of the Real Driving Conditions on the

NOx Emission of a Medium Duty Diesel Commercial Vehicle, SAE Tech. Pap. (2017) 1–6. doi:10.4271/2017-26-0124.

[11] X. Wang, Y. Ge, L. Yu, X. Feng, Effects of altitude on the thermal efficiency of a heavy-duty diesel engine, Energy. 59 (2013) 543–548. doi:10.1016/j.energy.2013.06.050.

[12] Á. Ramos Diezma, Emisiones contaminantes diésel en condiciones transitorias de motores y vehículos empleando combustibles alternativos, Universidad de Castilla-La Mancha, 2016.

[13] A. Ashtari, E. Bibeau, S. Shahidinejad, Using Large Driving Record Samples and a Stochastic Approach for Real-World Driving Cycle Construction: Winnipeg Driving Cycle, Transp. Sci. 48 (2014) 170–183. doi:10.1287/trsc.1120.0447.

[14] J.H. Roberts, W.R. Beyerly, M.W. Mason, J.R. Glazier, R.H. Wiley, PW4084 engine testing in altitude & sea level test facilities, (1994). doi:10.4271/942140.

[15] Y. Jun, I. Yang, C. Kim, S. Yang, D. Lee, Uncertainty Analysis and Improvement of an Altitude Test Facility for Small Jet Engines, KSAS Int. J. 5 (2004) 46–56.

[16] R.E. Smith, J. Ferrell, High-Altitude Tests of Rocket Engines in Ground Test Facilities, in: SAE Tech. Pap. 640811, 1964. doi:10.4271/640811.

[17] B. Bendz, M. Rostrup, K. Sevre, T.O. Andersen, P.M. Sandset, Association between acute hypobaric hypoxia and activation of coagulation in human beings., Lancet. 356 (2000) 1657–8. doi:10.1016/S0140-6736(00)03165-2.

[18] J.J. Cottrell, Altitude exposures during aircraft flight. Flying higher, Chest. 93 (1988) 81–84. doi:10.1378/chest.93.1.81.

[19] G. Osculati, M. Revera, G. Branzi, A. Faini, G. Malfatto, G. Bilo, A. Giuliano, F. Gregorini, F. Ciambellotti, C. Lombardi, P. Agostoni, G. Mancia, G. Parati, Effects of hypobaric hypoxia exposure at high altitude on left ventricular twist in healthy subjects: Data from HIGHCARE study on Mount Everest, Eur. Heart J. Cardiovasc. Imaging. 17 (2016) 635–643. doi:10.1093/ehjci/jev166.

[20] C.J. Bartholomew, W. Jensen, T. V Petros, F.R. Ferraro, K.M. Fire, D. Biberdorf, E. Fraley, J. Schalk, D. Blumkin, D. The, M. Levels, The Effect of Moderate Levels of Simulated Altitude on Sustained Cognitive Performance, Int. J. Aviat. Psychol. 9 (1999) 351–359. doi:10.1207/s15327108ijap0904.

[21] D.G. Gardner, V.A. Zaccardi, P.A. Jalbert, M. Denise Bryant, Reducing

the Cost of Aircraft Engine Emission Measurements, Proc. Int. Instrum. Symp. 49 (2003) 57–66.

[22] D. Testa, Apparatus and method for altimetric conditioning of internal-combustion engines, 2011. https://google.com/patents/EP2295950B1?cl=ja.

[23] J. Simperl, H. Erlach, Method for supplying an internal combustion engine with conditioned combustion gas, device for carrying out said method, method for determining the quantities of pollutants in the exhaust gases of an internal combustion engine, and device for carrying out, 2003. https://www.google.com/patents/WO2002042730A3?cl=en.

[24] N.G. Barton, The Expansion-Cycle Evaporation Turbine, J. Eng. Gas Turbines Power. 134 (2012) 51702–51707. http://dx.doi.org/10.1115/1.4004743.

[25] D.M. Human, T.L. Ullman, T.M. Baines, Simulation of High Altitude Effects on Heavy-Duty Diesel Emissions, SAE Tech. Pap. 900883. (1990). doi:10.4271/900883.

[26] C. He, Y. Ge, C. Ma, J. Tan, Z. Liu, C. Wang, L. Yu, Y. Ding, Emission characteristics of a heavy-duty diesel engine at simulated high altitudes, Sci. Total Environ. 409 (2011) 3138–3143. doi:10.1016/j.scitotenv.2011.01.029.

[27] C. Sistem, Engine Altitude Conditions Simulator, (n.d.). https://www.controlsistem.it/standard-products/eacs.html.

[28] AVL, Intake Air Conditioning Consys Air, (n.d.). https://www.avl.com/-/intake-air-conditioning.

[29] DieselNet. Emission Test Cycles - Worldwide Harmonized Light Vehicles Test Cycle (WLTC), (n.d.). https://www.dieselnet.com/standards/cycles/wltp.php.

[30] M. Tutuianu, A. Marotta, H. Steven, E. Ericsson, T. Haniu, N. Ichikawa, H. Ishii, Development of a World-wide Worldwide harmonized Light duty driving Test Cycle, Tech. Rep. 3 (2014) 7–10. doi:10.3141/2503-12.

[31] DieselNet. EU: Cars and Light Trucks Emissions Standards, (n.d.).

[32] G. Fontaras, P. Dilara, The evolution of European passenger car characteristics 2000-2010 and its effects on real-world CO 2 emissions and CO 2 reduction policy, Energy Policy. 49 (2012) 719–730. doi:10.1016/j.enpol.2012.07.021.

[33] T. Li, X. Chen, Z. Yan, Comparison of fine particles emissions of light-duty gasoline vehicles from chassis dynamometer tests and on-road

measurements, Atmos. Environ. 68 (2013) 82–91. doi:10.1016/j.atmosenv.2012.11.031.

[34] B. Daham, H. Li, G.E. Andrews, K. Ropkins, J.E. Tate, M.C. Bell, Comparison of Real World Emissions in Urban Driving for Euro 1-4 Vehicles Using a PEMS, Mater. Eng. (2009). doi:10.4271/2009-01-0941.

[35] L. Pelkmans, P. Debal, Comparison of on-road emissions with emissions measured on chassis dynamometer test cycles, Transp. Res. Part D Transp. Environ. 11 (2006) 233–241. doi:10.1016/j.trd.2006.04.001.

[36] M. Weiss, P. Bonnel, J. Kühlwein, A. Provenza, U. Lambrecht, S. Alessandrini, M. Carriero, R. Colombo, F. Forni, G. Lanappe, P. Le Lijour, U. Manfredi, F. Montigny, M. Sculati, Will Euro 6 reduce the NOxemissions of new diesel cars? - Insights from on-road tests with Portable Emissions Measurement Systems (PEMS), Atmos. Environ. 62 (2012) 657–665. doi:10.1016/j.atmosenv.2012.08.056.

[37] G. Fontaras, V. Franco, P. Dilara, G. Martini, U. Manfredi, Development and review of Euro 5 passenger car emission factors based on experimental results over various driving cycles, Sci. Total Environ. 468–469 (2014) 1034–1042. doi:10.1016/j.scitotenv.2013.09.043.

[38] Car emission testing facts - What is the Real Driving Emission (RDE) test?, (n.d.). http://www.caremissionstestingfacts.eu/rde-real-driving-emissions-test/#.

[39] Commission Regulations (EU) 2016/646, Euratom. (n.d.). doi:http://eur-lex.europa.eu/pri/en/oj/dat/2003/l_285/l_28520031101en00330037.pdf.

[40] D. Campos Navarro, Estudio de las emisiones de escape en motores de combustión interna alternativos utilizando diferentes sistemas de control de contaminantes, (2016). doi:10.4995/Thesis/10251/64066.

[41] J. Warnatz, U. Maas, R.W. Dibble, Combustion: Physical and chemical fundamentals, modeling and simulation, experiments, pollutant formation, 2006. doi:10.1007/978-3-540-45363-5.

[42] P. Dimitriou, R. Burke, Q. Zhang, C. Copeland, H. Stoffels, Electric Turbocharging for Energy Regeneration and Increased Efficiency at Real Driving Conditions, Appl. Sci. 7 (2017) 25. doi:10.3390/app7040350.

[43] S. Liu, L. Shen, Y. Bi, J. Lei, Effects of altitude and fuel oxygen content on the performance of a high pressure common rail diesel engine, Fuel. 118 (2014) 243–249. doi:10.1016/j.fuel.2013.10.007.

[44] B. Hu, J.W.G. Turner, S. Akehurst, C. Brace, C. Copeland, Observations on and potential trends for mechanically supercharging a downsized passenger car engine:a review, Proc. Inst. Mech. Eng. Part D J.

Automob. Eng. 231 (2017) 435–456. doi:10.1177/0954407016636971.

[45] A.M. Williams, A.T. Baker, C.P. Garner, R. Vijayakumar, Turbo-discharging turbocharged internal combustion engines, Proc. Inst. Mech. Eng. Part D J. Automob. Eng. 227 (2013) 52–65. doi:10.1177/0954407012455986.

[46] P. Leduc, B. Dubar, A. Ranini, G. Monnier, Downsizing of Gasoline Engine: an Efficient Way to Reduce CO2 Emissions, Oil Gas Sci. Technol. 58 (2003) 115–127. doi:10.2516/ogst:2003008.

[47] K. Nakata, S. Utsumi, A. Ota, K. Kawatake, T. Kawai, T. Tsunooka, The Effect of Ethanol Fuel on a Spark Ignition Engine, (2006). doi:10.4271/2006-01-3380.

[48] O.S. Azmir, A.J. Alimin, M.Y. Ismail, K.W. Hui, Performance and Emission Characteristics of Direct Injection C.I Engine Retrofitted with Mono-CNG System, Appl. Mech. Mater. 446–447 (2013) 443–447. doi:10.4028/www.scientific.net/AMM.446-447.443.

[49] P. Lu, C. Brace, B. Hu, C. Copeland, Analysis and comparison of the performance of an inverted brayton cycle and turbo-compounding with decoupled turbine and cvt driven compressor for small automotive engines, in: Proc. ASME Turbo Expo, 2016. doi:10.1115/GT2016-57675.

[50] S. Sawant, D. Prajapati, U.G. Student, N. Mumbai, A review on zero emissions vehicles, 8 (2017) 198–202.

[51] G. Wang, J.M. Ogden, D. Sperling, Comparing air quality impacts of hydrogen and gasoline, Transp. Res. Part D Transp. Environ. 13 (2008) 436–448. doi:10.1016/j.trd.2008.09.006.

[52] J.P. Meyers, Getting back into gear: fuel cell development after the hype, Electrochem. Soc. Interface. 17 (2008) 36–39.

[53] G. Wang, The role of hydrogen cars in the economy of California, Int. J. Hydrogen Energy. 36 (2011) 1766–1774. doi:10.1016/j.ijhydene.2010.10.083.

[54] B. van Wee, K. Maat, C. de Bont, Improving Sustainability in Urban Areas: Discussing the Potential for Transforming Conventional Car-based Travel into Electric Mobility, Eur. Plan. Stud. 20 (2012) 95–110. doi:10.1080/09654313.2011.638497.

[55] A. Tirez, P. Luickx, X. He, V. Rious, Possible impact of electric cars on electricity spot prices, in: Int. Conf. Eur. Energy Mark., 2010: pp. 1–6. doi:10.1109/EEM.2010.5558730.

[56] O.P.R. van Vliet, T. Kruithof, W.C. Turkenburg, A.P.C. Faaij, Techno-

economic comparison of series hybrid, plug-in hybrid, fuel cell and regular cars, J. Power Sources. 195 (2010) 6570–6585. doi:10.1016/j.jpowsour.2010.04.077.

[57] C.T. Bowman, Kinetics of pollutant formation and destruction in combustion, Prog. Energy Combust. Sci. 1 (1975) 33–45. doi:10.1016/0360-1285(75)90005-2.

[58] R.J. Levy, Carbon monoxide pollution and neurodevelopment: A public health concern, Neurotoxicol. Teratol. 49 (2015) 31–40. doi:10.1016/j.ntt.2015.03.001.

[59] J. a Raub, Health effects of exposure to ambient carbon monoxide, Chemosph. Glob. Charg. Sci. 1. 1 (1999) 331–351. doi:10.1016/S1465-9972(99)00005-7.

[60] M. Hosoya, M. Shimoda, The application of diesel oxidation catalysts to heavy duty diesel engines in Japan, Appl. Catal. B Environ. 10 (1996) 83–97. doi:10.1016/0926-3373(96)00025-2.

[61] Formation and control of nitrogen oxides, Catal. Today. 2 (1988) 369–379. doi:10.1016/0920-5861(88)80002-6.

[62] V. Vestreng, L. Ntziachristos, A. Semb, S. Reis, I.S.A. Isaksen, L. Tarrason, Evolution of NOx emissions in Europe with focus on road transport control measures, Atmos. Chem. Phys. 9 (2009) 1503–1520. doi:10.5194/acp-9-1503-2009.

[63] European Environment Agency, Air pollution at street level in European cities, 2006.

[64] P.E. Morrow, Toxicological data on nox: An overview, J. Toxicol. Environ. Health. 13 (1984) 205–227. doi:10.1080/15287398409530494.

[65] D. Norse, Non-point pollution from crop production: Global, regional and national issues, Pedosphere. 15 (2005) 499–508.

[66] M. Zheng, G.T. Reader, J.G. Hawley, Diesel engine exhaust gas recirculation - A review on advanced and novel concepts, Energy Convers. Manag. 45 (2004) 883–900. doi:10.1016/S0196-8904(03)00194-8.

[67] J. Theis, E. Gulari, A LNT+ SCR system for treating the NOx emissions from a diesel engine, SAE Tech. Pap. (2006). doi:10.4271/2006-01-0210.

[68] W.S. Epling, L.E. Campbell, A. Yezerets, N.W. Currier, J.E. Parks, Overview of the Fundamental Reactions and Degradation Mechanisms of NOx Storage/Reduction Catalysts, Catal. Rev. 46 (2004) 163–245. doi:10.1081/CR-200031932.

[69] G. Busca, L. Lietti, G. Ramis, F. Berti, Chemical and mechanistic aspects of the selective catalytic reduction of NO x by ammonia over oxide catalysts ：A review, Appl. Catal. B Environ. 18 (1998) 1–36. doi:10.1016/S0926-3373(98)00040-X.

[70] U.G. Alkemade, B. Schumann, Engines and exhaust after treatment systems for future automotive applications, 177 (2006) 2291–2296. doi:10.1016/j.ssi.2006.05.051.

[71] N.S. Ayoub, R.D. Reitz, Multidimensional modeling of fuel composition effects on combustion and cold-starting in diesel engines, SAE Tech. Pap. (1995). doi:10.4271/952425.

[72] J. Serras-Pereira, P.G. Aleiferis, D. Richardson, Imaging and heat flux measurements of wall impinging sprays of hydrocarbons and alcohols in a direct-injection spark-ignition engine, Fuel. 91 (2012) 264–297. doi:10.1016/j.fuel.2011.07.037.

[73] H. Sandquist, R. Lindgren, I. Denbratt, Sources of Hydrocarbon Emissions from a Direct Injection Stratified Charge Spark Ignition Engine, in: SAE Tech. Pap., 2000. doi:10.4271/2000-01-1906.

[74] P. Boffetta, N. Jourenkova, P. Gustavsson, Cancer risk from occupational and environmental exposure to polycyclic aromatic hydrocarbons., Cancer Causes Control. 8 (1997) 444–72. doi:10.1023/A:1018465507029.

[75] R. Snyder, Leukemia and benzene., Int. J. Environ. Res. Public Health. 9 (2012) 2875–2893. doi:10.1016/S1526-0046(03)00020-7.

[76] J. Appel, H. Bockhorn, M. Frenklach, Kinetic modeling of soot formation with detailed chemistry and physics: Laminar premixed flames of C2 hydrocarbons, Combust. Flame. 121 (2000) 122–136. doi:10.1016/S0010-2180(99)00135-2.

[77] S.J. Harris, M.M. Maricq, Signature size distributions for diesel and gasoline engine exhaust particulate matter, J. Aerosol Sci. 32 (2001) 749–764. doi:10.1016/S0021-8502(00)00111-7.

[78] D.W. Dockery, C.A. Pope, Acute Respiratory Effects of Particulate Air Pollution, Annu. Rev. Public Health. 15 (1994) 107–132. doi:10.1146/annurev.pu.15.050194.000543.

[79] M.R. Heal, P. Kumar, R.M. Harrison, Particles, air quality, policy and health, Chem. Soc. Rev. 41 (2012) 6606. doi:10.1039/c2cs35076a.

[80] S. Weichenthal, Selected physiological effects of ultrafine particles in acute cardiovascular morbidity, Environ. Res. 115 (2012) 26–36. doi:10.1016/j.envres.2012.03.001.

[81] M. Matti Maricq, Chemical characterization of particulate emissions from diesel engines: A review, J. Aerosol Sci. 38 (2007) 1079–1118. doi:10.1016/j.jaerosci.2007.08.001.

[82] C. Lin, B. Hillman, A. Williams, Performance of Slotted Metallic Membranes as Particulate Filters, (2018). doi:10.4271/2014-01-2807.Copyright.

[83] L. Shen, Y. Shen, Combustion Process of Diesel Engines At Regions With Different Altitude, SAE Tech. Pap. 950857. (1995). doi:10.4271/950857.

[84] A. Bell, Modern SI Engine Control Parameter Responses and Altitude Effects with Fuels of Varying Octane Sensitivity, SAE Tech. Pap. (2010) 25. doi:10.4271/2010-01-1454.

[85] R. Liu, Z. Zhang, S. Dong, G. Zhou, High-Altitude Matching Characteristic of Regulated Two-Stage Turbocharger With Diesel Engine, J. Eng. Gas Turbines Power. 139 (2017) 94501. doi:10.1115/1.4036283.

[86] P. Benjumea, J. Agudelo, A. Agudelo, Effect of altitude and palm oil biodiesel fuelling on the performance and combustion characteristics of a HSDI diesel engine, Fuel. 88 (2009) 725–731. doi:10.1016/j.fuel.2008.10.011.

[87] X. Wang, Y. Ge, L. Yu, X. Feng, Comparison of combustion characteristics and brake thermal efficiency of a heavy-duty diesel engine fueled with diesel and biodiesel at high altitude, Fuel. 107 (2013) 852–858. doi:10.1016/j.fuel.2013.01.060.

[88] X. Wang, Y. Ge, L. Yu, X. Feng, Effects of altitude on the thermal efficiency of a heavy-duty diesel engine, Energy. 59 (2013) 543–548. doi:10.1016/j.energy.2013.06.050.

[89] M. Yang, Y. Gu, K. Deng, Z. Yang, Y. Zhang, Analysis on altitude adaptability of turbocharging systems for a heavy-duty diesel engine, Appl. Therm. Eng. 128 (2018) 1196–1207. doi:10.1016/j.applthermaleng.2017.09.065.

[90] M. Lapuerta, O. Armas, J.R. Agudelo, C.A. Sánchez, Estudio del Efecto de la Altitud sobre el Comportamiento de Motores de Combustión Interna. Parte 1: Funcionamiento, Inf. Tecnológica. 17 (2006) 21–30. doi:10.4067/S0718-07642006000500005.

[91] J.R. Sodré, S.M.C. Soares, Comparison of engine power correction factors for varying atmospheric conditions, J. Brazilian Soc. Mech. Sci. Eng. 25 (2003) 279–284. doi:10.1590/S1678-58782003000300010.

[92] S.M.C. Soares, J.R. Sodré, Effects of atmospheric temperature and pressure on the performance of a vehicle, Part D J Automob. Eng. 216 (2002) 473–477. doi:10.1243/09544070260137499.

[93] G. Zhou, R. Liu, S. Dong, G. Liu, Z. Zheng, S. Hao, Experimental study on plateau matching performance of turbocharger and vehicle diesel engine, Proc. - 2010 Int. Conf. Digit. Manuf. Autom. ICDMA 2010. 1 (2010) 710–713. doi:10.1109/ICDMA.2010.305.

[94] H. Zhang, W. Zhuge, Y. Zhang, Study of the Control Strategy of the Plateau Self-adapted Turbocharging System for Diesel Engine, (2008). doi:10.4271/2008-01-1636.

[95] M. Szedlmayer, C.M. Kweon, Effect of Altitude Conditions on Combustion and Performance of a Multi-Cylinder Turbocharged Direct-Injection Diesel Engine, SAE Tech. Pap. 2016-01-0742. (2016) 4271. doi:10.4271/2016-01-0742.

[96] M. Yang, Y. Gu, K. Deng, Z. Yang, S. Liu, Influence of altitude on two-stage turbocharging system in a heavy-duty diesel engine based on analysis of available flow energy, Appl. Therm. Eng. 129 (2018) 12–21. doi:10.1016/j.applthermaleng.2017.09.138.

[97] Á. Ramos, R. García-Contreras, O. Armas, Performance, combustion timing and emissions from a light duty vehicle at different altitudes fueled with animal fat biodiesel, GTL and diesel fuels, Appl. Energy. 182 (2016) 507–517. doi:10.1016/j.apenergy.2016.08.159.

[98] Z.X. Zhu, F.J. Zhang, C.J. Li, K. Han, Calibration for Fuel Injection Parameters of the Diesel Engine Working at Plateau via Simulating, Adv. Mech. Eng. 2014 (2014). doi:10.1155/2014/621946.

[99] C.A. Chaffin, T.L. Ullman, Effects of Increased Altitude on Heavy-Duty Diesel Engine Emissions, (1994).

[100] G.H. Abd-Alla, Using exhaust gas recirculation in internal combustion engines: a review, Energy Convers. Manag. 43 (2002) 1027–1042. doi:10.1016/S0196-8904(01)00091-7.

[101] M. Yang, Y. Gu, K. Deng, Z. Yang, Y. Zhang, Analysis on altitude adaptability of turbocharging systems for a heavy-duty diesel engine, Appl. Therm. Eng. 128 (2018) 1196–1207. doi:10.1016/j.applthermaleng.2017.09.065.

[102] G.A. Bishop, J.A. Morris, D.H. Stedman, L.H. Cohen, R.J. Countess, S.J. Countess, P. Maly, S. Scherer, The effects of altitude on heavy-duty diesel truck on-road emissions, Environ. Sci. Technol. 35 (2001) 1574–1578. doi:10.1021/es001533a.

[103] X. Wang, H. Yin, Y. Ge, L. Yu, Z. Xu, C. Yu, X. Shi, H. Liu, On-vehicle emission measurement of a light-duty diesel van at various speeds at high altitude, Atmos. Environ. 81 (2013) 263–269. doi:10.1016/j.atmosenv.2013.09.015.

[104] X. Wang, Y. Ge, L. Yu, Combustion and Emission Characteristics of a Heavy-Duty Diesel Engine at Idle at Various Altitudes, SAE Int. J. Engines. 6 (2013) 2013-01–1516. doi:10.4271/2013-01-1516.

[105] D.B. Olsen, B.D. Willson, The Impact of Cylinder Pressure on Fuel Jet Penetration and Mixing, (2017) 1–7. doi:10.1115/ICEF2002-502.

[106] T. Lucchini, G. D'Errico, A. Onorati, G. Bonandrini, L. Venturoli, R. Di Gioia, Development of a CFD Approach to Model Fuel-Air Mixing in Gasoline Direct-Injection Engines, (2012). doi:10.4271/2012-01-0146.

[107] J.W. Dennis, Turbocharged Diesel Engine Performance at Altitude, in: Natl. Truck. Powerplant, Fuels Lubr. Meet., SAE International, 1971. doi:10.4271/710822.

[108] Z.F. Tan, L.Z. Shen, D.C. Jin, Y.W. Bin Ou, A Research on the Performance of a Common Rail Diesel Engine Fueled with Different Blending Ratio of Biodiesels, Adv. Mater. Res. 860–863 (2013) 555–559. doi:10.4028/www.scientific.net/AMR.860-863.555.

[109] M. Ghazikhani, M. Ebrahim Feyz, O. Mahian, A. Sabazadeh, Effects of altitude on the soot emission and fuel consumption of a light-duty diesel engine, Transport. 28 (2013) 130–139. doi:10.3846/16484142.2013.798743.

[110] M. Lapuerta, O. Armas, J.R. Agudelo, A.F. Agudelo, Estudio del efecto de la altitud sobre el comportamiento de motores de combustión interna. Parte 2: Motores diesel, Inf. Tecnol. 17 (2006).

[111] L. Yu, Y. Ge, J. Tan, C. He, X. Wang, H. Liu, W. Zhao, J. Guo, G. Fu, X. Feng, X. Wang, Experimental investigation of the impact of biodiesel on the combustion and emission characteristics of a heavy duty diesel engine at various altitudes, Fuel. 115 (2014) 220–226. doi:10.1016/j.fuel.2013.06.056.

[112] B. Guan, R. Zhan, H. Lin, Z. Huang, Review of the state-of-the-art of exhaust particulate filter technology in internal combustion engines, J. Environ. Manage. 154 (2015) 225–258. doi:10.1016/j.jenvman.2015.02.027.

[113] J. Agudelo, A. Agudelo, J. Pérez, Análisis energético y exergético de un motor diesel de automoción operando en diferentes altitudes, Rev. Fac. Ing. (2009) 45–54.

CHAPTER 3

Altitude simulator development

Contents

Figures

Tables

3.1 Introduction

One of the main objectives of this doctoral thesis is the development of an altitude simulator. This system will offer an alternative to the actual technologies available to perform altitude tests, which are real altitude tests and hypobaric chambers.

The initial idea came from the CMT-Motores Térmicos, which patented a concept of an altitude simulator whose main novelty with respect to other systems was the use of a VGT in the expansion of the atmospheric air. A VGT allows cooling air as a function of altitude in a similar way as ISA and in some cases using the energy of this expansion to help in the vacuum objective of the altitude simulator [1].

In this chapter, it is explained in detail the operation principle of the altitude simulator and its different elements. Then, the performance maps of the altitude simulator are shown and analyzed, focusing on its altitude, mass flow and temperature range. In parallel, a computational 1-dimensional model is developed in order to deeper understand the operation principle of the altitude simulator and to improve the design of the different elements. With the information of the model and the experimental tests, the layout of the altitude simulator is redesign, introducing new elements and changing the design of others in order to improve the operation range of the altitude simulator.

These changes in the design of the altitude simulator lead to two new patents [2,3], that introduced the new changes in the layout of the altitude simulator.

3.2 Operation principle

The altitude simulator conditions pressure and temperature of the air sucked by an internal combustion engine, depending on the operating height above sea level. Only the engine intake and exhaust are at that created low pressure and temperature atmosphere, while the rest of the test bench is at room pressure and temperature.

The operation principle of the altitude simulator is based on the use of radial turbomachines to create the desired atmosphere at the engine intake. Despite the fact that the design has been evolved and has become more sophisticated, the core of the system is the same.

Figure 3.1 shows the scheme of the altitude simulator. It sucks the air from the room atmosphere and decreases its pressure and temperature, creating

a low pressure atmosphere. The engine intake and exhaust are connected to this low pressure atmosphere, while the rest of the test cell is at room pressure.

Going now deeper into detail, the altitude simulator layout is represented in Figure 3.2.

The installation can be divided into two parts: the inlet line, which covers from altitude simulator inlet to the engine intake connection; and the exhaust line, which is defined from the engine exhaust connection to the installation outlet. Both lines are connected by the dilution pipe where the low pressure and low temperature atmosphere is generated.

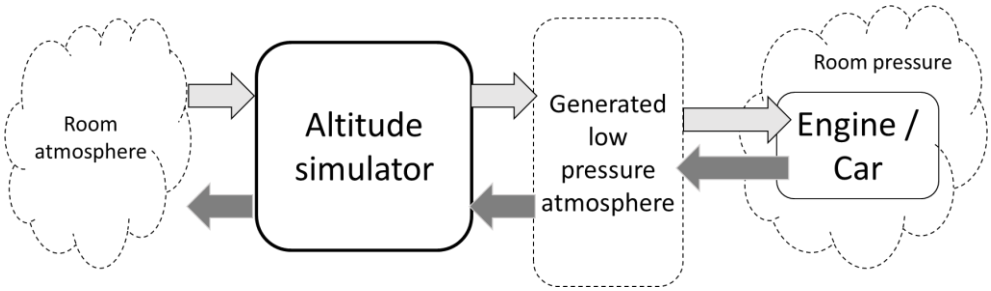

Figure 3.1 – Altitude simulator operation principle

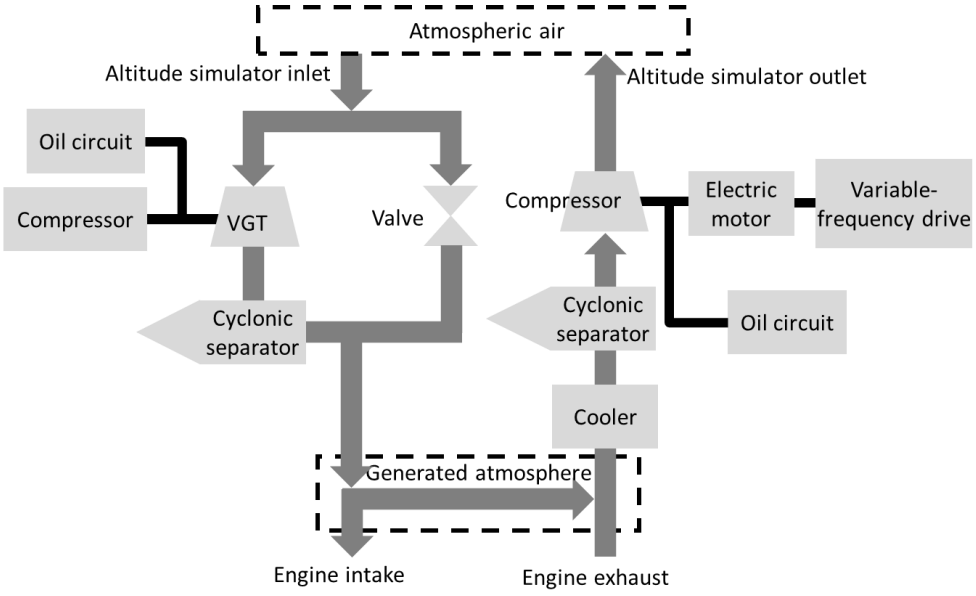

Figure 3.2 – Sketch of the altitude simulator layout

The room air passes through the VGT where it is expanded and cooled down from room conditions to the pressure of the altitude that is being simulated. The VGT power is dissipated in an independent compressor. Downstream of the VGT, a cyclonic separator is installed to separate the possible water or ice generated because of below dew point or below frozen point temperatures respectively.

Alternatively, a Valve can be managed in parallel with the VGT, allowing the air to be expanded at a constant temperature, in contrast to the VGT air flow, which is cooled down. When both flows, the one from the VGT and the other from the Valve are mixed, an intermediate temperature is obtained at engine intake. This valve is similar to the waste-gate valves mechanism in the engine turbines. For that reason, this control valve will also be called WG valve in the rest of the document.

Then, the air is aspirated by the engine intake and the excess air is by-passed through the dilution pipe from engine intake connection to engine exhaust connection; and following to the tailpipe of the installation, it is further diluted with exhaust gas from the engine. This dilution pipe ensures engine operation with equal intake and exhaust pressure. This mix of exhaust air and dilution air passes through a cooler to ensure the safe operation of the mechanical compressor because can be at high temperature. It additionally reduces the compressor power consumption.

To avoid the effects of condensates formed when the exhaust gases are cooled down [4,5], what may damage compressor blades [6], another cyclonic separator is installed just upstream of the mechanical compressor. The risk of condensates and its generation rate is depending mainly on the equivalence ratio, dilution ratio, and the cooler outlet temperature. The mechanical compressor speed is controlled by means of the electric motor speed with a variable-frequency drive.

Finally, the diluted exhaust gases are discharged to the atmosphere.

The layout represented in Figure 3.2 is the one used as a first approach to study the altitude simulator viability and does not include the overpressure operation mode, i.e. cannot generate higher pressure than room pressure. However, the prototype built following Figure 3.2 scheme can be manually modified to operate in overpressure mode. This solution was taken into account because made the design of the prototype much simpler and cheaper, which is a key point in the first steps of the project.

The overpressure mode layout is represented in Figure 3.3. The atmospheric air is forced to pass through the mechanical compressor where

its pressure is increased. Then, this air is directly aspired by the engine intake and the excess air is bypassed and mixed with the exhaust gases. As in vacuum mode, the dilution pipe ensures that the engine intake and exhaust operate at the same high pressure.

Then, the exhaust gases are cooled down in the cooler and the droplets generated are removed from the gas in the cyclonic separator. Then, the air is expanded again up to room pressure in the control valve. In this case, the VGT fully closed because it is not needed as the gas temperature at the altitude simulator outlet does not need to be controlled.

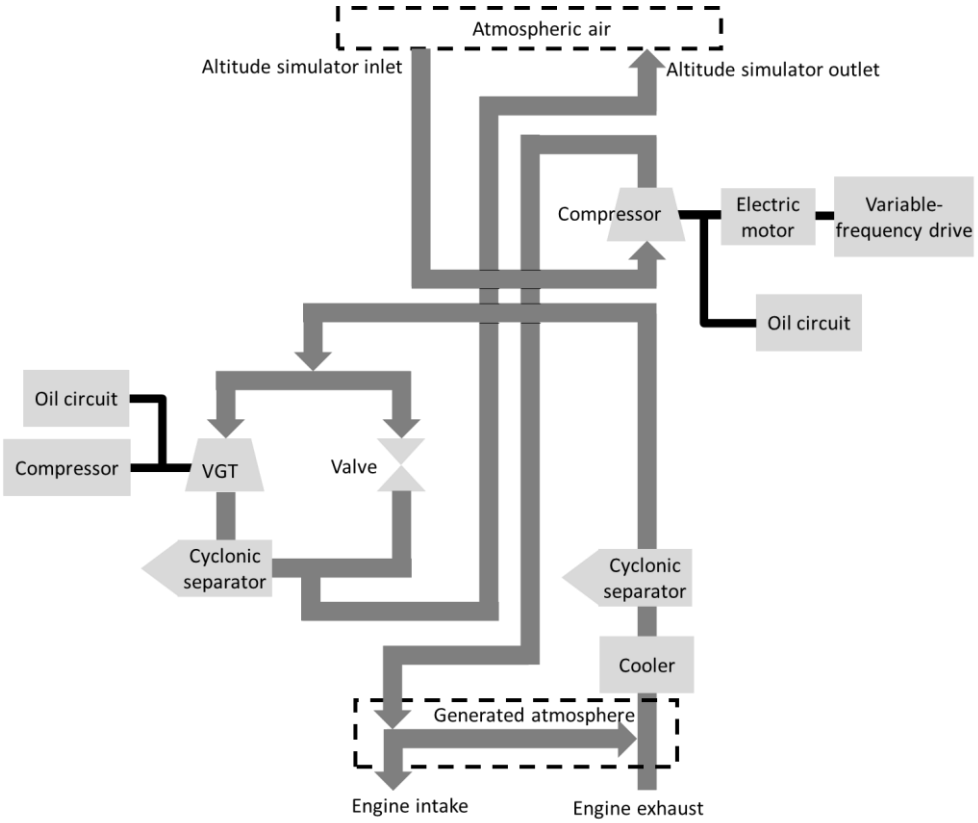

Figure 3.3 – Sketch of the altitude simulator layout when manually changed to operate in overpressure mode

Comparing Figure 3.2 and Figure 3.3, it can be observed that only two pipes have to the exchanged to change from vacuum to overpressure operation mode.

3.3 Altitude simulator prototype

Once the initial layout has been described and discussed, the altitude simulator prototype was built. This prototype main purpose was to study the performance of the altitude installation and its potential to be used in altitude engine testing. Figure 3.4 shows the altitude simulator first prototype.

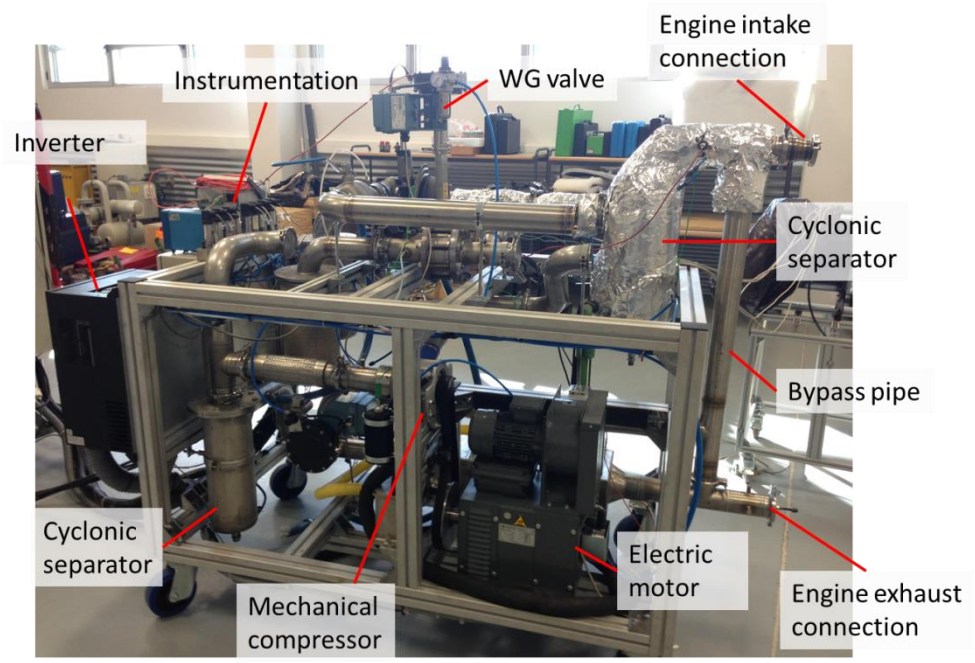

Figure 3.4 – Altitude simulator first prototype

3.3.1. Main elements

The altitude simulator is composed of different elements to reach its objective. The elements described in Section 3.2 that compound the altitude simulator have to be chosen from the real world in order to build the prototype. In the following paragraphs are described these main elements

Control valve (WG)

The WG control valve is an electro pneumatic control valve specially designed for fine pressure control with a very linear operation. Physically, it has one fixed gate with racks and other mobile gate with the

complementary racks. When the mobile gates are in the closed position, its racks are blocked by the fixed gate and the racks of the fixed gate are block by the mobile gate. However, when the valve is open, their racks are in the same position, leaving the air passing through.

The model is GS8021 from Schubert and Salzer manufacturer (shown in Figure 3.5) and its diameter is DN80, which corresponds to a 73 mm internal diameter. This diameter was chosen to be similar to the VGT diameter while costs and size are kept small [7].

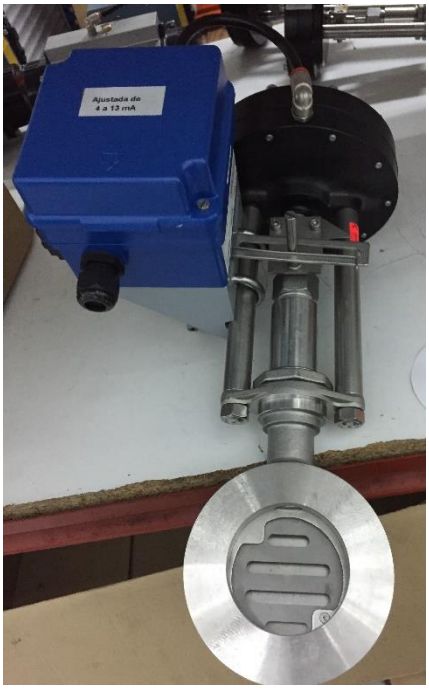

Figure 3.5 – WG picture in the altitude simulator

VGT

The VGT is a truck size, with variable nozzle opening, electronically moved by CAN bus communication. The size of the turbocharger has been selected as big as possible and as efficient as possible (biggest available VGT with high efficiency at low openings and with CAN control in the market), in order to be able to move the bigger amount of air as possible with the lowest pressure drop. The size is not as big as would be desirable but a balance between performance and turbomachinery size must be maintained. The amount of air that can pass through the VGT depending

on the position of the blades is given by its map (represented in Figure 3.6), that has been measured in the department in before the start of this doctoral thesis in previous projects.

The VGT model is Holset HY40V [8], and is shown in Figure 3.7 circled in green.

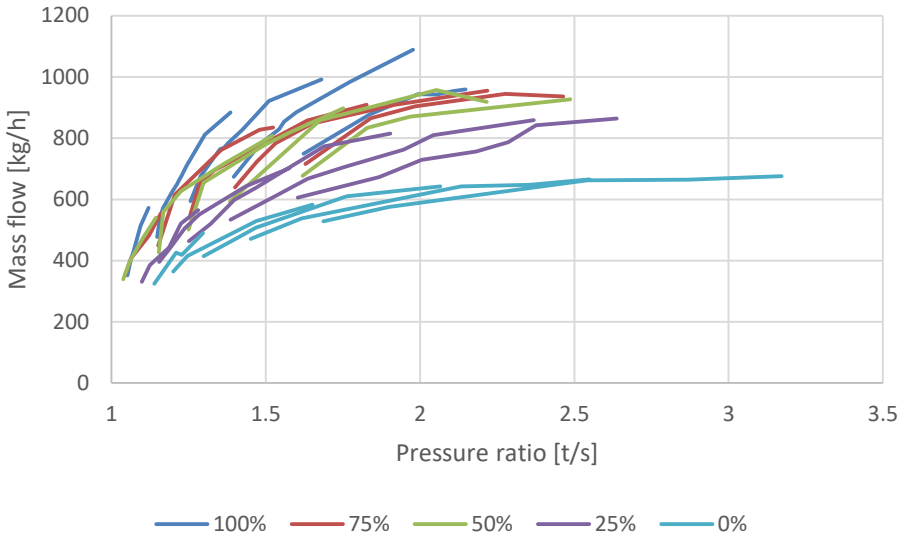

Figure 3.6 – VGT map

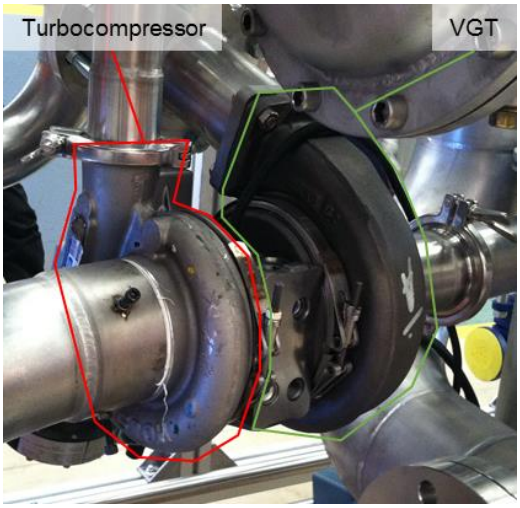

Figure 3.7 – VGT and turbocompressor picture in the altitude simulator

Turbocompressor

The turbocompressor is the other element that compounds the turbocharger. In the altitude simulator, the turbocompressor dissipates the energy extracted by the turbine from the room air. It just sucks room air which is returned to the room atmosphere through a calibrated orifice.

In this application, the turbocompressor is a secondary element, being its design subject to the VGT, as both elements are coupled and commercial available elements must be chosen for keeping contained the cost of the prototype and of the final product. The turbocompressor picture is shown in Figure 3.7 circled in red.

Cyclonic separator

The cyclonic separator is designed to remove the droplets generated in the air when it is cooled down. Figure 3.8 shows the design of a cyclonic separator.

Figure 3.8 – Frontal section of the cyclonic separator

This kind of separators has been studied in detail in the literature for other application [9–12] and its operation principle is as follow. The air goes into the cyclonic separator through the horizontal pipe which is tangent to the cylindrical container. Then, air flow follows an elliptical pattern inside the separator. As the water droplets have higher density than the air, they

strike outside the wall and fall to the bottom of the cyclone where they are accumulated in a small deposit to be later extracted. With respect to the clean air, it goes out from the cyclone through the pipe in the top cup of the cylinder.

Cooler

The cooler (shown in Figure 3.9) ensures a low temperature in the mechanical compressor, because too high temperature could damage it [13,14].

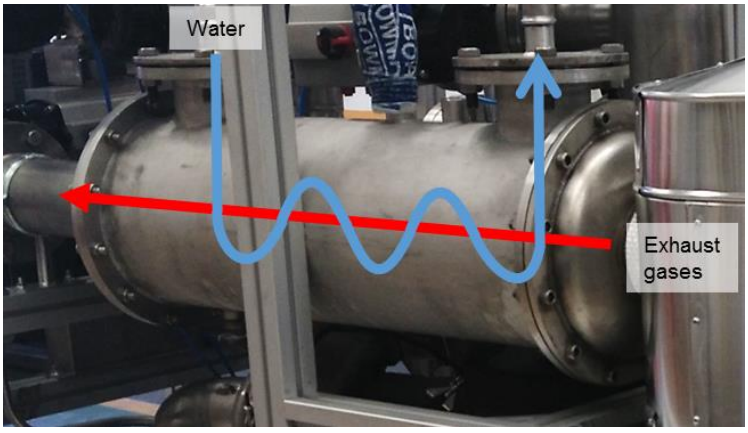

Figure 3.9 – Water-to-air cooler in the altitude simulator

The criterion to choose its size is based on the maximum cooling requirements, following Equation (3.11). For example: in a Diesel engine the most unfavorable scenario is when all the air is sucked by the engine and there is none dilution air and the engine is at maximum exhaust temperature point. In this case, the expected inlet temperature to the cooler is around 600 ºC. The outlet temperature has to ensure safe operation of the mechanical compressor. This temperature can be around 50 ºC, as lower temperature would generate too high amount of condensates in the cyclonic separator. If the maximum mass flow expected, according to the VGT operation map, would be around 1000 kg/h, the cooler power has to be higher than 171 kW.

$$Cooler\ power = \dot{m} c_p (T_{in} - T_{out}) \qquad (3.11)$$

Mechanical compressor

The mechanical compressor generates vacuum in the altitude installation by sucking the air and compressing it up to room pressure. It is moved by an electric motor which controls its rotor speed.

As done with the VGT sizing, the mechanical compressor has been chosen to be as big as possible among those available in the market, according to the high volumetric flow needed to be moved at vacuum conditions. The model is Rotrex C38-92 [15], shown in Figure 3.10.

Figure 3.10 – Mechanical compressor Rotrex C38-92

Figure 3.11 shows mechanical compressor map. It is corrected at 1.013 bar and 15 °C. The x-axis represents the corrected mass flow in kg/s (Equation (3.12)). In the y-axis is represented the pressure ratio (Equation (3.14)). If the mechanical compressor is at its maximum speed, the maximum corrected mass flow is 0.63 kg/s (2268 kg/h). However, as the altitude simulator generates vacuum at the compressor inlet, the inlet pressure will be lower than the corrected pressure of 1.013 bar, and therefore the real mass flow will be lower than 0.63 kg/s (Equation (3.12)), and it is dependent on the vacuum generated. For example, at 0.54 bar (which corresponds to an altitude of 5000 m), the maximum theoretical real mass flow is 0.34 kg/s (1200 kg/h). In Chapter 4, the link between the mechanical compressor and the altitude simulator performance will be explained in more detail.

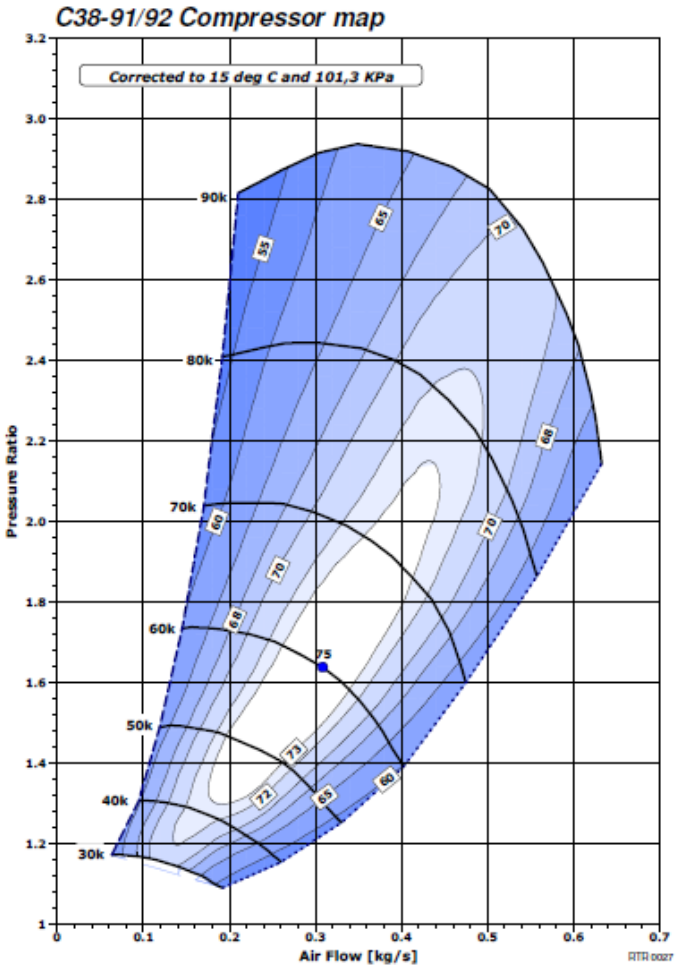

Figure 3.11 – Mechanical compressor map [16]

$$m = m^* \frac{\sqrt{T_{RI}/T_0}}{p_{RI}/p_0} \tag{3.12}$$

$$\Pi_C = \frac{p_{out}}{p_{in}} \tag{3.13}$$

Electric motor and variable-frequency drive

The electric motor is the element that moves the mechanical compressor. Therefore, its power, speed and gears are specially designed for this

application. The electric motor maximum power is about 45 kW with a maximum current of 100 A; and it is directly coupled to the mechanical compressor, as can be seen in Figure 3.12.

The configuration parameters and power are calibrated to operate in this application by the mechanical compressor manufacturer.

The Variable Frequency Drive is Parker AC30V, frame H, with an output maximum power of 75 kW [17] and is shown in Figure 3.13.

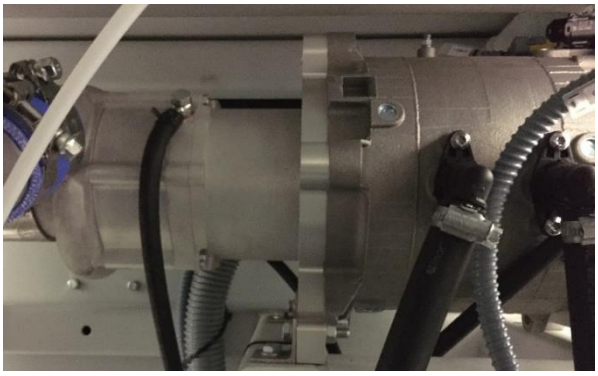

Figure 3.12 – Electric motor of the mechanical compressor

Figure 3.13 – Parker AC30V inverter in the altitude simulator

3.3.2. Auxiliary elements

The altitude simulator needs also auxiliary elements for a proper operation. These elements are not directly related with the altitude generation, but are also necessary for the operation of the different elements.

Air filter

In order to remove any particle or dust from the air that goes to the altitude simulator, it is required the use of air filters in the altitude simulator intake and in the turbocompressor inlet. This air filters protect the elements and the engine to be damaged.

Turbocharger oil circuit

The turbocharger needs an oil circuit for its proper operation. Figure 3.14 is de diagram of the oil circuit connections.

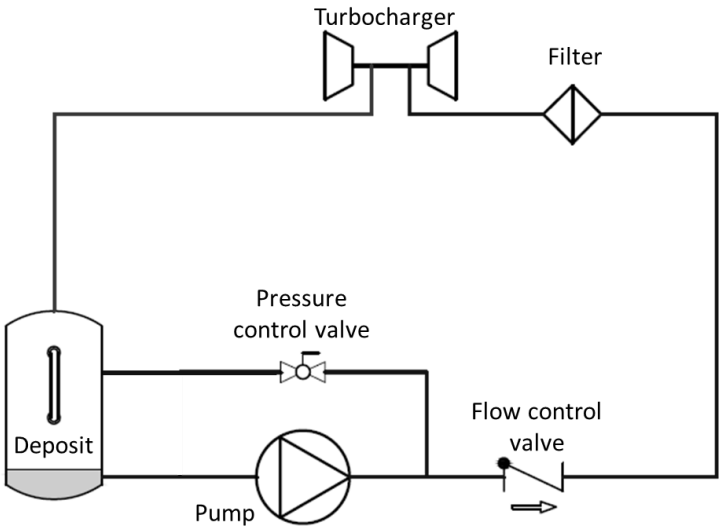

Figure 3.14 – Turbocharger oil circuit

This oil circuit consists in:

- Oil deposit, with a peephole to visually check the oil level.
- Oil pump, to move the oil through all the oil circuit.
- Flow control valve, to regulate the oil mass flow.

- Pressure control valve, to reduce the backpressure generated by the flow control valve and avoid breaking the oil pump.
- Oil filter, to remove from the oil any particle or dust.
- Turbocharger hose.

Mechanical compressor oil circuit

Similarly to the turbocharger oil circuit, the mechanical compressor also has its own oil circuit for its proper operation. In this case, Figure 3.15 represents the mechanical compressor oil circuit. In this case, a pressure control valve or flow control valve is not necessary, but it is needed a water-to-oil cooler.

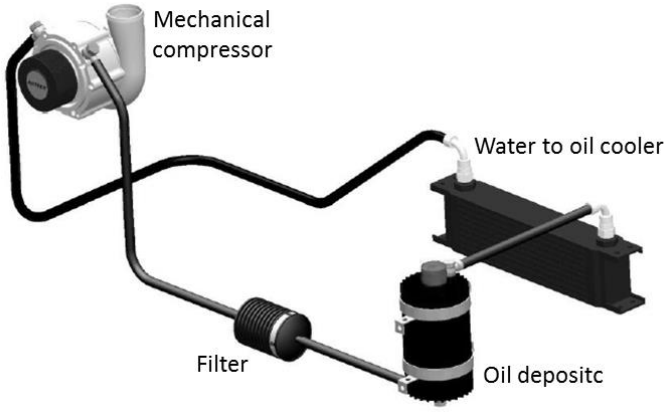

Figure 3.15 – Mechanical compressor oil circuit

Pressure sensors

There are a total number of five pressure sensors in the altitude simulator. The exactly position and function of them will be explained in detail in Chapter 4, Section 4.7.3.

The pressure sensors are WIKA S20, a piezoresistive sensor with a pressure range from 0 bar to 4.5 bar for four of them, and from 0 bar to 6 bar for one of them, and the analogue output signal ranges from 0 V to 10 V [18].

Temperature sensors

The temperature sensors are type K. There are a total number of nine type K temperature sensors in the altitude simulator. The exactly position and function of them will be explained in detail in Chapter 4, Section 4.7.3.

Acquisition modules

The signal from the sensors and actuators is managed by the acquisition modules. The modules are produced by Beckhoff [19]. The different modules are listed below.

- CX9020-0111: Is the CPU module.
- EL3318: Is the temperature module with 8 type K temperature sensors connectors.
- EL3008: Is an analogue input module that processes signals in the range between -10 and +10 V, used to read the measurement of the pressure sensors.
- EL4018: Is an analogue output module that generates analog output signals in the range between 0 and 20 mA, used to manage the different control valves.
- EL4004: Is an analogue output module that generates signals in the range between 0 and 10 V, used to manage the water cooler valve and the inverter.
- EL1259: Is a digital module with 8 input channels and 8 output channels, used to control the actuation valves and read the signal of the status of different elements in the altitude simulator (oil pump, inverter, power supply and water level in the cyclonic separators).
- CP2912-0000: Is the touch screen used to manage the altitude simulator.
- EL6751: Is a CANopen module, used to control the VGT blades position.

3.4 Operation maps

3.4.1. Vacuum operation range

The first step to assess the prototype flow test rig performance and analyze its capability to operate in vacuum mode covered a set of tests without coupling to any other system, i.e. by-passing all the flow from the intake to the exhaust of the installation.

In order to explore the mass flow and vacuum pressure range, its dependence and the available range for temperature control, a parametric study was carried out. The speed of the mechanical compressor was swept for five combinations of VGT and WG opening, whose values are shown in

Table 3.1. The tested mechanical compressor speeds and its corresponding electric power are shown in Table 3.2. Therefore, the total number of tested points is 50.

Table 3.1. WG and VGT opening in the parametric studies.

VGT opening [%]	WG opening [%]
20	0
50	0
100	0
100	50
100	100

Table 3.2. Mechanical compressor speed and its correspondent power in the tested points of the parametric study.

Mechanical compressor speed [rpm]	Electric power [kW]
9000	0.2
18000	0,5
27000	1.6
36000	3.0
41000	4,1
46000	5.2
55000	8.6
63000	12,3
71000	16.0
78000	22.0

Figure 3.16 shows the results for the described test. The x-axis on the top of the plot represents the pressure at the engine intake connection to the altitude simulator, just downstream the WG and VGT joint. On the other hand, the x-axis on the bottom represents its corresponding altitude according to ISA. As example, at 3000 m, the pressure is 0.70 bar. The y-axis represents the air mass flow for each operation point.

Figure 3.16 shows that for the maximum mechanical compressor speed and the minimum VGT and WG opening (VGT 20% - WG 0%), the maximum altitude is simulated. It makes sense because the mechanical compressor is at its maximum power for that position and the free section through the VGT-WG is minimal, increasing expansion capability and therefore producing the highest vacuum and altitude. For this position, more than 0.1 kg/s air mass flow is obtained at 6000 meters of altitude (0.47 bar).

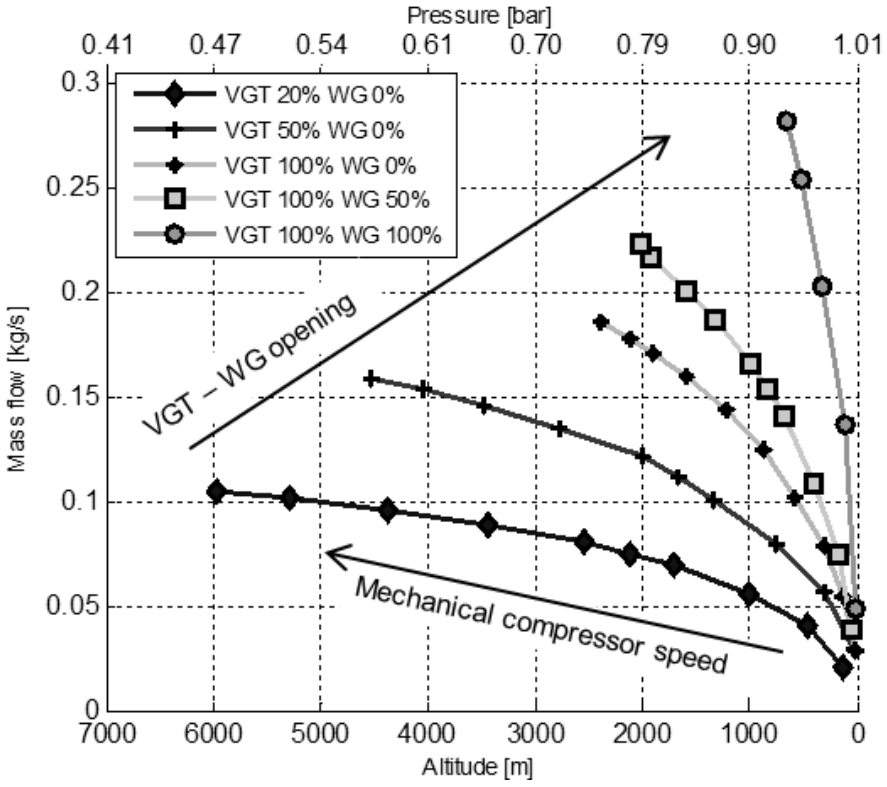

Figure 3.16 – Altitude simulator prototype operation map in vacuum mode

Similarly, the maximum air mass flow is obtained when the installation operates with the maximum mechanical compressor speed and maximum

VGT and WG opening (VGT 100% - WG 100%). The reason is that with a bigger opening, increases the permeability of the VGT and WG and more air can pass through them at the expense of lower expansion ratio. The maximum air mass flow is obtained at 660 meters of altitude (0.915 bar). If the altitude is lower, the maximum air mass flow decreases according to the slope of the VGT 100% - WG 100% line. This slope is caused by the inlet line losses (pipe friction, elbows and valves).

3.4.2. Vacuum temperature range

Once analyzed the altitude and mass flow range, the other important variable to be controlled by the altitude simulator is the temperature range that it can generate at the engine intake. Figure 3.17 and Figure 3.18 show the maximum and the minimum temperature decrease that the installation can generate for each operation point, respectively.

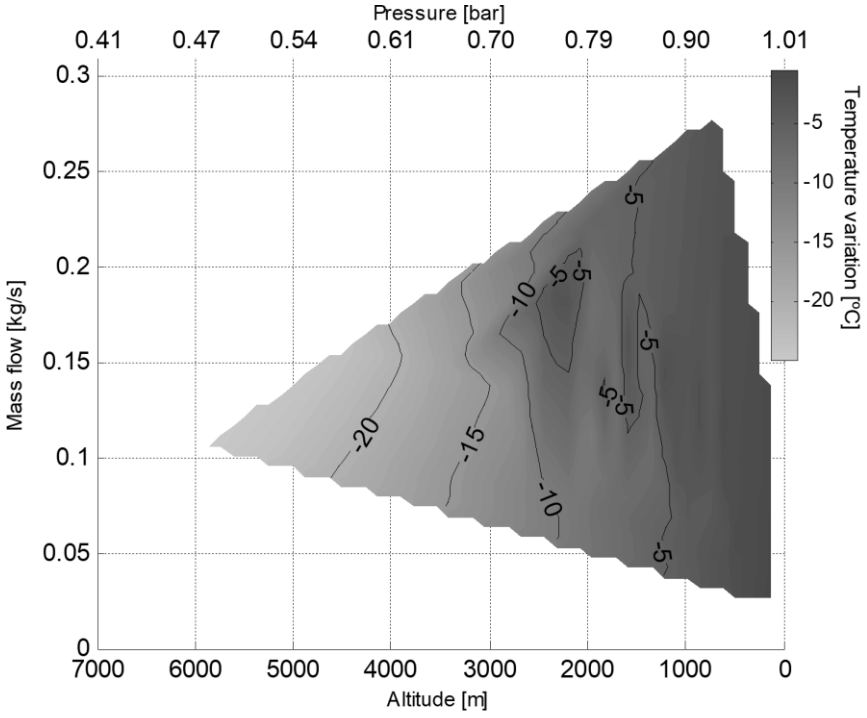

Figure 3.17 – Maximum temperature decrease between outlet VGT-WG outlet and atmospheric temperature

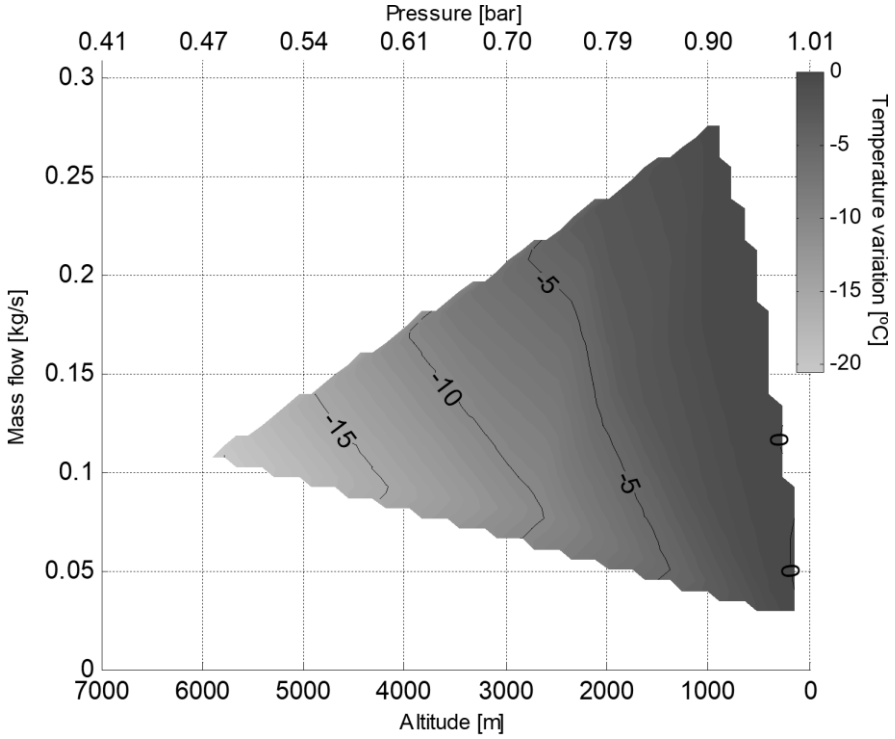

Figure 3.18 – Minimum temperature decrease between VGT-WG outlet and atmospheric temperature

As the temperature range is obtained by the expansion in the turbine, the engine intake temperature value is dependent on the room temperature. What is kept quite constant is the temperature variation between the engine intake and the atmosphere. For that reason, in Figure 3.17 and Figure 3.18 has been colored the temperature decrease between the ambient and the engine intake for each tested point.

Table 3.3 shows the strategy of WG and VGT control to generate the maximum and the minimum temperature decrease. In the case of maximum temperature decrease, the WG valve must remain close while setting up the VGT position. Once the VGT position is fully open, the WG valve must be opened. For minimum temperature decrease purpose, the WG valve should be managed keeping the VGT closed, which must be opened only when the WG is fully open.

Table 3.3. Sequence of variation the opening of VGT and WG valves to generate the maximum and the minimum temperature decrease available.

	Maximum temperature		*Minimum temperature*	
Steps order	VGT opening [%]	WG opening [%]	VGT opening [%]	WG opening [%]
1st	0 ÷ 100	0	0	0 ÷ 100
2nd	100	0 ÷ 100	0 ÷ 100	100

Comparing Figure 3.17 and Figure 3.18, it can be deduced the control range over temperature that can be obtained with different VGT and WG opening strategies. Higher control range is available at higher simulated altitude, where temperature range can vary until 10 ºC for some points. At lower altitudes less temperature control is available because the WG is more open and much less air passes through the VGT and also because the expansion in the VGT is much smaller.

Another interesting way to represent the temperature range is just taking into account the maximum mass flow line, i.e. the line where the mechanical compressor speed is maximum, for the maximum and minimum temperature decrease, as shown in Figure 3.19. It is a different way to see the line at maximum speed of the Figure 3.17 and Figure 3.18 in the same graph. This is interesting as allows knowing the temperature range at a given altitude for the maximum mass flow. The strategy to move through both lines is the one shown in Table 3.3.

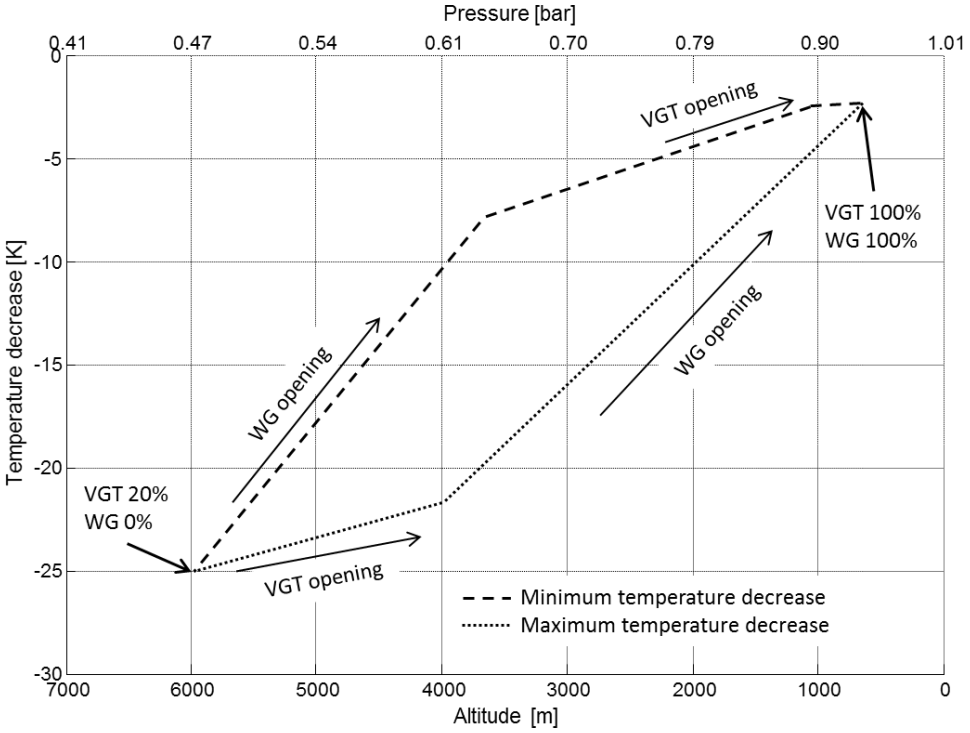

Figure 3.19 – Temperature range between VGT-WG outlet and atmospheric temperature for the maximum mass flow at each altitude

As can be seen, for the maximum and minimum altitude, both strategies converge. On the other hand, the maximum temperature range is obtained around 3750 m, being 13 ºC.

3.4.3. Overpressure operation range

In some situations a flow test rig simulating overpressure conditions is of interest. It is the case of a test rig at high altitude requiring sea level pressure simulation; or the case of that an engine needs to operate over sea level pressure, like an engine in a mine.

The parametric experimental study that was carried out with this configuration is the same as that for vacuum mode (Table 3.1 and Table 3.2). Figure 3.20 shows overpressure performance of the installation. In this case, the x-axis refers to the altitude of a test cell that where sea level pressure can be simulated. For example, the altitude simulator can

reproduce sea level conditions in a test cell located at 3000 meters above sea level for a maximum mass flow of 0.35 kg/s. Comparing with Figure 3.16, it can be concluded that in overpressure mode higher mass flow passing through the installation is obtained. The maximum altitude where the test bench is able to simulate sea level conditions is close to 6000 meters.

On the other hand, the VGT 100% - WG 100% line reach the maximum mass flow at 4000 m altitude. In order to reach higher altitudes, the WG must be closed at the expense of lower maximum mass flow. In order to reach higher air mass flow below 4000 m a better piping and elements design is required to minimize pressure losses.

Concerning the temperature increase, it is in all cases bigger than the temperature increase necessary to reproduce ISA atmosphere at sea level. For this reason, an air chilling unit between the mechanical compressor outlet and engine intake connection is necessary in overpressure mode.

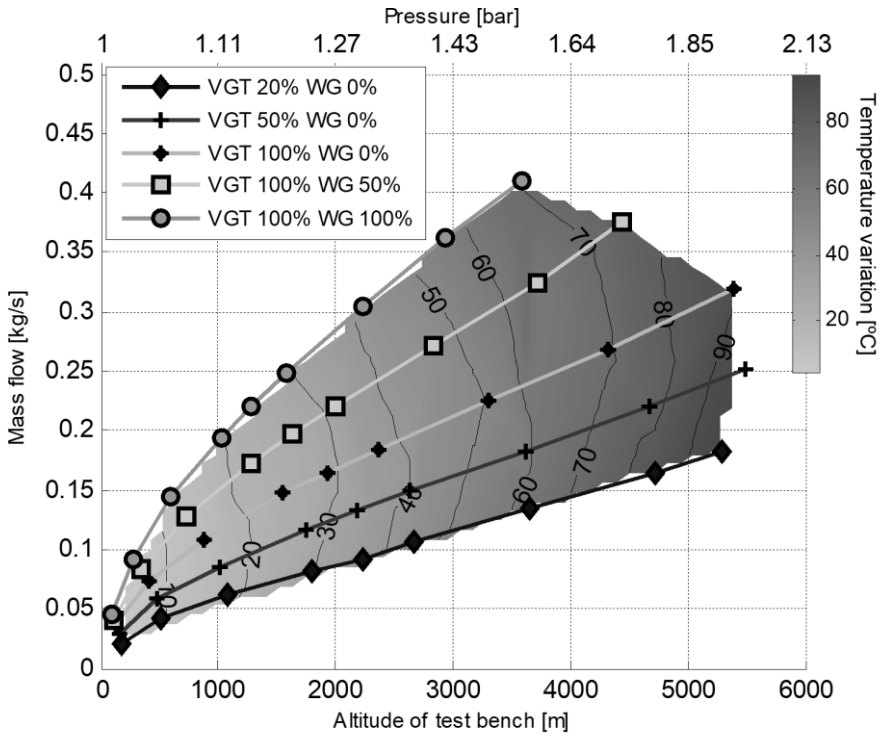

Figure 3.20 – Altitude simulator prototype operation map in overpressure mode

3.4.4. Limitations in the operation maps

The operation maps show good results with respect to maximum mass flow and altitude. The maximum mass flow in vacuum operation mode is 0.27 kg/s, which covers most of the light and medium duty engines. In overpressure mode, the maximum mass flow is 0.41 kg/s, even higher than in vacuum mode.

With respect to the altitude, the maximum altitude that can reach the prototype in vacuum mode is 6000 m, which also covers most of the automotive situations, as there aren't roads at such a high altitude.

Finally, the temperature reached at the engine intake is also very low. If the results obtained are compared with the ISA atmosphere, the temperature generated by the altitude simulator is only 2 ºC to 10 ºC higher than the ISA temperature at every altitude.

However, there are also some limitations in the operation ranges that will be detailed in the following paragraphs.

Maximum mass flow at altitudes close to ambient pressure

As can be seen in the vacuum and overpressure operation maps, the maximum mass flow that can be reached at altitudes close to the test cell altitude is limited.

In vacuum mode, the maximum mass flow peak is at 700 meters above sea level. Then, this mass flow decreases when the altitude is increased or decreased. The decrease of the mass flow with the altitude is related with the decrease of the air density at the mechanical compressor inlet. This will be explained in detail in Chapter 4, Section 4.5.1. This decrease in the mass flow also occurs in an engine, when the turbocharger has not energy enough to keep the boost pressure constant and the mass flow in the manifold decreases [20]. However, the decrease of the mass flow when the simulated altitude is close to room conditions limits the number of tests that the altitude simulator can perform, as an engine cannot be tested with the altitude simulator prototype at altitudes ranging from sea level to 700 m.

In overpressure mode, the 'dead area' is even larger, being the maximum mass flow peak at 3600 m, and the same analysis than in vacuum mode can be done.

Maximum mass flow in vacuum mode is much lower than in overpressure mode

Other limitation is that the maximum mass flow in vacuum mode is 0.27 kg/s, while the maximum mass flow in overpressure mode is 0.4 kg/s.

The altitude simulator can be used in three different ways, and that difference in the maximum mass flow in both operation modes leads to different engine sizes that can be tested.

- If the altitude simulator wants to be used only in vacuum mode, for example if the test cell is already at sea level, the maximum engine that can be tested is 0.27 kg/s, and only in a limited altitude range.
- If the altitude simulator wants to be used only in overpressure mode, for example, if the test cell is at a certain altitude and only sea level tests are needed, the maximum engine that can be testes is 0.4 kg/s.
- Finally, if both operation modes are needed, this would be the case of a test cell at a certain altitude that needs sea level tests but also higher altitude tests. In this case, the maximum size of the engine is limited by the vacuum maximum mass flow.

As can be seen, the lower maximum mass flow in vacuum mode limits the size of the engine that can be tested with the altitude simulator in most of the situations.

Narrow temperature range in vacuum mode

As shown in Figure 3.19, the temperature range in vacuum mode is dependent on the altitude. At the maximum and minimum altitude, there is not temperature control and the maximum temperature control range of 14 °C is obtained around 3750 m. However, for lower altitudes, that temperature control range decreases, being for example at 2000 m only 6 ^{o}C.

In addition, the maximum temperature that can be obtained is much lower than the room temperature. This leads to the problems that the altitude is not independent to the temperature. Pressure and temperature are modified at the same time (coupled). This fact limits the tests that can be done with the altitude simulator. For example, if only the pressure wants to be modified at constant room temperature.

Engine intake temperature in overpressure mode is too high

In overpressure mode, the atmospheric air is compressed in the mechanical compressor and goes directly to the engine intake connection. During that

compression, the air is warmed up and is not cooled down again before the engine intake. This also limits the possible tests to be performed, where only the pressure wants to be changed.

All this limitations are going to be analyzed in detail in the following sections.

3.5 Fluid dynamic 1-D model

The altitude simulator prototype has shown good results, but also some areas that need to be improved. For that reason, a 1-dimensional model of the altitude simulator was developed. The model will offer big potential to study how every element of the altitude simulator behaves and its effect on the system operation maps (Figure 3.16 and Figure 3.20). This will also allow studying different layouts of the vacuum and overpressure operation modes.

The software was created in OpenWAM [21]. OpenWAM is a free open source tool for gas dynamics modelling, mainly developed for Internal Combustion Engines. This code was initially developed in CMT-Motores Térmicos in 1984 using the Method of Characteristics [22] and it was initially based on the Benson's work [23], but has been improved over the years [24–26] and now uses a more modern finite differences scheme.

Therefore, OpenWAM is a powerful tool to be used in the altitude simulator modelling. The next step is to model the different elements as accurate as possible to the reality in order to get reliable results from the model.

3.5.1. Altitude simulator model description

Valves model

The valves in OpenWAM are modelled as nodes that connect a pipe with a deposit. These nodes are zero dimensional elements. The different valve positions are achieved by modifying its discharge coefficient, from 0 (fully closed valve) to 1 (fully open valve).

The prototype has only the WG valve. The WG valve has also some pressure losses even when it is fully open, therefore its discharge coefficient is never 1. Its maximum value when it is fully open can be calibrated from the tests performed in the prototype.

Cyclonic separators model

The cyclonic separators are modelled as zero dimensional elements, only defined by its turbulent pressure loss (K), which follows Equation (3.14). This value can be also calculated from the tests performed in the prototype.

$$\Delta p = \frac{1}{2}\rho v^2 K \qquad (3.14)$$

Air-to-water cooler

In OpenWAM, a cooler is defined as a group of many pipes, with its correspondent inlet and outlet diameters and length. However, the cooling power cannot be imposed, only the thermal losses through the walls. As the thermal losses are also dependent on the water flow and temperature, in the model it was imposed the outlet temperature to a value of 50 ºC. This value is low enough to protect the mechanical compressor but also high enough to avoid water vapor condensates going into the cyclonic separator.

Turbocharger model

In OpenWAM, turbocharger is formed by three separated elements: a compressor, a turbine and the shaft that connects both elements and transmits the power from the turbine to the compressor [27]. The turbine is the object that generates energy from the air that passes through it and the compressor is the object that transforms that rotational energy into compression work.

The turbocharger model uses the turbine and compressor maps for a more accurate result. With these maps, the model calculates the output variables: outlet turbine pressure and temperature, outlet compressor temperature, inlet compressor pressure and axis speed. The maps of the VGT and turbocompressor used in the prototype were introduced also in the model.

Mechanical compressor and electric motor models

The mechanical compressor and the electric motor are modelled as a turbocharger where the speed is imposed. In the prototype, the electric motor imposes the speed of the mechanical compressor. Therefore, in the OpenWAM model, this can be simulated by a turbocharged where the shaft speed is imposed and a compressor with its map equal to the mechanical compressor map.

3.5.2. Altitude simulator model flow path

Figure 3.21 shows schematically the main components of the altitude simulator model.

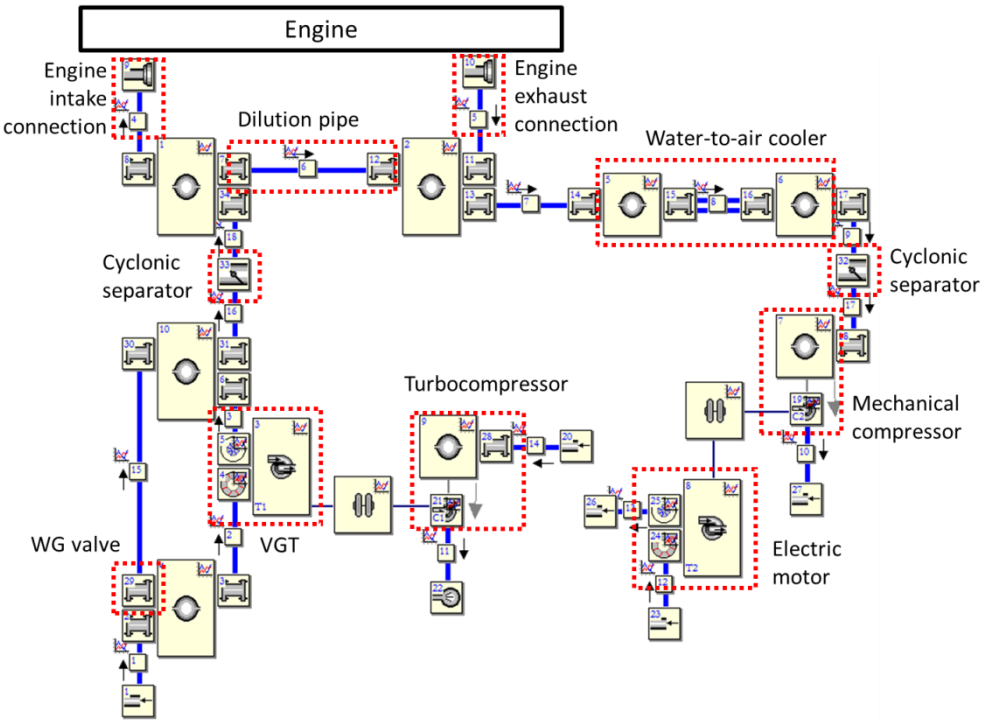

Figure 3.21 – Altitude simulator modelled in OpenWAM

3.5.3. Model validation

First of all, the altitude simulator model was validated to proof its capability to reproduce the real installation behavior. Figure 3.22 is a comparison between experimental tests and fluid-dynamic modeling of the installation in vacuum mode. Figure 3.22 shows that the simulation reproduces the operation behavior and range of the installation with a small error at high mechanical compressor speeds. This difference can be attributed to the fact that in the tests, the temperature at the inlet of the mechanical compressor changed with altitude (lower temperature with higher altitude), obtaining a better performance for higher altitudes than the simulation, where that temperature was constant, as explained in section 3.5.

The line in the right of the map, which corresponds to the line where the WG valve and VGT are fully open and only the mechanical compressor speed changes, has been adjusted with the discharge coefficient in the WG valve of the model.

The same comparison has been done for the overpressure configuration, as shown in Figure 3.23. In this case, the WG valve maximum discharge coefficient value is the same than in vacuum mode. As can be seen, the model shows very similar operation map with respect to the prototype.

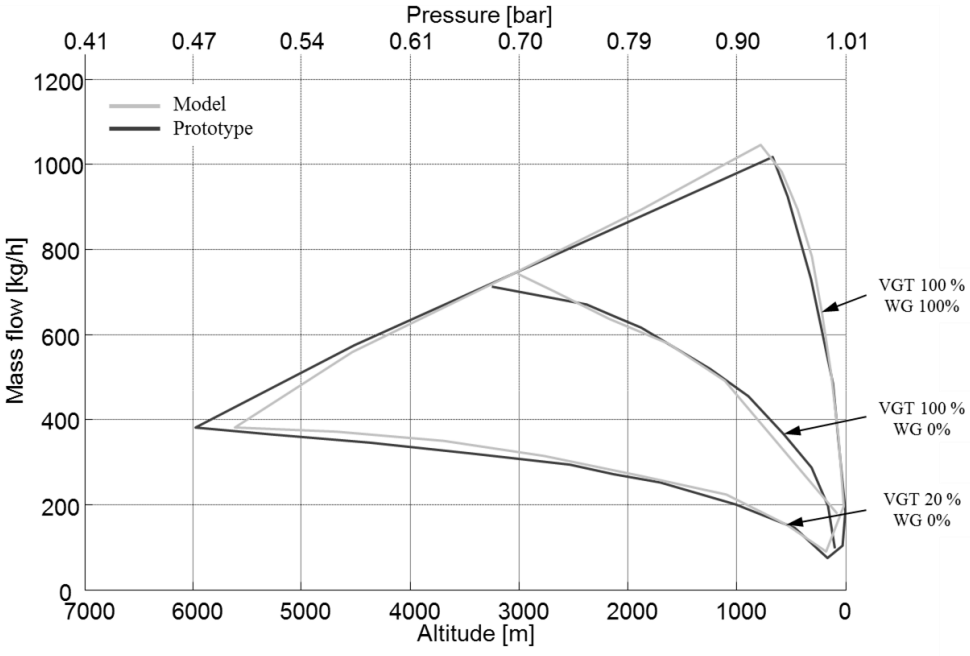

Figure 3.22 – Comparison between prototype and model results in vacuum mode

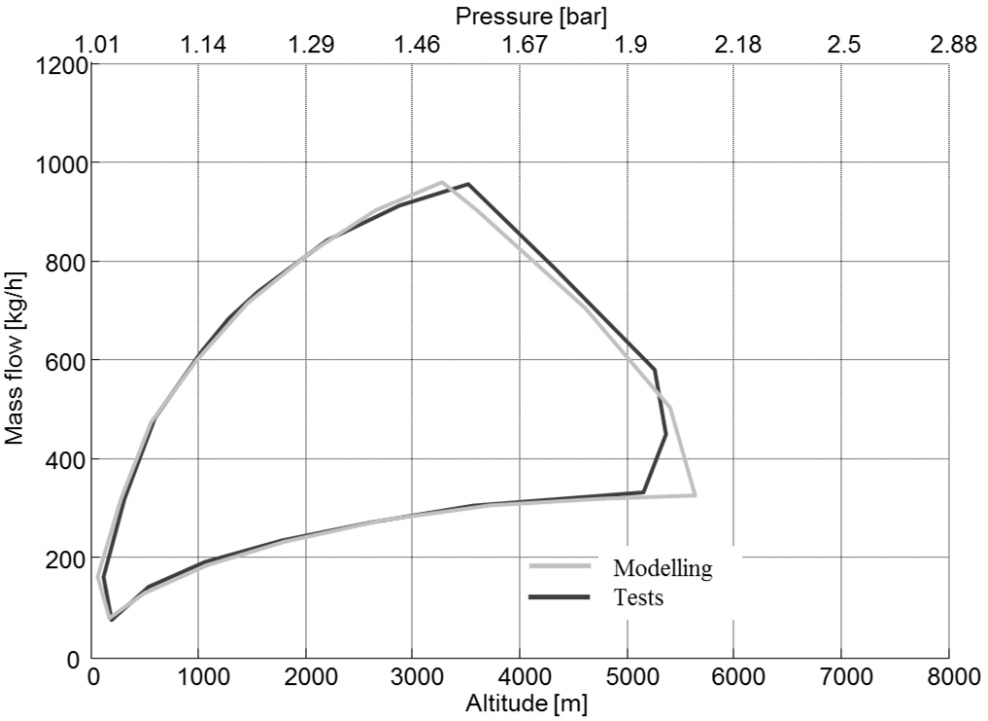

Figure 3.23 – Comparison between prototype and model results in overpressure mode

3.5.4. Elements analysis

Once all the elements of the altitude simulator prototype have been defined and modelled and the model has been validated, it can be used to deep understand the effect of the design of the different elements of the altitude simulator in the operation maps.

Pipes diameter

The pipes diameter is the first parameter to be analyzed, studying its effect in the performance maps. The altitude simulator prototype has DN80 pipes, which corresponds to an inner diameter of 73 mm. In the model, the entire pipes diameter can be changed. However, in the prototype there are some constrains. On one side, the diameter of the mechanical compressor inlet and outlet is imposed, as well as the diameter of the VGT. On the other side, the cyclonic separators are designed according to their diameter. Thus, increasing their diameter will increase also their dimensions and consequently the dimensions of the entire altitude simulator. For these

reasons, the parametric study of the pipes diameter was limited to the diameter of the WG pipes, which covers from the air filter to the engine intake connection, but without effect on diameter of the VGT branch.

Therefore, a parametric study was done for the following inner diameters: 73 mm (actual prototype), 90 mm, 110 mm and 130 mm.

Figure 3.24 shows the results. As can be seen, the increase in the diameter of the inlet part of the prototype only affects to the low altitude area. This makes sense, as the WG valve is fully open in that area and the slope of that speed line is caused by the pressure losses in the intake line. If the engine intake was directly connected to the atmosphere, the line would be vertical, as occurs when the engine is operating without the altitude simulator.

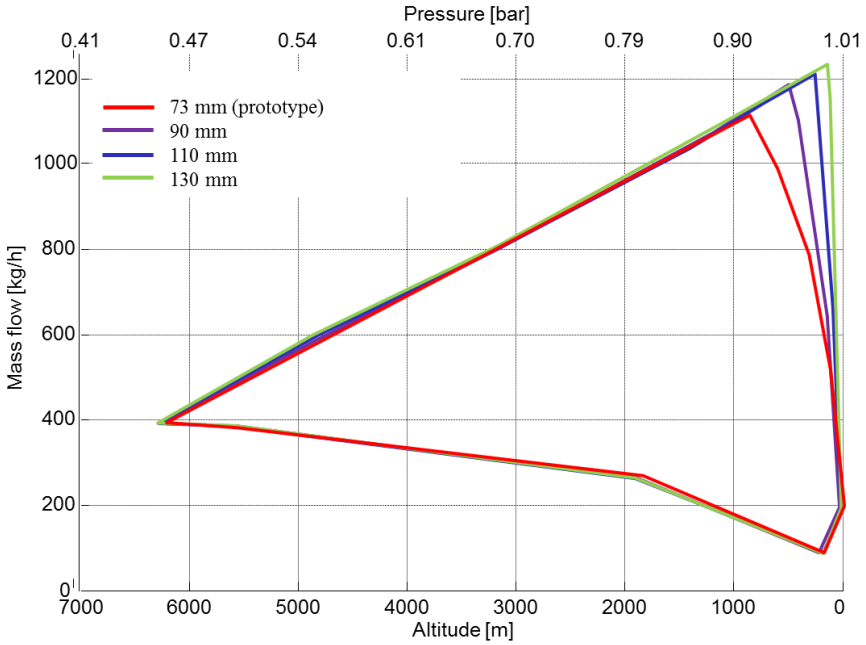

Figure 3.24 – Inlet pipes diameter effect on the operation map

The increase of the inlet pipes is limited by the increase in size and costs. The altitude simulator has to be kept as small as possible in order to be movable and the costs are affected directly by the pipes diameter, but also by the increase in the WG valve diameter. The inlet pipes and the WG

diameter have to be the same; therefore, the study of the effect of the WG diameter has to be studied also in detail.

WG diameter

As can be seen in Figure 3.24, the diameter increase reduces the 'dead zone' near to the room altitude. However, the WG valve has a big effect also in the pressure losses, which are the cause of that dead zone. In fact, the WG pressure losses are much higher than the pipes pressure losses. As the OpenWAM model cannot reproduce with enough accuracy the effect of the WG diameter, this parametric study has to be done with the flow coefficient (K_v) values for the different diameters that can be found in the valve datasheet [7].

The K_v is defined as the water flow in cubic meters through the valve in one hour at a pressure drop across the valve of 1 bar (Equation (3.15)). Its value is determined by the manufacturer and it is a relative measure of the permeability of the valve to allow the flow moving through it. In other words, the higher the value of the K_v, the lower the pressure losses across the valve for a given amount of air.

$$K_v = \frac{Q}{\sqrt{\Delta p}} \; [m^3/h] \qquad (3.15)$$

Table 3.4 shows the K_v when the valve is fully open according to the valve diameter given in the valve datasheet.

Table 3.4. K_v of the GS8021 valve according to its diameter.

DN	80	100	125	150	200
K_v	92	154	237	338	560

Then, for given pressure losses, the mass flow that can pass through the valve follows Equation (3.16). Assuming that the test cell is at sea level, according to ISA, the valve inlet conditions are 1.01325 bar and 15 ºC. Varying the pressure losses, different values of mass flow are obtained. Besides, the inlet and outlet WG valve pressure can be expressed as altitude, being therefore at the inlet sea level and at the outlet the generated altitude caused by the pressure losses across the WG valve.

If that procedure is done for the different diameters, the result obtained is shown in Figure 3.25.

$$\dot{m} = K_v \rho \sqrt{\Delta p} \quad [m^3/h] \qquad (3.16)$$

The first thing that can be observed is that the DN80 line fits with the experimental results. Therefore, the values of the data sheet are reliable.

Then, to choose the diameter of the WG valve, four factors have to be balanced: pressure losses, rangeability (flow yield), cost and space occupied by the valve. As explained, a big valve will have very low pressure losses when fully open, which leads to very low 'dead area'. However, this valve will present some disadvantages. On one side, the flow yield of the valve, which is defined as the maximum to minimum flow rate that can be controlled by this type of linear valves, is 40:1 and independent on the valve diameter, according to the manufacturer. This means that a very big valve will have some problems to control low mass flow. On the other hand, both the size and cost of a big valve increase exponentially. Taking into account all these factors, the valve size chosen has been DN150, which presents a good balance.

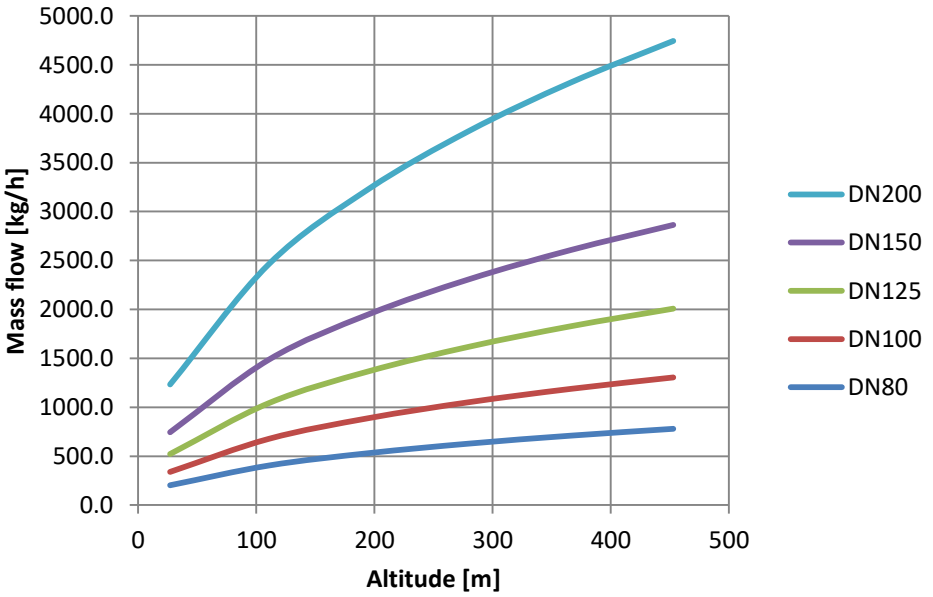

Figure 3.25 – Maximum mass flow for each altitude depending on the WG diameter

Cyclonic separators

A cyclonic separator is an element that uses the centrifugal force to separate solid or liquid particle from a gas [10].

Figure 3.26 shows the geometry of a generic cyclonic separator. The air with the particles goes into the cyclonic separator in the top part of the

cylinder (horizontal duct in the top left side of the Figure 3.26). This entry duct is usually tangential to the filter walls and internal outlet duct. The gas moves in its interior through a downward spiral creating a field of centrifugal forces depending on the tangential velocity of the fluid in each section. Due to this force, the particles suspended in the gas are concentrated along the inner walls of the filter. The collected particles are drawn through a duct located in the lower region of the filter, while the gas changes its axial direction and exits through the outlet duct located in the upper zone, in the center of the cylinder.

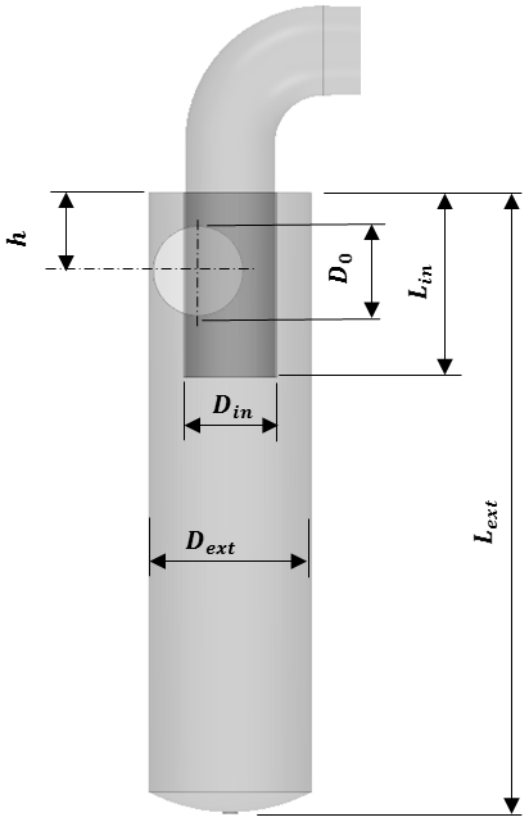

Figure 3.26 – Frontal section of the cyclonic separator

Commercial cyclonic separators usually work with higher pressure than room pressure, for that reason, the cyclonic separators used in the altitude simulator had to be specially design and built in the CMT-Motores

Térmicos department, as their inner pressure will be lower than the outer pressure.

The prototype design of the cyclonic separator is based on commercial separators. However, it presented some critical points that had to be improved:

- The pressure losses of the air across it are too high, being this element the main source of pressure losses in the system.
- The noise produced by the cyclonic separator located upstream the mechanical compressor is too high for some altitude simulator operation points.

Therefore, its design has been studied by means of CFD tools in order to improve these two points while the filtration efficiency is not modified, because it has been working fine [28,29].

Despite the fact that the study of the cyclonic separator redesign is out of the scope of this thesis, the results can be summarized in the dimensions for an optimum performance of the cyclonic separator (variables are referred to Figure 3.26):

- $h = 0.8\ D_0$
- $L_{in} = 2\ D_0$
- $D_{in} = D_0$
- $D_{ext} = 2\ D_0$
- $L_{ext} \geq 6\ D_0$

3.6 Redesign of the prototype

The altitude simulator prototype and model has been very useful for the redesign of the main elements, understanding its influence in the operation maps and performance. Besides, the model has also been used to study different layouts and designs of the altitude simulator.

3.6.1. VGTv valve

As was shown in Figure 3.18 and Figure 3.19, the temperature range is limited in vacuum mode. This is a big disadvantage especially when the test bench has its own temperature control, because the altitude simulator modifies it. The reason is that the altitude simulator always decreases the

temperature when operates in vacuum mode because the VGT allows some air passing through them even when its blades are fully closed. Therefore, the altitude and temperature are coupled.

To solve this problem, another control valve has been proposed to be installed upstream the VGT. This control valve, named VGTv, is of the same type than the WG valve.

When the VGTv is fully closed, the altitude simulator does not modify the ambient temperature, as all the pressure drop occurs in the WG.

Also, modifying its opening the mass flow through the VGT can be controlled. Therefore, the VGTv introduces an extra dimension in the temperature control, allowing increasing the temperature range shown in Figure 3.19 in the area between the minimum temperature decrease and the horizontal line (that means no temperature decrease).

Taking this into account, the final design of the inlet line of the altitude simulator is shown in Figure 3.27.

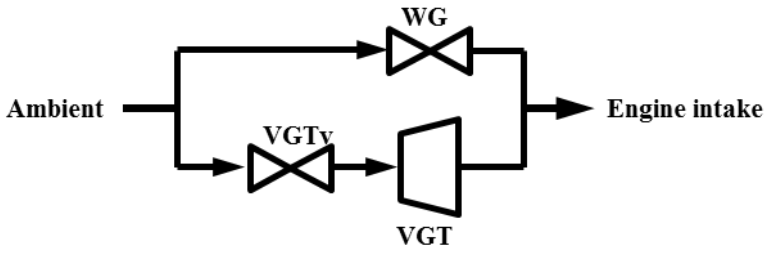

Figure 3.27 – New layout of the altitude simulator inlet line

3.6.2. Cooler upstream the engine intake in overpressure

With respect to the temperature range in overpressure mode, Figure 3.20 showed that the ambient temperature is highly increased because of the compression in the mechanical compressor.

To solve this problem and decrease the engine intake temperature, it should be necessary to install a chiller or cooler upstream the engine connection.

The first solution would be to install an extra cooler. This solution seems simple, but increases the dimensions of the altitude simulator and its cost.

The other solution is to modify the overpressure layout in order to use the same water-to-air cooler than the vacuum mode. In the prototype, this

cooler is used to cool down the exhaust temperature. However, this is not needed, as there is not any element in the exhaust line in overpressure that needs to be protected from high temperature. This solution will increase the complexity of the pipes and the valves needed to operate the altitude simulator. But as is going to be shown in the following paragraphs, the layout in overpressure has to be also modified to reduce the 'dead area' close to the room pressure. This modification in the layout allows using the cooler with the same number of elements and pipes than in the vacuum circuit.

3.6.3. Overpressure valves

The dead area in overpressure mode is bigger than the dead area in vacuum mode, as shown in Figure 3.20.

In section 3.5.4, the reasons of the dead area in vacuum mode have been discussed and analyzed. The solution proposed is to install a bigger WG valve in order to reduce the pressure losses in the inlet line of the altitude simulator. In overpressure mode, the WG valve is used as backpressure valve, downstream the engine exhaust connection.

Using the model, the layout of the overpressure mode has been modified. First, the WG valve size and piping has been increased. Secondly, the cooler has been moved from downstream the engine connections to upstream it, in order to cool down the compressed air in the mechanical compressor. And finally, the cyclonic separator has been also removed from the exhaust line in overpressure mode, because it is not necessary once the cooler has been removed.

Figure 3.28 shows the comparison between the prototype map in the model and the new modified map. As can be seen, the dead area has been reduced. However, this can be smaller if the bigger pipes diameter and shorter length. In the extreme case where the engine exhaust was connected directly to the atmosphere, the exhaust pressure would be the ambient pressure. This means that the left line of the operation map in overpressure mode (Figure 3.28) would be vertical. Therefore, to be as close as possible to that ideal case, the exhaust line of the altitude simulator in overpressure mode has to have as low pressure losses as possible.

Theoretically, the WG valve can be used in the overpressure mode to generate the backpressure, as it is a DN150 valve with low pressure losses and the pipes are also DN150. However, when the altitude simulator has to be built, to connect the engine exhaust with the WG valve introduces many

elbows and a big distance in the piping that increases the pressure losses, as has been shown in Figure 3.28.

Therefore, the new solution adopted has been to introduce a new valve that operates generating the backpressure in overpressure mode and that is fully closed in vacuum mode. This valve connects the engine exhaust to the atmosphere with a very short pipe.

The first approach was to select a control valve identical to the WG valve. However, the higher exhaust temperature increases also the pressure losses across the valve (Equation (3.16)), so the valve diameter should be DN200. This big diameter would have a poor control for low mass flows.

To solve this problem, the solution adopted has been to install two valves in parallel. One control valve similar to the WG valve with a DN80 diameter for the fine pressure control and a butterfly valve with a big diameter to generate low pressure losses when fully open.

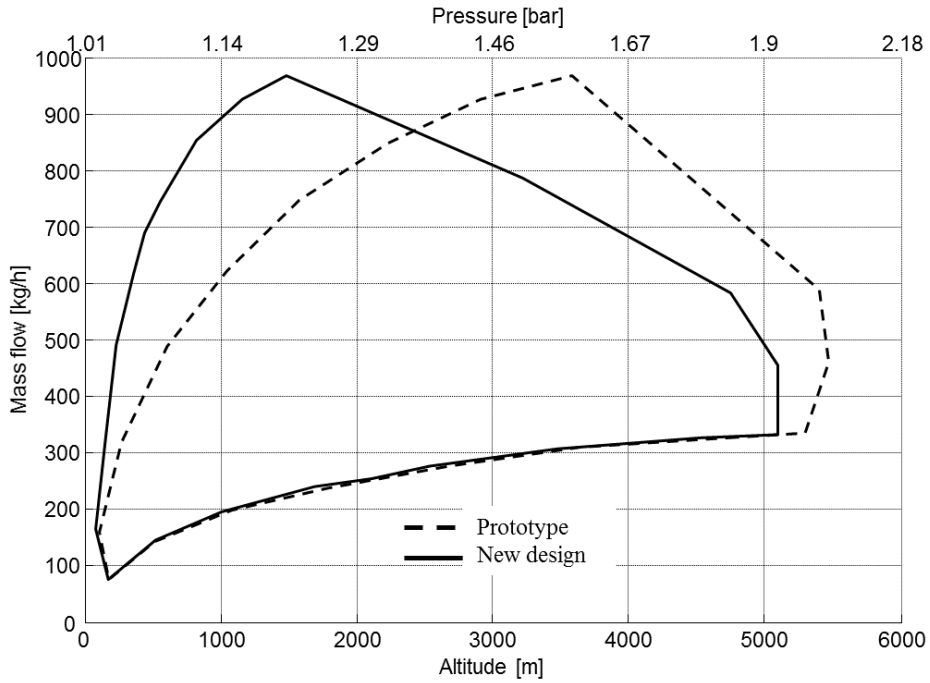

Figure 3.28 – Overpressure operation map modelled with the new design

3.6.4. On-off valves

Finally, the prototype could change from vacuum to overpressure mode manually. This was enough to test that both operation modes worked and to study the behavior and operation maps of the altitude simulator. However, it is not useful when the altitude simulator is operating in a test cell connected to an engine, because to change the operation mode the engine has to be stopped and the altitude simulator has to be partially disassembled, which takes some hours.

The use of several on-off valves has been proposed to solve this problem. These on-off valves change their position automatically depending on the operation mode. The position of each on-off valve will be explained in section 3.7, where the final design is presented and explained in detail.

3.7 Altitude simulator flow path

By means the tests of the prototype and the simulations with the OpenWAM model, the altitude simulator has been understood in deeper detail and the different elements analyzed and optimized. In order to integrate all the proposed changes in the altitude simulator, a change in the layout has been mandatory.

Figure 3.29 shows the layout of the final design of the altitude simulator, where all the upgrades proposed have been taken into account. The different elements are listed in Table 3.5

The new flow path is explained in the following paragraphs.

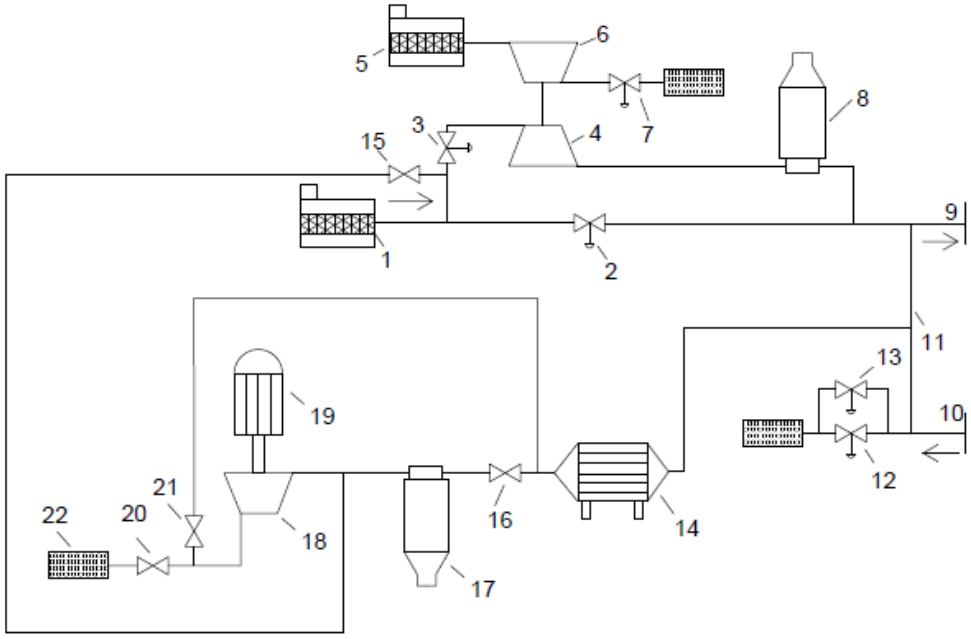

Figure 3.29 – Altitude simulator layout.

Table 3.5. Elements numbered in Figure 3.29.

1	Air filter	12	OP valve
2	WG valve	13	OP valve
3	VGTv	14	Water to air cooler
4	VGT	15	On-off valve
5	Air filter	16	On-off valve
6	Turbocompressor	17	Cyclonic separator
7	Backpressure valve	18	Mechanical compressor
8	Cyclonic separator	19	Electric motor
9	Engine intake connection	20	On-off valve
10	Engine exhaust connection	21	On-off valve
11	Dilution pipe	22	Silencer

3.7.1. Vacuum Operation Mode

In vacuum operation mode, the room air passes through the VGT (4) where it is expanded and cooled down from room conditions to the pressure of the altitude that is being simulated. The VGT power is dissipated in an independent compressor (6). In addition, a control valve (3) can be managed in series with the VGT, allowing expanding the air at constant temperature in the WG valve (2) or expanding and decreasing its temperature at the same time in the VGT. The on-off valve which connects the air intake with the mechanical compressor inlet is closed (15).

Downstream of the VGT, a cyclonic separator (8) is installed to separate the possible ice generated because of very low temperature.

Alternatively, the WG valve can be managed in parallel. Basically, it allows increasing the engine intake mass flow rate and pressure for a given VGT opening; VGTv (3) position and mechanical compressor speed; and without effect on flow temperature. When both flows, the one from the VGT and the other from the WG join, an intermediate temperature is obtained at engine intake.

Then, the air is aspirated by the engine intake (9) and the excess air is by-passed through the dilution pipe (11) from engine intake connection to engine exhaust connection (10); and following to the tailpipe of the installation, it is further diluted with exhaust gas from the engine. This dilution pipe ensures engine operation with equal intake and exhaust pressure. As both OP_Ex1 (12) and OP_Ex2 (13) valves are closed, this mix of exhaust air and dilution air passes through a cooler (14) to ensure the safe operation of the mechanical compressor (18), because can be at high temperature. It additionally reduces the compressor power consumption. To avoid the effects of condensates formed when the exhaust gas is cooled down, what may damage compressor blades, another cyclonic separator (17) is installed just upstream of the mechanical compressor. The risk of condensates and its generation rate is depending mainly on the equivalence ratio, dilution ratio and the cooler outlet temperature. The mechanical compressor speed is controlled by means of the electric motor speed (19) with a variable-frequency drive. Finally, the diluted exhaust gases are discharged to the atmosphere (22) at a maximum gas temperature of 200ºC, as the on-off valve which connects the mechanical compressor outlet and the cooler (21) is closed and the one connecting the compressor outlet and the silencer is opened (20).

3.7.2. Overpressure Operation Mode

In Overpressure operation mode, the position of the on-off valves changes, the VGTv (3) and WG (2) are shut and the OPEx1 (12) and OPEx2 (13) valves are open. Therefore, the atmospheric air is forced to pass through the mechanical compressor (18) where its pressure and temperature increases. Downstream the mechanical compressor, the air passes through the water to air cooler (14) where its temperature can be controlled depending on the water flow.

Then, the air is aspired by the engine intake and the excess air is by-passed to the tailpipe of the installation and diluted with the exhaust gas of the engine. This by-pass pipe ensures engine operation with equal intake and exhaust pressure.

Finally, this mixed exhaust gas with intake air passes through two control valves (OP valves Ex1 and Ex2) positioned parallel, where is expanded until atmospheric pressure.

3.7.3. Altitude simulator operation maps

This new design of the altitude simulator was constructed in order to test the new results. Figure 3.30 shows the operation map of the altitude simulator for vacuum and overpressure mode. It is equivalent to the one shown in Figure 3.16 and Figure 3.20, but showing both modes in the same figure.

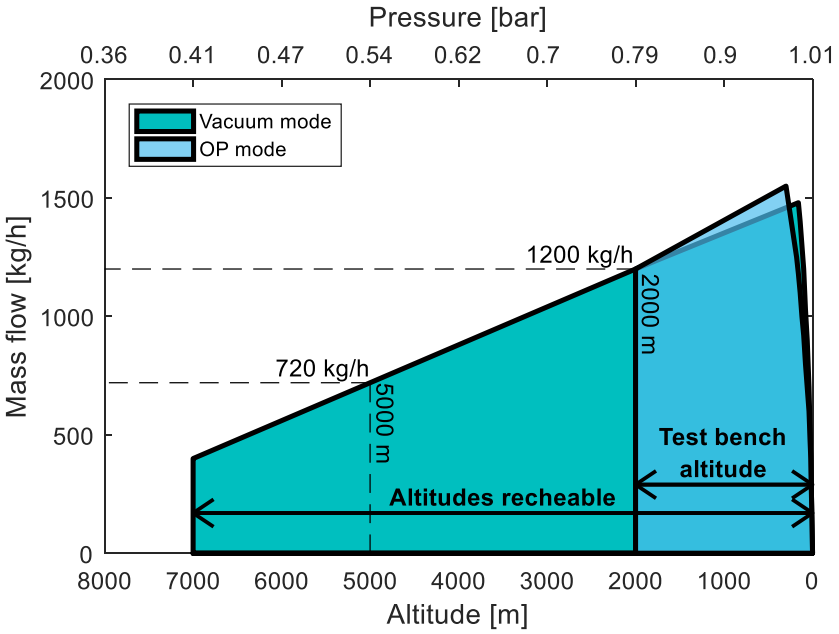

Figure 3.30 – Altitude simulator operation map in vacuum and overpressure mode

The blue area represents where the test bench can be located, and ranges from sea level up to 2000 meters above sea level. The green area represents all the reachable altitude with the altitude simulator, and ranges from sea level up to 7000 meters above sea level. For example, a test cell at 2000 meters above sea level can simulate sea level pressure if operates in overpressure mode, and can simulate 7000 meters above sea level if operates in vacuum mode.

As can be seen, the main upgrades have been reached in the low altitude area, caused by the bigger pipes diameter and control valves size (WG and OPEx2). Besides, the operation map has also been increased in the top left area, in the maximum mass flow line, where the maximum mass flow at 2000 m has been increased from 820 kg/h to 1200 kg/h and at 5000 m has been increased from 540 kg/h to 720 kg/h. This increase is caused mainly by the improved design of the cyclonic separator located upstream the mechanical compressor.

With respect to the temperature range, shown in Figure 3.31 analogue to Figure 3.19 and Figure 3.20, it can be seen how the minimum temperature in vacuum mode has not being modified, but the maximum temperature with the new design can be the same than the room temperature, caused by

the installation of the VGTv valve upstream the VGT. In overpressure mode, the temperature now can be controlled because of the use of the water-to-air cooler used to cool down the air compressed in the mechanical compressor, upstream the engine connection.

Therefore, in both operation maps and both operation modes, the new proposed design improves the behavior of the previous design.

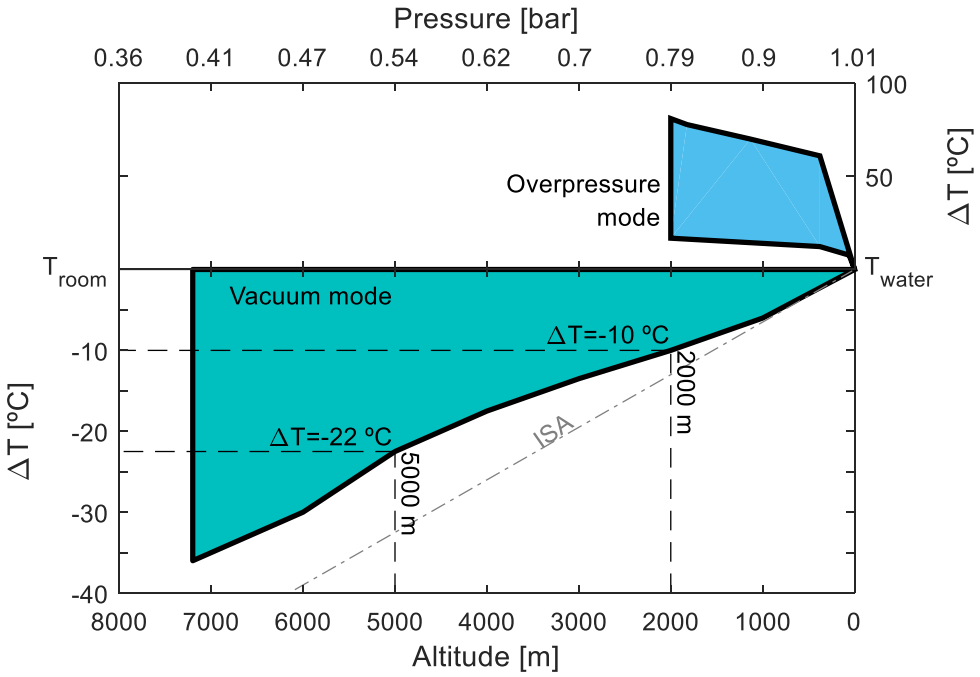

Figure 3.31 – Altitude simulator temperature range control in vacuum and overpressure mode

3.8 Altitude simulator aspect

One of the objectives of this doctoral thesis is to build a product to be commercialized in the automotive industry as an alternative or complement to the tools available in their R&D centers for the altitude simulation (in Chapter 4 will be detailed other important aspects to achieve these objectives).

Therefore, the altitude simulator has to look like a product to be commercialized and installed in a test cell. The first prototype shown in Figure 3.4 is useful as a development system, but cannot be commercialized as a product in the industry. Figure 3.32, Figure 3.33 and Figure 3.34 show the new external aspect of the altitude simulator and Figure 3.35 shows the internal aspect. The system has been body-built, installing doors around the frame in order to access the internal elements. Besides, all the connections have been located in the same side of the frame (Figure 3.34), in order to simplify the installation in the test cell (it will be explained in detail in Chapter 4).

Figure 3.32 – Altitude simulator overview of the external aspect

Figure 3.33 – Altitude simulator external aspect of one of the lateral frames

Figure 3.34 – Altitude simulator external aspect of the connections side

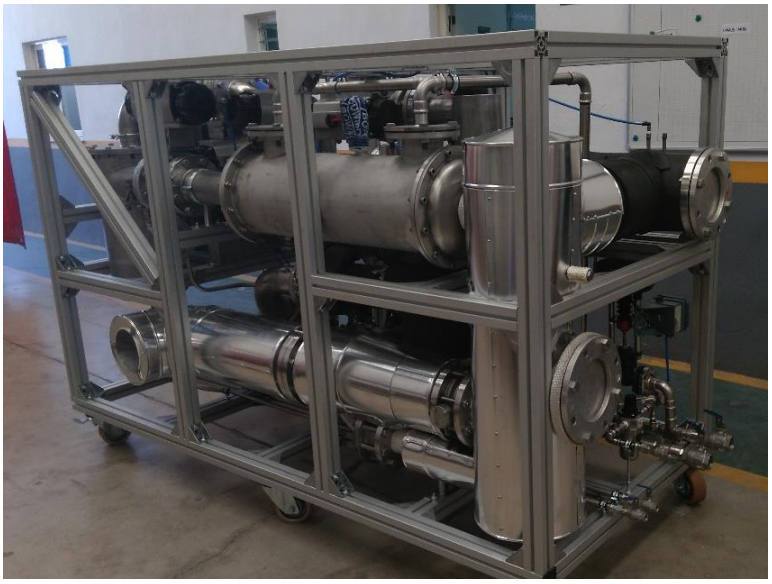

Figure 3.35 – Altitude simulator internal aspect

3.9 Conclusions

In the present chapter, an altitude simulator is presented. This altitude simulator operates connected to the engine intake and exhaust, generating vacuum only inside the engine, while the rest of the test cell is at room pressure.

A first prototype has been built and tested in order to study the potential of the altitude simulator, analyze its performance and know its potential to be used as a real alternative in the automotive industry during the development of new engines and control strategies in altitude conditions. The results showed that the altitude simulator could simulate altitudes higher than 6000 m and mass flow up to 1000 kg/h. Moreover, the altitude simulator could also operate in overpressure mode in order to simulate higher pressure than the room pressure. This allows, for example, simulating sea level conditions in a test cell located in altitude.

With the promising results shown in the prototype, a model in OpenWAM, a fluid-dynamic 1D software, was created. With this model, new designs of the different elements were studied, in order to improve the performance of the altitude simulator, as well as new layouts in order to add new features to the altitude simulator, such as automatic changes between vacuum and overpressure mode, and better performance.

Finally, with this information, a new design of the altitude simulator is proposed and another prototype is built. This new prototype aspect is closer to the aspect of a final product design, as one of the objectives is to develop a system to be sold in the automotive industry. The results of the tests performed with this prototype showed better performance in all the operation maps limits, such as low altitude dead zone, maximum mass flow and temperature range in vacuum and overpressure mode.

3.10 References

[1] F. Payri, J.M. Desantes, J. Galindo, J.R. Serrano, P. Piqueras, Unit for simulating the pressure and temperature conditions of the air drawn in by a reciprocating internal combustion engine, ES2398095B1 Spanish Pat. Date 20/01/2014. PCT/ES2012/070010. USA Pat. Nº 9038578. Japan Pat. Nº 5788025. Eur. Pat. Appl. No. 12742066.9 - EP2672248. Chinese Pat. Appl. Nº 201280007012.6. (2011).

[2] J.M. Desantes, J.G. Lucas, F.P. González, P. Piqueras Cabrera, J.R. Serrano Cruz, Dispositivo de acondicionamiento de atmósfera para el ensayo de motores de combustión, procedimiento y uso relacionados, ES2485618B1 (P201430071) PCT/ES23015/070037, 2014.

[3] J.M. Desantes Fernández, J.G. Lucas, F. Payri González, P. Piqueras Cabrera, J.R. Serrano Cruz, Dispositivo para acondicionar la atmósfera en ensayos de motores de combustión interna alternativos, procedimiento y uso de dicho dispositivo, ES2544516B1 (P201530075), WO 2015/110683 A1, 2015.

[4] J.R. Serrano, P. Piqueras, E. Angiolini, C. Meano, J. De La Morena, On Cooler and Mixing Condensation Phenomena in the Long-Route Exhaust Gas Recirculation Line, (2015). doi:10.4271/2015-24-2521.

[5] A. Warey, A.S. Bika, D. Long, S. Balestrino, P. Szymkowicz, Influence of water vapor condensation on exhaust gas recirculation cooler fouling, Int. J. Heat Mass Transf. 65 (2013) 807–816. doi:10.1016/j.ijheatmasstransfer.2013.06.063.

[6] S. Karstadt, J. Werner, S. Münz, R. Aymanns, Effect of Water Droplets Caused by Low Pressure EGR on Spinning compressor Wheels, in: 19th Supercharging Conf. Dresden, 24th Sept. 2014, 2014.

[7] Schubert & Salzer, Control Systems, Control Valve GS8021, (n.d.). http://schubertsalzerinc.com/products/gs-valves/type-8021/.

[8] Holset HY40V - Service Repair Manual, (2007).

[9] D. Bogdanov, S. Poniaev, Numerical simulation of turbulent flow in a cyclonic separator, J. Phys. Conf. Ser. 572 (2014). doi:10.1088/1742-6596/572/1/012056.

[10] S. Akhter, N. Nabi, Design , Construction and Performance Testing of a Cyclonic Separator to Control Particulate Pollution from Diesel Engine Exhaust, (2005).

[11] W. Peng, A.C. Hoffmann, H.W.A. Dries, M.A. Regelink, L.E. Stein, Experimental study of the vortex end in centrifugal separators: The nature of the vortex end, Chem. Eng. Sci. 60 (2005) 6919–6928. doi:10.1016/j.ces.2005.06.009.

[12] A.C. Hoffmann, L.E. Stein, Gas Cyclones and Swirl Tubes, New York. (2007) 434.

[13] X. Zheng, L. Jin, T. Du, B. Gan, F. Liu, H. Qian, Effect of temperature on the strength of a centrifugal compressor impeller for a turbocharger, Proc. Inst. Mech. Eng. Part C J. Mech. Eng. Sci. 227 (2013) 896–904. doi:10.1177/0954406212454966.

[14] EJ Bowman - Exhaust gas heat exchanger, (n.d.). https://www.ejbowman.co.uk/products/ExhaustGasHeatExchangers.htm.

[15] Rotrex A/S - C38-92, (n.d.). http://www.rotrex.com/.

[16] T.D. Sheet, Rotrex C38 Supercharger range, (n.d.) 1–7.

[17] Parker AC Frequency Drive Inverter AC30 Frame H, (n.d.).

[18] WIKA - Piezoresistive pressure sensor S20, (n.d.). https://en-co.wika.de/s_20_en_co.WIKA.

[19] Beckhoff, (n.d.). https://www.beckhoff.com/.

[20] H. Li, L. Shi, K. Deng, Development of turbocharging system for diesel engines of power generation application at different altitudes, J. Energy Inst. (2015). doi:10.1016/j.joei.2015.04.001.

[21] OpenWAM webpage, CMT-Motores Térmicos, Universitat Politècnica de València, (n.d.). http://openwam.webs.upv.es.

[22] J.M. Corberan, Contribución al modelado del proceso de renovación de la carga en motores de combustión interna alternativos, Universitat Politècnica de València, 1984.

[23] R.S. Benson, The Thermodynamics and Gas Dynamics of Internal Combustion Engines, 1 (1982).

[24] F. Payri, J.M. Corberan, F. Boada, Modifications to the method of characteristics for the analysis of the gas exchange process in internal

combustion engines., Proc. Inst. Mech. Eng. Part D, Transp. Eng. 200 (1986) 259–266. https://www.scopus.com/inward/record.uri?eid=2-s2.0-0022877864&partnerID=40&md5=332bdd1f2512d04f22f88ec2bec7820c.

[25] F. Payri, J. Benajes, M.D. Chust, Programme pour étude assistée par ordinateur de systèmes d'admission et d'échappement de moteurs, Entropie. 27 (1991) 17–23.

[26] J.M. Desantes, M.D. Chust, J. Llorens, Análisis comparativo de métodos numéricos para la resolución del flujo no estacionario en colectores de motores de combustión interna alternativos, II Congr. Métodos Numéricos En Ing. (1996).

[27] J. Ramón, F. José, L.M. García-cuevas, A. Dombrovsky, Development and validation of a radial turbine efficiency and mass flow model at design and off-design conditions, 128 (2016) 281–293. doi:10.1016/j.enconman.2016.09.032.

[28] S.J.G. Arias, Análisis CFD y optimización de un separador ciclónico, Universitat Politècnica de València, 2015.

[29] S.G. Barberá, Estudio CFD de separadores inerciales centrífugos de un simulador de altitud: estudio paramétrico de las condiciones de operación, Universitat Politècnica de València, 2015.

CHAPTER 4

Altitude simulator analysis

Contents

Figures

Tables

4.1 Introduction

The altitude simulator development has been analyzed in the previous chapter (Chapter 3) and the different steps followed to reach the final design of the system have been detailed. However, once the system has been fully defined, there are still some analyses that can be done.

First of all, a deeper analysis of the altitude simulator map will be performed, that links it with the mechanical compressor map. This analogy allows better understanding the effect of different ambient conditions and designing changes.

Then, it is proposed a control of the different actuators to automatically reach any given operation points. This way, the operator of the system only needs to introduce in the software the target pressure, temperature and mass flow setpoint and the system will reach them if they are inside its operation maps.

Finally, the operation of the altitude simulator; the different interfaces and things to take into account when installed in a test cell with an engine and the different screens of the control touch panel are explained.

4.2 Operation points in the mechanical compressor map

In the previous chapter, Figure 3.11 showed the operation map of the altitude simulator when VGTv and VGTb are kept in a constant position and only WG opening and mechanical compressor speed are modified. When the WG opens, the speed lines are more vertical. If the only actuator changed is the mechanical compressor speed, keeping WG, VGTv and VGT blades constant, operation point moves in the same line. Increasing mechanical compressor speed, decreases engine intake pressure and increases the mass flow.

These operation points can be also be represented in the mechanical compressor map, as shown in Figure 4.1. With this representation of the operation points, the different regions and limits of the altitude simulator can be deeply understood and analyzed.

On the one hand, if the WG valve closes, but the mechanical compressor speed is kept constant, the operation points move to the left, following a constant speed line in the map. This is caused by the increment of the pressure losses in the WG valve, what decreases the mechanical compressor inlet pressure, while its outlet pressure is not modified because is directly connected to the atmosphere. This leads to an increment on the pressure ratio in the mechanical compressor. Finally, as the speed in the mechanical compressor is also constant, the mass flow in the installation has to decrease.

On the other hand, when the WG is kept in a constant position and the mechanical compressor speed is increased, the operation point moves at a

constant load curve and the pressure ratio in the mechanical compressor increases. As explained before, as the outlet pressure is room pressure, this increment in the pressure ratio decreases the pressure inside the installation. With respect to the mass flow, it is also increased.

A similar analysis can be done with the overpressure operation map. When the overpressure valve opens, the back pressure decreases and consequently the mechanical compressor outlet pressure also decreases. While, the outlet pressure does not changes, because it is directly connected to the atmosphere. Therefore, the compression ratio in the mechanical compressor decreases and, as the speed is kept constant, the mass flow increases. On the other hand, when the overpressure valve is kept in a constant position and the mechanical compressor speed is increased, the operation point moves at a constant load curve and the pressure ratio in the compressor increases. This increment leads to an increment in the mechanical compressor outlet pressure. Besides, the mass flow also increases.

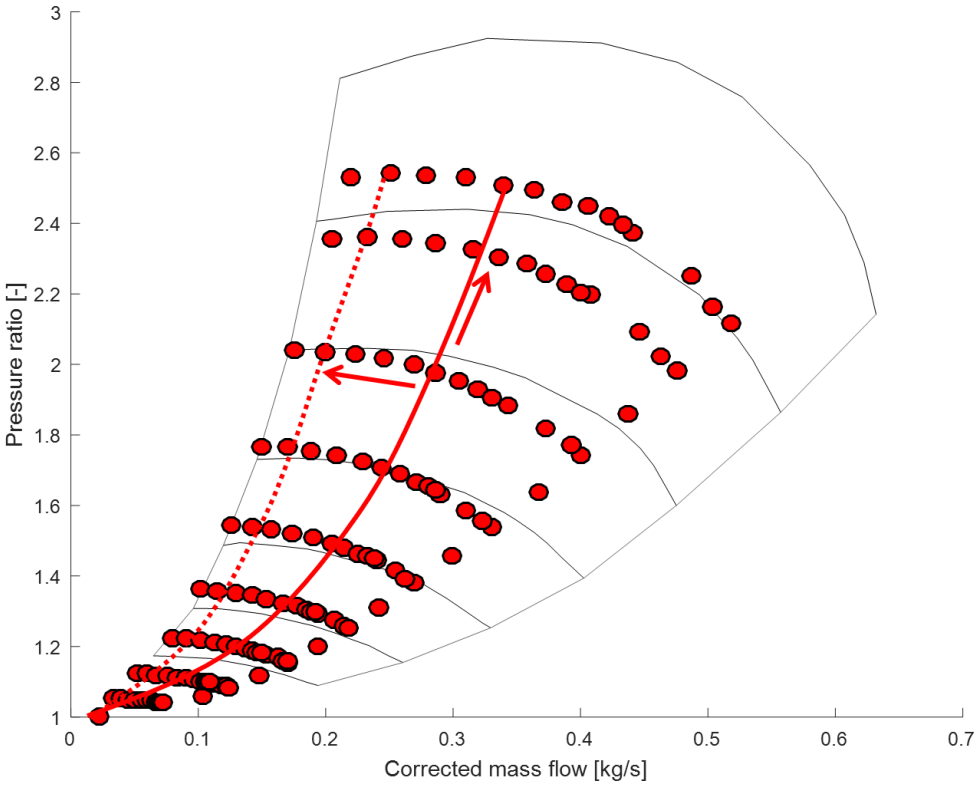

Figure 4.1 – Mechanical compressor map and load line for a given WG valve position.

The representation of the altitude simulator map in the mechanical compressor speed and the relation between them is going to be used in the following paragraphs in order to deep understand the altitude simulator operation maps and limits.

4.3 Ambient conditions effect on the operation maps

The altitude simulator has been mapped in the CMT-Motores Térmicos facilities, which are located in Valencia (Spain). This means that the ambient pressure has been around 1.013 bar, as Valencia is at sea level, and the ambient temperature has been around 25 ºC.

However, the altitude simulator can operate also in other locations at different ambient conditions. Therefore, it is important to study the effect of the ambient pressure and temperature in the operation maps, in order to be able to predict its behavior and identify any possible risk or limitation.

To do these studies, different simulations in OpenWAM have been launched. These simulations covered different pressures and temperatures. For each ambient condition, a parametric study similar to that shown in Table 3.1 and Table 3.2 has been done.

Table 4.1. Parametric studies at different ambient temperature and pressure.

VGT opening [%]	WG opening [%]
20	0
50	0
100	0
100	50
100	100

Figure 4.2 shows the results when the ambient pressure is 1013 mbar (sea level), 800 mbar (2000 m), 700 mbar (3000 m) and 500 mbar (5600 m). As can be seen, the mass flow is reduced when the altitude increases. This mass flow reduction is caused by the lower mechanical compressor inlet pressure. For a given mechanical compressor speed and inlet temperature, the mass flow through it is only dependent on its inlet and outlet pressure.

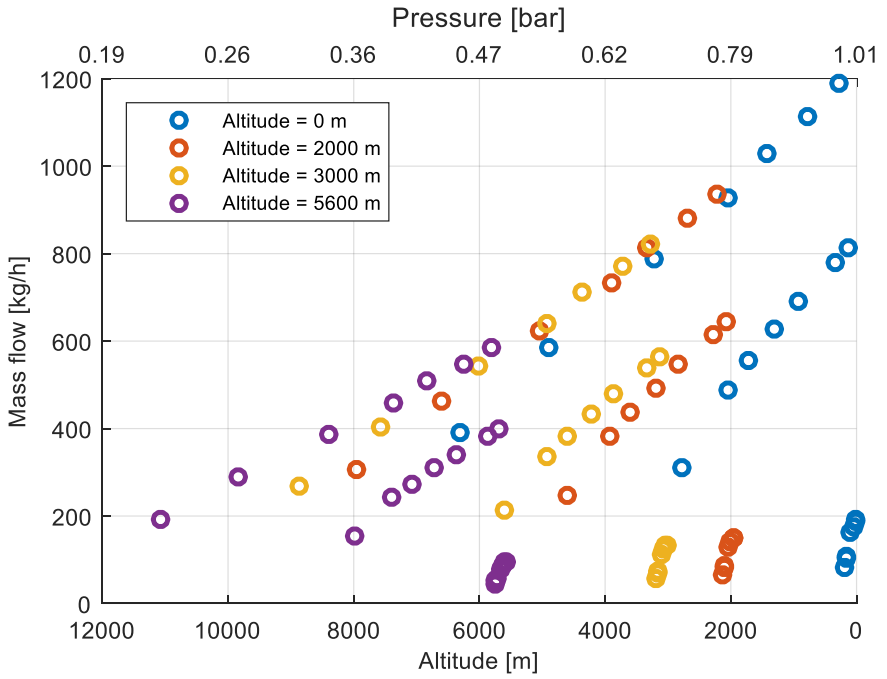

Figure 4.2 – Altitude simulator operation map at different room pressures

For example, for a given altitude simulator operation point, i.e. the mechanical compressor speed and the rest of the valves (WG, VGTv and VGT) are at given position, the engine intake pressure (p_{EI}) is only dependent on the mass flow and the pressure losses of the inlet elements (valves, VGT and cyclonic separator), following Equation (3.14).

$$p_{EI} = p_{atm} - \Delta p_{intake} \tag{4.17}$$

Where,

$$\Delta p_{intake} = \frac{1}{2} K_{intake} \rho_{atm} v_{atm}^2 \tag{4.18}$$

And,

$$\rho = \frac{p}{TR} \tag{4.19}$$

$$\rho = \frac{\dot{m}}{Q} \tag{4.20}$$

Then, the pressure losses in the exhaust line (cooler and cyclone) leads to a lower mechanical compressor inlet pressure (Equation (4.21)).

$$p_{RI} = p_{EI} - \Delta p_{exhaust} \quad (4.21)$$

Where the exhaust pressure losses ($\Delta p_{exhaust}$) can be also calculated following Equation (4.18), Equation (4.19) and Equation (4.20) for the engine intake conditions instead of the atmospheric conditions.

Then, the mechanical compressor inlet pressure is only dependent on the ambient pressure (p_{atm}) and on the pressure losses of the altitude simulator from the air filter to just upstream the mechanical compressor ($\Delta p_{exhaust}$ and Δp_{intake}).

Therefore, if the ambient pressure decreases, the mechanical compressor inlet pressure also decreases if the actuators are kept constant. Besides, the variation in the mechanical compressor inlet pressure is similar to the variation of the atmospheric pressure, as the pressure only affects the density and air velocity in the pressure losses term (Equation (4.18)), and its effect is small in comparison with the variation of the absolute pressure term, as can be seen in Figure 4.3, where the values of the K_{intake} and $K_{exhaust}$ have been obtained experimentally.

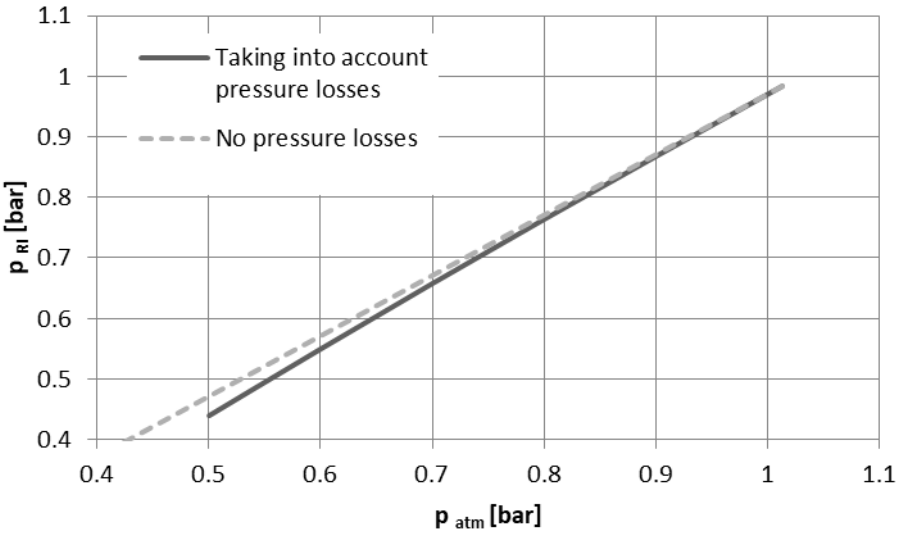

Figure 4.3 – Mechanical compressor inlet pressure (p_{RI}) with respect to the atmospheric pressure (p_{atm}) and their deviation with respect to the bisector.

Besides, the mechanical compressor outlet pressure also decreases with the ambient pressure, as is directly connected to the atmosphere.

Attending to the previous analysis, the pressure ratio in the mechanical compressor is almost constant with the altitude where it is located, for a

given position of the altitude simulator actuators. Then, as the speed of the mechanical compressor is also kept constant, this leads to a constant corrected mass flow with the altitude, according to the compressor map.

However, the real mass flow has to be corrected with the mechanical compressor inlet pressure (Equation (4.22)), which decreases with the altitude. Therefore, for a given operation point, the mass flow decreases with the altitude, with an almost linear trend.

As a summary, changing the ambient pressure where the altitude simulator is running modifies almost linearly the mechanical compressor inlet pressure. This leads to a decrease of the mass flow though the altitude simulator, if the operation point of the mechanical compressor does not change (constant speed and actuators position).

$$m_{SP} = m_{SP}^{*} \frac{p_{RI}}{\sqrt{T_{RI}}} \approx m_{SP}^{*} \frac{p_{atm}}{\sqrt{T_{RI}}} \qquad (4.22)$$

Figure 4.2 also shows the other effect of the ambient pressure in the operation range of the altitude simulator. This is the horizontal displacement of the operation map. At sea level, the dead area and the limit between vacuum and overpressure mode is located close to sea level. However, with the altitude, these limits move to the altitude of the test cell. For example, in a test cell at 2000 meters above sea level, the dead area is around 2000 meters.

With respect to the temperature range, the ambient pressure does not modify it, only moves it horizontally. Therefore, the engine intake temperature at a given operation point is the ambient temperature minus a temperature decrement, which is independent on the ambient pressure and it is only affected by the pressure ratio in the VGT.

The other variable that can be modified in the ambient condition is the temperature.

Figure 4.4 shows the effect of the ambient temperature on the operation map while the cooler water temperature it kept constant. As can be seen, the operation maps are not modified. This can be explained with an analogue analysis to the one done with the ambient pressure. The pressure losses are the only term dependent on the ambient pressure, but these are small in comparison with the ambient pressure, which is kept constant. Then, as the cooler is modifying this ambient temperature, cooling or warming it depending on the ambient and water temperature, the mechanical compressor inlet temperature is almost constant and independent of the ambient temperature. Therefore, the operation point on the mechanical compressor is also independent of the ambient temperature and the mass flow is not modified.

With respect to the temperature range, the ambient temperature does not modify it. The engine intake temperature at a given operation point is the ambient temperature minus a temperature decrement, which is independent on the ambient temperature and it is only affected by the pressure ratio in the VGT.

However, if the ambient temperature is kept constant but the cooler water temperature is modified, the mechanical compressor inlet temperature changes, what modifies the corrected speed (Equation (4.23)) and therefore the mass flow, as the corrected mass flow has changed, as can be seen in Figure 4.5.

$$N_{SP} = \frac{N_{SP}}{\sqrt{T_{RI}}} \qquad (4.23)$$

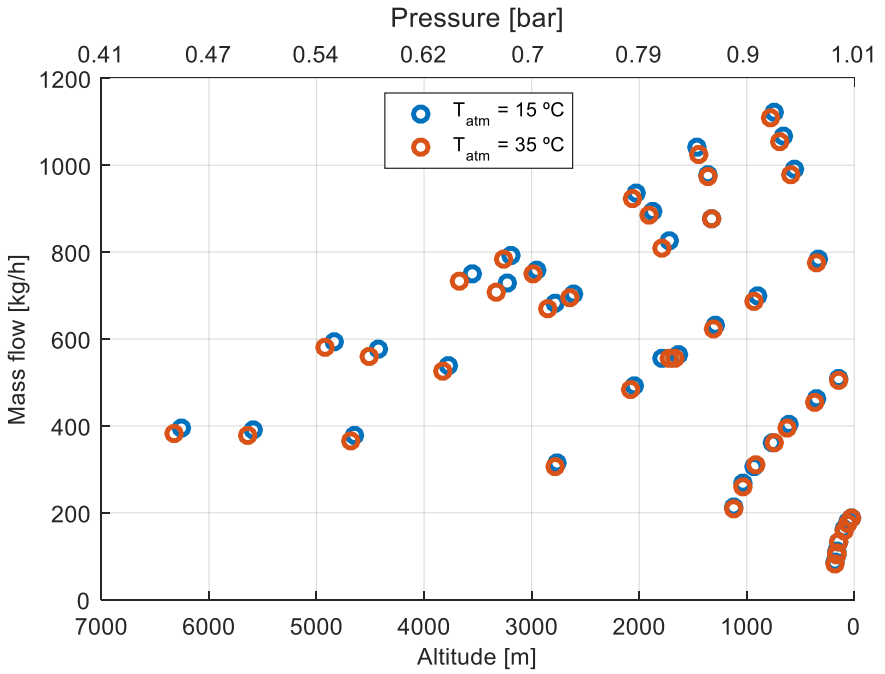

Figure 4.4 – Altitude simulator operation map at different room temperatures

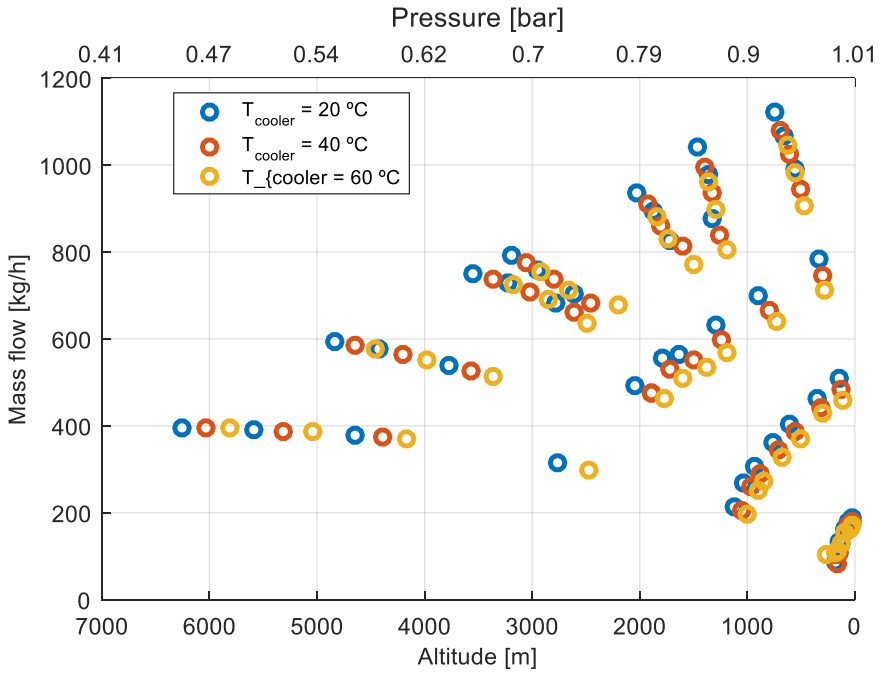

Figure 4.5 – Altitude simulator operation map at different water temperatures

4.4 Altitude simulator reduced maps

In conclusion, it could be said that the operation map of the altitude simulator represented in Figure 3.16 is a modified representation of the mechanical compressor map. Therefore, a reduced map of the altitude simulator can be obtained, analogue to the operation map of the mechanical compressor. This altitude simulator reduced map will be independent on the ambient conditions.

In the previous section, it has been shown that the ambient pressure, ambient temperature and cooler temperature affect the altitude simulator operation map, as they modify the mechanical compressor inlet conditions. For example, for a given cooler water temperature, the ambient temperature does not modify the altitude simulator operation map, as the mechanical compressor inlet conditions are kept constant, what leads to constant mechanical compressor corrected variables.

In a compressor map (Figure 4.1), in the x-axis is represented the corrected mass flow and in the y-axis is represented the pressure ratio. In the altitude simulator map, the x-axis represents the simulated pressure, which is analogue to the pressure ratio in the compressor map, because the outlet pressure is always room pressure. The y-axis in the altitude simulator map

represents the mass flow, also analogue to the reduced mass flow in a compressor map.

Therefore, also reduced variables can be used to represent the operation map of the altitude simulator.

On the one hand, the x-axis can be converted in a pressure ratio between the pressure generated in the altitude simulator and the room pressure (Equation (4.24)).

$$PR = p_{EI}/p_{Atm} \qquad (4.24)$$

As explained in Section 4.3, the mechanical compressor inlet pressure is only dependent on the engine intake pressure and the pressure losses of the exhaust line of the altitude simulator. As the exhaust line has not any active element (it is formed by the cooler and the cyclonic separator and the connection pipes), the pressure losses coefficient is constant for all the operation points. This means that for a given operation point, the engine intake pressure and the mechanical compressor inlet pressure are unique and knowing one of them, the other one can be calculated.

Analogously, the mechanical compressor outlet pressure and the ambient pressure are also unique for a given operation point, as both pressures only differ on the pressure losses between the mechanical compressor and the altitude simulator outlet.

It could be said that the engine intake pressure is a transformation of the mechanical compressor inlet pressure and that the atmospheric pressure is a transformation of the mechanical compressor outlet pressure.

On the other hand, the y-axis can by represented by the reduced mass flow following Equation (4.25). In this case, the mass flow is corrected with the mechanical compressor inlet pressure and temperature, as done in a compressor map. However, it could be also corrected with the engine intake pressure, because as has been explained is analogue to the mechanical compressor inlet pressure.

$$m^* = m\frac{\sqrt{T_{RI}}}{p_{RI}} \qquad (4.25)$$

Figure 4.6 represents the reduced operation map of the altitude simulator. The reduced map is not affected by the room pressure or temperature, as happens with a compressor map.

With respect to the temperature range map in reduced variables, the x-axis is also the pressure ratio (Equation (4.24)) and the y-axis is the temperature

variation between atmosphere and engine intake temperature, as represented in Figure 3.12.

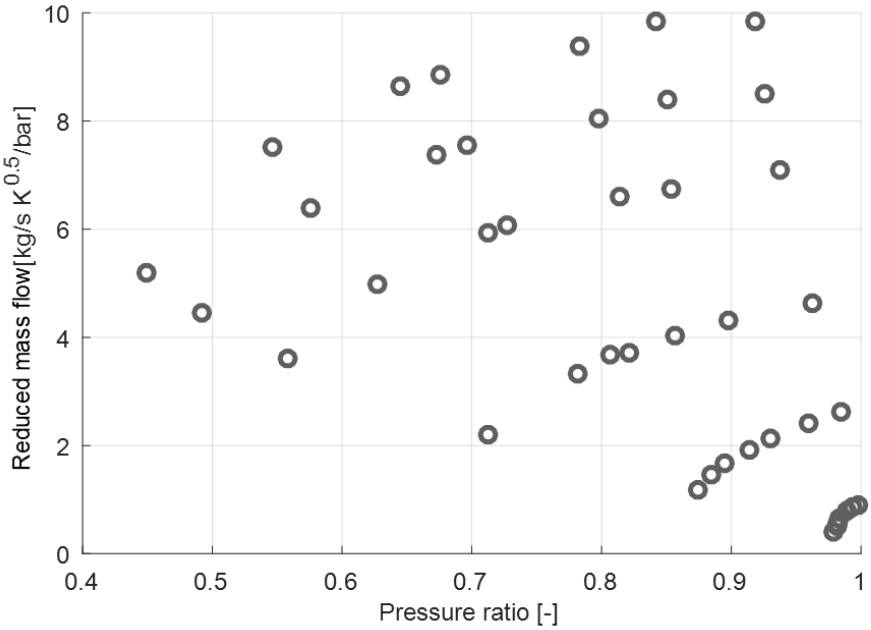

Figure 4.6 – Altitude simulator reduced operation map

4.5 Limits on the operation map of the altitude simulator

Using the analogy between the altitude simulator map and the mechanical compressor map, the limits on the operation map of the altitude simulator can be analyzed. Figure 4.7 shows the three areas in the altitude operation map that are going to be analyzed: maximum mass flow area colored in blue in Figure 4.7), maximum altitude (colored in green in Figure 4.7) and minimum mass flow (colored in red in Figure 4.7).

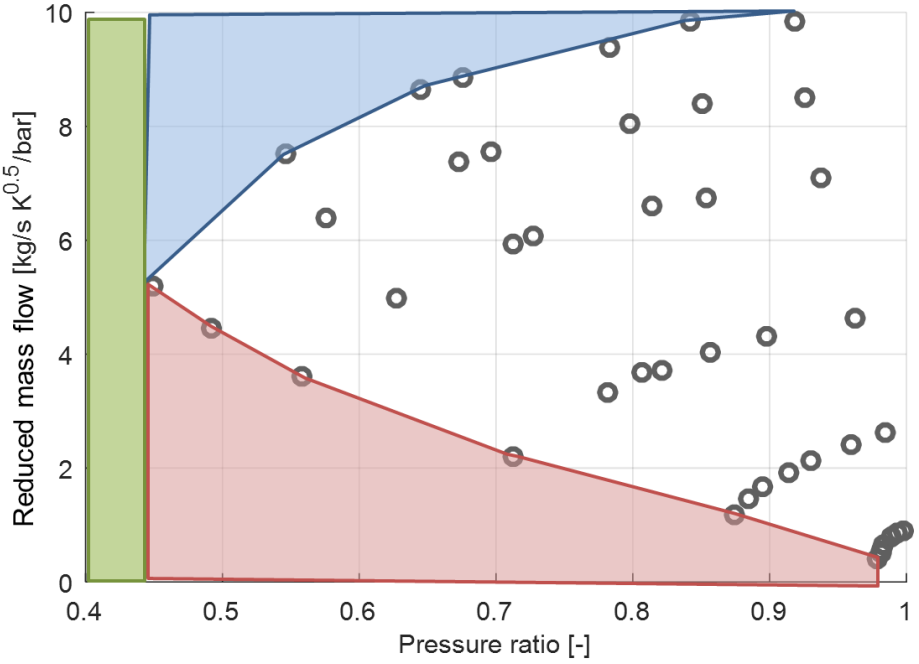

Figure 4.7 – Altitude simulator limit areas

4.5.1. Maximum mass flow area

The maximum altitude simulator mass flow is limited by the maximum mass flow that can pass through the mechanical compressor.

As explained in previous section, in vacuum mode, for a given engine intake pressure and mass flow, the mechanical compressor inlet pressure is known and only dependent on the pressure losses of the exhaust elements (Equation (4.21)).

Ideally, without any pressure losses in the exhaust line, both pressures are the same. Then, to get the potential maximum mass flow that the altitude simulator generates at each altitude, the mechanical compressor is operating in the maximum speed line and the pressure ratio is given by the corresponding pressure at each altitude and the ambient pressure. The results of these calculations are shown in Table 4.2, where the ambient pressure has been fixed in 1.013 bar.

As can be seen, the maximum mass flow decreases with the altitude. The cause is that at maximum speed, the maximum corrected mass flow sucked by the mechanical compressor is 0.63 kg/s and slightly decreases with the

altitude increase. Then, to obtain the real mass flow that the mechanical compressor is sucking, this corrected mass flow is multiplied by the mechanical compressor inlet pressure, which decreases with the altitude. Therefore, the real mass flow also decreases with the altitude.

This is the ideal case, where there aren't pressure losses in the exhaust of the altitude simulator. However, the elbows, the on/off valve, the water-to-air cooler and the cyclonic separator generate pressure losses. Minimizing the pressure losses with an improved design of these elements would lead to an increase of the maximum mass flow line.

Table 4.2. Theoretical maximum mass flow at each engine intake pressure.

P_{EI} [bar]	Mass flow [kg/h]
1	2274
0.9	2047
0.8	1820
0.7	1592
0.6	1366
0.54	1228
0.5	1137
0.4	839

The analysis in overpressure mode is analogue. For a given engine intake pressure and mass flow, the pressure at the mechanical compressor outlet is given by the pressure losses between this and the engine intake connection. Then, minimizing the pressure losses of the elements in between would increase the maximum mass flow in overpressure mode.

4.5.2. Minimum mass flow area

As can be seen in Figure 3.16 in Chapter 3, the altitude simulator minimum mass flow line corresponds to the WG and VGTb most closed positions, where the pressure losses are higher. In the mechanical compressor map, that line corresponds to the left line, close to surge limit.

In some situations, operating the altitude simulator with low mass flow is interesting. For example, if the tested engine is small, reducing the mass flow through the altitude simulator also decreases the power consumption.

However, the minimum mass flow that the altitude simulator can move is limited by the surge line of the mechanical compressor.

To calculate the minimum potential mass flow for each altitude, the same analysis than the one followed to determine the maximum mass flow area can be done. The mechanical compressor outlet pressure is given by the room pressure; and in the ideal case, the mechanical compressor inlet pressure is the same than the engine intake pressure. Then, following the surge line, Table 4.3 is obtained, where the ambient pressure has been fixed in 1.013 bar.

Table 4.3. Theoretical minimum mass flow at each engine intake pressure.

P_{EI} [bar]	Mass flow [kg/h]
1.013	0
0.9	192
0.8	242
0.7	274
0.6	288
0.54	288
0.5	284
0.4	277

The analysis in overpressure mode is analogue, but in this case the restriction in the mass flow is done by the overpressure valves closed.

4.5.3. Maximum altitude

The maximum altitude is limited by the mechanical compressor maximum pressure ratio. With an analogue analysis than the one done in the previous sections, the maximum altitude of the altitude simulator is reached at the point of maximum pressure ratio in the compressor. Looking into the compressor map given by the manufacturer (Figure 3.11), this point corresponds to a pressure ratio of 2.94. Then, following Equation (4.26) and assuming that there are not any pressure loss between the engine intake connection to the mechanical compressor and that the mechanical compressor outlet pressure is the same than the room pressure (in this example sea level pressure), the maximum engine intake pressure is 0.344 bar, which corresponds to an altitude of 8223 m. At this altitude, the altitude simulator would move 440 kg/h of mass flow.

Taking into account the pressure losses of the altitude simulator, the maximum altitude is 6900 meters above sea level.

$$\Pi_c = \frac{p_{RO}}{p_{RI}} \qquad (4.26)$$

4.6 Control strategies

One of the objectives of the altitude simulator that has been developed in this thesis is to make it simple to operate. The final user should be able to choose the desired setpoints of altitude, temperature and mass flow and the system should provide automatically those conditions at the engine intake and keep them constant during the entire test, even during engine transients. To achieve this, it has been necessary to understand the physics behind the altitude simulator and to explore different approaches to optimize its behavior, i.e. to reach fast the desired setpoints and to keep them constant during its operation with an engine.

In the following sections, it will be detailed how every actuator affects the main variables and how the control has been designed.

4.6.1. Control variables and actuators

On the one hand, the main control variables in the altitude simulator are pressure, mass flow and temperature at the engine intake. In order of importance, pressure is the most important variable, followed by the mass flow and then the temperature.

On the other hand, the altitude simulator has four actuators that affects the main variables (WG, VGTv, VGTb and mechanical compressor speed) in vacuum mode and other four actuators (OPEx1, OPEx2, cooler valve and mechanical compressor speed) in overpressure mode.

The objective of the altitude simulator automatic control is to control the three variables with the different actuators in order to reach a given operation point by the operator of the system.

Vacuum operation

The engine intake pressure is the more important variable. Its value should be reached fast, but also its variations should be small when the setpoint altitude has been reached and the engine is operating in a dynamic cycle. Also, the actuator has to be able to modify the engine intake pressure value from room pressure up to 0.54 bar (which corresponds to an altitude of 5000 m according to ISA).

The VGTv and VGTb are not suitable actuators to control pressure, because its pressure control range is limited: when they are fully closed, if the WG

valve is fully open, the engine intake pressure is very similar to the atmospheric pressure. The mechanical compressor speed has also small influence in pressure when the WG valve is fully open.

With respect to the WG, when it is fully open, as it generates low pressure losses, engine intake pressure is very similar to atmospheric pressure. When the WG is fully closed, the intake air has to go through the VGTv, VGTb and cyclonic separator, which generates high pressure losses. Therefore, even with the VGTv and VGTb fully open, the engine intake pressure is much lower than atmospheric pressure.

For those reasons, the WG is chosen to control the pressure. Closing the WG decreases the pressure.

Then, the mechanical compressor controls the mass flow, because its effect in the mass flow is more direct than its effect in the temperature (since pressure has been already decided to be controlled by WG valve). Increasing the mechanical compressor speed directly increases the mass flow. However, increasing the mechanical compressor speed do not directly affects the temperature, because the temperature is directly related with the mass flow ratio between the VGTv and the WG.

Finally, the temperature is controlled by the VGTv and VGTb. Opening the VGTv and VGTb decreases the temperature. This temperature control mechanism is not as direct as the mass flow and pressure control. The mechanism is as follow: if the engine intake temperature needs to be decreased, the VGTb and VGTv open. Then, the intake air has lower pressure losses and the engine intake pressure increases. Finally, to compensate it, the WG closes. Once the system is stable again, the mass flow through the VGT has been increased but the engine intake pressure has not been modified. Therefore, the engine intake temperature is lower.

Figure 4.8 represents these controls, where in the x-axis is represented the controlled variable and in the y-axis is represented the actuator action.

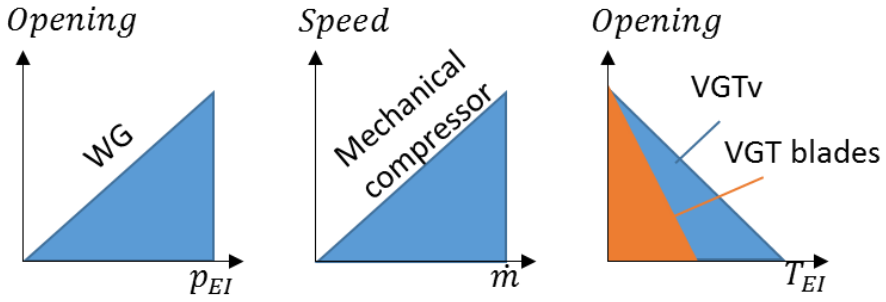

Figure 4.8 – Main variables control strategies in vacuum mode

Overpressure operation

In overpressure operation, the three main variables have to be controlled with the mechanical compressor speed, the opening of the water valve of the water-to-air cooler and the opening of both overpressure valves.

As in vacuum operation, the mass flow is controlled by the mechanical compressor speed. Increasing its speed, mass flow is increased, but also pressure for a given loading of the flow circuit.

The water valve controls the engine intake temperature, also because it has not influence in the pressure. The atmospheric air is warmed up in the mechanical compressor. Then, it is cooled down in the water-to-air cooler. Its cooling power is controlled by the water valve position.

Finally, the pressure is controlled by the position of both overpressure valves. Opening its position decreases the engine intake pressure. When both valves are fully open, the engine intake pressure is almost the same than room pressure.

Analogue to Figure 4.8, Figure 4.9 represents these controls, where in the x-axis is represented the controlled variable and in the y-axis is represented the actuator action.

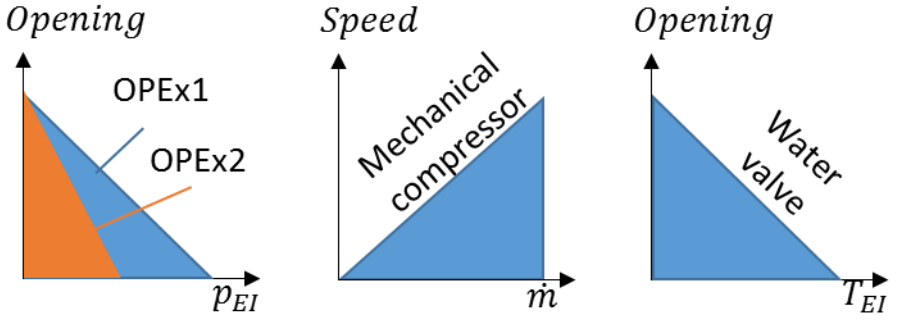

Figure 4.9 – Main variables control strategies in overpressure mode

4.6.2. Control by reduced maps

Vacuum mode

Once the main variables to be controlled are assigned to the different actuators, the next step is to define how to operate them to achieve the setpoints.

A control done just by PIDs presents some problems. First of all, the time to reach the desired setpoint can be too long. For example, if the altitude simulator is stopped, the time for the mechanical compressor to reach the

target speed to get the setpoint mass flow can take too long. If the speed of the PID is increased, then might appear problems with the stability of the system once the setpoints are reached and the system can overreact to small pressure oscillations produced by the engine. Finally, depending on the setpoints, the mechanical compressor has risks to go into surge and being broken. For example, for a high altitude and low mass flow setpoint, the pressure PID would close very fast the WG valve, as the setpoint pressure is very far from the ambient pressure. However, if the mechanical compressor speed would not be reduced so fast (because the initial mass flow setpoint was high); this could lead the mechanical compressor going transitory into surge, because the WG valve is too close (mass flow too low) and the mechanical compressor speed is still too high, providing a small surge margin.

To solve these problems, a different approach to control the altitude simulator is needed. In Section 4.4, in the paragraph named "Reduced operation map", the altitude simulator map represented with the reduced variables is described (Figure 4.6), similarly to the representation of a turbo compressor map. Therefore, the altitude simulator can be mapped at different WG positions and mechanical compressor speeds, creating a map where each pressure ratio and reduced mass flow can be obtained only with one WG position and mechanical compressor speed. It would lead to the following control by reduced maps:

1. The user chooses the setpoint pressure, mass flow and temperature.
2. With these setpoints, the system calculates the reduced setpoints, following Equation (4.27) and Equation (4.28) and represented with a star in Figure 4.10.

$$PR_{SP} = p_{SP}/p_{Atm} \tag{4.27}$$

$$m_{SP}{}^{*} = m_{SP}\frac{\sqrt{T_{RI}}}{p_{RI}} \tag{4.28}$$

3. Then, the reduced setpoint is compared with the mapped points at known WG position and mechanical compressor speed. The system calculates which of the points of the map is closer to the reduced setpoint, circled in Figure 4.10.
4. Finally, the system increases or reduces gradually the speed of the mechanical compressor up to the speed of the closer point and closes or opens the WG valve up to the position of the WG of the closed point.

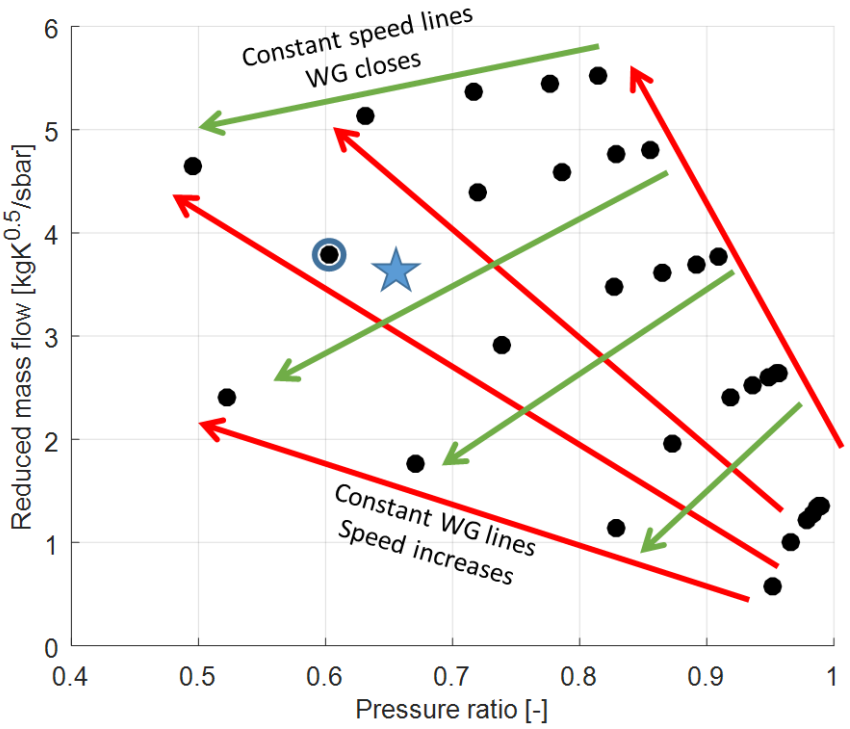

Figure 4.10 – Reduced map point for different WG openings and mechanical compressor speeds for a given VGTv and VGT position

After that, the engine intake pressure and mass flow is close to the setpoints. The final tuning of the pressure and mass flow is adjusted with PIDs.

With respect to the VGTv and VGTb control, it is not necessary to define its position with maps, because their position have not a big influence in the pressure or mass flow, as the WG valve diameter is much bigger, and including the temperature would increase the number of maps exponentially, as it would be necessary a map for each position of the VGTv and VGTb.

Overpressure mode

In overpressure mode, a similar control approach has been followed. In this case, there are two valves for the pressure control. On the one hand, a big butterfly valve that provides low pressure losses for altitudes close to the room altitude, but with not very precise pressure control. On the other hand, a small control valve that generates big pressure losses but fine pressure control.

The objective of the control is to be able to fine control the pressure in all the altitudes range. The big butterfly valve cannot be constantly trying to control

the pressure with a PID, because its control over pressure is rough and it has big peaks and oscillations. Therefore, the position of the butterfly valve has to change as little as possible.

Therefore, the reduced maps in overpressure are obtained by changing the mechanical compressor speed and the position of the big butterfly valve, with the small control valve at 50% of opening. With that, the position of the butterfly valve is previously defined by the setpoints and the fine control of pressure is done by the small control valve. Just in case the control valve is fully open or closed, the butterfly valve changes its position until the control valve can control again the pressure.

4.6.3. Other controls

Besides the control of the three main variables, the altitude simulator has to control other variables for the safety operation of its elements.

Mechanical compressor temperature

The maximum compressor outlet temperature is 200 ºC. In order to protect it from breaking, that outlet temperature is controlled by the cooler water valve in vacuum mode. To decrease the outlet compressor temperature, the valve in the cooler opens, this decreases the inlet and outlet mechanical compressor temperature. However, of decreasing too much, the exhaust gases temperature can generate a lot of condensates in the cyclonic separator, decreasing the testing time available before having to empty it. For that reason, the cooler water valve also controls the inlet mechanical compressor temperature to be at 50 ºC. Both controls are managed at the same time with a PID which controls the inlet compressor temperature following the Equation (4.29).

$$T_{RI,SP} = \max(50, 50 + T_{RI} - 150)\ °C \qquad (4.29)$$

In overpressure mode there isn't any control in the compressor outlet or inlet temperature, because the inlet temperature is room temperature, which is always low in comparison with the exhaust gases temperature that is sucking the compressor in vacuum mode.

Turbocharger oil circuit

As explained in Section 3.2.2 of the Chapter 3, the turbocharger has its own oil circuit with an oil pump. This oil pump has to be turned on only when the VGT is spinning and has to be turned off in the rest of the cases. Therefore, the oil pump is only working when the altitude simulator is in vacuum mode and the VGTv is open.

4.6.4. Operation mode changes

As has been explained in Section 3.2 of Chapter 3, the altitude simulator can operate in two different modes, depending on the test bed altitude and the simulated altitude. If the simulated altitude is higher than the test bed altitude, then the altitude installation operates in Vacuum Mode. When the simulated altitude is lower than the test bed altitude, it operates in Overpressure Mode.

To change from one mode to other, it is needed to close some valves and to open others, following a series of steps. Table 4.4 summarizes the position of the valves depending on the operation mode.

Table 4.4. Valves position depending on the operation mode

Valve name	*Valve number in Figure 3.29*	*Vacuum mode*	*Overpressure mode*
WG	2	Controlled	Closed
VGTv	3	Controlled	Closed
VGTb	4	Controlled	Closed
OPEx1	12	Closed	Controls
OPEx2	13	Closed	Controls
V_VGT_Ro	15	Closed	Open
V_Coo_Sep	16	Open	Closed
V_Ro_Ex	20	Open	Closed
V_Ro_Coo	21	Closed	Open

However, the valves speed to close or open can be different from one model to other. For example, the WG valve is DN150 valve, while the VGTv is DN80. Also the on/off valves reaction time is slower than the one from the control valves. For that reason, the changes between vacuum and overpressure cannot be done just in one step changing the position of all the valves. Besides, the altitude cannot suddenly change from a big altitude to a big overpressure, and vice versa. It has to be done gradually, ensuring a safe operation of the altitude simulator and controlling the pressure inside installation.

Taking all of this into account, the steps followed to change from vacuum to overpressure are as follows (Figure 4.11):

1. The system detects that the new setpoint has to be reached in overpressure mode by comparing the atmospheric pressure with the new setpoint pressure.

2. The system freezes all the PIDs.
3. Then, the WG valve fully opens with a ramp.
4. Once the WG valve is fully open (being therefore the engine intake pressure similar to the room pressure), the on/off valves switch their position, i.e. the on/off valves that are closed, opens; and vice versa. Also the OPEx2 valve (butterfly valves) opens. In this step the system waits 5 seconds to stabilize the pressure, slightly higher than room pressure.
5. Then, the WG, VGTv and VGTb valves fully close.

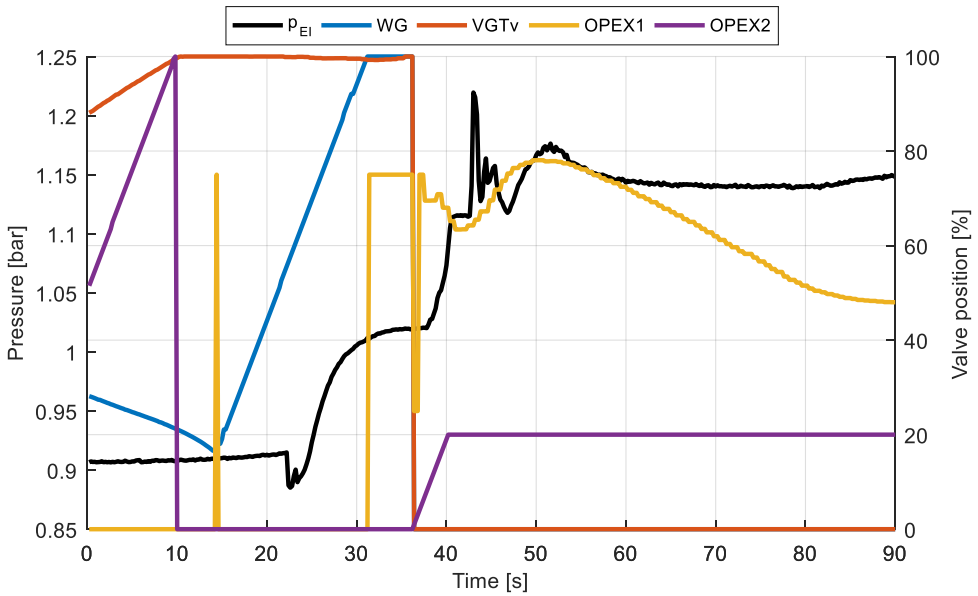

Figure 4.11 – Vacuum to overpressure operation mode change

In this step, the system is already in overpressure mode. The OPEx2 valve and the mechanical compressor speed go to the value defined by the reduced map control.

If the altitude simulator has to change from overpressure to vacuum mode, the steps are as follow (Figure 4.12):

1. The system detects that the new setpoint has to be reached in vacuum mode by comparing the atmospheric pressure with the new setpoint pressure.
2. The system freezes all the PIDs.

3. Then, the OPEx2 valve fully opens with a ramp.
4. Once the OPEx2 valve is fully open (being therefore the engine intake pressure similar to the room pressure), the on/off valves switches its position, i.e. the on/off valves that are closed, opens; and vice versa. Also the WG, VGTv and VGTb valves open. At the same time, the OPEx1 and OPEx2 valves fully close. In this step the system waits 5 seconds to stabilize the pressure, slightly lower than room pressure.

In this step, the system is already in vacuum mode. The WG valve and the mechanical compressor speed go to the value defined by the reduced map control.

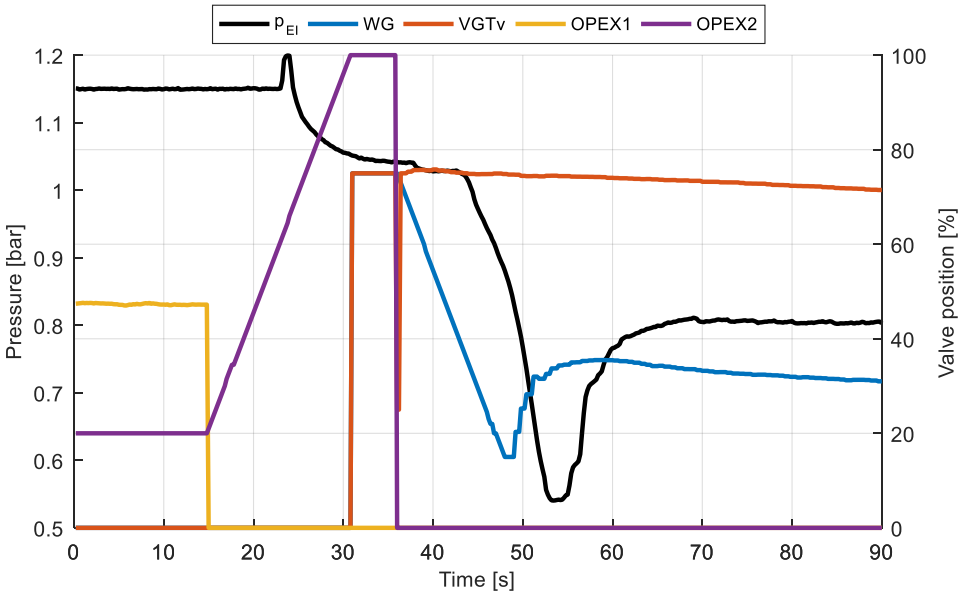

Figure 4.12 – Overpressure to vacuum operation mode change

4.6.5. Dynamic operation

The previous sections describe how the altitude simulator operates at a constant altitude. However, real driving also includes altitude changes, for example when ascending a mountain. This means that the pressure changes with time. As has been explained, the altitude simulator control has two parts. The first one is a ramp approximation to the setpoint pressure and mass flow with the use of reduced maps. The second one is the final adjustment to the setpoints with different PIDs.

When the pressure and temperature setpoints are slightly changed with the time, as done during the dynamic operation, the ramp approximation cannot be done, as it would introduce pressure oscillations when the actuators move to the close mapped point.

With respect to the PIDs, the setpoint pressure and temperature have to be updated with each new setpoint introduced during the dynamic operation. As the setpoint variation when ascend or descend a mountain is slow, the new setpoint is very close to the current setpoint and the altitude simulator components are not in risk, such as surge in the mechanical compressor.

Figure 4.13 and Figure 4.14 show two dynamic cycles with the altitude simulator. In both cases, the altitude simulator is operating without an engine or any other system connected, being the connections closed and all the air bypassed through the dilution pipe.

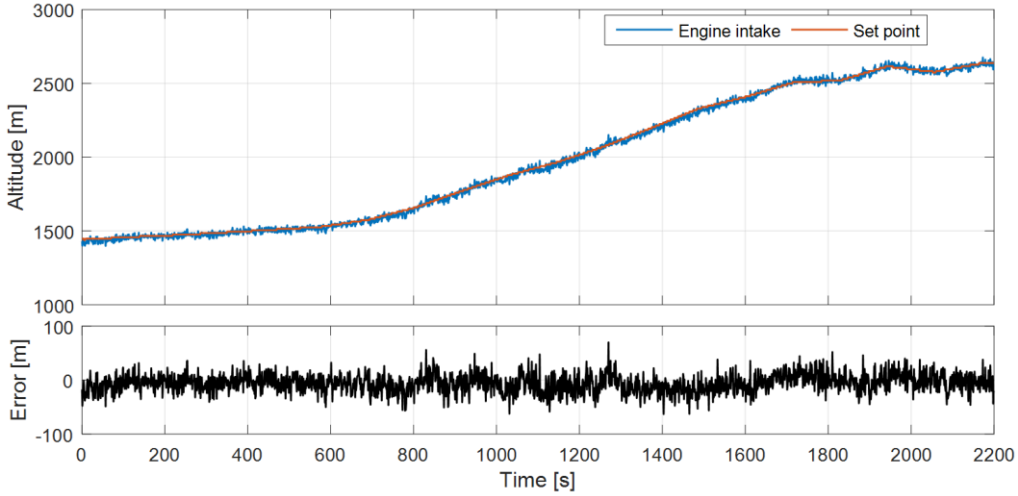

Figure 4.13 – Deviation of the pressure at the engine intake during dynamic altitude changes. Simulation of an ascend to Los Lagos de Covadonga mountain (Asturias, Spain)

Figure 4.13 shows the altitude profile of a very famous mountain in Spain, with big slopes and long distance, named Los Lagos de Covadonga in Asturias [1]. Its mean slope is 6.3%, being the maximum 13.2% (equivalent to 0.95 meters of vertical ascension per second). The starting point of the altitude has been shifted in order to avoid the dead area of the altitude simulator close to room pressure. The results show that the maximum altitude error during the complete ascension is lower than 100 m.

Figure 4.14 show another dynamic cycle with the altitude simulator. In this case, the generated pressure has been changed from 1.25 bar (-1800 meters below sea level) to 0.54 bar (5000 meters of altitude) and again to 1.25 bar in

3500 s. This is equivalent to a slope of 20%, with the vehicle speed at 70 km/h and 3.88 meters of vertical ascension per second. This is a very aggressive ascension, probably unrealistic, but has been used to study the limits of the altitude simulator dynamic mode. However, the results show also small pressure error (lower than 20 mbar) for all the altitude range, with only two areas with higher error, corresponding to the areas where the operation mode changes from overpressure to vacuum (between second 500 sec. and 1000 sec.) and from vacuum to overpressure (between second 3000 sec. and 3500 sec.) This error corresponds to the dead area close to the room pressure, and the oscillations created by the change of the position of the different valves.

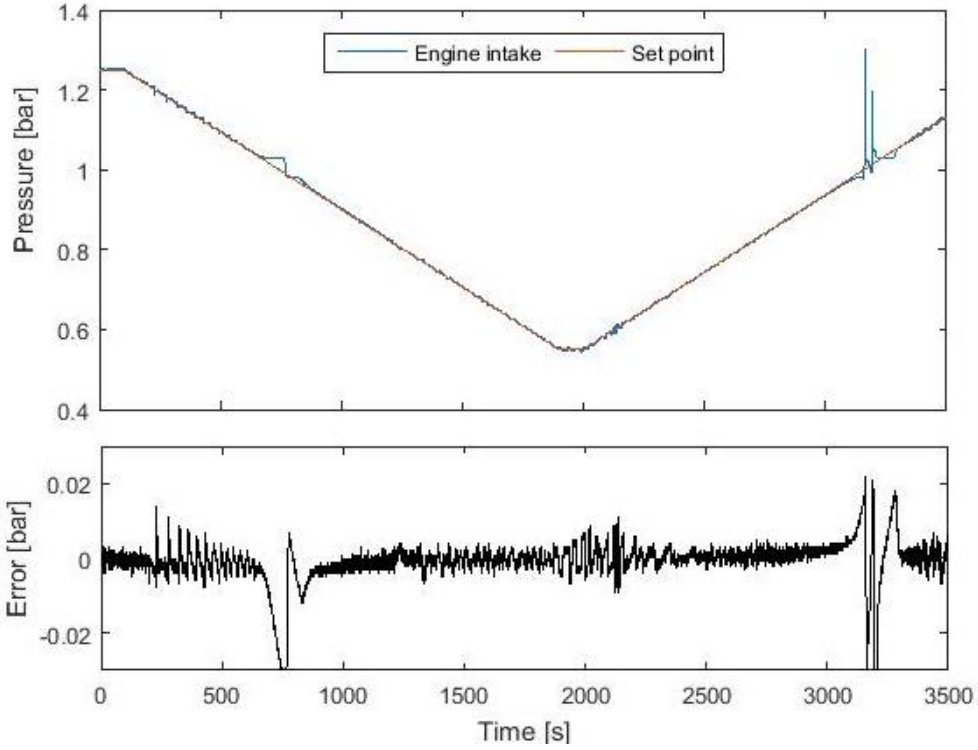

Figure 4.14 – Deviation of the pressure at the engine intake during dynamic altitude changes, with changes in the operation mode from overpressure to vacuum, and vice versa

4.7 Altitude simulator operation

The altitude simulator described in this work, as any other equipment, has its own way to be operated when installed in a test cell. There is list of things to be done and to take into account before being able to test a car or an engine with the altitude simulator.

In this section, all the requirements needed to operate the altitude simulator properly are detailed.

4.7.1. Interfaces

The altitude simulator needs some supplies from the test cell to operate.

Power

The main source of power consumption is the variable-frequency drive, required to move the electric motor coupled to the mechanical compressor. The rest of the equipment's power consumption is much lower in comparison.

The maximum power consumption is 45 kW and the connection is through a three-phase connection, with neutral and ground connection (3P+N+E 400 V).

Water

The water is used in the altitude simulator as a cooling fluid in the water-to-air cooler to cool down the exhaust gases, in the oil-to-air cooler in the mechanical compressor oil circuit and in the external jacket of the mechanical compressor for a better heat dissipation.

The cooling flow rate is 15 m^3/h and its inlet temperature is around 20 ºC. If the water temperature is lower, it will generate more condensates in the cyclonic separator that is just downstream the cooler, if the temperature is higher, a higher flow rate will be needed and the minimum temperature in overpressure mode will be limited, as the engine intake temperature is controlled by the cooler.

The altitude simulator is connected to the water supply by means of two threaded ball valve DN 50, one for the inlet and other for the outlet.

The position of the water connections is shown in Figure 4.15 and pointed with the number 6.

Pressurized air

All the valves of the altitude simulator are electro-pneumatic. Therefore, they need pressurized air to be moved. The air needed to move them is not a constant air flow, as it is used only to pressurize the actuator diaphragm.

The pressurized air has to be between 4 and 6 bar and is connected to the altitude simulator by means of a threaded ball valve DN15.

The position of the pressurized air is shown in Figure 4.15 and pointed with the number 5.

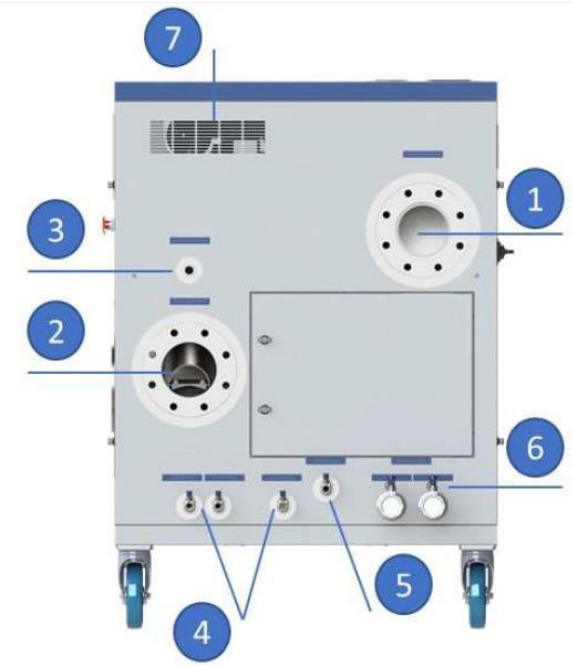

Figure 4.15 – Altitude simulator back frame with all the mechanical connections numbered

Emergency stop

As the altitude simulator will operate inside a test cell, it is necessary to have an external emergency stop connected to the test cell or in the operator desk, in order to stop the system in case any problem happens.

This emergency stop is connected by means of a DIN 8-pole circular connector (SV60 [cable] & KFV60 [panel]).

Remote control

The altitude simulator has a touch screen in one side. With that touch screen, the altitude simulator can be completely managed. However, when it is operating inside the test cell, it has to be operated from the control room. The altitude simulator has two different connections to be operated from an external PC. On the one hand, it can be operated by means of an Ethernet cable and installing a remote desktop from the touch screen manufacturer webpage in the PC. On the other hand, it can be controlled by means of an EtherCAT connection. If the connection is done by Ethernet, the way to operate the altitude simulator is the same than with the touch screen, as the screen shown in the PC is the same than in the touch screen. If the connection is done by EtherCAT, it is necessary to integrate the altitude simulator variables and controls in the control software of the test bench.

This solution takes more time and effort, but allows the altitude simulator control to be integrated with the rest of the systems in the test cell.

Engine connections

The altitude simulator has three different connections to the engine. All these connections ensure that all the elements of the engine are at the desired pressure during the test. Figure 4.15 shows the position of the different connections to the engine in the altitude simulator front.

Engine intake

The altitude simulator is connected to the engine intake through a DN150 flange. This connection feeds the engine with its necessary mass flow at the setpoint pressure.

On the one side, when an engine operates at high altitude, the pressure in the airbox is the same than the ambient pressure. On the other side, when an engine is operating with the altitude simulator, the airbox is connected through a pipe to the altitude simulator, where it is the simulated atmosphere. If the connection pipe is too long or the diameter is too small, the pressure losses through it will be too high and the pressure at the airbox will be different depending on the operation point, as the pressure losses are related with the mass flow, and its pressure lower than the setpoint pressure. Therefore, the real altitude in the engine will be higher than expected and will change with the engine load. For that reason, it is important to reduce the pressure losses in this connection to reproduce as accurate as possible a real atmosphere, with short pipes and big diameters.

The position of the engine intake connection is shown in Figure 4.15 and pointed with the number 1.

Engine exhaust

The altitude simulator is connected to the engine exhaust through a DN150 flange. This connection sucks the engine exhaust gases at the setpoint pressure. For the same reason given with the engine intake connection, it is important to reduce the pressure losses in this connection to reproduce as accurate as possible a real atmosphere, with short pipes and big diameters.

The position of the engine intake connection is shown in Figure 4.15 and pointed with the number 2.

Engine sump

The blow-by connects the engine sump to the compressor inlet. This connection is used to evacuate the exhaust gas and oil filtered from the combustion chamber through piston rings. Without the blow-by connection,

the sump would pressurized and these pollutants would go to the atmosphere [2].

When the altitude simulator is operating, the engine sump has to be also in vacuum. In some engines, the blow-by connection might be too small to evacuate the exhaust gas in the sump, when the engine is operating in altitude, being the ambient pressure at room pressure. If that happens, the sump pressurizes, even with the air that could come into the sump from the room pressure atmosphere through the crankshaft retainers. If crank case is pressurized, then high quantity of oil mist is sucked by the compressor and burned in the engine with abnormal oil consumption and quite evident white smoke emissions.

To ensure that the engine sump is at the same pressure than the engine intake, the altitude simulator has a connection, different than the engine intake and exhaust connection, but at the same simulated pressure. This connection, as explained before, is not always needed, only when the blow-by connection of the tested engine does not operates properly and the sump pressure increases.

The position of the engine intake connection is shown in Figure 4.15 and pointed with the number 3.

Other connections

There are some other elements in the car that have to be connected to the simulated pressure to reproduce real altitude conditions. However, not all the cars have these connections.

Some ECUs have an atmospheric pressure sensor [3]. If the car is operating with the altitude simulator at a given altitude, but the pressure sensor of the ECU is measuring a different pressure, it can think that something wrong is happening and it can go into a safety operation mode to protect the engine elements. To solve this problem, the ECU pressure sensor has to be at the same pressure than the rest of the engine. It can be done by encapsulating the sensor and connecting it to the engine intake or to the engine sump connection of the altitude simulator.

Also if open ECU is available and constant altitude wish to be simulated, is possible tricking the sensor read, by changing it to the desired altitude to be simulated.

Also, some cars have a connection to the atmosphere in the fuel canister [4]. This connection has to be also encapsulated and connected to the engine intake or altitude simulator sump connection.

4.7.2. Engine modifications

When a car is running in altitude, the air that surrounds the engine is at the same pressure than the engine intake and exhaust air. However, when a vehicle or an engine is operating with the altitude simulator, the surrounding air is at a different pressure than the air inside the engine intake and exhaust. For example, when the test bench is at sea level (which corresponds to a pressure of 1.013 bar) and the altitude simulator is generating an atmosphere at 1000 m of altitude above sea level, the pressure inside the engine is 0.9 bar. This pressure difference can make some soft ducts to collapse, such as compressor inlet or compressor outlet pipes. These pipes have to be rigidized.

Also, this pressure difference can generate some air leaks, mainly in the airbox that is not sufficiently airtight, and have to be fixed. The airbox, or any other element that can generate leaks, has to be sealed. Otherwise system will consume more power to cope with air leakages. In the limit, if leakages are huge, the system performance will be reduced up to the level that set points cannot be achieved.

4.7.3. User interface description

The altitude simulator can be controlled from the touch screen (or from the PC with the remote desktop), as explained in Section 4.7. The user interface has been designed and elaborated along this thesis for HORIBA. The interface is accessible through the touch screen and it has different screens, which at the same time are divided in different boxes to show all the information and to allow a complete interaction with the different actuators.

The interface has three different screens, which will be described in detail in the following paragraphs.

Main Screen

Figure 4.16 shows the main screen of the altitude simulator touch screen. It is divided in seven main boxes, numbered in the figure.

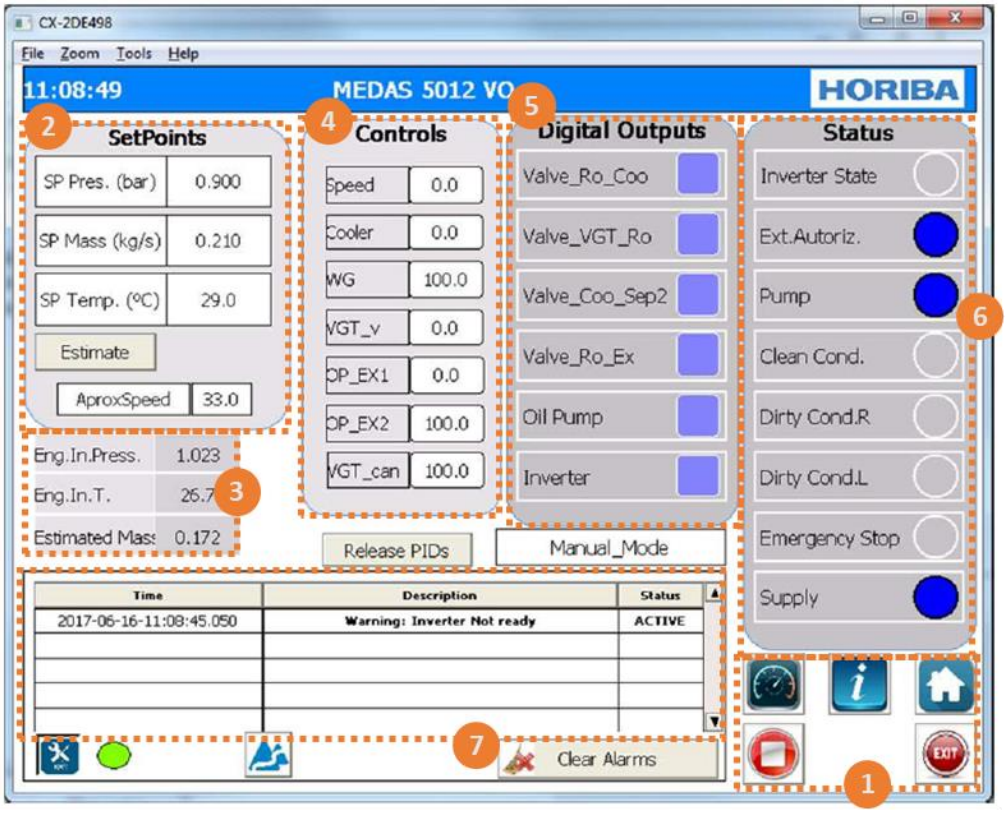

Figure 4.16 – Main screen of the altitude simulator touch screen

Operation box (number 1 in Figure 4.16)

This box contains the buttons to change between the different screens, to start the altitude simulator and to stop it. Figure 4.17 shows the different buttons of the operation box in detail.

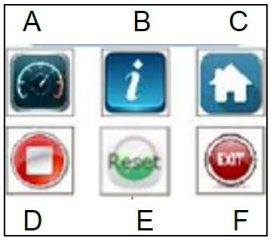

Figure 4.17 – Operation box in the main screen of the altitude simulator touch screen

- A: When pressing this button, the Sensors Screen is shown.
- B: When pressing this button, the SCADA Screen is shown.

- C: When pressing this button, the Main Screen is shown.
- D: When pressing this button, the altitude simulator stops. This is the button to stop the altitude simulator normally.
- E: When pressing this button, the power elements of the altitude simulator (variable-frequency drive) are turned on.
- F: When pressing this button, the software is closed. This button has to be pressed always before switching off the power from the altitude simulator.

Setpoints box (number 2 in Figure 4.16)

This box contains the information of the current setpoints values for the three control variables (engine intake pressure, engine intake temperature and altitude simulator mass flow). Its value can be also modified by pressing in the current value.

Once desired setpoints are chosen, the user has to press the estimate button, so the system can calculate the closest point in the reduced map. After that, the user can press the run button and the system automatically will reach the setpoint values.

Main variables value box (number 3 in Figure 4.16)

This information box contains the current value of the three main control variables in order to compare it with the setpoint value.

Analogue actuators box (number 4 in Figure 4.16)

The analogue actuators box shows the analogue actuators of the altitude simulator. The value of each actuator can be also changed. The name of the different actuators are:

- Speed: corresponds to the speed of the mechanical compressor, being 0% when it is fully stopped and 100% when it is operating at its maximum speed.
- Cooler: corresponds to the opening position of the water-to-air cooler, being 0% when the valve is fully closed and 100% when it is fully open.
- WG: corresponds to the opening position of the Waste-Gate valve, being 0% when the valve is fully closed and 100% when it is fully open.
- VGT_V: corresponds to the opening position of the VGTv valve, being 0% when the valve is fully closed and 100% when it is fully open.

- OP_Ex1: corresponds to the opening position of the OPEx1 valve, being 0% when the valve is fully closed and 100% when it is fully open.
- OP_Ex2: corresponds to the opening position of the OPEx2 valve, being 0% when the valve is fully closed and 100% when it is fully open.
- VGT_can: corresponds to the blades position of the VGTb, being 0% when the blades are more open and 100% when they are more closed.

Digital actuators box (number 5 in Figure 4.16)

The digital actuators box shows the digital actuators of the altitude simulator. The value of each actuator can be also changed.

- Valve_Ro_Coo: corresponds to the on/off valve that connects the mechanical compressor outlet with the cooler. It is a normally open valve, therefore, when the light of the box next to the valve is glowing, means that the valve is closed.
- Valve_VGT_RO: corresponds to the on/off valve that connects the VGT outlet with the mechanical compressor inlet. It is a normally open valve, therefore, when the light of the box next to the valve is glowing, means that the valve is closed.
- Valve_Coo_Sep2: corresponds to the on/off valve that connects the water-to-air cooler outlet with the cyclonic separator just upstream the mechanical compressor. It is a normally open valve, therefore, when the light of the box next to the valve is glowing, means that the valve is closed.
- Valve_Ro_Ex: corresponds to the on/off valve that connects the mechanical compressor outlet with altitude simulator exhaust. It is a normally open valve, therefore, when the light of the box next to the valve is glowing, means that the valve is closed.
- Oil pump: corresponds to the bit that turns on the turbocharger oil pump. When pressing this button, the oil pump starts to turn immediately.
- Inverter: corresponds to the bit that powers on the inverter. When pressing this button, the electric motor do not turns; it is only feeding with power to the variable-frequency drive.

Status box (number 6 in Figure 4.16)

The status box shows all the digital inputs of the altitude simulator. It is an informative panel that shows the status of different sensors and elements in the system.

- Inverter state: ON means electric power supply to the variable-frequency drive.
- Ext. Autoriz.: ON means that there isn't any external signal from the test cell avoiding the altitude simulator to be started. For example, if the test cell has a sensor avoiding the altitude simulator to be started.
- Pump: ON means that the turbocharger oil pump has power connection.
- Clean Cond.: ON means that the clean condensates separator (downstream VGT) is full and needs to be emptied.
- Dirty Cond. R.: ON means that dirty condensates (right one) is full and needs to be emptied.
- Dirty Cond. L.: ON means that dirty condensates (right one) is full and needs to be emptied.
- Emergency Stop: ON means that the emergency stop has been pressed.
- Supply: ON means that the altitude simulator is connected to the electric power.

Alarm box (number 7 in Figure 4.16)

The alarm box is an informative panel indicating any warning or error in the altitude simulator. It also indicates if the alarm is currently active or not. The inactive alarms can be removed by pressing the "Clear Alarms" button. There are two kind of alarms:

- Warning: there alarms are not critical for the altitude simulator integrity and only informative. For example, when the deposits of the cyclonic separators are full.
- Error: there alarms are critical for the altitude simulator. When any error happens, the altitude simulator automatically stops and cannot be turned on again until the error disappears. For example, if the outlet mechanical compressor temperature is too high.

Other elements in the Main Screen

There are also some other buttons and elements in the Main Screen that are not in boxes. These is the case of:

- Language menu: by pressing in the top left part of the touch screen (above the setpoints box, where is the current hour), the altitude installation language interface can be changed.
- User level menu: by pressing in the top right part of the touch screen (above the status box), the user level can be changed.
- Can communication button: by pressing this button the used can communicate with the altitude simulator via CAN.
- Dynamic mode button: by pressing this button, the dynamic mode is enable.
- Informative box showing the operation mode:
    - Manual mode: this is the normal mode, when the altitude simulator is in vacuum or overpressure mode.
    - OptoV: this mode is active when the altitude simulator is changing from overpressure mode to vacuum mode.
    - VtoOP: this mode is active when the altitude simulator is changing from vacuum mode to overpressure mode.
    - Safe_Stop: this mode is active when the altitude simulator is stopping in a safe way, whether the Stop button has been pressed or an error has appeared.
- Release PIDs button. By pressing this button, all the PIDs are released and allows modifying all the actuators position manually.

Sensors Screen

Figure 4.18 shows the sensors screen of the altitude simulator touch screen. It has many elements in common with the main screen. The only boxes that are not in the sensors screen with respect to the main screen are Setpoints box, Analogue Actuators box and Release PIDs button. On the other hand, it shows information of all the temperature and pressure sensors.

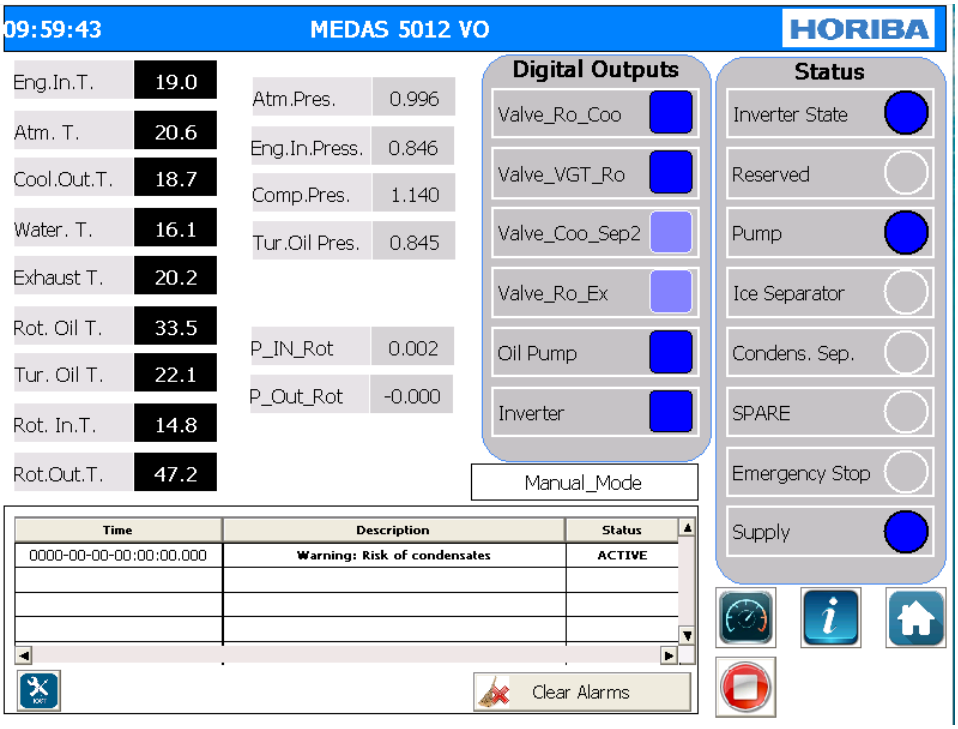

Figure 4.18 – Sensors screen of the altitude simulator touch screen

Temperature sensors

- "Eng. In. T" (T_EI): Air temperature at the engine intake temperature.
- "Atm. T" (T_atm): Atmospheric temperature.
- "Cool. Out. T." (T_CO): Water-to-air cooler outlet temperature.
- "Water. T." (T_WO): Water outlet temperature from altitude simulator.
- "Exhaust T." (T_EE): Engine exhaust temperature inside altitude simulator.
- "Rot. Oil T." (T_OR): Mechanical compressor oil temperature.
- "Tur. Oil T." (T_TO): Turbocharger oil temperature.
- "Rot. In. T." (T_RI): Mechanical compressor inlet temperature.
- "Rot. Out. T." (T_RO): Mechanical compressor outlet temperature.

Pressure sensors

- "Atm. Pres." (p_atm): altitude simulator air inlet pressure.

- Eng. In. Pres." (p_EI): Air pressure at the engine intake.
- "Comp. Pres." (p_CO): Air pressure at the turbocompressor outlet.
- "Tur. Oil Pres." (p_OT): Turbocharger oil pressure.
- "P_IN_Rot" (p_RI): Air pressure at the mechanical compressor inlet.
- "P_Out_Rot" (p_RO): Air pressure at the mechanical compressor outlet.

SCADA screen

Figure 4.19 shows the SCADA screen of the altitude simulator touch screen. It shows the information of the different temperature and pressure sensors and actuators position in real time and in a similar position they are in the layout of the altitude simulator.

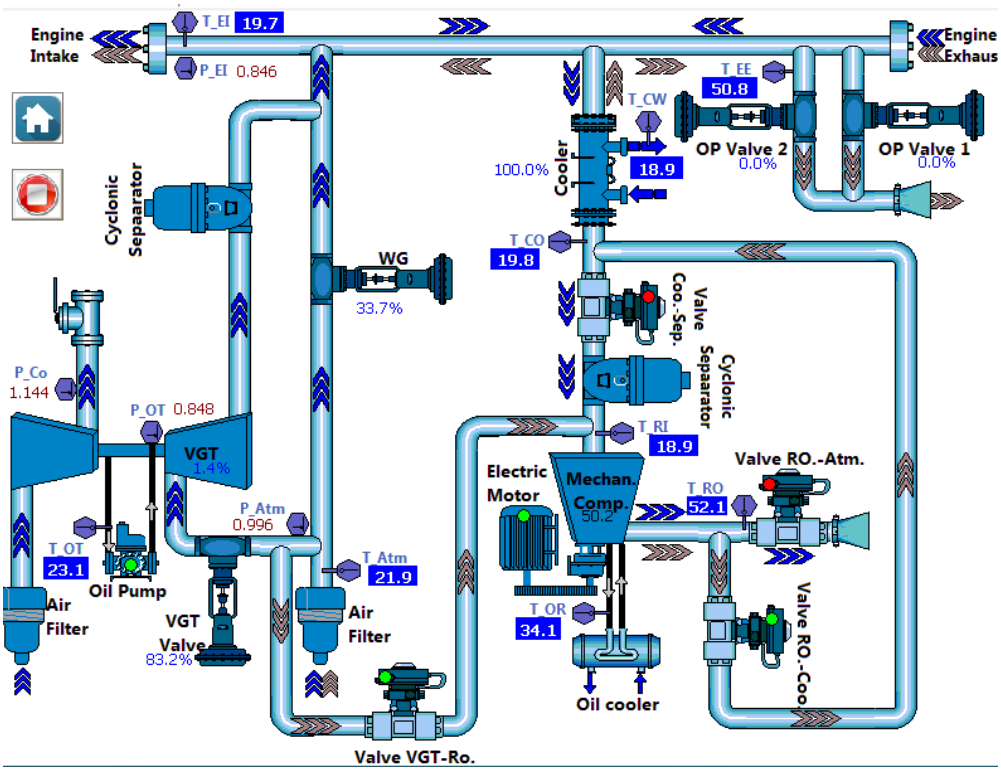

Figure 4.19 – SCADA screen of the altitude simulator touch screen

4.8 Variables stability when coupled to an engine

When an engine is operating in real conditions, whether in altitude or at sea level, the surrounding pressure and temperature are constant, even during engine accelerations or decelerations. The altitude simulator here in after will be called as MEDAS (movable, efficient and dynamic altitude simulator) which has been the commercial name registered by Horiba. MEDAS has to ensure also constant pressure and temperature even during engine transients in order to be as accurate as possible to a real atmosphere.

To analyze the pressure and temperature variation in the altitude simulator when operating with an engine, a test campaign has been performed with the altitude simulator. Two different cycles (NEDC and WLTC) have been performed at 6 different altitudes: four altitude above sea level (150 m, 1000 m, 2000 m and 3000 m) and two altitude below sea level (-1000 m and -2000 m).

The pressure and temperature have been measured just upstream the engine connection with MEDAS, where the altitude simulator is controlling both variables in order to keep constant the setpoint altitude and temperature.

Figure 4.20 shows the results of the test performed. In the left graphs it is represented the pressure variation (top) and temperature variation (bottom) for the NEDC tests and in the right graphs is it represented also the pressure variation (top) and temperature variation (bottom) for the WLTC tests. The differences are calculated with respect to the setpoint value, following Equation (4.30).

$$Difference = SP - Measure \qquad (4.30)$$

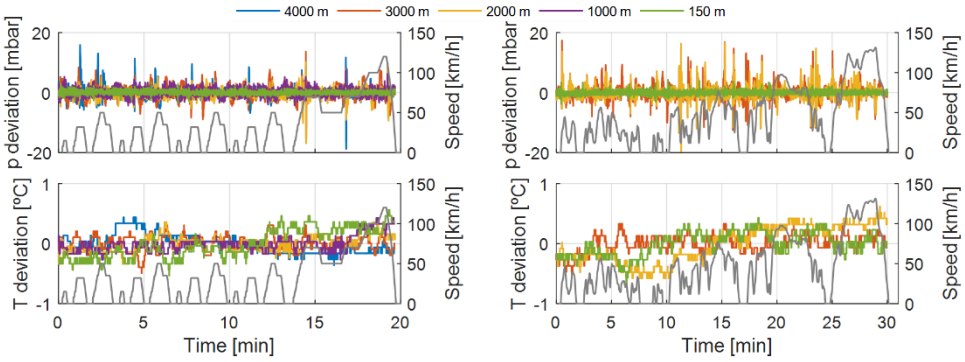

Figure 4.20 – Pressure (top) and temperature (bottom) variation at the engine connection with the altitude simulator for NEDC tests (left) and WLTC tests (right) at different altitudes.

As can be seen, the differences in pressure are lower than 20 mbar, which approximately corresponds to 200 m and temperature variations are lower than 1 ºC.

The pressure peaks are mainly produced during the engine accelerations and decelerations. They are caused by two main physical phenomena. On one hand, when the engine accelerates, the mass flow increases a few seconds earlier at the intake connection than at the exhaust connection with the altitude simulator. Consequently, the total mass flow in the dilution pipe decreases, leading to a slight decrement in the engine intake pressure. The WG valve must open quickly to compensate this vacuum increment. The opposite effect happens during the engine deceleration.

On the other hand, when the engine accelerates, the exhaust gas temperature increases and the altitude simulator dilution mass flow decreases. Therefore, the temperature at the mechanical compressor inlet also increases. This increment in the temperature leads to an increment in the corrected mass flow and a reduction in corrected speed, which leads to a step reduction in pressure ratio. Then, the vacuum generated by the mechanical compressor reduces and the engine intake pressure increases. The WG valve must close quickly to compensate this vacuum reduction. The opposite effect happens during the engine deceleration.

In the previous paragraphs, the variation in the engine intake pressure and temperature has been analyzed. The effect of 1 ºC variation in the engine intake temperature is small and can be neglected. However, the effect of 20 mbar (around 200 m) in the engine intake pressure cannot be directly neglected and its real effect in the engine behavior has to be analyzed in more detail. For that reason, the pressure difference at the engine turbocompressor inlet when the engine is operating with the altitude simulator and when is operating without it has been compared. Figure 4.21 shows the results for the NEDC test (on the top) and for the WLTC test (on the bottom). As can be seen, the pressure at the compressor inlet present the same trends and values independently whether the altitude simulator is connected or not to the engine.

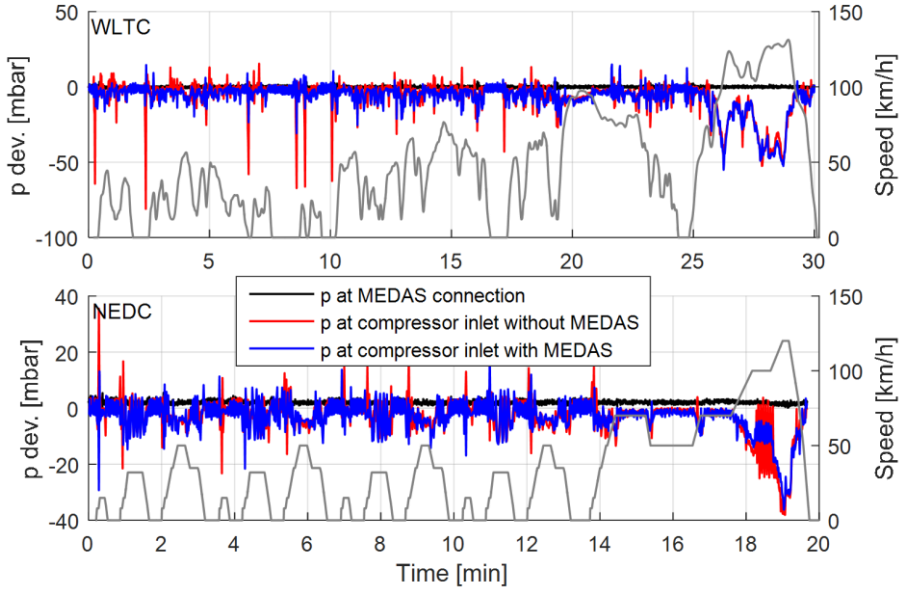

Figure 4.21 – Turbocompressor inlet pressure variation comparison when the engine is at sea level or operating with the altitude simulator.

To study in more detail the effect of the difference in the mass flow in the altitude simulator during engine accelerations, an engine load transient [5] was modeled with the engine intake and tailpipe connected to the altitude simulator. The installation was in vacuum mode and with constant mechanical compressor speed (40000 rpm), constant inlet mechanical compressor temperature (22 ºC) and constant VGT and WG position (100% and 0%, respectively) in order to operate with constant pressure and air mass flow. This operation point was chosen because low dilution air mass flow through the dilution pipe is generated, what is worst for the installation behavior during an engine transient. The technical specifications of the engine are in Table 4.5.

Table 4.5. Engine specifications of the modeled engine.

Type	*HSDI Diesel passenger car engine*
Displacement	1997 cm3
Bore	85 mm
Stroke	88 mm
Number of cylinders	4 in line
Number of valves	4 per cylinder
Compression ratio	18:1
Maximum power @ speed	100 kW @ 4000 rpm
Maximum torque @ speed	320 Nm @ 1750 rpm

The engine was at constant 4500 rpm and a transient from 0% to 80% of load was simulated. Figure 4.22 represents the variation in time of the engine torque (top left graph in Figure 4.22), mass flow to the engine, through the dilution pipe and the total mass flow through the altitude simulator (top right graph in Figure 4.22), pressure at altitude simulator connection with the engine intake and exhaust (bottom left graph in Figure 4.22), temperature in the engine intake connection (bottom left graph in Figure 4.22), and mass flow in the engine compressor outlet and intercooler outlet (bottom right graph in Figure 4.22).

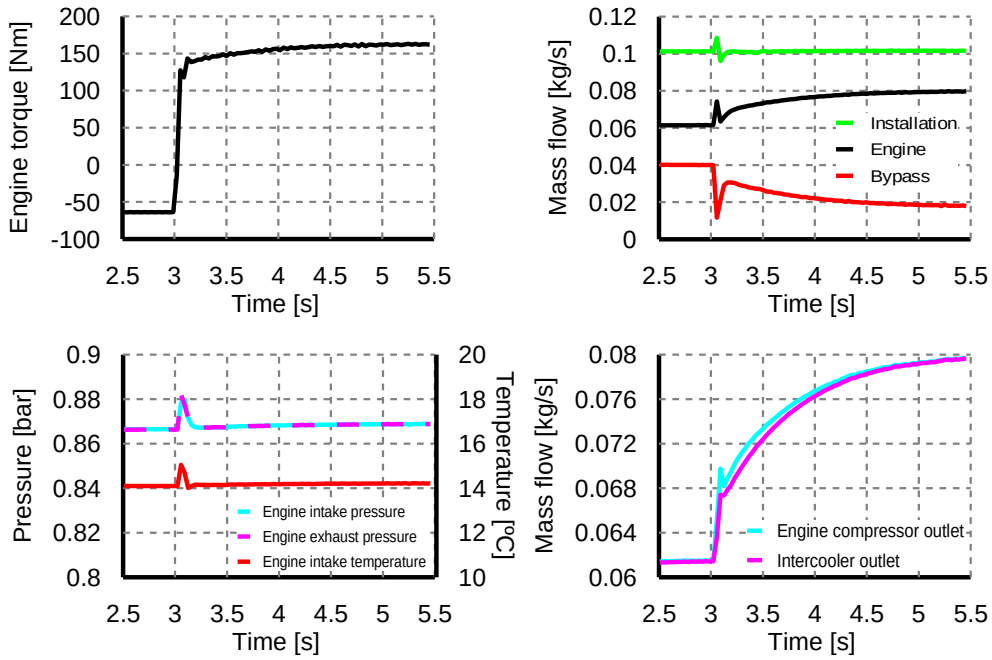

Figure 4.22 – Installation behavior during an engine load transient

Figure 4.22 shows that the pressure peak introduced by an engine transient operation is small when the inlet compressor temperature is not modified.

Attending to all these results, it can be said that the engine behavior is not affected by the pressure oscillations in the compressor inlet, as the pressure at the compressor inlet is the same and the oscillations are not transmitted to the engine with the same amplitude and its duration is reduced in time.

4.9 Conclusions

In the present chapter, it has been analyzed the altitude simulator that was developed in Chapter 3.

First, the analogy between the altitude simulator operation map and the mechanical compressor map has been explained. This analogy has been useful to deeper understand the operation of the altitude simulator: the effect of the ambient conditions in the performance of the altitude simulator, the theoretical limits of the maximum and minimum mass flow that can be moved by the altitude simulator depending on the altitude and the maximum altitude that can be reached.

Then, the control strategies of the altitude simulator have been explained. The main objective of the control algorithm is to reach the pressure, temperature and mass flow setpoints introduced by the operator automatically and keep their value constant even during engine transients.

Finally, how to install and operate the altitude simulator in a test cell has been explained. On the one hand, the main things that have to be taken into account when an engine or a vehicle is coupled to the altitude simulator in order to reproduce as accurate as possible a real altitude test. On the other hand, the different menus of the software interface and how it has to be operated.

4.10 References

[1] Lagos de Covadonga, Asturias (Spain), (n.d.). https://www.climbbybike.com/climb.asp?Col=Lagos-de-Covadonga&qryMountainID=4590.

[2] M.J. Hu, Optimizing Crankcase Ventilation System of Gasoline Engine, Appl. Mech. Mater. 58–60 (2011) 171–176. doi:10.4028/www.scientific.net/AMM.58-60.171.

[3] Y. Ohno, K. Funato, K. Kajita, An integration approach on powertrain control system, SAE Tech. Pap. (1989). doi:10.4271/890762.

[4] J.J. Streicher, Automobile fuel system vapor emission following evaporation canister breakthrough, J. Environ. Sci. Heal. - Part A Toxic/Hazardous Subst. Environ. Eng. 34 (1999) 1035–1060. doi:10.1080/10934529909376880.

[5] F. Payri, J. Benajes, J. Galindo, J.R. Serrano, Modelling of turbocharged diesel engines in transient operation. Part 2: Wave action models for calculating the transient operation in a high speed direct injection engine, Proc. Inst. Mech. Eng. Part D J. Automob. Eng. 216 (2002) 479–493. doi:10.1243/09544070260137507.

CHAPTER 5

Altitude simulator and hypobaric chamber correlation

Contents

Figures

Tables

5.1 Introduction

In the previous chapters, the development of an altitude simulator by means of 1-D models has been described and experimental tests to shows its operation maps have been shown and discussed. The altitude simulator has shown good performance with respect to the operation range and stability in altitude, temperature and mass flow, with low energy consumption.

However, in order to be used in altitude testing as a real alternative to hypobaric chambers or real altitude tests, it is good to validate its performance when operating with an engine. When an engine is operating in altitude, its behavior changes caused by the lower ambient pressure. However, when the engine is operating with the altitude simulator, only some elements are at low pressure, most of the elements in the engine are at room pressure. Therefore, it is necessary to quantify its impact in the engine performance and emissions.

In the present chapter, the engine performance and emissions when it operates inside a hypobaric chamber and when it is connected to the altitude simulator are compared.

A turbocharged diesel engine has been tested at different altitudes in a hypobaric chamber. Then, the same engine has been tested at sea level but connecting its intake and exhaust to the altitude simulator, generating the same altitudes than in the hypobaric chamber tests.

Finally, the results obtained using both systems have been compared and engine emissions and performance differences analyzed.

In this chapter the changes in the engine behavior and emissions are not analyzed in detail, this analysis will be done in Chapter 6.

In the literature, it can be found different altitude studies with engines or vehicles operating connected to altitude simulators with a similar operation principle to the altitude simulator developed in this work. However, none of them compare the results obtained with a hypobaric chamber or real altitude [1–8]. The trends in the engine performance and emissions shown in the studies performed with an altitude simulator are similar to the ones shown in hypobaric chamber or real altitude tests. However, the accuracy of the results has not been studied.

5.2 Methodology

In order to show the differences between the altitude simulator and the hypobaric chamber, a test campaign has been designed. The comparison has to be done testing the same engine, at the same temperature and pressure conditions, with the same layout and in the same operation conditions.

In the following paragraphs it will be described the different elements of the test cell and the tested points in the engine.

5.2.1 Test bench description

The CMT-Motores Térmicos has a hypobaric chamber where the comparison tests have been performed. However, it had to be adapted in order to be able to connect the altitude simulator without modifying the engine layout. Figure 5.1 shows the test bench layout and connections. In the right image, it can be seen the hypobaric chamber, where the engine and the brake are placed. The left image shows the altitude simulator, which is outside the hypobaric chamber, separated from the engine by one of the chamber walls with three holes to connect both systems when they have to operate coupled. The three holes in the wall are connecting the engine intake to the altitude simulator, as well as the engine exhaust. Besides, the altitude simulator intake air is also sucked from the hypobaric chamber by means of the third connection, in order to have the same temperature when the engine is operating with the hypobaric chamber than when is operating with the altitude simulator. The ambient temperature during all the tests was controlled between 10 to 15 °C.

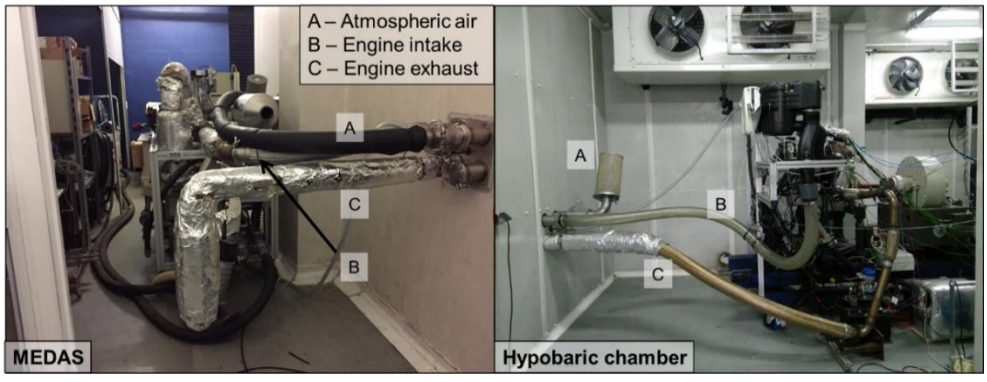

Figure 5.1. Altitude simulator (left) and engine (right) connections.

When the altitude simulator is connected to the engine and operating, the altitude chamber is not generating vacuum and only controls the temperature inside the test cell. Therefore, the air that surrounds the engine is at sea level pressure, but the intake and exhaust air are at the altitude imposed by the altitude simulator.

The engine sump was not connected to the altitude simulator as the engine has a blow by connection to the compressor inlet through an oil box which are both, box and connection, rigid enough to operate at the maximum altitude without pressurizing engine sump. However, the engine sump pressure was measured and monitored during the tests to compare its value between the altitude simulator and the hypobaric chamber tests.

To avoid any air leaks from the atmosphere to the engine during the tests with the altitude simulator, the compressor inlet and outlet pipes were reinforced and the airbox was completely sealed. These modifications were done before the tests with the hypobaric chamber. Therefore, the engine geometry was not modified between the tests with both systems.

With respect to the ECU pressure sensor, as it is at sea level, the pressure that is measuring had to be modified internally my means of INCA software when the engine is operating with the altitude simulator. This way, the engine is cheated and thinks it is operating in altitude. If the engine intake is at lower pressure than the value measured by the ECU pressure sensor, its behavior can be different than when operates in real altitude, as the ECU is measuring very different pressures at the compressor inlet and in the ECU.

5.2.2 Tested points

The engine was tested at the same operation points with both systems. The engine was operating in steady state at different speeds (1500 rpm, 2000 rpm, 2500 rpm and 3000 rpm) and pedal positions (3 bar BMEP, 6 bar BMEP, 9 bar BMEP and full load), being in total 16 steady state points. Besides, the engine was tested at two different altitudes: 1300 m and 2300 m for each system.

Therefore, a total number of 64 different operation points in the engine were performed:

- 2 systems: altitude simulator and hypobaric chamber.
- 2 altitudes: 1300 m and 2300 m.
- Engine speeds: 1500 rpm, 2000 rpm, 2500 rpm and 3000 rpm.

- 4 pedal positions: 3 bar BMEP, 6 bar BMEP, 9 bar BMEP and full load.

5.2.3 Engine tested

The engine tested is described in Table 5.1.

Table 5.1. Specifications of tested Euro IV turbocharged engine

Type	HSDI Diesel passenger car engine, Euro V
Displacement	2953 cm3
Bore	96 mm
Stroke	102 mm
Number of cylinders	4 in line
Number of valves	4 per cylinder
Turbocharger model	Variable Geometry Turbine
Compression ratio	17.9:1
Maximum power @ speed	110 kW @ 3400 rpm
Maximum torque @ speed	380 Nm @ 1500 rpm
Maximum mass flow @ speed	750 kg/h @ 4500 rpm & full load
EGR type	Cooler, high pressure with intake throttle

5.3 Results

In the following paragraphs the results obtained from the tests are exposed and discussed.

5.3.1 Boundary conditions

As explained before, the tested points and altitudes have been the same with the altitude simulator and with the hypobaric chamber, in order to be able compare the results and to analyze the engine performance and emissions differences between them. Then, it is necessary a previous

analysis of the boundary conditions of the engine to be ensured that both test campaigns can be compared.

Figure 5.2 shows the compressor inlet pressure for all the tested points and conditions. The graphs on the top of the figure are the tests done with the hypobaric chamber and the graphs on the bottom of the figure are the tests done with MEDAS. Then, the graph on the left side of the figure are 1300 m tests and the graphs on the right side of the figure are 2240 m tests. Each graph has as x-axis the engine speed and as y-axis the engine torque. Every tested point is represented as a black dot in the different graphs.

As can be seen in Figure 5.2, for a given altitude, the compressor inlet pressure is the same when operating with altitude simulator or with the hypobaric chamber. The small decrease of the compressor inlet pressure is caused by the pressure losses increase in the pipes and in the air filter when the engine mass flow increases.

With respect to the temperature, the compressor inlet temperature is also the same in both cases, as shown in Figure 5.3, with differences lower than 4 ºC in all the operation map.

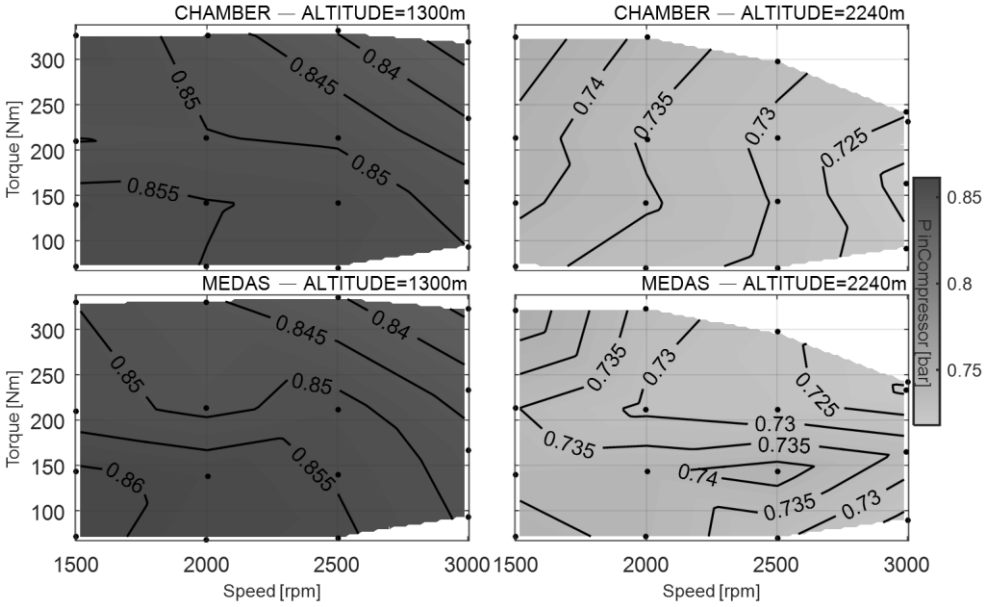

Figure 5.2. Compressor inlet pressure

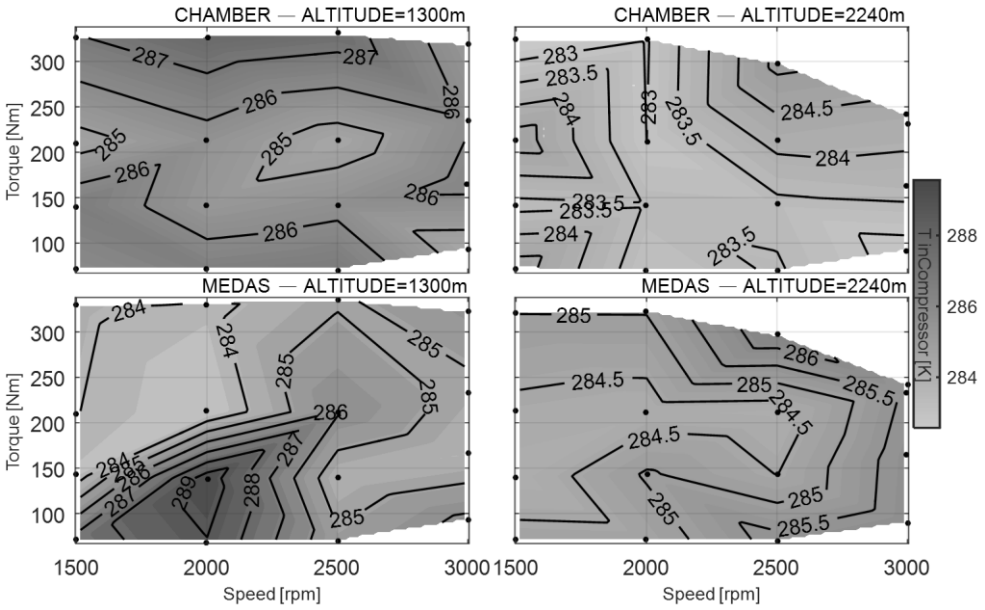

Figure 5.3. Compressor inlet temperature

With respect to the outlet engine conditions, Figure 5.4 and Figure 5.5 show turbine outlet pressure and temperature, respectively.

As in the compressor inlet conditions, the turbine outlet pressure and temperature are very similar in the tests with the altitude simulator and the hypobaric chamber. The bigger pressure differences are below 16 mbar at very high speed and load, probably caused because the engine exhaust connection is longer when operating with the altitude simulator than when operating in the hypobaric chamber. The Mean Square Error is 5 mbar, what shows that the ambient pressure was very similar in both test campaigns.

The turbine outlet temperature biggest difference is 20 ºC at 2240 m, maximum load and 2000 rpm. In that point, the turbine outlet temperature is 20 ºC higher when the engine is coupled to the altitude simulator than when it operates with the hypobaric chamber. This temperature increment in altitude simulator is not a trend, but only a punctual effect in that operation point. In fact, the Mean Percentage Error (MPE) is 1.04% for all the points at 2240 m. Therefore, it is probably caused by measurement uncertainties and not by the altitude simulator influence.

Turbine outlet temperature refers to turbine efficiency that refers to VGT operative point. As T_3 and T_4 are equal in the altitude simulator and chamber, it means that VGT operative point is the same in both.

From the results shown in the previous figures, it can be concluded that the tests results obtained from altitude simulator and the ones obtained from the hypobaric chamber can be compared, as the boundary conditions in both cases are very similar and the effect of differences observed can be considered negligible.

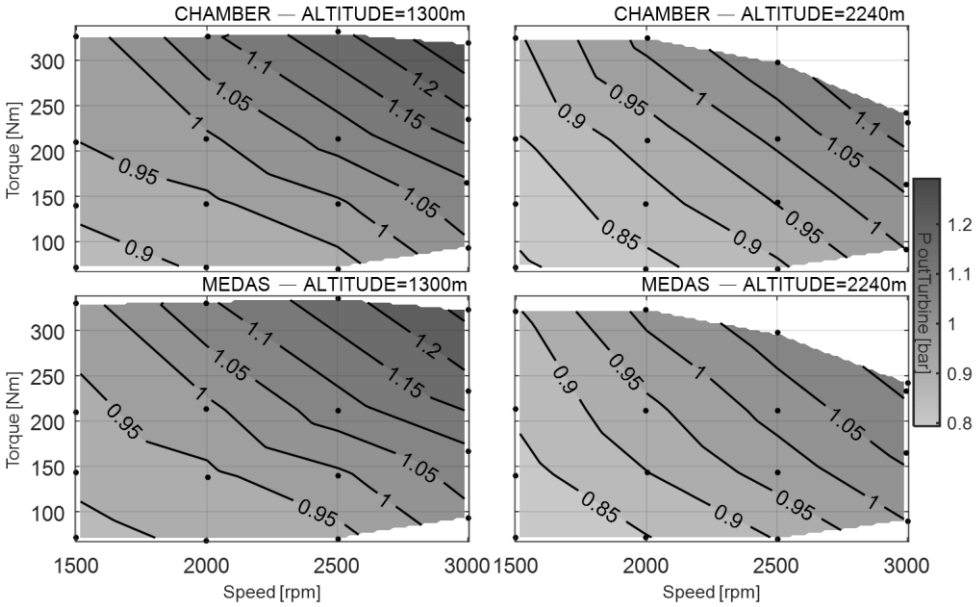

Figure 5.4. Turbine outlet pressure

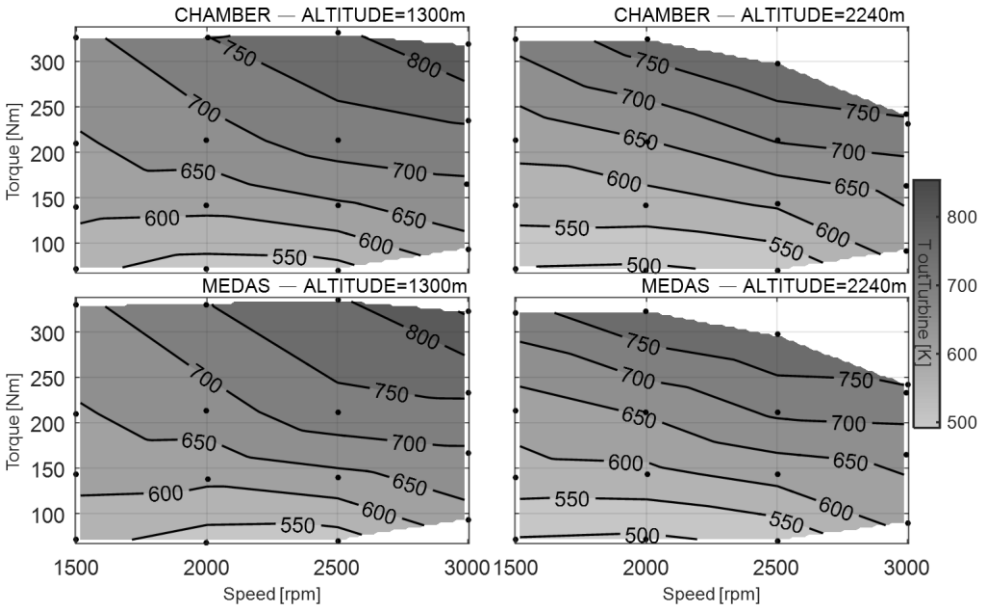

Figure 5.5. Turbine outlet temperature

5.3.2 Compressor behavior

The first element of the engine to be analyzed is the turbocharger. Figure 5.6 and Figure 5.7 show the tested points in the compressor map at 1300 m and 2300 m, respectively. As can be seen, the altitude simulator points (represented by circles) and hypobaric chamber points (represented by crosses) are very close when homologue points are compared. Only small differences at 2240 meters tests can be observed, for example in the high load points at 2000 rpm. These differences are small and could be explained by the dispersion of the measurements, as they do not follow any trend. Therefore, the compressor behavior is not being modified by the use of the altitude simulator and its behavior with the altitude simulator is the same than when operating in a full environment altitude.

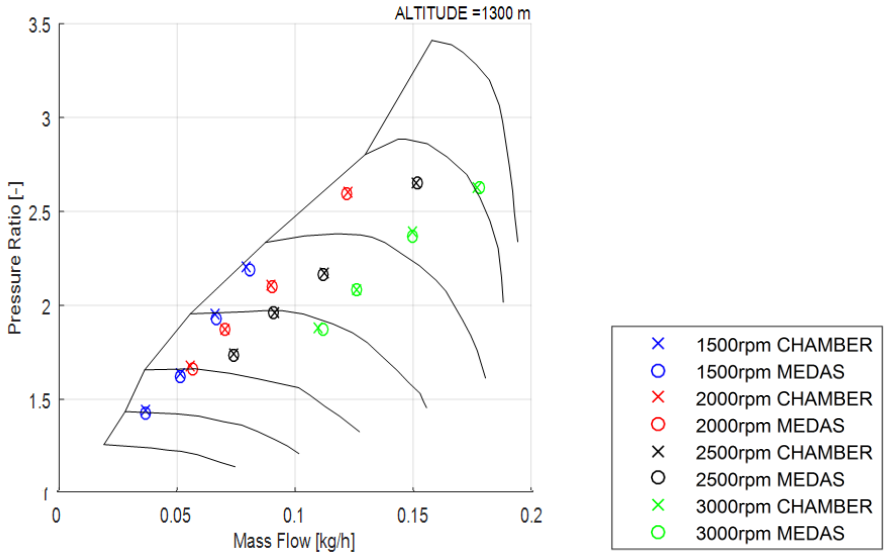

Figure 5.6. Compressor map at 1300 m test

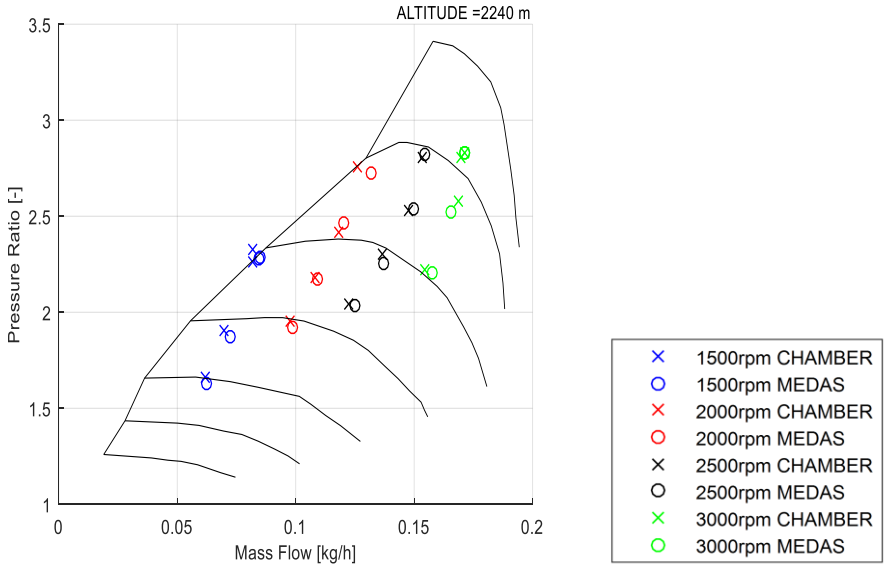

Figure 5.7. Compressor map at 2300 m test

5.3.3 Engine sump pressure

Other important element in the engine that can modify its behavior by the altitude simulator is the blow-by connection. When the engine is operating, some gases can pass through the piston rings from the combustion chamber to the sump. If these gases, which are a mix of oil vapors, unburned fuel and exhaust gases, are not correctly removed from the engine sump, its pressure would increase and they would be emitted to the atmosphere, increasing the engine emissions. In order to avoid it, the blow-by connects the engine sump with the compressor inlet. This way, the gas in the sump goes back to the combustion chamber through the compressor, and is not emitted to the atmosphere.

When the engine is operating in altitude, the blow-by pipe has similar pressure in the inner and outer part, being therefore fully open and operating as it does at sea level. Similarly happens with the crankshaft retainers. They are designed to work with higher pressure in the sump than in the atmosphere, sealing the gases in the sump to be emitted to the atmosphere.

However, when the engine is operating with the altitude simulator, the blow-by pipe can collapse and partially block the sump gases to pass through it. Besides, as the atmospheric pressure is higher than the pressure in the crankshaft, the crankshaft retainers can have some leaks, increasing the pressure in the sump. Also the lower density of blow-by gases can increase pressure losses in the oil-mist-cleaning-box and increase pressure in the engine sump. All these effects affect the general behavior of the engine.

For these reasons, the engine sump pressure was measured during the tests and the results are shown in Figure 5.8. As can be seen, only small differences at medium load and high speed at 2240 meters are observed, being the maximum pressure difference lower than 15 mbar, being the altitude simulator pressure higher than the pressure measured when operating with the hypobaric chamber. However, for the same points at 1300 m, the sump pressure is similar in both cases. However, the points next to this medium load and high speed point haven't any difference in pressure between both experiments, and the difference is very small (lower than 15 mbar). Therefore, previous differences could be also dispersion in the measurement.

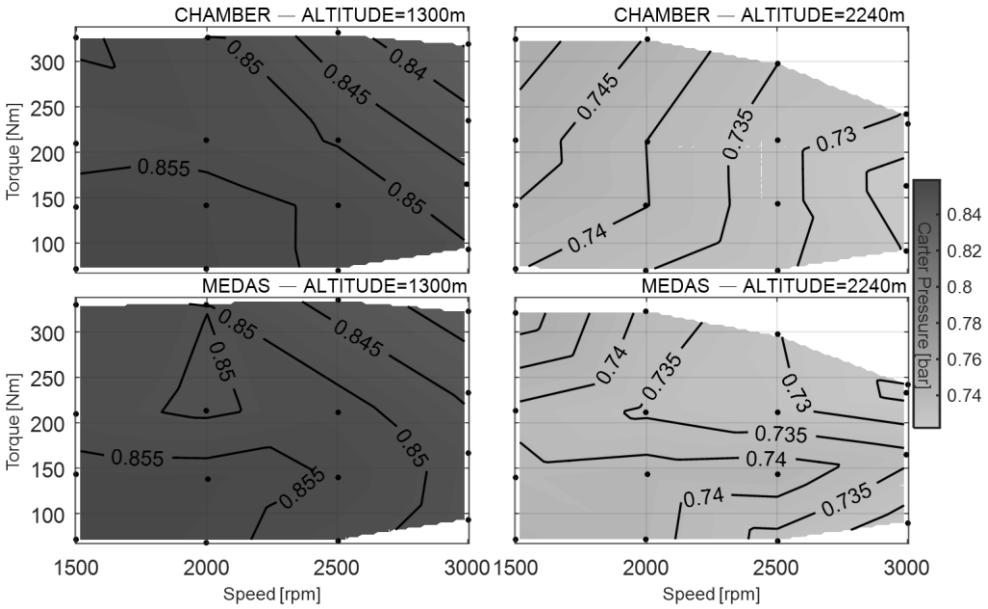

Figure 5.8. Engine sump pressure

5.3.4 EGR and VGT

Figure 5.9 shows the EGR valve opening. As can be seen, at 2240 m the EGR valve is fully closed in both tests. At 1300 m, the EGR valve is partially open in all the tested points, except in the full load line. As can be seen, the results are the same in altitude simulator than in the hypobaric chamber test. EGR position is perfectly reproduced by the altitude simulator.

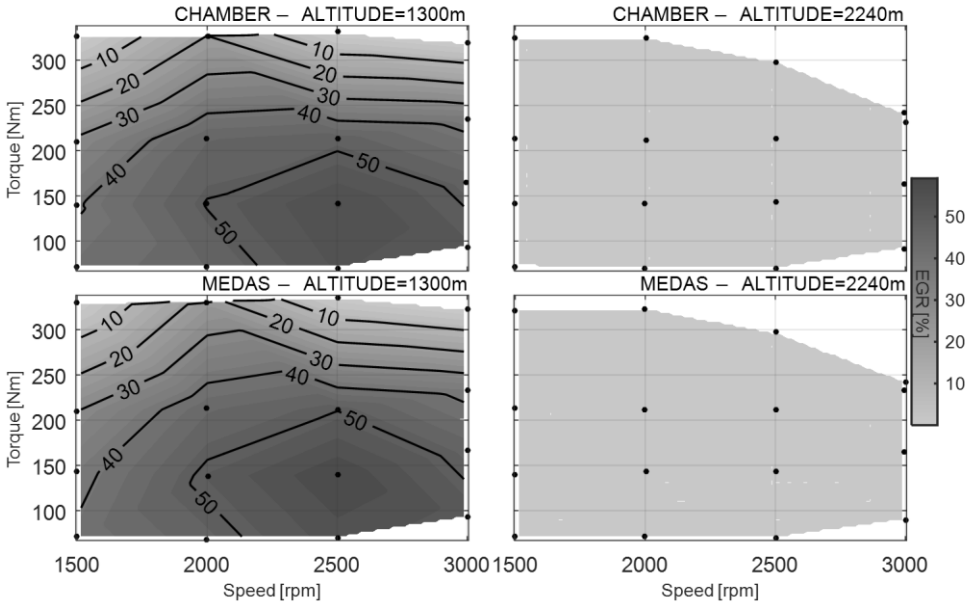

Figure 5.9. EGR opening

Figure 5.10 shows the VGT position estimated by the ECU. In this engine, the vacuum to move the actuator of the VGT is generated by a vacuum pump with some extra help coming from the compressor inlet connection. The help is in form of an atmosphere were vacuum is released to control VGT actuation, and this is the compressor inlet. Since compressor inlet is at high vacuum with respect to test room ambient vacuum the release valve has to open a lot to release. This means the simulated altitude helps the vacuum pump to work less. Since this release valve position is main feedback to ECU about VGT opening, the reading from the ECU about VGT opening is wrong. This is not a big issue when VGT is generally closed loop with p_2. Actual VGT position will be the same even reading is wrong.

It is advised to disconnect vacuum release from compressor inlet and let connected to test room ambient to minimize this effect. In the short term all VGTs will be actuated by wire and this small issue will disappear.

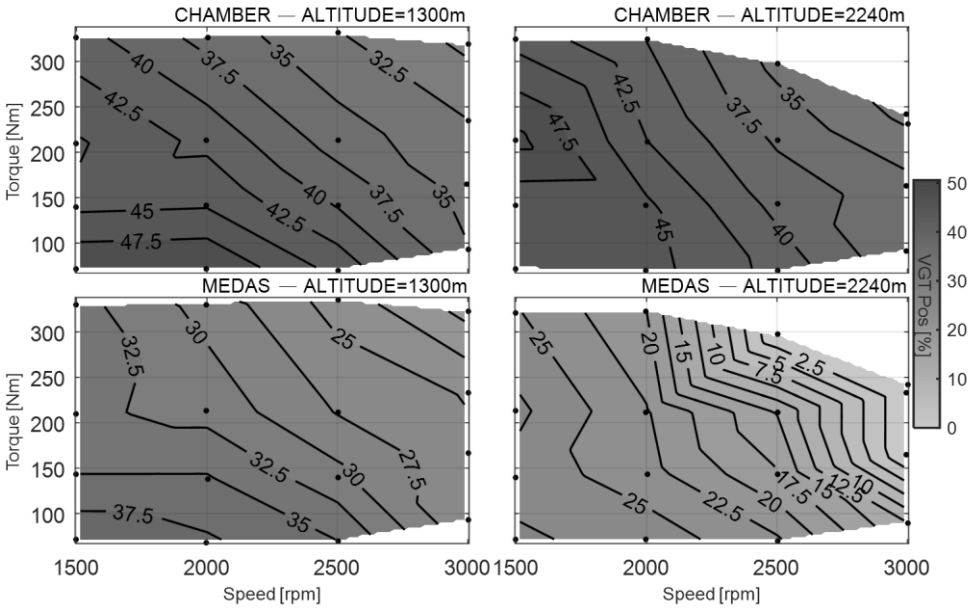

Figure 5.10. VGT opening

5.3.5 Torque

Once the engine actuators has been analyzed and its behavior has been shown that is the same with both systems, it will be analyzed the rest of the engine variables.

The first variable to be analyzed is going to be the torque, shown in Figure 5.10 for 1300 m and 2300. As can be seen, the torque is the same for both systems at a given altitude. It can be seen that the maximum torque is limited for the altitude tests. At sea level, the maximum torque is 380 Nm at 2000 rpm. However, the maximum torque at 1300 m and 2300 m is limited to 320 Nm. This limitation can be observed both in the hypobaric chamber tests and in the altitude simulator tests.

5.3.6 Fresh air

With respect to the fresh air, the results in Figure 5.11 show the same values for the tests with the hypobaric chamber and the altitude simulator, also the different trend in the slope of the lines.

For example, the effect of the EGR closing can be observed in both tests, as the fresh air is higher at 2300 m than at 1300 m in the area where the EGR

is open at 1300 m but closed at 2300 m. However, the points where the EGR valve is fully closed at both altitudes, the fresh air mass flow decreases with the altitude, caused by the lower compressor outlet pressure. Despite the increment of the compressor pressure ratio with the altitude, it is not big enough to compensate the effect of the lower ambient pressure.

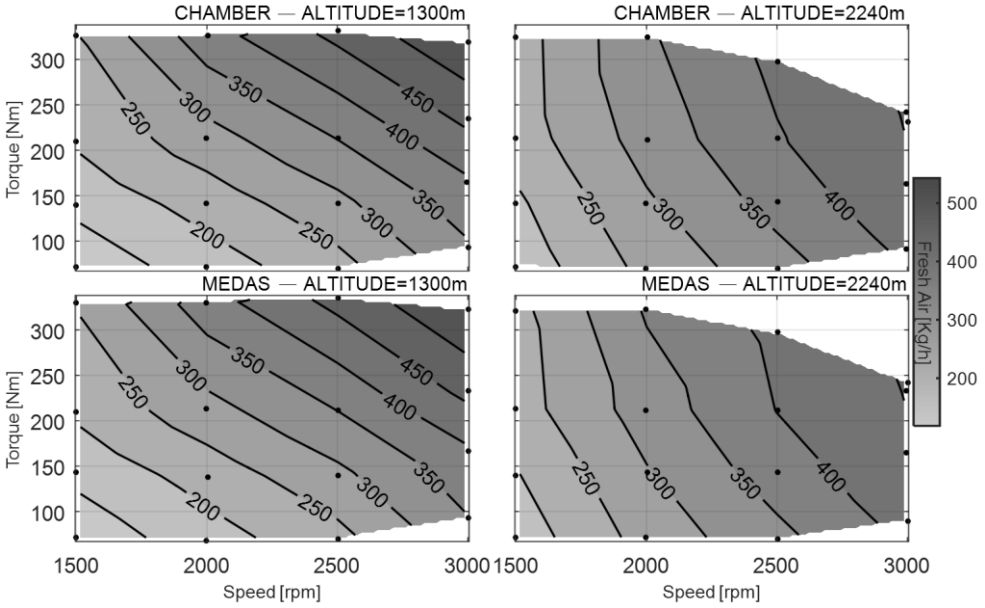

Figure 5.11. Fresh air

5.3.7 BSFC

Figure 5.12 shows the BSFC for the tested points with both systems. The trends observed are the same in both cases. For example, the top left area where the BSFC reaches its minimum value or the high values at the low load area.

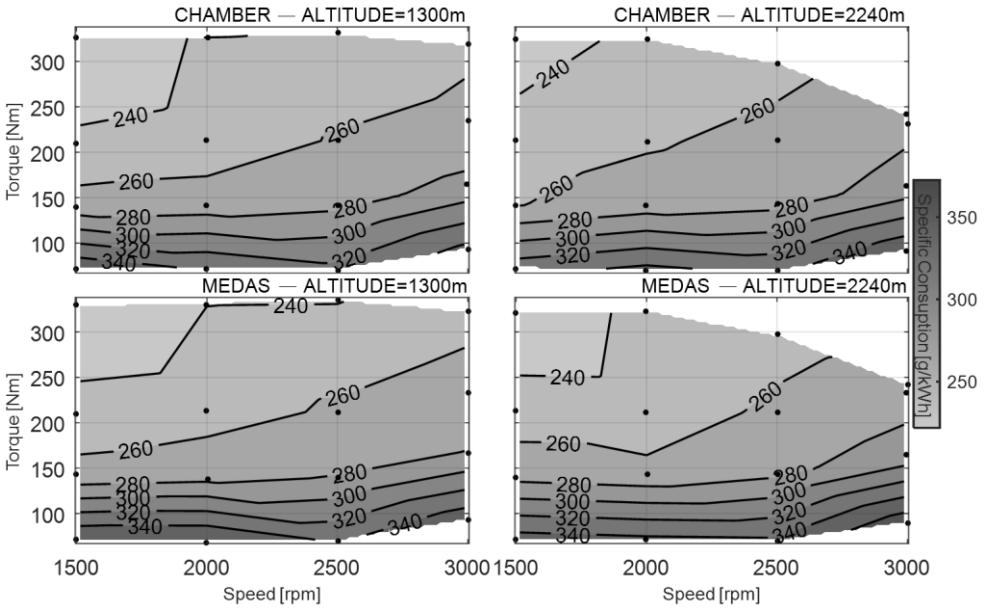

Figure 5.12. BSFC

5.3.8 Emissions

In the previous sections the differences between testing an engine in a hypobaric chamber and in an altitude simulator has been analyzed. The results show that the differences are very small. However, with the new directives from European Commission, the emissions measurement in altitude is also an important parameter to be controlled. Therefore, if the altitude simulator wants to be a real alternative to the hypobaric chambers and a better approximation to the RDE tests, an engine tested with the altitude simulator has to emit the same emissions than the same engine but tested in a hypobaric chamber.

For that reason, also the emissions differences between the altitude simulator and the hypobaric chamber have been compared. Figure 5.13 shows hydrocarbons emissions in grams per hour, Figure 5.14 shows NO_x emissions and Figure 5.15 shows CO_2 emissions, all of them in grams per hour, for all the tested points.

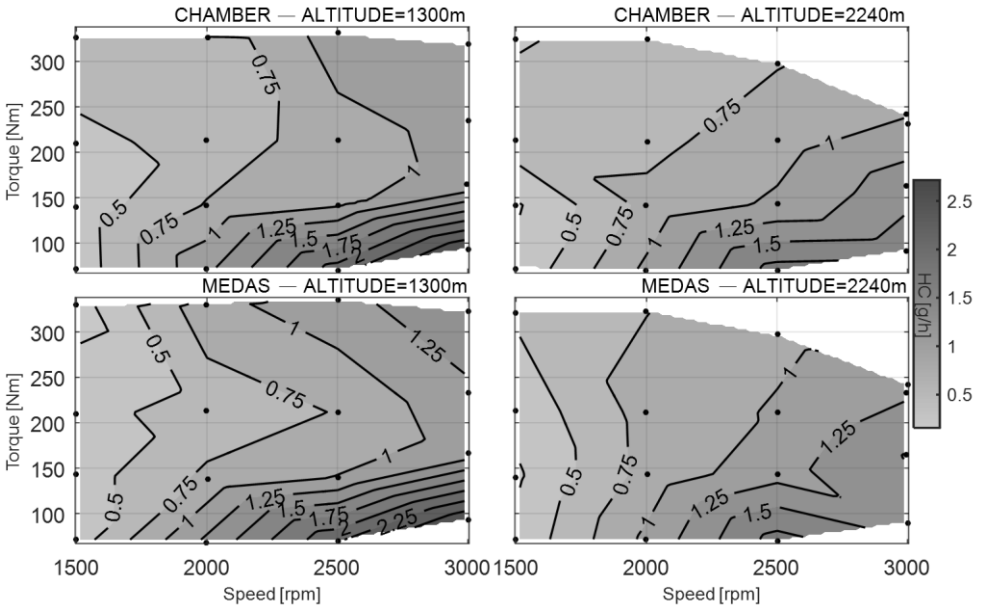

Figure 5.13. HC emissions

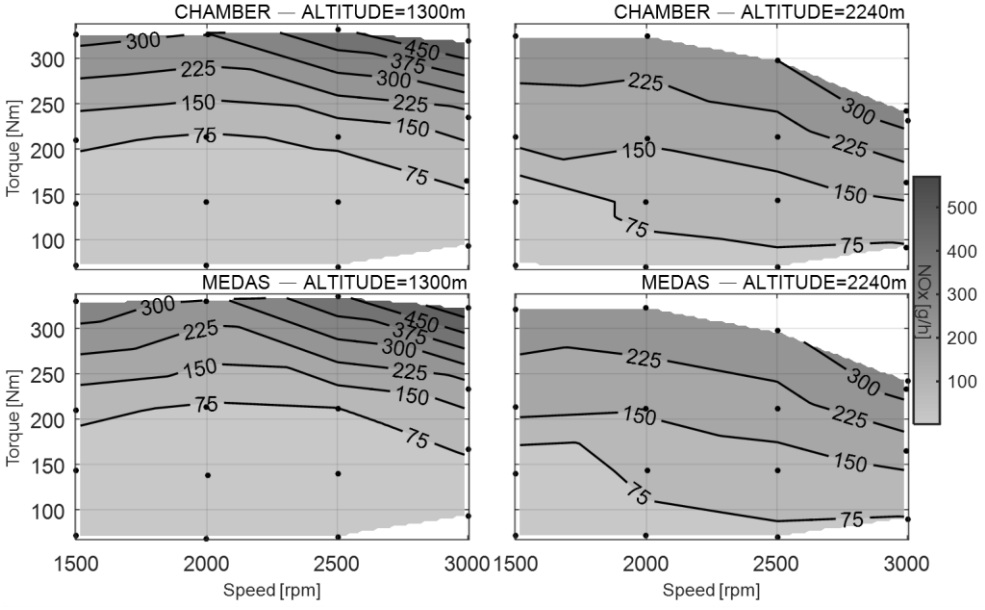

Figure 5.14. NOx emissions

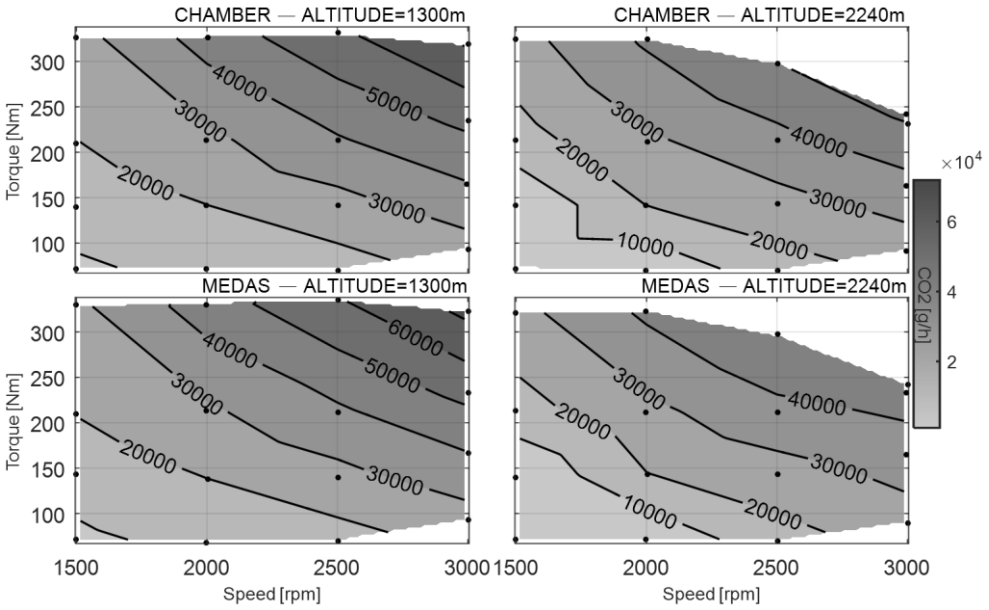

Figure 5.15. CO2 emissions

Comparing the results differences between the altitude simulator and the hypobaric chamber, it can be shown that the differences are small; the MSE is lower than 2%. Some points show bigger absolute differences, mainly in the HC emissions, but these points are insulated cases and do not show a trend, what can be explained by the dispersion in the emission measurement systems.

5.4 Error analysis

In the previous sections it has been observed that some of the measurements and variables present small differences between the altitude simulator tests and the hypobaric chamber. In this section, an error analysis will be performed, in order to identify if the errors observed are caused by the measurement system or by the altitude simulator.

To perform the analysis, the six operation points with higher error were tested again. Table 5.1 shows the repeated points.

Table 5.2. Repeated points with higher error

Point	*Speed [rpm]*	*BMEP [bar]*	*Altitude [m]*
#1	1500	6	2300
#2	3000	7	2300
#3	3000	10	2300
#4	2500	Full load	2300
#5	2000	Full load	1300
#6	2500	Full load	1300

Figure 5.16 shows the average percentage error (APE) of the different variables measured during the tests for the altitude chamber and the two tested altitudes with the altitude simulator. In the x-axis, the different measured variables are represented. In the y-axis, the APE is represented, following Equation (5.31). Therefore, the error of the measurement systems is obtained with the APE of the altitude chamber; and the error of the altitude simulator is obtained for each tested altitude with each corresponding APE.

$$APE = \frac{AQE}{RMS} \tag{5.31}$$

Where AQE is the Averaged Quadratic Error.

$$AQE = \sqrt{\frac{1}{n}\sum(x_i - \bar{x})^2} \tag{5.32}$$

And RMS is the Root Mean Square.

$$RMS = \sqrt{\frac{1}{n}\sum(\bar{x})^2} \tag{5.33}$$

Figure 5.16 presents many information that will be explained in detail in the following paragraphs.

- The average percentage error most of the variables is below 4%. Only three of the variables present bigger errors: compressor inlet temperature, CO emissions and THC emissions.
    - The compressor inlet temperature difference is related with the ambient temperature (with also an error close to 4%).

During the tests, the ambient temperature in the test cell was kept constant at around 15 ºC (as shown in Figure 5.3), and the absolute error was around 4 ºC. However, the ambient temperature error is then mitigated at the compressor outlet, where the APE is 2%.

  - The CO error of the measurement is 5%, what shows that the measurement of the emissions is more difficult and present bigger error than other variables such as pressure and temperature.
  - The THC error of the measurement system is 7%, also higher than other errors.

- The average percentage error of the tests at 2300 m is higher than in the tests at 1300 m. This can be explained by the increase of the instabilities in the engine when the altitude is increased; i.e. with the altitude increase, the repeatability of the engine decreases.
- The APE of the tests at 1300 m is lower than the error of the measurement equipment. Only the water temperature and the THC shows slightly higher errors in the 1300 m tests with the altitude simulator, being the difference negligible.
- The APE of the tests at 2300 m is closer to the APE of the measurement systems, being slightly higher in some variables and slightly lower in other. The higher difference is found in the CO emissions, which can be explained by the decrease of the repeatability of the engine with the altitude and the big inherent error in the emissions measurement.

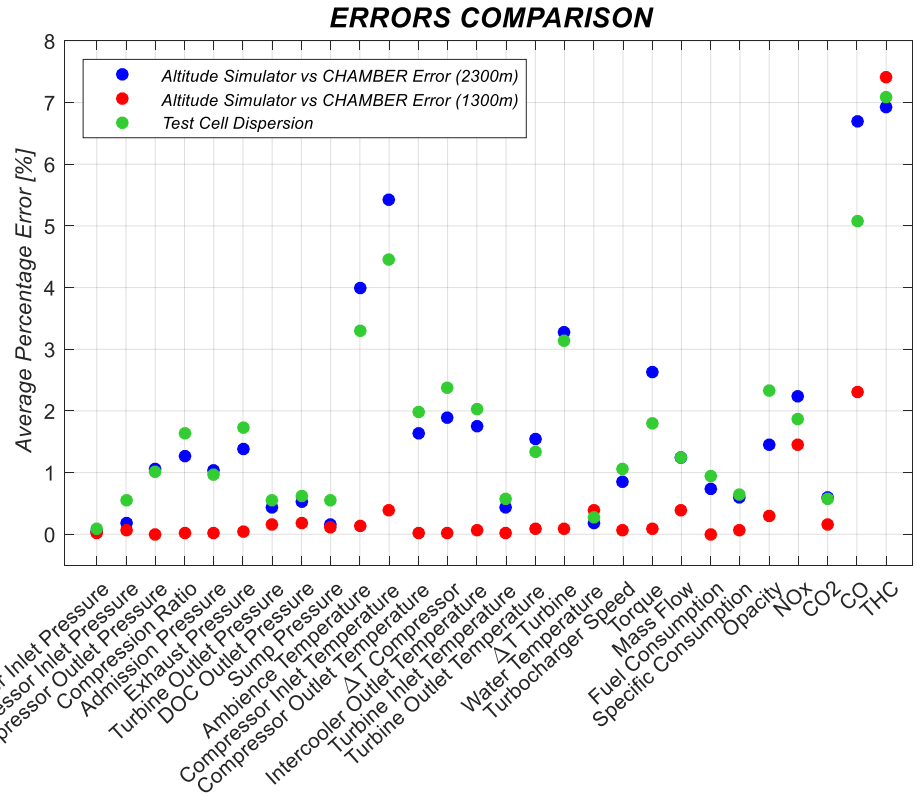

Figure 5.16. Averaged percentage errors for the different variables

5.5 Summary and conclusions

In this chapter, the differences of performance and emissions of an engine operating in altitude in a hypobaric chamber and connected to an altitude simulator has been discussed. The hypobaric chamber reduces the pressure inside the test cell where the engine is being tested, creating an altitude atmosphere for the engine as if it were operating in real altitude. However, the altitude simulator only decreases the pressure in the engine intake and exhaust. The test cell where the engine is tested is at sea level.

To analyze the differences, two different altitudes (1300 m and 2240 m) and 16 different steady state points covering a wide range in the engine operation map have been tested with the hypobaric chamber and with the altitude simulator.

The results show very similar engine performance and emissions at both altitudes with the altitude simulator and with the hypobaric chamber. Besides, the errors in the measurements and repeatability with the altitude simulator are similar to the hypobaric chamber.

Therefore, the altitude simulator has shown a big potential to be used in the engine test campaigns in altitude conditions. Besides, the altitude simulator has many advantages in comparison with a hypobaric chamber. The altitude simulator is movable and can be installed in any normal test cell. Besides, it is much cheaper than a hypobaric chamber and the energy consumption is also lower. With respect to the advantages in the operators' security, the altitude simulator is installed in a chassis dyno, where the driver is at room pressure while the car is being tested at different altitudes, while in the hypobaric chamber the driver is also at low pressure. Therefore, the altitude simulator presents lower health risks for the driver, as the human body cannot withstand repeated pressure changes around. Also in case of any failure, it is easier to evacuate the driver from the test bench.

In the next chapter the altitude simulator is used to analyze the influence of the altitude in the engine performance and emissions.

5.6 References

[1] D.M. Human, T.L. Ullman, T.M. Baines, Simulation of High Altitude Effects on Heavy-Duty Diesel Emissions, SAE Tech. Pap. 900883. (1990). doi:10.4271/900883.

[2] M. Ghazikhani, M. Ebrahim Feyz, O. Mahian, A. Sabazadeh, Effects of altitude on the soot emission and fuel consumption of a light-duty diesel engine, Transport. 28 (2013) 130–139. doi:10.3846/16484142.2013.798743.

[3] L. Shen, Y. Shen, Combustion Process of Diesel Engines At Regions With Different Altitude, SAE Tech. Pap. 950857. (1995). doi:10.4271/950857.

[4] C.A. Chaffin, T.L. Ullman, Effects of Increased Altitude on Heavy-Duty Diesel Engine Emissions, (1994).

[5] G. Zhou, R. Liu, S. Dong, G. Liu, Z. Zheng, S. Hao, Experimental study on plateau matching performance of turbocharger and vehicle diesel engine, Proc. - 2010 Int. Conf. Digit. Manuf. Autom. ICDMA 2010. 1 (2010) 710–713. doi:10.1109/ICDMA.2010.305.

[6] M. Yang, Y. Gu, K. Deng, Z. Yang, S. Liu, Influence of altitude on two-stage turbocharging system in a heavy-duty diesel engine based on analysis of available flow energy, Appl. Therm. Eng. 129 (2018) 12–21. doi:10.1016/j.applthermaleng.2017.09.138.

[7] C. He, Y. Ge, C. Ma, J. Tan, Z. Liu, C. Wang, L. Yu, Y. Ding, Emission characteristics of a heavy-duty diesel engine at simulated high altitudes, Sci. Total Environ. 409 (2011) 3138–3143. doi:10.1016/j.scitotenv.2011.01.029.

[8] J.-L. Lei, Z. Tan, S. Liu, Y.-H. Bi, L.-Z. Shen, Performance of Diesel Engine Fueled with Ethanol-diesel Blends in Different Altitude Regions, 2010 Int. Conf. Digit. Manuf. Autom. (2010) 82–85. doi:10.1109/ICDMA.2010.45.

CHAPTER 6

Turbocharged diesel engines behavior when operating at high altitude

Contents

Figures

Tables

6.1 Introduction

In the previous chapter, the altitude simulator has been correlated with a hypobaric chamber and the results show that the engine performance and emissions operating with both systems are very similar, being therefore the altitude simulator a good tool to test engine in altitude.

However, the engine behavior at different altitudes was not analyzed, but the differences could be observed.

The reduction of ambient pressure with altitude also reduces the air density [1], what has a major effect on the engine response. For example, the decrease of the in-cylinder density causes smaller droplet size, which leads to coalescence reduction [2,3]. This lower coalescence would decrease jet-to-wall impingement, but the lower density also decreases the spray angle thus leading to increased spray penetration [4]. In parallel, the combustion start is advanced as altitude increases producing higher maximum in-cylinder pressure which results in an increase of mechanical load on the cylinder walls [5]. Another effect of the lower density is the increase of the lift-off, which increases the fresh air penetration into the jet decreasing initial soot formation [6,7]. However, the lower oxidation rate of the soot caused by the lower density in the combustion chamber globally increases soot formation at the end of the combustion process.

These examples show how many factors are affected by the altitude at which the engine works, hence the diversity of published studies analyzing the influence of the altitude on engine performance and emissions. Some of them are based on the use of computational tools; for example Zhu et al. [8] optimized injection parameters using a genetic neuronal network in order to improve engine performance but without taking into account emissions. Other researchers focused on real driving emissions at different plateau altitudes; for example, in the work of Wang et al. [9], a vehicle powered by a 2.8 l turbocharged diesel engine was driven at altitudes of 1000, 2400 and 3200 m and at constant vehicle speeds ranging from 10 to 90 km/h in order to analyze regulated emissions. It was observed that CO, HC and PM emissions increased with altitude. However, NO_x emissions also increased up to 2400 m but a decrease was found at 3200 m. However, these conclusions are only based on 10 steady-state operating points focusing on the influence of engine speed and relying on intake charge variation because of the decrease in density as altitude increases to explain the variation in emissions.

Another group of studies on the influence of altitude are performed in hypobaric tests benches [10]. The tests are performed by simulating altitude conditions in the test cell environment, what involves a large volume because of the need for high mass flow renewal without pressure and temperature variations. This contrasts with the proposed equipment in this thesis, which is based on a mobile solution able to be shared by conventional engine test cells and ensuring fast dynamic response to engine requirements in a compact package. Concerning the improvements of the engine response, some techniques have been proposed to solve the penalty on performance caused by altitude. Due to the fact that at low ambient pressure the intake air mass flow decreases, some studies are driven to analyze the potential of enriched oxygen fuel [11] as a way to improve the engine performance. NO_x emissions have been discussed not to be directly affected by fuel oxygen [12], so that can be proposed as a potential improvement. Another solution is based on two-stage sequential turbocharging system to increase the maximum available pressure ratio so that boosting pressure at sea-level conditions can be kept at high altitude [13]. This kind of boosting architecture was shown to allow the same engine power output that is reached at sea level to be reached at up to 2000 m recovering up to 80% at 5500 m. However, it involves an oversized boosting system for sea-level operation increasing the engine cost and size. In addition, concerns about the turbocharger maximum temperature, surge margin and engine emissions should be addressed.

In this chapter, a turbocharged diesel engine under different altitudes is tested using the altitude simulator. The engine was operating under steady state operation at different engine speeds and loads, and also in dynamic operation modes in the NEDC. The combination of steady-state and transient operation tests provides a comprehensive range for engine performance and emissions analysis.

Finally, the results obtained in the engine performance and emissions are analyzed and compared with the sea level behavior.

6.2 Methodology

The test campaign has been divided in two parts. In the first part, the engine has been tested at four different altitudes (150 m, 1000 m, 2000 m and 3000 m) at different steady state points covering a wide range in the engine operation map. These tests are useful to see the operation range of the engine and to analyze its behavior without the effect of the dynamic variability of the engine. In the second part, the engine has been tested at

the same four altitudes in the dynamic cycle NEDC. In these tests, the engine behavior and emissions are also compared and analyzed.

6.2.1. Test bench description

Figure 6.1 shows the test bench layout. The engine and the altitude simulator were in different test cells connected through a gate. The engine intake and exhaust were coupled to the altitude simulator, as well as the engine sump. The altitude simulator could not be in the same room as the engine due to the lack of space. However, the length of the connection pipes is short enough to ensure low pressure losses between the generated atmosphere in the altitude simulator and the engine intake and exhaust pressure.

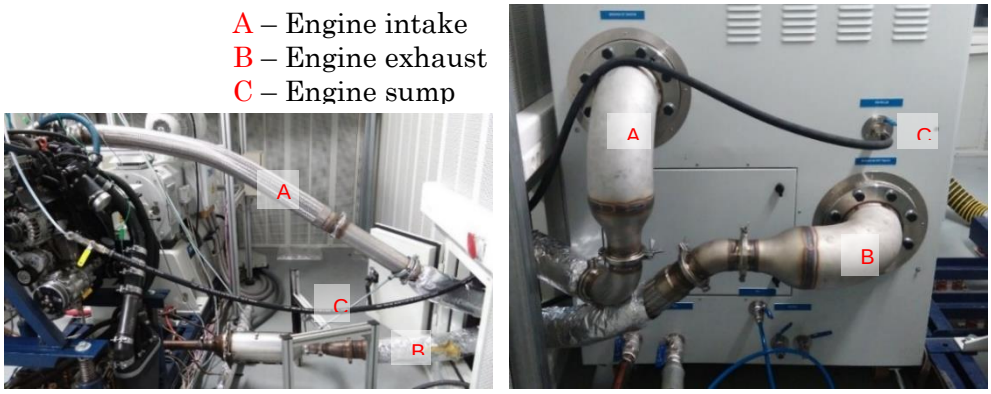

Figure 6.1 – Altitude simulator (left) and engine (right) connections

6.2.2. Tested points

First, the engine was tested at different steady state points covering a wide range on the operation map, testing in total 100 points.

- 4 altitudes: 150 m, 1000 m, 2000 m and 3000 m.
- Engine speeds: 800 rpm, 1000 rpm, 1500 rpm, 2000 rpm and 2500 rpm.
- 5 pedal positions: 1 bar BMEP, 25 %, 50 %, 75 % and 100 %.

Then, the NEDC were performed at the different altitudes. The tests campaign was performed in two different days following Table 6.1. In the first day, it was performed three tests in a row at 150 meters. The first one

was run in cold conditions and the following two with the engine once completed the warm-up. In the second day, three tests were performed in the same corresponding conditions but at different altitudes (1000 m, 2000 m and 3000 m). Therefore, each altitude test can be compared with its corresponding 150 m test. Cold test at 1000 m is compared with the cold test at 150 m, whilst hot tests at 2000 m and 3000 m are compared with each hot test at 150 meters. Additionally, both second and third hot tests at 150 m are compared between them. This last comparison of the hot tests at 150 m is used to check repetitiveness of the testing campaign.

Table 6.1 – Dynamic tests campaign

Order	Day 1	Day 2	Engine temperature
1st	150 m	1000 m	Cold
2nd	150 m	2000 m	Hot
3rd	150 m	3000 m	Hot

6.2.3. Engine tested

The engine tested is described in Table 6.2.

Table 6.2 – Specifications of tested Euro IV turbocharged engine

Type	HSDI Diesel passenger car engine, Euro IV
Displacement	1997 cm3
Bore	85 mm
Stroke	88 mm
Number of cylinders	4 in line
Number of valves	4 per cylinder
Turbocharger model	Variable Geometry Turbine
Compression ratio	15.5:1
Maximum power @ speed	120 kW @ 3750 rpm
Maximum torque @ speed	340 Nm @ 2000 rpm
Maximum mass flow @ speed	640 kg/h @ 4500 rpm & full load
EGR type	Cooled high pressure with intake throttle

6.3 Results

In this section, the tests results in steady state and dynamic cycles will be exposed and analyzed.

6.3.1. Steady tests

Torque, EGR and fresh air

Figure 6.2 shows EGR valve position colored for every altitude chart, where 0% means EGR valve is completely closed and 100% means EGR valve is completely open. Besides, each tested point has been plotted as a function of engine speed and torque as a black dot to show steady-state tests results.

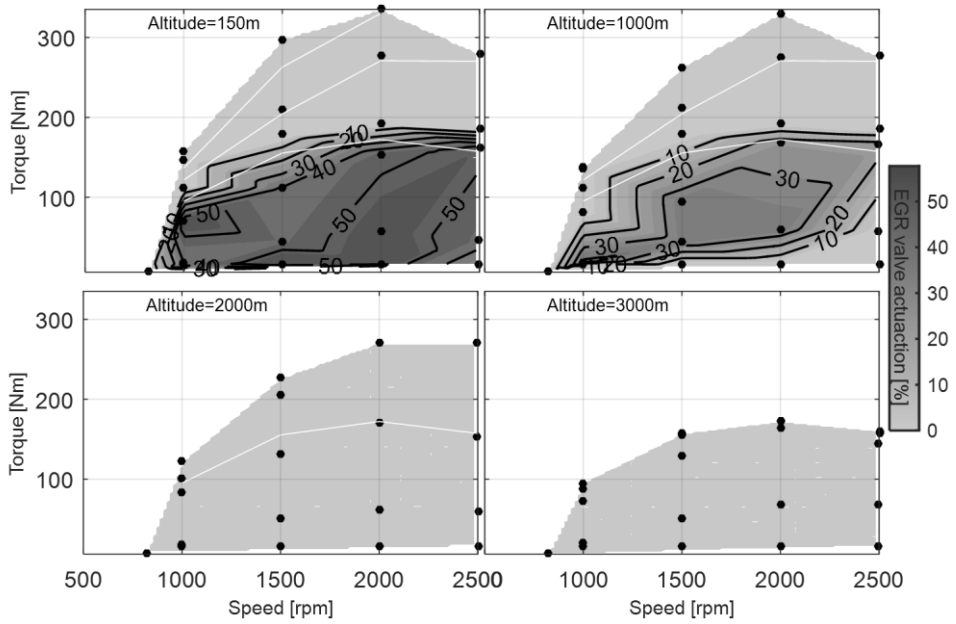

Figure 6.2 – EGR valve position at different altitudes

Figure 6.2 to Figure 6.5 show that maximum engine torque decreases with the altitude, being at 3000 meters much lower than maximum torque at any other altitude. This is caused because the engine is in a safe mode at 3000 m for pedal positions higher than 50% and torque does not change when pedal is increased. The safe mode protects compressor of surge but also of high compressor outlet air temperature, which reaches values

slightly over 160 ºC, and high turbine inlet gas temperature, which reaches values slightly over 800 ºC.

This can be explained by two opposite effects. On one hand, p_2 decreases because p_1 also decreases, which should lead to a decrease of the engine air mass flow. But the pressure ratio in the compressor is kept constant. However, to compensate this effect, EGR closes with the altitude, being completely closed at 2000 m and 3000 m, as shown in Figure 6.2. EGR closing slightly increases fresh air for same engine torque and speed conditions, as shown in Figure 6.3. But due to the absence of EGR, the addition of both gases (EGR and fresh air mass flow) decreases with the altitude. This means the in-cylinder trapped mass decreases at the intake valve closing, what reduces maximum in-cylinder pressure and increases adiabatic flame temperature (due to EGR absence).

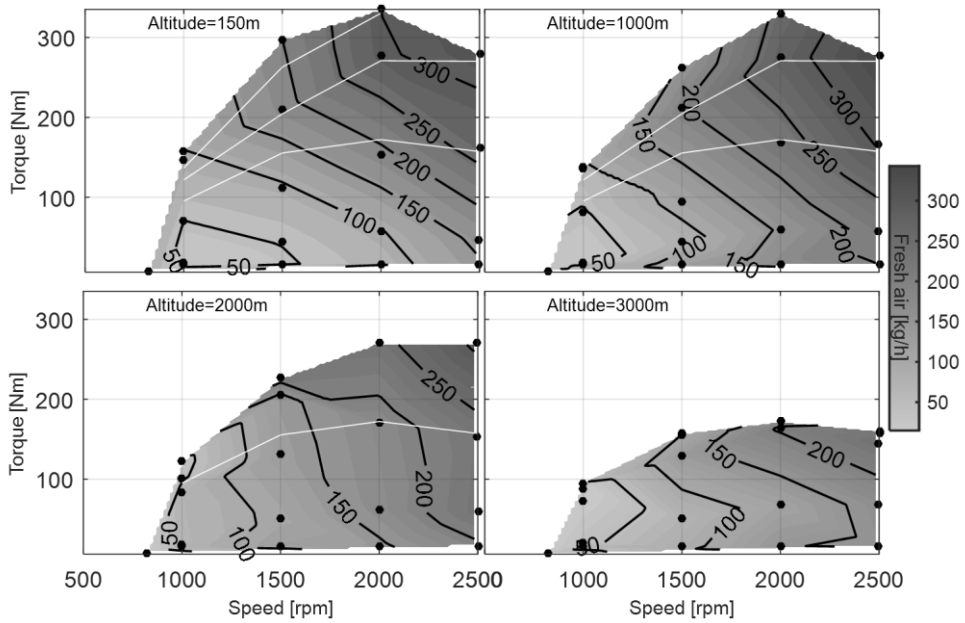

Figure 6.3 – Fresh air mass flow at different altitudes

VGT and p_2

With respect to the VGT behavior, there are not relevant differences in VGT position at the different altitudes, as can be seen in Figure 6.4, in spite of the fact that there are two main strategies for VGT control depending on the engine operative area. On one side, the VGT position is within an open loop control at engine low load and low speed. In this area,

the VGT position is set by ECU look-up tables, which are independent of the altitude. Nevertheless, some dynamic corrections with altitude are considered, as will be further described during transient behavior analysis. This operative area covers most of the points where the engine is during the NEDC, except those at very high speed in the EUDC cycle. On the other side, the operative area at which the VGT position is set in order to keep boosting pressure constant. This area is at high load and high speed, where the turbine recovers enough energy from the exhaust gases.

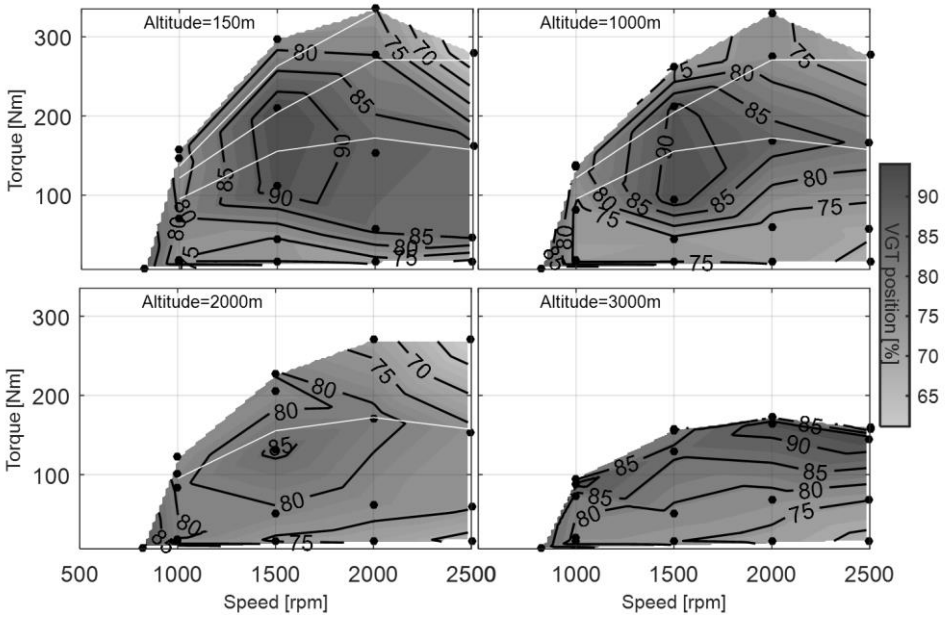

Figure 6.4 – VGT position at different altitudes

Nevertheless, under steady state operation, and for the same engine torque and speed values than at 150 m, VGT remains at quite the same position independently of altitude (Figure 6.4). Therefore p_2 is not recovered, but shows values from 200 to 300 mbar lower than at 150 m for the same engine torque and speed (Figure 6.5). It can be said that control is protecting compressor and therefore keeps quite constant pressure ratio(Π_c) instead of p_2, like in a pure open loop control strategy even at full load.

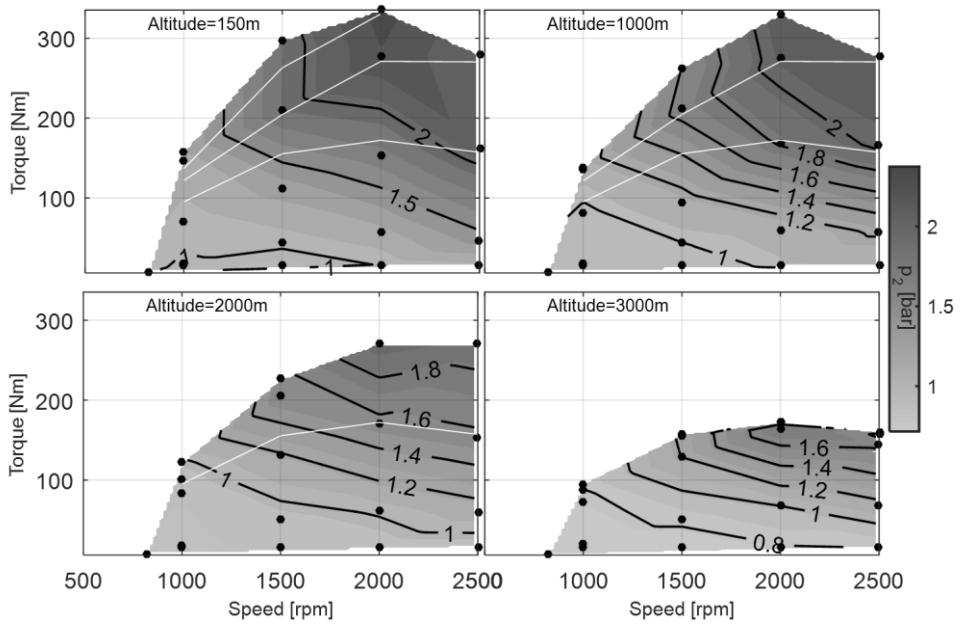

Figure 6.5 – Compressor outlet pressure (p_2) at different altitudes

Compressor behavior

Figure 6.6 (a) shows the full load lines, where EGR is closed, in the compressor map for the studied altitudes. All points with same engine speed should collapse in the compressor map if the volumetric efficiency does not vary with altitude. This can be deduced from Equation (6.1) and Equation (6.2):

$$\dot{m} = \eta_v \left[\frac{n}{2}\right] V_D \frac{p_2 - \Delta p_{cooler}}{R T_{co}} \tag{6.1}$$

$$\dot{m}^* = \left[\left(\frac{V_D}{2}\right)\frac{\sqrt{T_{10}}}{R T_{co}}\left(1 - \frac{\Delta p_{cooler}}{p_2}\right)\frac{p_2}{p_{20}}\right] \Pi_c n \eta_v \tag{6.2}$$

Equation (6.1) defines the engine mass flow as a function of the volumetric efficiency. If Equation (6.1) is multiplied by $\sqrt{T_{10}}/p_{10}$, the expression obtained is Equation (6.2). The expression between brackets in Equation (6.2) can be said not to change with the altitude since $(1 - \Delta p_{cooler}/p_2)\, p_2/p_{20}$ variation with the altitude is lower than 1% and T_{10} was controlled to be same in all tests. Therefore, for a given compression ratio (Π_c) and engine speed, only volumetric efficiency (η_v) variation

explains the horizontal movement of the points with the altitude. This volumetric efficiency variation can be explained by the exhaust gas back-flows during open loop period of the engine cycle. Thus, the decrease of p_2 with the altitude (Figure 6.5), while keeping constant VGT position, increases exhaust gas back-flows. Especially at 3000 m, η_v is a reduced, moving full load points closer to surge limit (Figure 6.6 (a)).

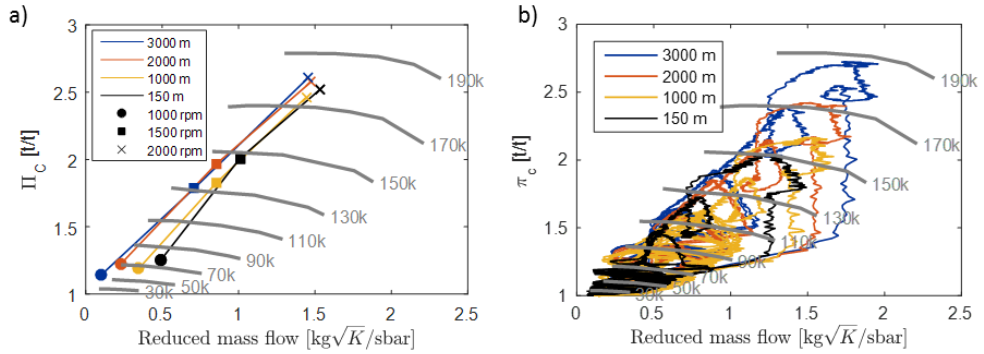

Figure 6.6 – Engine operation at compressor map for points at different altitudes: Full-load steady-state tests (a) and transient NEDC tests (b)

6.3.2. Dynamic tests

Once the steady state tests have been analyzed and the main trends of the engine behavior with the altitude have been explained and understood, the NEDC was tested at the same four altitudes. The results obtained are shown in the following paragraphs and the results are also analyzed.

The main objective of these tests is to analyze engine performance and emissions during a NEDC. A gas test bench HORIBA 7100DEGR was used for the measurement of gaseous emissions. The HORIBA analyzer specifications, measuring ranges and response time are adequate to the requirements established by the standard ISO16183 to measure the concentrations of the exhaust gas components under transient conditions [14]. The sample line of the equipment is connected directly to the exhaust pipe and it is heated to maintain wall temperature around 191 ºC and to avoid the condensation of hydrocarbons into the line. The line is extended from the exhaust pipe to the equipment units where the different analyzers are located. The hydrocarbons analyzer is a heated flame ionization detector (HFID) type, with detector, valves, pipe work, etc. heated so as to maintain a gas temperature of 190 ± 10 ºC. Oxides of nitrogen are measured on a dry basis by means of a heated chemiluminescent detector

(HCLD) type with a NO_2/NO converter. The sampling path is maintained at a wall temperature of 190 ± 10 ºC up to the converter. The carbon monoxide and dioxide are measured with an analyzer of the non-dispersive infrared (NDIR) absorption type.

VTG and EGR position

Figure 6.7 shows EGR position during the NEDC in absolute value. As can be observed, EGR closes as altitude increases. In fact, EGR is fully closed at 2000 m and 3000 m during all the driving cycle. This result was already observed in the steady tests (Figure 6.2). In addition to the steady state tests, very relevant differences are noticed at EGR opening even at EUDC between 150 m and 1000 m tests. About min 16 in Figure 6.7 is shown how EGR closes at 1000 m and EUDC much more than at UDC, but opposite trend is shown at 150 m.

Figure 6.8 shows the difference in the VGT position during NEDC according to Equation (6.3), where positive values at higher altitudes indicate that the VGT vanes are more closed. Figure 6.9 and Figure 6.10 shows also differences of variables using Equation (6.3) philosophy.

$$Variable\ difference^{t}_{altitude} = Variable^{t}_{altitude} - Variable^{t}_{150m} \qquad (6.3)$$

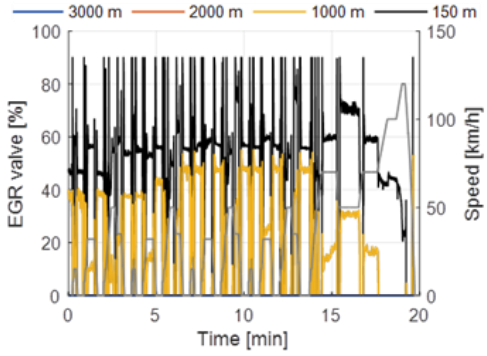

Figure 6.7 – Instantaneous EGR vale position (%) for different altitudes during NEDC

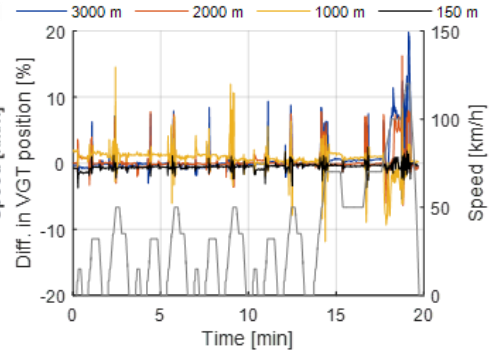

Figure 6.8 – Instantaneous VGT position difference with respect to sea level for different altitudes during the NEDC

During UDC, the VGT is controlled in open loop with dynamic correction of the VGT position during the accelerations. At EUDC, VGT controls p_2 in order to keep boosting pressure constant. For that reason, at EUDC, VGT closes a lot with altitude. This results in a high increase in p_3, as shown in Figure 6.9. During the open loop control (UDC), p_2 and many times p_3

decrease with altitude. Similarly, p_1 and p_4 also decrease with the altitude increasing the turbine pressure ratio (Π_T), which increases turbine energy given to the compressor. Consequently, compressor pressure ratio (Π_C) increases, as shown in Figure 6.6 (b) and Figure 6.10. In spite of this increase in turbine and compressor pressure ratios, they are not big enough to compensate the decrease in p_1. Even with dynamic corrections of VGT, and corresponding p_3 peaks, p_2 is barely recovered. Just sometimes p_2 overcome 150 m values and just in case of 1000 m.

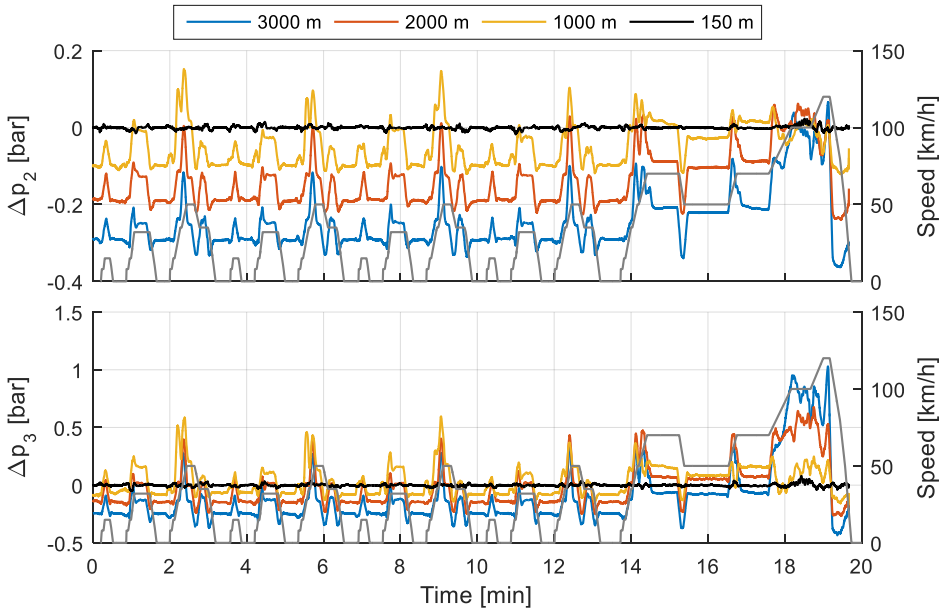

Figure 6.9 – Instantaneous differences during NEDC and with respect to 150 m of p_2 (top) and p_3 (bottom) for different altitudes

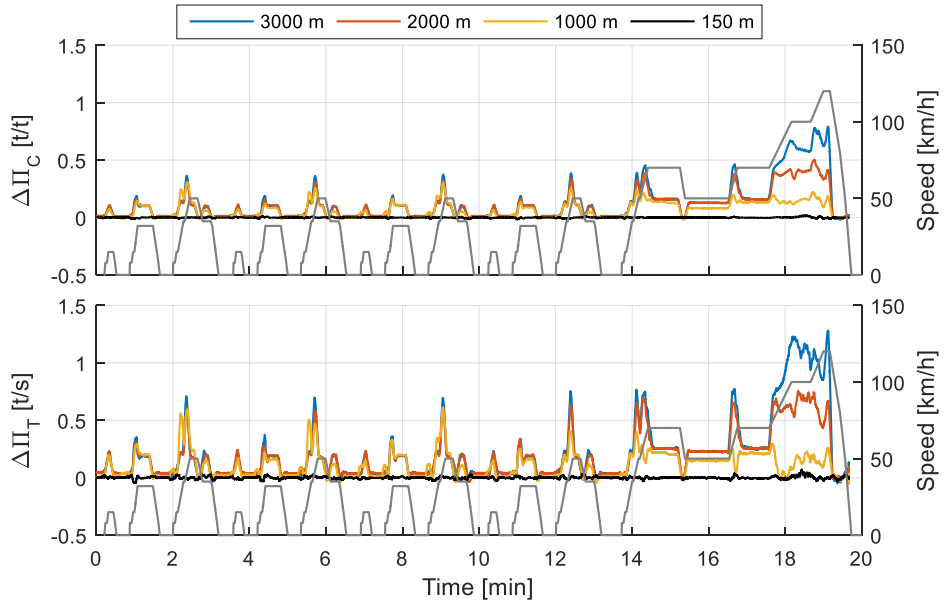

Figure 6.10 – Instantaneous differences during NEDC and with respect to 150 m of Π_c (top) and Π_T (bottom) for different altitudes

Regarding the compressor operating conditions during NEDC, Figure 6.6 (b) shows its performance on the compressor map at the four studies altitudes. It can be said that Π_c growing at EUDC, as shown in Figure 6.10, increases the risk of over speed during transient cycles. Figure 6.6 (b) shows also that surge risk is not high during NEDC, and barely increases at UDC (Π_c < 1.5) due to the higher pressure ratio as altitude increases.

VGT and EGR valve control strategies have, as can be deducted, a key influence in the operation at altitude. These effects in engine performance and emissions will be further analyzed in the following sections.

In Chapter 4 Section 4.8, the peaks in the engine intake pressure were analyzed. It was pointed that there are some peaks with a maximum amplitude of 20 mbar caused during the engine transients that are difficult to eliminate with the control actuators. In Figure 6.9, it can be seen how the pressure peaks at the altitude simulator connection with the engine disappear at the compressor outlet because they are muffled in the engine air filter, the pipes and the compressor. Therefore, these 20 mbar peaks have not any influence in the engine performance.

Air mass flow

Fresh air mass flow increases with the altitude, as shown in Figure 6.11, where the variation has been represented following Equation (6.4). The maximum fresh air mass flow is obtained at 1000 m above sea level, decreasing at 2000 m and 3000 m with respect to the 1000 m case. This is caused by the decrease in p_2 with the altitude. Nevertheless, measured total air mass at altitude has always been higher than at 150 m, due to the particular EGR and VGT control.

$$Variable\ deviation^{t}_{altitude} = \frac{\sum_{i=0}^{t} Variable_{\ altitude} - \sum_{i=0}^{t} Variable_{\ 150m}}{\sum_{i=0}^{total} Variable_{\ 150m}} \times 100 \qquad (6.4)$$

Therefore, the increase in fresh air mass flow can be explained by the different strategies in the VGT and EGR position during the NEDC.

At UDC (zone A in Figure 6.11), fresh air mass flow is increased at 1000 and 2000 m because EGR is progressively closed with altitude, in spite of average p_2 is lower because VGT is open loop controlled. At 3000 m, fresh air is lower than at 2000 m because EGR is already fully closed at 2000 m and at 3000 m p_2 is much lower and exhaust gas back-flows become much higher. At the beginning of the EUDC (zone B in Figure 6.11), VGT is still open loop controlled. However, EGR trends to open at 150 m whilst trends to close at 1000 m with respect to zone A (Figure 6.7). Consequently, the growing trend in fresh air increases with respect to zone A. As the EGR trends to open at 150 m the difference also increases with respect to zone A for tests at 2000 m and 3000 m. Moreover, dynamic actuations to VGT open loop control are also more aggressive at zone B. In zone C, the VGT is controlling p_2 constant for all the altitudes and EGR is still more open at 150 m than at the rest of the altitudes. Both effects together increase fresh air mass flow even more with altitude. Finally, in the first part of zone D air mass flow is constant for all the altitudes because EGR is closed for all the altitudes and p_2 is constant controlled by the VGT. In the second part of zone D air mass flow decreases with the altitude, because VGT stops controlling (opens), causing p_2 decrease with altitude because the VGT does not provide energy and EGR is closed even at 150 m.

Other important phenomenon during operation in the VGT open loop region (zones A and B) is that p_2 and p_3 are higher at 1000 m than at sea level in some of the accelerations. Also a big increase at 2000 m and 3000 m can be appreciated. This is caused by the dynamic corrections on the VGT

open loop control and increases fresh air mass flow in these regions (circles in Figure 6.11), which increases further p_3 and pumping losses.

Must be said that as effective torque is the same at all altitudes, all this extra air mass flow is not used to burn more fuel, but mainly means more pumping losses for the engine.

Fuel

Figure 6.12 shows fuel consumption accumulated differences in percentage (Equation (6.4)). It shows also two different trends, very influenced by VGT and EGR control strategies. At UDC, VGT is open loop controlled, decreasing p_2 and hence effective pressure ratio in the engine. On the other side, the dynamic actuations increase air mass flow and p_3 and therefore pumping losses. In addition, at 1000 m the increment is higher than at the rest of the altitudes because the engine is colder, causing the VGT to be even closer (Figure 6.8). Besides it, at 1000 m still there is some EGR in the combustion chamber. As a consequence, 1000 m case shows lower combustion temperature and lower maximum in-cylinder pressure than 2000 m and 3000 m cases, at which EGR valve was fully closed. So 1000 m shows even lower indicated efficiency than 2000 m and 3000 m. During the accelerations in the UDC, marked with red and dotted squares in Figure 6.12, fuel consumption has peaks at high altitude, caused by the dynamic actuation of the VGT, which closes to follow the vehicle acceleration imposed by the cycle.

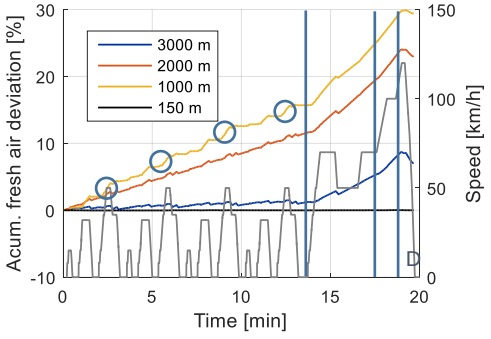

Figure 6.11 – Accumulated differences with respect to 150 m of fresh air for different altitudes during NEDC

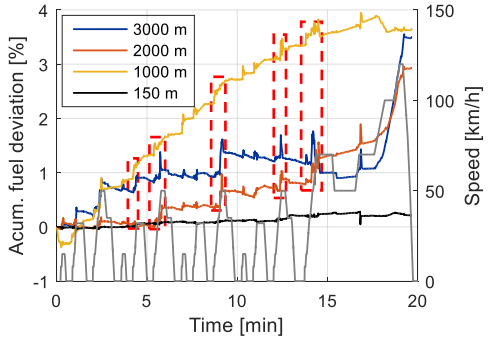

Figure 6.12 – Accumulated differences with respect to 150 m of fuel injected for different altitudes during the NEDC

In the part of the EUDC where the VGT is controlling p_2, pumping losses increment is more significant due to higher p_3 (Figure 6.9), increasing fuel

consumption very fast at 2000 m and 3000 m. At 1000 m, there is not any fuel increment during EUDC because p_1 is not so low and the increment of p_2 is mostly achieved by the closer position of the EGR valve with respect to 150 m.

Emissions

Finally, the analysis of the emissions at different altitudes is performed. All the emissions represented in Figure 6.13 are calculated as a difference in percentage with respect to the corresponding test at sea level, according to Equation (6.4).

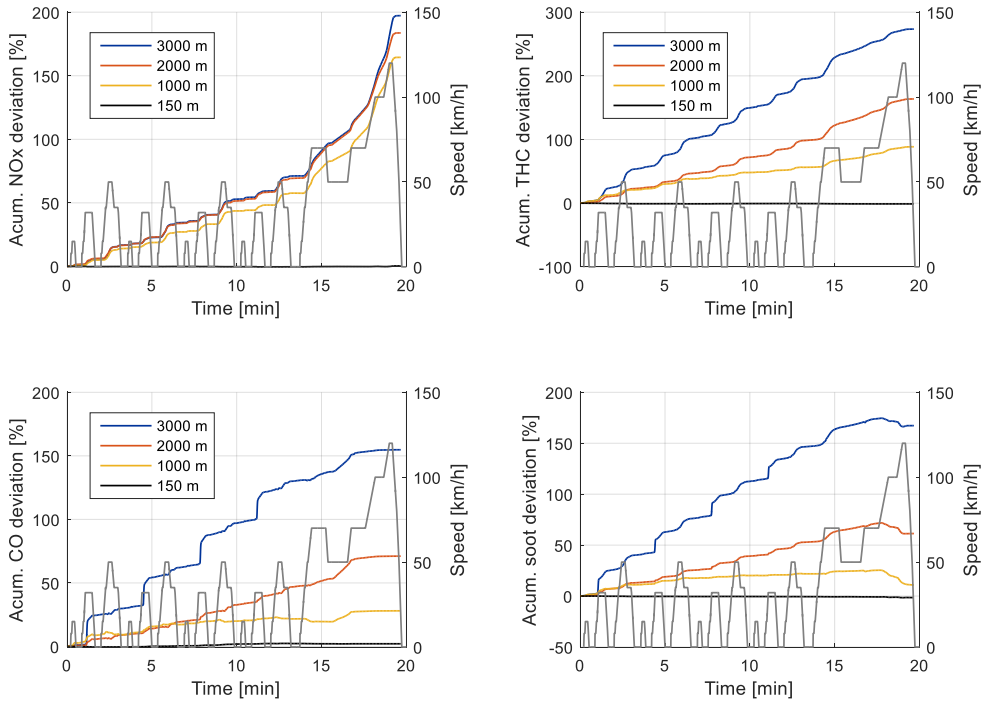

Figure 6.13 – Accumulated percentage differences with respect to 150 m for different altitudes during NEDC of NOx (top left), THC (top right), CO (bottom left) and Soot (bottom right) emissions

NOx emissions are higher at any altitude than at sea level. The main reason for the NOx increase is the EGR closing. At 2000 m and 3000 m the EGR is fully closed during all the NEDC, being NOx emissions very similar between them. This result is slightly different if compared with results

shown by Xin Wang, et. al [9], where NOx emissions decrease at 3200 m with respect to 2800 m. However, results are similar to the one obtained by Linxiao, et. al. [15] where NOx emissions barely change with altitude. These different NOx emissions trends can be strongly affected by EGR behavior in each tested engine and remarks the importance of an appropriate control strategy at high altitude.

THC and CO emissions increase with altitude. Both were measured downstream of the DOC. Therefore their emissions are very affected by DOC performance. Anyway, DOC is not activated until late in the EUDC part of the NEDC, where Figure 6.13 shows that CO and THC emissions do not suffer further increments. Their increase before catalyst activation is partly explained by the increment of the jet-to-wall impingement, caused by the lower pressure in the combustion chamber during fuel injection, due to lower p_2. CO and THC emissions are especially relevant in the accelerations at UDC, when p_2 is low but p_3 grows suddenly due to VGT closing. CO and THC emissions are then increased by the exhaust gas back-flows caused by the increase of p_3 during the VGT closing peaks as a consequence of the dynamic corrections to the open loop control.

Finally, soot emissions increase with altitude. The cause is very similar to the increase of CO, also with peaks at the highest altitude. At the last part of the EUDC, soot emissions decreases at altitude because VGT controls p_2, what balance jet-to-wall impingement at high altitude and contributes to decrease soot emissions. In addition, EGR is fully closed at altitude but still open at sea level, what also increases soot formation at sea level with respect to altitude operation.

Regulated emissions have been summarized in

Figure 6.14, which shows emissions in grams per kilometer differentiating between the UDC and the EUDC for the NEDC at 150 m, 1000 m, 2000 m and 3000 m. Measured emissions at sea level are very close to Euro IV limits, as would be expected. However, all the emissions increase with the altitude from two to three times 150 m emissions caused mainly by the EGR closing (high temperature in combustion chamber), VGT closing (exhaust back-flows) and lower p2 (jet-to-wall impingement).

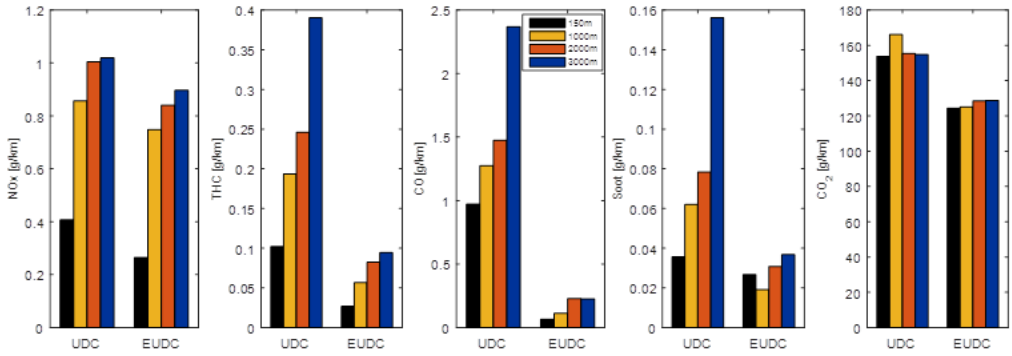

Figure 6.14 – Emissions at different altitudes in UDC and EUDC of the NEDC

6.4 Summary and conclusions

In this chapter, the behavior of an engine as a function of the altitude of operation has been discussed. Altitude tests have been performed with an altitude simulator which is connected to the engine intake and exhaust in order to generate pressure from sea level up to 7000 meters above sea level, while the rest of the room pressure is kept constant at sea level pressure.

With respect to the engine behavior in altitude, steady-state tests show different trends than dynamic tests due to dynamic control corrections. The most relevant change observed in steady state is the reduction of the maximum torque with altitude, specially reduced at 3000 meters because the engine goes into a safe mode protecting the compressor from surge and turbine from too high temperature. Also with altitude, EGR closes, being completely closed at 2000 m and 3000 m, this increases fresh air mass flow. With respect to the VGT, it is in an open loop control strategy for all the steady points tested but applying dynamic corrections in the accelerations during the dynamic tests. Only during the EUDC, VGT closes with the altitude in order keep p_2 constant.

In conclusion, control strategies should be reoriented from just performance and mechanical protection criteria to emissions abatement in order to be able to meet upcoming emissions standards. It could be proposed a change in the VGT and EGR control strategies.

For example, the EGR valve might not close as altitude increases, keeping total gas flow (fresh air and exhaust gas) to the cylinders constant with the altitude. A more efficient use of the burn gas ratio (BGR) could be done if BGR were estimated by the ECU considering O_2 contents in the exhaust

gases. Therefore, the same BGR could be kept in the cylinders in altitude, what would help to keep overall engine performance. This probably would reduce NOx compared to the results shown in this paper. Meanwhile, the VGT might controls p_2 constant even during the UDC. Constant p_2 would decrease jet-to-wall impingement, what would decrease CO, THC and soot emissions. Besides, this would keep fresh air mass flow through the compressor constant, avoiding surge risk. Because of the low load, turbocharger over-speed would be also far. However, VGT closing might highly increase pumping losses and therefore fuel consumption would be drastically increased.

If the increase of the EGR rate would lead to an increase even higher of soot, CO and THC emissions that could not be controlled by the VGT closing, other technologies such de-NOx aftertreatment systems should be considered in passenger cars as responsible to control tailpipe NOx emissions.

With the altitude, the aftertreatment systems become more important to reduce emissions, as the decrease of the pressure force to close the EGR and the VGT if the engine performance wants to be kept constant. This leads to an increment in the pollutants that have to be reduced by the aftertreatment systems.

However, the new homologation cycles will force to reduce emissions also at -7 ºC and the temperature in the aftertreatment systems is a key parameter for its proper operation, as it is much related with its efficiency. In the next chapter, different strategies to increase aftertreatment temperature will be studied, as one of the many potential strategies to control the emissions increment with the altitude.

6.5 References

[1] ISO, Standard Atmosphere, ISO 2533:1975, Int. Stand. Organ. 2533 (1975).

[2] H. Hiroyasu, M. Arai, M. Tabata, Empirical Equations for the Sauter Mean Diameter of a Diesel Spray, SAE Tech. Pap. 890464. (1989). doi:10.4271/890464.

[3] K.D. Kihm, D.P. Terracina, S.E. Payne, J.A. Caton, Synchronized Droplet Size Measurements for Coal-Water Slurry Sprays Generated from a High-Pressure Diesel Injection System, J. Inst. Energy. 67 (1994) 2–9.

[4] Y. Zama, W. Ochiai, T. Furuhata, M. Arai, Experimental study on spray angle and velocity distribution of diesel spray under high ambient pressure conditions, At. Sprays. 21 (2011) 989–1007. doi:10.1615/AtomizSpr.2012004722.

[5] L. Shen, Y. Shen, Combustion Process of Diesel Engines At Regions With Different Altitude, SAE Tech. Pap. 950857. (1995). doi:10.4271/950857.

[6] J.E. Dec, A conceptual model of DI diesel combustion based on laser sheet imaging, SAE Tech. Pap. (1997). doi:10.4271/970873.

[7] H. Wu, K. Nithyanandan, N. Zhou, T.H. Lee, C.F. Lee, C. Zhang, Impacts of acetone on the spray combustion of Acetone–Butanol–Ethanol (ABE)-Diesel blends under low ambient temperature, Fuel. 142 (2015) 109–116. doi:10.1016/j.fuel.2014.10.009.

[8] Z. Zhu, F. Zhang, C. Li, T. Wu, K. Han, J. Lv, Y. Li, X. Xiao, Genetic algorithm optimization applied to the fuel supply parameters of diesel engines working at plateau, Appl. Energy. 157 (2014) 789–797. doi:10.1016/j.apenergy.2015.03.126.

[9] X. Wang, H. Yin, Y. Ge, L. Yu, Z. Xu, C. Yu, X. Shi, H. Liu, On-vehicle emission measurement of a light-duty diesel van at various speeds at high altitude, Atmos. Environ. 81 (2013) 263–269. doi:10.1016/j.atmosenv.2013.09.015.

[10] D.M. Human, T.L. Ullman, T.M. Baines, Simulation of High Altitude Effects on Heavy-Duty Diesel Emissions, SAE Tech. Pap. 900883. (1990). doi:10.4271/900883.

[11] X. Li, S. Xu, Y. Xiong, X. Liu, Effects of oxygenated fuel on diesel engine performance under the simulated condition of plateau area, Shiyou Xuebao, Shiyou Jiagong/Acta Pet. Sin. (Petroleum Process. Sect. 32 (2016) 215–220. doi:10.3969/j.issn.1001-8719.2016.01.030.

[12] H. Zhu, S. V. Bohac, Z. Huang, D.N. Assanis, Emissions as functions of fuel oxygen and load from a premixed low-temperature combustion mode, Int. J. Engine Res. 15 (2014) 731–740. doi:10.1177/1468087413501317.

[13] X. Shi, T. Wang, C. Ma, Simulations of the diesel engine performance with a two-stage sequential turbocharging system at different altitudes, Proc. Inst. Mech. Eng. Part D J. Automob. Eng. 228 (2014) 1718–1726. doi:10.1177/0954407014535919.

[14] ISO-16183:2002, Heavy duty engines - Measurement of gaseous emissions from raw exhaust gas and of particulate emissions using

partial flow dilution systems under transient test conditions, (2002).

[15] L. Yu, Y. Ge, J. Tan, C. He, X. Wang, H. Liu, W. Zhao, J. Guo, G. Fu, X. Feng, X. Wang, Experimental investigation of the impact of biodiesel on the combustion and emission characteristics of a heavy duty diesel engine at various altitudes, Fuel. 115 (2014) 220–226. doi:10.1016/j.fuel.2013.06.056.

CHAPTER 7

Strategies to reduce emissions in extended conditions

Contents

Figures

Tables

7.1 Introduction

In the previous chapter, a turbocharged diesel engine has been tested at different altitudes during transient and dynamic operation. The results have shown that control strategies applied at sea level are not working at altitude to reduce emissions. The lower pressure leads to a decrease in the fresh air, which has to be balance by closing the EGR. However, closing the EGR leads to an increase in NO_x emissions. Also p_2 decreases, which leads to an increment in the jet-to-wall impingement, increasing CO, HC and soot emissions. In order to recover p_2, VGT has to close, increasing the pumping losses and therefore the fuel consumption. But not only, turbocharger speed turbine inlet temperature and compressor outlet temperature approach to risky limits. As can be seen, the solution is not straightforward; especially concerning emissions, since EGR cannot be massively used without compromising turbocharger performance.

In this scenario, aftertreatment systems will gain a more important role to mitigate emissions increment with the altitude. Moreover, considering that the extended conditions of the in force regulations with World-wide harmonized Light duty Test Cycle (WLTC) [1] will require to control emissions up to 1300 meters of altitude and -7 ºC, in order to approach regulated emissions to real driving emissions, contrary to what happened with NEDC [2–4].

However, despite advances in purely aftertreatment aspects [5] and control strategies [6], the performance of the diverse aftertreatment devices is very dependent on the operating temperature. For example, a standard DPF needs around 500 ºC to reach target conversion efficiency and to complete regeneration processes [7]. This makes them rely on the engine design and calibration because of the imposed turbine outlet temperature, besides processes required to control additional parameters during engine setup [3].

For these reasons, exploring the potential of different solutions to increase inlet aftertreatment temperature (T_4) is becoming a critical topic that will also help to overcome extended altitude conditions for homologation. Nevertheless, such studies cannot be tackled without considering concerns on the engine fuel consumption, which can be penalized as T_4 is increased.

Due to this increasing interest, many studies have been published. Ranganathan et al. [8] collected data from 67 naturally aspirated spark ignited engines during vehicle operation and proposes a correlation to predict exhaust manifold temperature with some geometrical measures of

the engine. Alkidas et al. [9] analyses the effect in the temperature of the pulsating flow in the exhaust manifold, which enhances heat transfer to the walls, and how this heat transfer enhance decreases with the attenuation of pulsations as the exhaust gas goes through the exhaust pipes.

There are also several publications studying the influence of some engine parameters in T_4 and bsfc. For example, Deng and Stobart [10] simulated effect of different variable valve timing and valve lift profiles for exhaust and intake valves of a Caterpillar C6.6 heavy duty diesel engine. In their parametric studies fuel injection timing and quantity were kept constant. Results show that bsfc can be significantly improved with proper valve timing, decreasing T_4 as well.

Also D'Ambrosio et al. [11] designed an integrated exhaust manifold in the cylinder head for a diesel engine to study its effect in bsfc, NOx emissions, exhaust temperature and warm-up time. Results show this new design promising because maintains bsfc, performance and emissions while appreciably faster engine and aftertreatment warm-up is achieved.

On the other hand, to achieve target conversion efficiency, Payri et al. [12] propose a change of the positioning of DPF and DOC systems in a diesel engine. A pre-turbo aftertreatment positioning is analyzed and results show a remarkable increase in DPF temperature because exhaust gas has not been expanded and cooled down in the turbine.

As can be seen, exhaust temperature estimation is still a critical topic and heat losses reduction in the exhaust line is being studied, but most of the studies are focused in bsfc and emissions reduction and their effect in inlet aftertreatment temperature has not been specifically addressed but as a second order effect.

However, in this chapter all the studies are focused on aftertreatment inlet temperature increase looking for minimizing bsfc penalty. The influence of several design parameters is studied by modelling approach under steady state operating conditions in the turbocharged diesel engine studied in this thesis document. An engine model has been setup with experimental data using GT-Power software coupled to an external heat transfer and friction losses turbocharger model to predict correctly turbine outlet temperature. The analysis covers parametric studies focused on the exhaust and intake valves diameter, valves timing as well as the use of multi-step openings. The exhaust ports total length and distribution into several branches are also explored. Differences in the potential of every proposal are also considered as a function of the engine operating range. Finally, discussions on the influence on turbine outlet temperature and fuel consumption are

conducted to define general guideline criteria. These are affected by the need to look for solutions providing a suitable balance between exhaust temperature increase and minimized impact on engine fuel economy.

7.2 Methodology

7.2.1. Heat transfer model description

To perform the simulations has been used the commercial software GT-Power [13], a 1D fluid dynamic engine modelling. Standard GT-Power elements has been used to build up the model, but the turbocharger has been replaced and its linked to OpenWAM software [14], which is the same software used to model the altitude simulator, explained in Section 3.4 from Chapter 3 [16, 17]. OpenWAM has an advanced model to simulate heat transfer in the turbocharger, improving T_4 prediction and therefore obtaining more accurate results in the parametric studies carried out. This heat transfer model in the turbocharger is explained in detail by Serrano et al. in [15] and the turbocharger heat transfer and mechanical losses influence in the prediction of the engine performance in [16]. Figure 7.1 shows the scheme of the lumped turbocharger heat transfer model. The model accounts for 5 nodes. These have been chosen in order to keep the balance between accuracy and simplicity. Only one node could have been used for each different metal component (i.e. turbine case, bearing housing and compressor case) as proposed by Baines [17]. Nevertheless, the high temperature gradients in the bearing housing, which are due to the active cooling in this component (oil and sometimes water cooling) and the high temperature difference between turbine and compressor back-plates, suggests the convenience of including 3 nodes in this element. One of the nodes is placed in the hot turbine back-plate (H1 in Figure 7.1); another is located in the cold compressor back-plate (H3 in Figure 7.1); and a third one is placed in the central bearing housing (H2 in Figure 7.1), where oil and water ports are located and heat sink usually takes place.

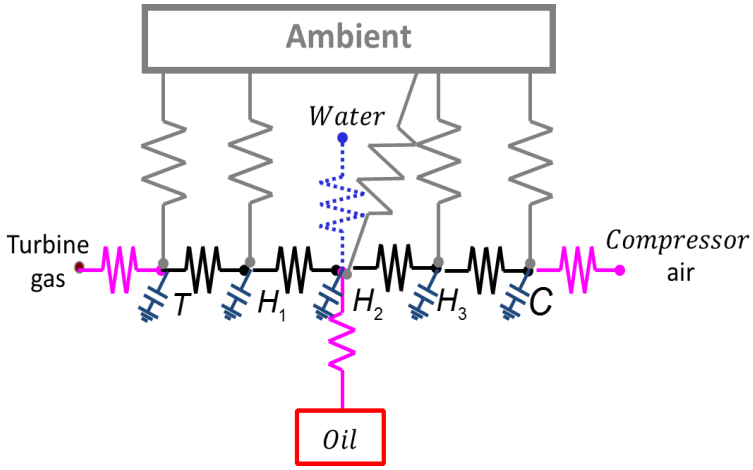

Figure 7.1 – Scheme of the lumped turbocharger heat transfer model

In the heat transfer model, radial temperature distribution is considered negligible compared to the axial one. Besides, the thermal properties of the turbocharger are calculated from measurements on a thermohydraulic test rig. Measurements in a hot flow gas stand allowed obtaining the correlations for both internal heat transfer and external heat transfer. In addition, in order to adapt a mathematical model for turbocharger mechanical losses, adiabatic measurements from gas stand have been used. Therefore, using these models, the calculation of heat transfer and mechanical losses for any operating condition of the turbocharger in the engine is possible. In addition, all temperatures are not time but mass averaged, which results in a more accurate temperature prediction [18].

7.2.2. Engine model specifications

The basic characteristics of the simulated engine (already used in the previous chapter) are again detailed in Table 7.1 for reader convenience.

Table 7.1. Engine specification of simulated engine

Type	Turbocharged HSDI diesel Euro IV
Displacement	1997 cm3
Bore	85 mm
Stroke	88 mm
Number of cylinders	4 in line
Number of intake valves	2 per cylinder
Number of exhaust valves	2 per cylinder
Turbocharger model	VGT
Compression ratio	15.5:1
Maximum power @ speed	120 kW @ 3750 rpm
Maximum torque @ speed	340 Nm @ 2000 rpm
EGR type	Cooled, high pressure with intake throttle

7.2.3. Simulated operation points

Six engine operating points has been simulated, as shown in Table 7.2. These conditions have been chosen to cover a wide range in the engine operation map. In following figures, #A, #B and #C operating points are defined as low load conditions whereas #D, #E and #F are referred as high load points. Thus, these sets of operating points are shown separately to address properly different trends and magnitude in variations.

Table 7.2. Specifications of tested Euro IV turbocharged engine

Point ID	Speed [rpm]	Load [%]
#A	1500	0
#B	1500	25
#C	2000	25
#D	1250	75
#E	2000	75
#F	3500	100

7.3 Results

First of all, engine model was adjusted with experimental data in order to have a predictive model able to produce reliable results in the following parametric studies. Figure 7.2 shows the comparison between measured and modelled data. In overall, all variables have admissible errors and the model can be considered as predictable in the following parametric studies.

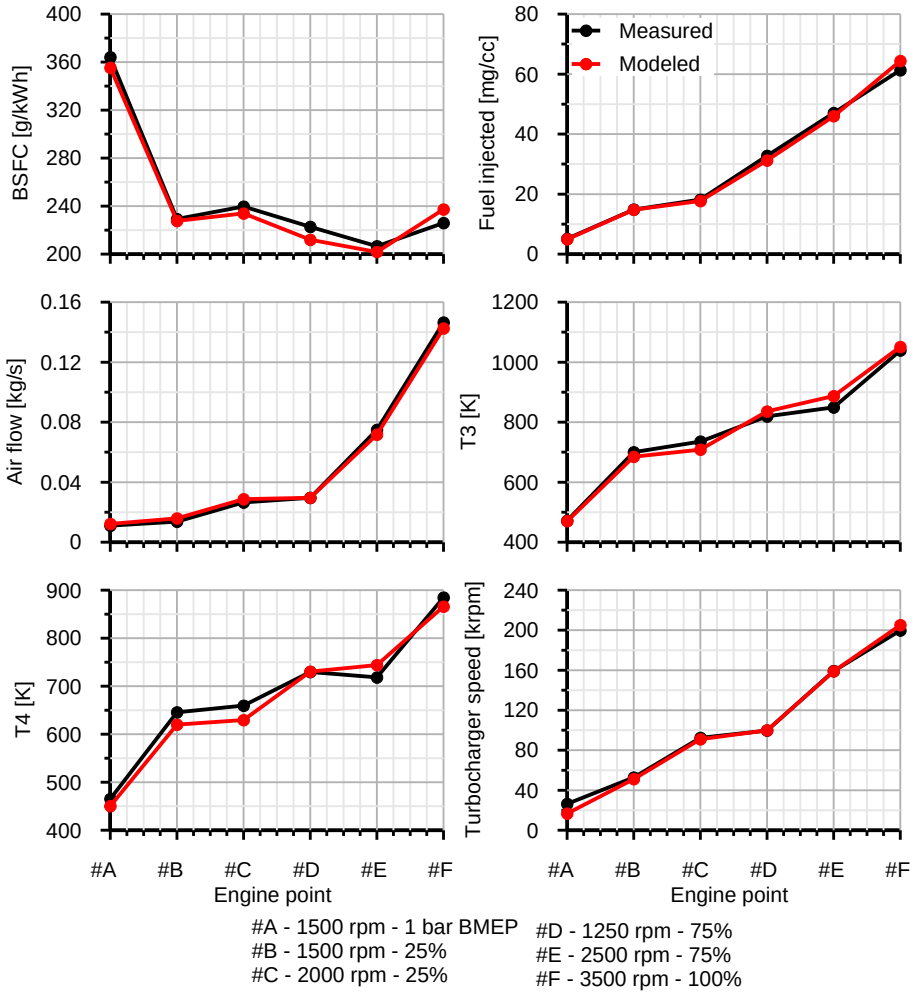

Figure 7.2 – Engine measured and modeled results comparison for the six operation points

In all parametric studies some variables have been controlled to keep them in a constant value by means of PIDs. Torque has been controlled changing the injected fuel; the intake manifold pressure is governed by the VGT opening; and the oxygen concentration in the intake manifold after the mixing between fresh air and high pressure EGR has been controlled by the EGR valve opening. Once the EGR valve is fully open and the oxygen concentration is still too high, an intake valve upstream the EGR junction throttles the air charge.

Parametric studies were carried out trying to obtain higher T_4 with low or lack of bsfc penalty, identifying general trends and potential engine optimizations. These studies are focused in the exhaust line and in cylinder valves.

Figure 7.3 shows the exhaust manifold layout, where stations and their lengths have been indicated, from the exhaust valve (station 1) to the turbine inlet (station 4). The exhaust ports length (station 1 to 3) is 130 mm and the exhaust manifold length (station 3 to 4) is 83 mm.

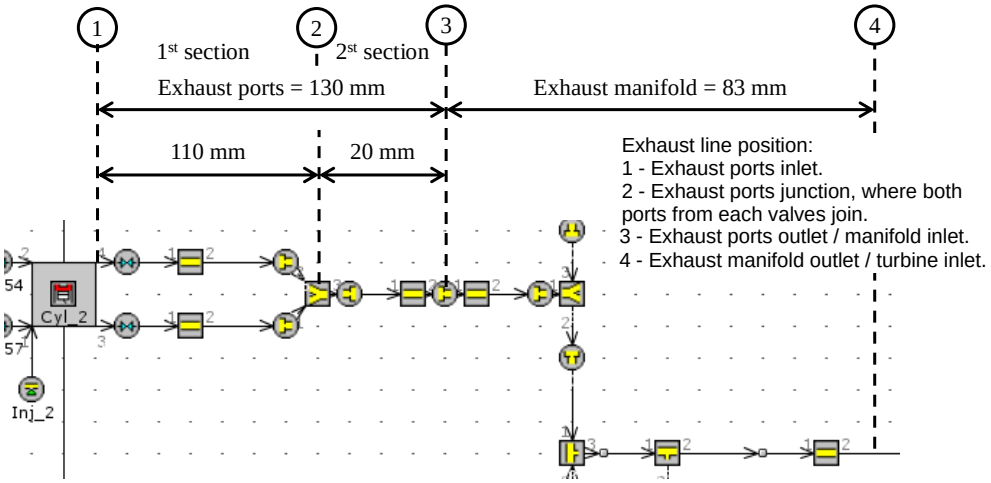

Figure 7.3 – Scheme of the baseline exhaust. Exhaust ports length and distribution

The temperature evolution through the exhaust line for the six chosen operation points is shown in Figure 7.4. The x-axis of Figure 7.4 corresponds to the stations identified in Figure 7.3, with the addition of the station 5, which represents turbine outlet.

Figure 7.4 shows that the exhaust ports are the elements where the temperature drop is higher along the exhaust line. Based on this result, the

parametric studies have been focused on them, i.e. region between stations 1 and 2 in Figure 7.3.

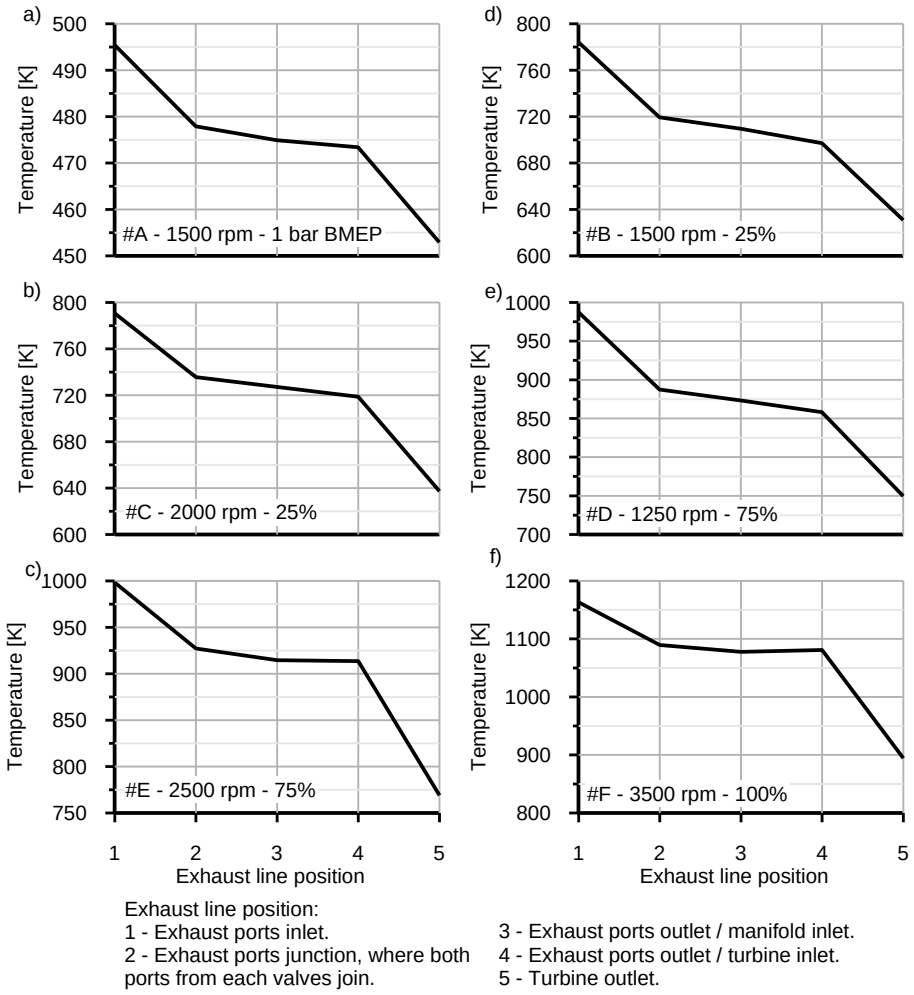

Figure 7.4 – Temperature variation across exhaust line in the baseline configuration for the six operation engine points

The other element with high temperature drop is the turbine (between station 4 and 5) and is caused by the expansion of the exhaust gas to produce energy and by wall heat transfer. Just the second cause can be reduced, for example with thermal insulation. However, turbine studies to reduce heat transfer are out of the scope of this chapter. In this doctoral

thesis, just exhaust ports and intake and exhaust valves effect in T_4 and bsfc will be studied.

7.3.1. Exhaust ports length and distribution

The exhaust ports are divided into two different sections, as can be seen in Figure 7.3. The first section is formed by two ports from the respective exhaust valve up to their junction, from station 1 to station 2 in Figure 7.3. Its baseline length is 110 mm. The second section links the junction of the ports to the exhaust manifold inlet, from station 2 to station 3 in Figure 7.3. The baseline length of this section is 20 mm.

The first parametric study to characterize the influence of the exhaust ports is focused on the analysis of the length reduction. Table 7.3 describes the simulated geometries. Case #1 is the baseline. Case #2 and Case #3, the first section pipe is gradually reduced. In Case #4, the first section is kept constant, but the second section is removed, therefore, first section is directly connected to the exhaust manifold. Despite some of them are considered non-feasible from a mechanical design point of view, these are included to provide a more detailed trend.

Table 7.3. Exhaust port length of each case of the parametric study

Case	L_{total} [mm]	First section pipe		Second section pipe	
		L [mm]	D in/out [mm]	L [mm]	D in/out [mm]
#1	130	110	22 / 25.5	20	41.5 / 41.5
#2	80	60	22 / 25.5	20	41.5 / 41.5
#3	40	20	22 / 25.5	20	41.5 / 41.5
#4	20	20	22 / 25.5	0	- / -

Figure 7.5 shows the variation in temperature at the aftertreatment inlet (T_4) and bsfc for the described parametric study. In all cases, x-axis represents the total length of the exhaust port, i.e. second column in Table 7.3. Variations are expressed with respect to the baseline case (Equation (7.2)), which is detailed in Figure 7.2. Absolute value is used for temperature and percentage for bsfc (Equation (7.1)).

$$\Delta T_4 = T_{4_{case\ \#i}} - T_{4_{baseline}} \qquad (7.1)$$

$$\Delta bsfc\ [\%] = \frac{bsfc_{case\ \#i} - bsfc_{baseline}}{bsfc_{baseline}} \times 100 \qquad (7.2)$$

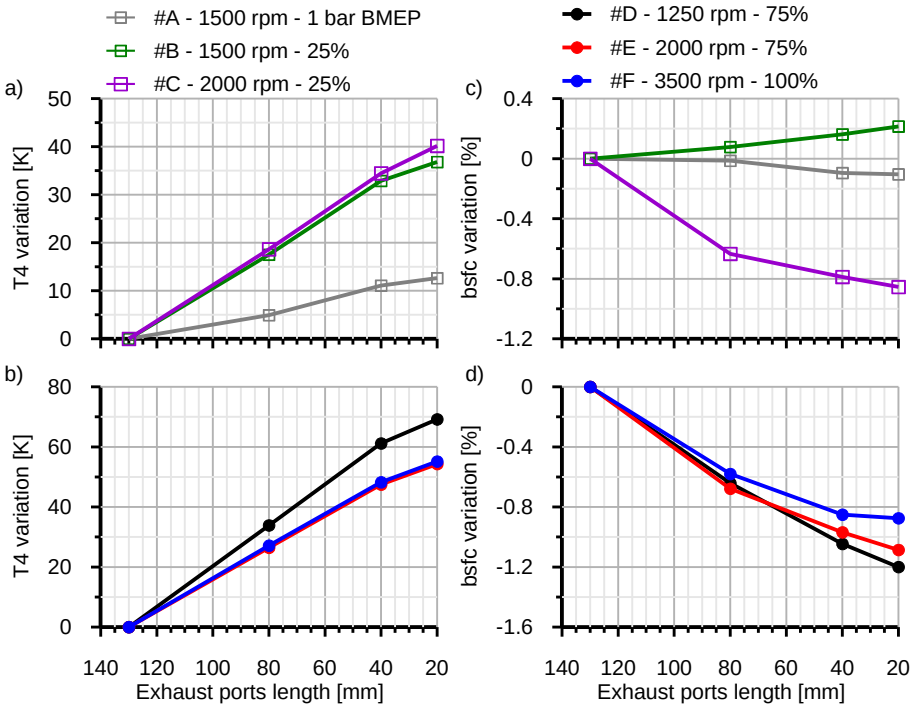

Figure 7.5 – Aftertreatment inlet temperature and bsfc variations at low and high load operating points as a function of the exhaust ports length

As shown in Figure 7.5 (a) and (b), the exhaust ports reduction in the first section produces a linear increment of T_4. However, T_4 is less sensitive to changes in second section. Cross-section area is higher in second section so that the instantaneous flow velocity is lower with respect to first section. Hence, the heat transfer coefficient is lower in second section. In addition, the external surface is higher in the first section, thus contributing to higher heat losses with respect common port in every exhaust valve. According to this behavior, a reduction in 50 mm of the first section is able to provide 20ºC of aftertreatment inlet temperature at low load. This increase varies between 30ºC and 40ºC in the medium-high load range. This sensitivity underlines the interest for an optimum design of the exhaust ports integrating both fluid mechanics and heat transfer criteria.

Besides benefits in aftertreatment inlet temperature, fuel economy improvements are also expected, especially at high load. In this operating region, the turbine inlet temperature increase, because of heat loss reduction in exhaust ports, leads to VGT opening and, hence, PMEP reduction. As represented in Figure 7.5 (d) all operating points show a similar bsfc decrease, which reaches 0.5% with 50 mm in first section length reduction. On the contrary, bsfc variation in partial load region, which is represented in Figure 7.5 (c), reveals different behavior. Noticeable bsfc reduction alternates with slight bsfc increase as a function of the particular operating point. In these cases the benefits in pumping losses brought by VGT opening are in trade-off with the penalty caused by the need to close EGR valve or intake throttle to keep constant O_2 concentration. The trade-off refers to the reduction of engine back pressure that takes place when the VGT opens. VGT position (100% fully open), which is represented in plot (a) of Figure 7.6 for low load operation points, produces the reduction of engine pumping losses. However, in engine operative conditions where EGR valve opening has reached its maximum (cases 2, 3, & 4 in operating point #C, as represented in Figure 7.6 (b) it is needed to throttle the intake manifold. This is to generate enough pressure difference to pump the required EGR to the intake line keeping constant O_2 concentration. Therefore, the potential benefit for pumping losses due to VGT opening can be cancelled by the intake throttling that reduces boost pressure and increases pumping losses accordingly.

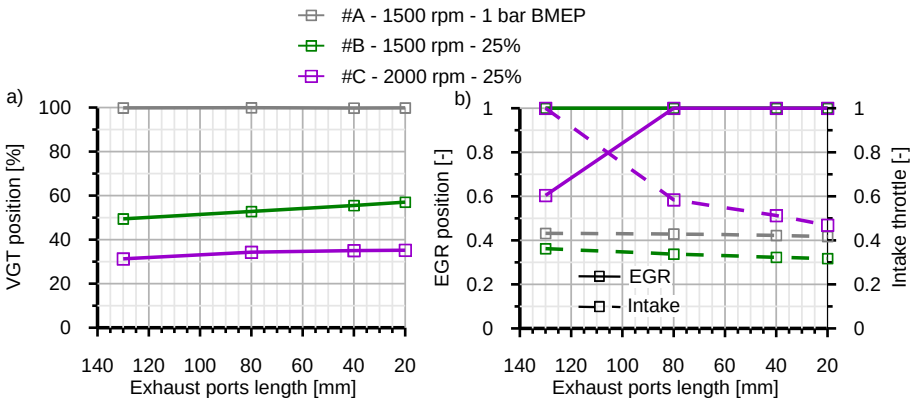

Figure 7.6 – VGT and EGR valve position at low load operating points as a function of the exhaust ports length

A second parametric study has been approached in order to analyze further the influence of the exhaust ports division into two different sections. In

this study, the total length has been set to 80 mm being the length of every section changed to identify the influence of the distribution. The geometry of the cases composing the study is sketched in Figure 7.7. Case #1 in which first section and total lengths coincide, has been set as baseline layout. The geometry of case #2 has been already considered in the previous study (case #2 in Table 7.3). Finally, only one exhaust valve is considered in case #5 since the first section is completely removed. The criterion to define the valve diameter has been to keep constant the perimeter to that in two-valve configuration i.e. to keep the exhaust curtain area.

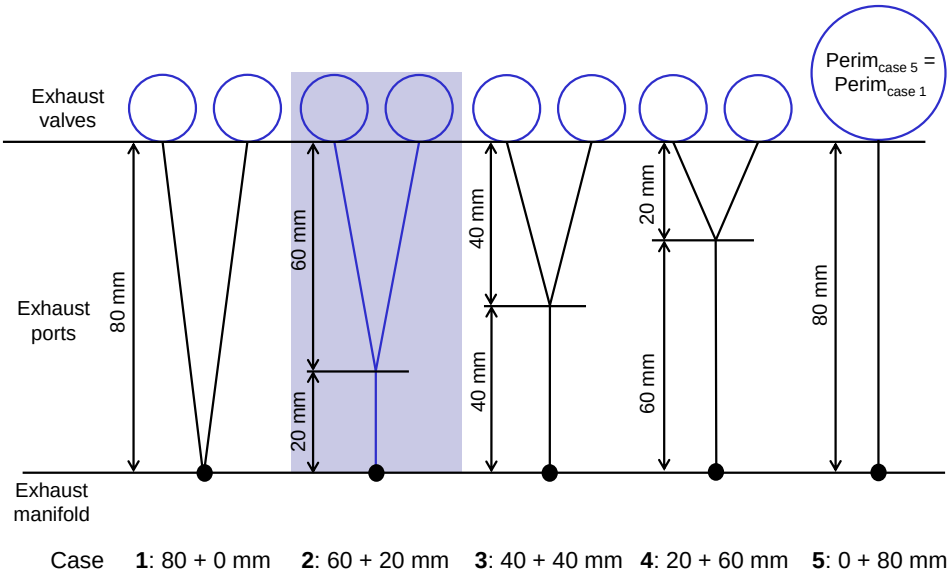

Figure 7.7 – Definition of the cases composing the exhaust ports length distribution study

Figure 7.8 shows the variation in aftertreatment inlet temperature and brake specific fuel consumption for low and high load operating. General response is the increase of gas temperature and fuel economy benefit as the common branch of the exhaust port in every cylinder gets longer. Aftertreatment inlet temperature benefit ranges between 12 K and 22 K with the only exception of operating point #1, which is of very low load. These results are consistent with previous study (total length variation), in which was observed that the first section shortening is more positive.

Fuel economy results point out a slight benefit, which is around 0.1% with the only exception of case #5. The particular characteristics of case #5 have

as a result a change in the rate of variation. The use of one exhaust valve ensuring the same curtain area provides an increase of the cross-section in the entire port. As a result the trend in aftertreatment inlet temperature is kept at the same time the reduction of bsfc is further improved. Besides pumping losses reduction caused by the higher VGT opening additional pressure drop reduction in the exhaust ports is obtained.

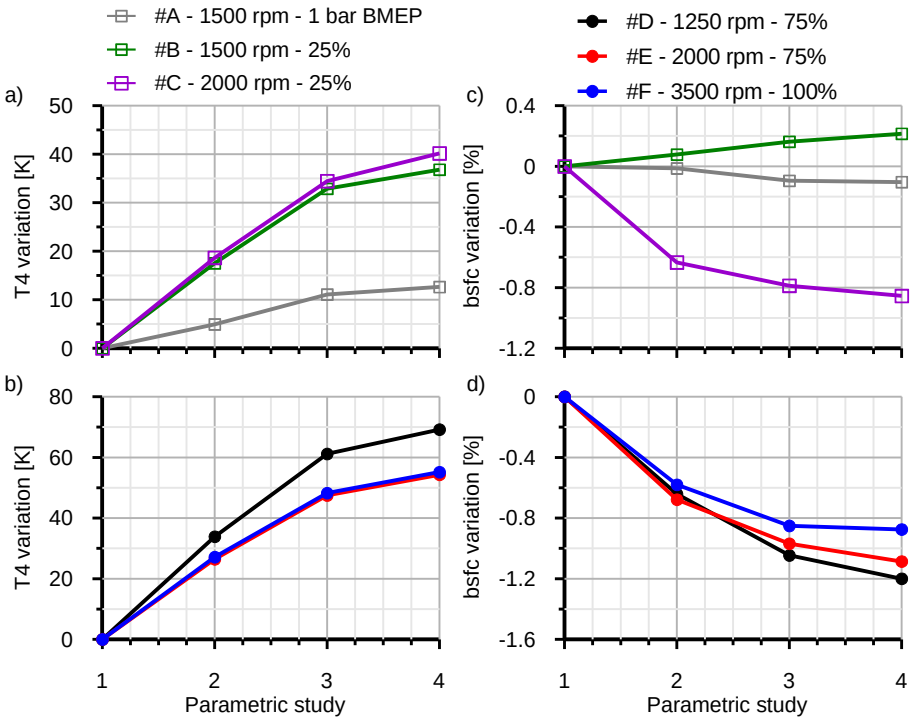

Figure 7.8 – Aftertreatment inlet temperature and bsfc variations at low and high load operating points as a function of the exhaust ports length distribution

7.3.2. Valves and ports diameter

In order to complete the analysis on the exhaust ports geometry, next parametric study covers the exhaust valve diameter influence. Due to cylinder head space limit, the change in diameter of the exhaust valves produces a complementary variation in intake valves so that the total valves area is kept the same as the baseline configuration. In addition, the inlet and outlet diameter of the ports is changed. The section next to the valves has always the same diameter as the corresponding valve, as in the baseline case. The end diameter is changed so that the tapered duct

geometry is maintained with the same slop. Baseline geometry of the intake and exhaust valves and ports is detailed in Figure 7.9.

Table 7.4 details the geometric parameters defining the different cases of study. The intake to exhaust valve area ratio is selected as parameter to define the three cases composing the study. Case #1 corresponds to the baseline configuration. It is characterized by higher area in intake than in exhaust valves. In case #2, the diameter of the intake and exhaust valves is equal. Finally, case #3 represents a design condition in which exhaust valve diameter is higher than that in the intake valve. Indeed, the intake to exhaust valve area ratio is the inverse ratio than in case #1.

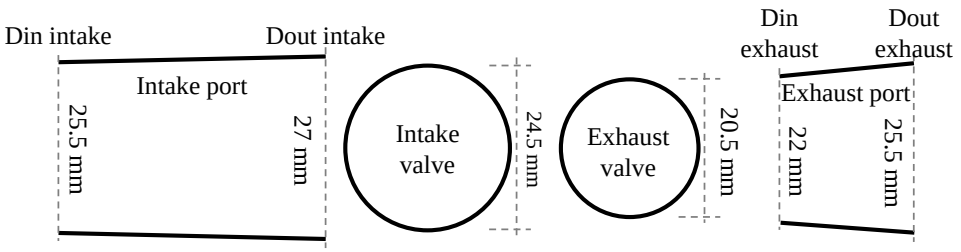

Figure 7.9 – Baseline geometry of valves and ports

Table 7.4. Intake and exhaust ports and valves geometry variation in each case of the parametric study

Case	Intake valve	Exhaust valve	Intake ports		Exhaust ports	
	Ø [mm]	Ø [mm]	$Ø_{in}$ [mm]	$Ø_{out}$ [mm]	$Ø_{in}$ [mm]	$Ø_{out}$ [mm]
#1	24.5	20.5	25.5	27	22	25
#2	22.59	22.59	21.34	22.59	22.59	25.67
#3	20.5	24.5	19.36	20.5	24.5	27.84

One of the consequences of the intake valve diameter reduction is the decrease in volumetric efficiency. To offset this effect, an alternative control strategy to constant boost pressure has been considered. Thus the effect of keeping constant fresh mass flow while boost pressure varies is also analyzed.

The influence of this alternative control strategy has been applied to high load #D, #E and #F operating points. Figure 7.10 shows the variation in

aftertreatment inlet temperature and bsfc in conditions as a function of the valves diameter and the boost control strategy. Plots (a) and (b) are referred to constant p_2' control strategy and plots (c) and (d) represent the results corresponding to constant fresh air control strategy. Comparing plots (a) and (c) can be concluded that the control of boost pressure provides more benefits in aftertreatment inlet temperature than constant mass flow strategy. In addition, benefit is increasing as the intake to exhaust valve area ratio decreases. Nevertheless these benefits, which are limited to average maximum around 10 K, are accompanied by a penalty in fuel consumption, which is caused by intake valve area decrease. The fuel penalty trend is similar in both control strategies but it reaches higher magnitude when fresh mass flow control is applied.

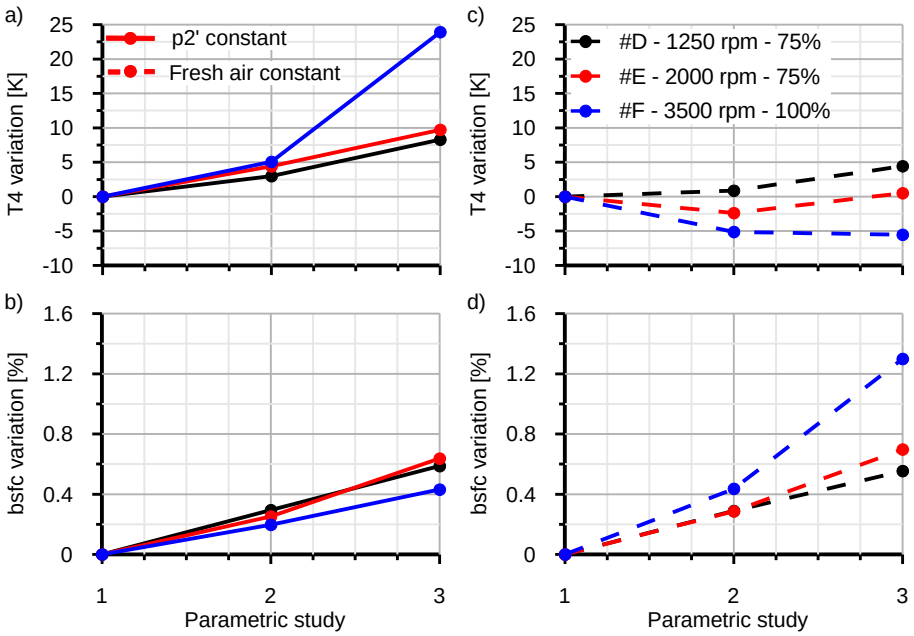

Figure 7.10 – Aftertreatment inlet temperature and bsfc variations at high load operating points as a function of the valves diameter and the control strategy

The reason for the higher fuel penalty in fresh mass flow control is because of the consequences of the volumetric efficiency reduction on different engine parameters. One of the effects is the VGT closing in order to keep fresh mass flow constant by increasing boost pressure. Consequently, turbine inlet pressure also increases and finally PMEP gets damaged. This

PMEP increase is especially evident in operating point #F, as shown in Figure 7.11 (a) by dashed blue series.

The reduction of the volumetric efficiency has as an additional consequence a decrease of the air-to-fuel ratio, which is represented in Figure 7.11 (b). Although this response is much more constraining in the case of boost pressure control, it is obtained regardless the control strategy due to the fact that the torque is kept constant. Consequently, the air to fuel ratio decreases even when fresh mass flow is controlled. As a result an increase in maximum in-cylinder temperature is obtained, as represented in Figure 7.11 (c). Therefore the indicated efficiency decreases. This process is the responsible of the bsfc penalty in the case of boost pressure control. Despite its lower influence when fresh mass flow control is imposed, the final damage on fuel economy is higher because of its combination with previously described PMEP increase. Since the injected fuel mass is varied to keep constant the torque, it must be higher in the case of constant fresh air control strategy, as plot Figure 7.11 (d) certifies.

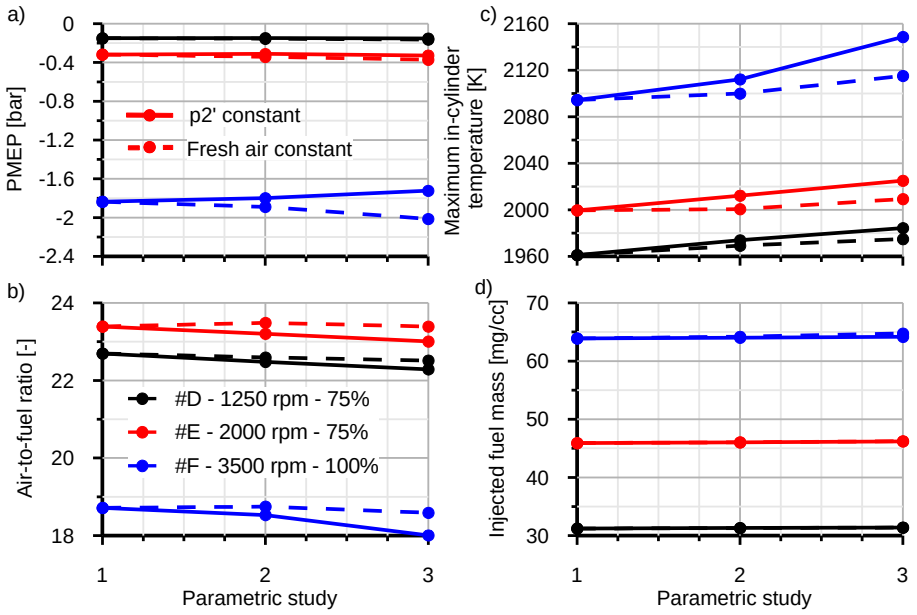

Figure 7.11 – PMEP, air-to-fuel ratio, maximum in-cylinder temperature and injected fuel mass variations at high load operating points as a function of the valves diameter and the boost control strategy

Due to the better results obtained in the case of boost pressure control, only this strategy has been applied to low load operating points. Variation in

aftertreatment inlet temperature is shown in Figure 7.12 (a) for this operating range. Its magnitude is low, being maximum temperature increase around 5 K. However, the penalty in bsfc, which is shown in Figure 7.12 (b), is close to 1% and higher than that obtained at high load. Therefore, efforts on valve and ports geometry optimization for aftertreatment inlet temperature increase are to be focused on length concerns. On the other hand, fuel economy criteria must determine intake to exhaust valve area ratio.

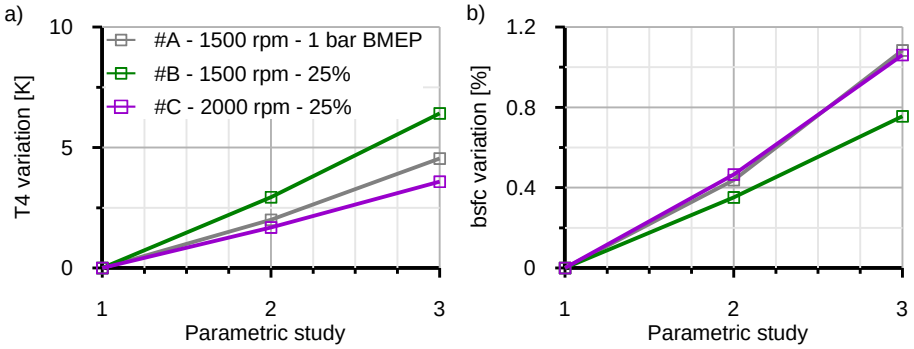

Figure 7.12 – Aftertreatment inlet temperature and bsfc variations at low load operating points as a function of the valves diameter

7.3.3. Exhaust valve timing

Exhaust valve timing is well-known to have direct influence on engine fuel economy but it is also relevant on the exhaust gas temperature. Since the baseline setup is optimized for fuel consumption, the variation in the exhaust valve timing has been analyzed looking for T_4 increase and quantification of the damage on bsfc. Figure 7.13 shows the exhaust valve lift as function of the timing and the crankshaft angle. It can be observed that the maximum delay of the exhaust valve timing with respect to baseline one is 15º in order not to impact against the piston. Based on these results, 7 cases have been simulated between ±15º with a step of 5º.The variation in timing affects the whole exhaust valve profile, from opening to closing.

Aftertreatment inlet temperature and bsfc variation with respect to baseline timing are represented in Figure 7.14 for low and high load operating points. Minimum bsfc correspond to baseline timing, as represented in plots (c) and (d) in Figure 7.14. Only operating points of very low load such as #A seem not to fulfill this condition. As shown in Figure

7.15, baseline timing is that of maximum volumetric and indicated efficiency. PMEP is also in the minimum region for all operating points, being operating point #F the only exception for this variable. Hence its lower rate of bsfc increase as the exhaust valve opening is advanced.

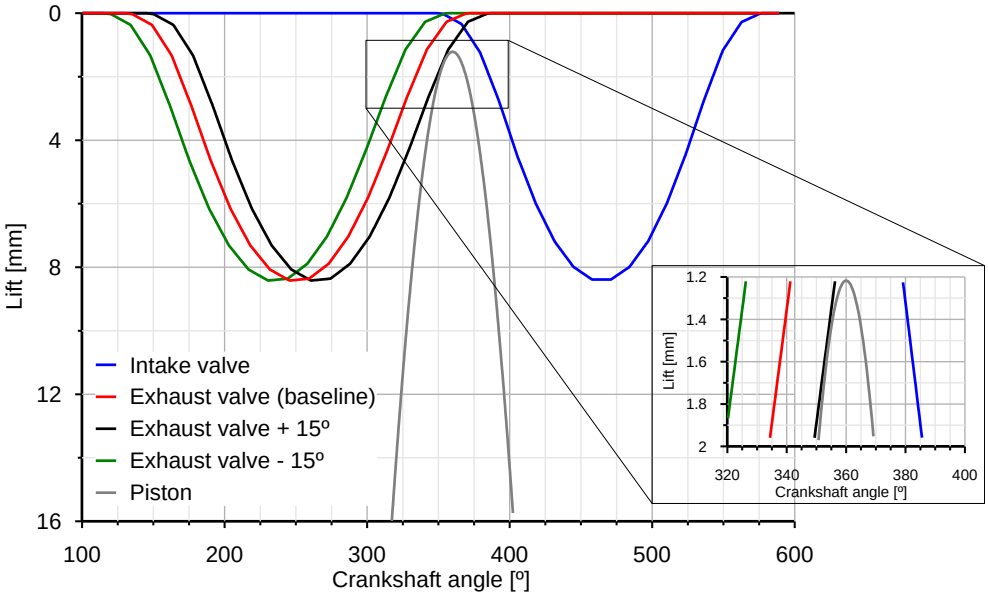

Figure 7.13 – Detail of piston position with respect to TDC and exhaust and intake valves lift

Regarding aftertreatment inlet temperature, any delay of the exhaust valve timing leads to bsfc increase but gas temperature remains almost unaffected. By contrast, advancing exhaust valve timing produces a noticeable increase in exhaust gas temperature with a slightly higher damage on fuel economy. The reason is that when the exhaust valve timing is advanced (negative timing change in Figure 7.14), the gas temperature exiting the cylinder is higher with respect to baseline because the in-cylinder pressure at the opening is also higher. In addition, the valve overlap is reduced. Consequently, the induced exhaust by the fresh air is less efficient. This process leads to an increase of the burned gases fraction inside the cylinder at the combustion start and results in the decrease of volumetric and indicated efficiency as shown in Figure 7.15. At the aftertreatment inlet, temperature increase around 15 K in low load operating region. In the high load operating points, range is much more wide ensuring between 20 K and 60 K of temperature increase.

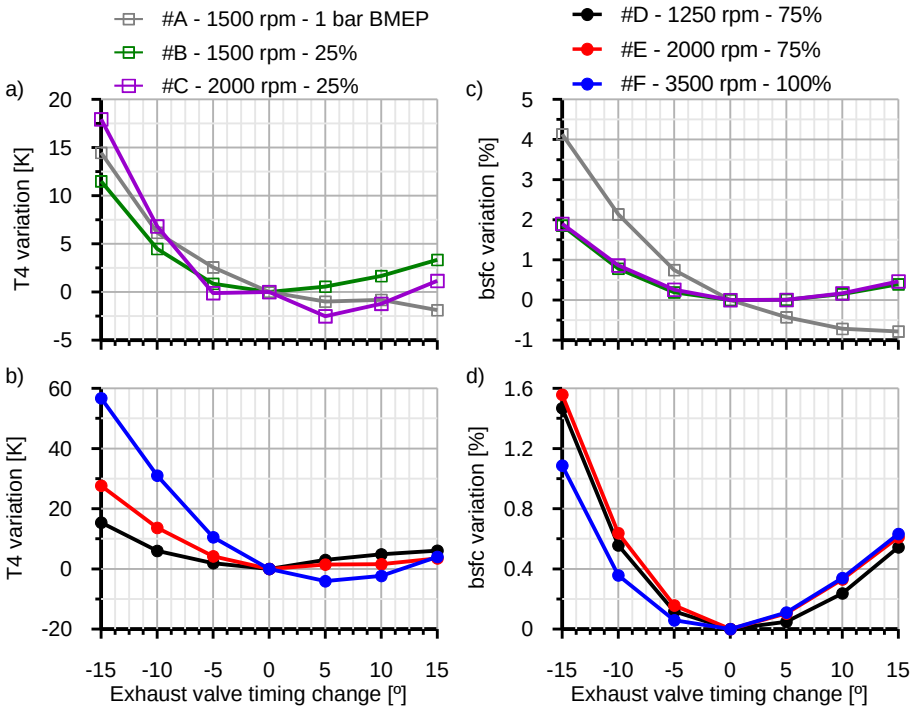

Figure 7.14 – Aftertreatment inlet temperature and bsfc variations at low and high load operating points as a function of the exhaust valve opening change with respect to baseline setup

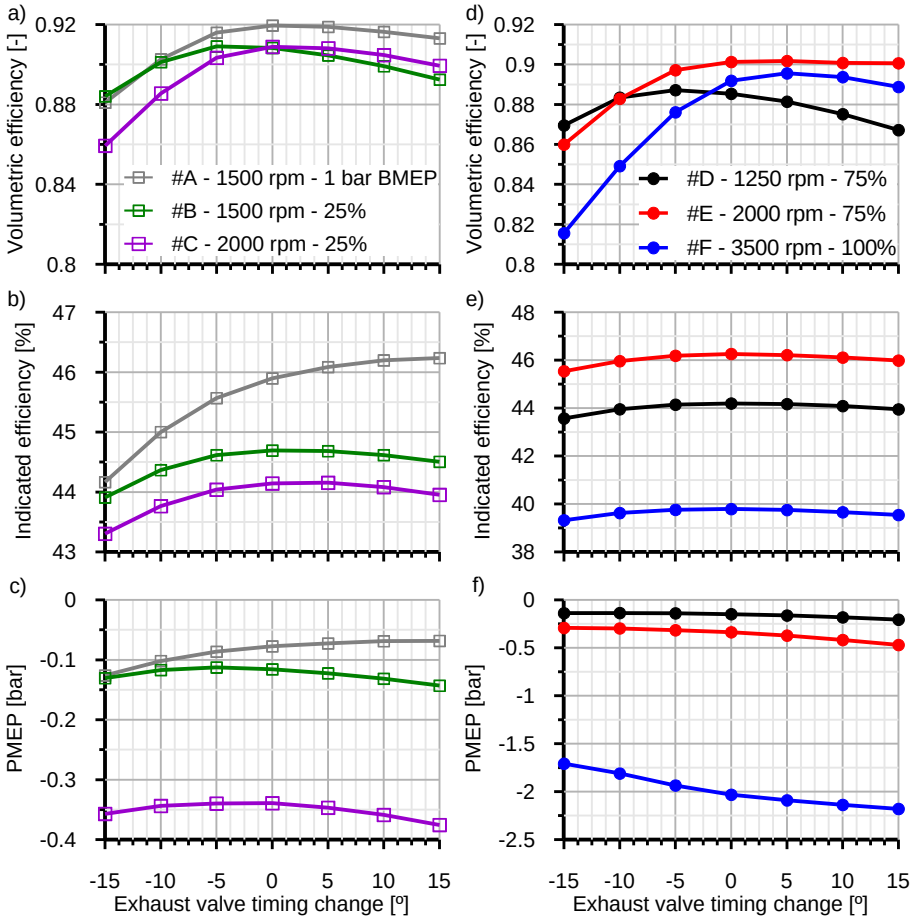

Figure 7.15 – Variation of volumetric efficiency, indicated efficiency and PMEP at low and high load operating points as a function of the exhaust valve opening change with respect to baseline setup

7.3.4. Multi-step valve opening

Multi-step valve opening parametric study analyses the influence on T_4 and bsfc of the increase of internal EGR due to the addition of a second step valve opening [19]. Three different strategies covering intake valve pre-opening, exhaust valve post-opening as well as their combination have been considered.

The intake pre-opening strategy is to be applied when the in-cylinder pressure is higher than intake pressure during the exhaust phase. The

objective is that part of the burned gases moves back towards the intake port where are buffered up to the intake phase initiation.

Figure 7.16 shows the instantaneous intake, exhaust and in-cylinder pressure and the valves lift as a function of the crankshaft angle. Blue-colored areas identify the range in which intake pre-opening strategy may be applied in every operating point.

The application of the exhaust post-opening strategy looks for an increase of the internal EGR making part of the exhaust gases go back to the cylinder during the intake phase. Red-colored areas in plots of Figure 7.16 identify the range in which in-cylinder pressure is lower than the exhaust gas pressure during the intake phase and thus allows exhaust post-opening application.

Overlapping in the same plot the areas in which intake pre-opening and exhaust post-opening can be performed in the operation points it is possible to define common regions for their application. These are shown in Figure 7.17. It should be noted that the pre-opening or post-opening window may change considering additional operating points. Nevertheless, a wide operation range of the engine has been covered. Therefore no relevant variations should be expected for the particular case analyzed in this work.

The proposed valve lift profiles fulfilling these constraints are also represented in Figure 7.17. The profiles of these second opening events have been scaled to the available useful window from the nominal profiles. The maximum lift has been defined to obtain the same maximum acceleration in the re-opening than in the main valve opening. With this procedure, an intake pre-opening window of 60 CAD with a maximum lift of 0.42 mm has been imposed. The exhaust post-opening window reaches 100 CAD with a maximum lift of 0.80 mm.

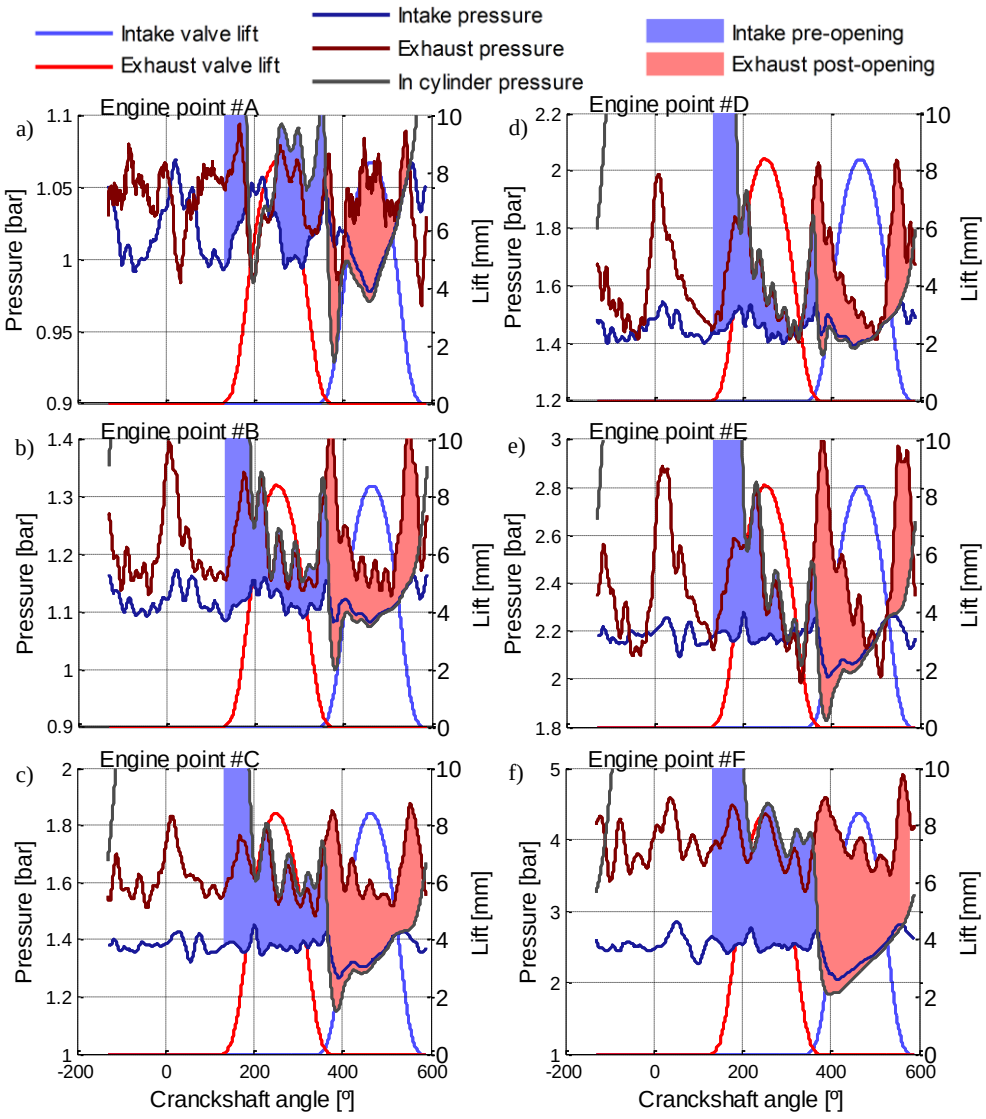

Figure 7.16 – Identification of the crankshaft angle range for application intake pre-opening and exhaust post-opening strategies

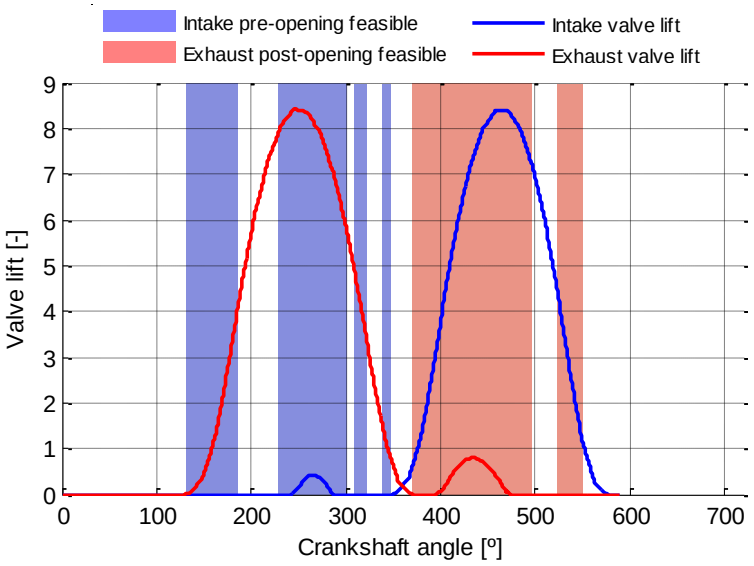

Figure 7.17 – Proposed valve lift profiles for intake pre-opening and exhaust post-opening application.

Figure 7.18 to Figure 7.20 show the results corresponding to the parametric study. Four cases have been considered. Baseline (case #1); separated application of intake pre-opening (case #2) and exhaust post-opening (case #3) and case #4 that includes the combination of both strategies.

Figure 7.18 shows the influence of the proposed strategies on the burned fraction present in the cylinder at the beginning of the combustion process. This magnitude increases, especially when exhaust valve post-opening is considered. As a result, the high temperature of the internal EGR and the decrease of the mass flow make the maximum in-cylinder temperature to increase. Figure 7.19 shows the effect of the different multi-step valve opening strategies on the instantaneous mass flow through intake and exhaust ports corresponding to operating point #E. This behavior leads the volumetric efficiency to decrease.

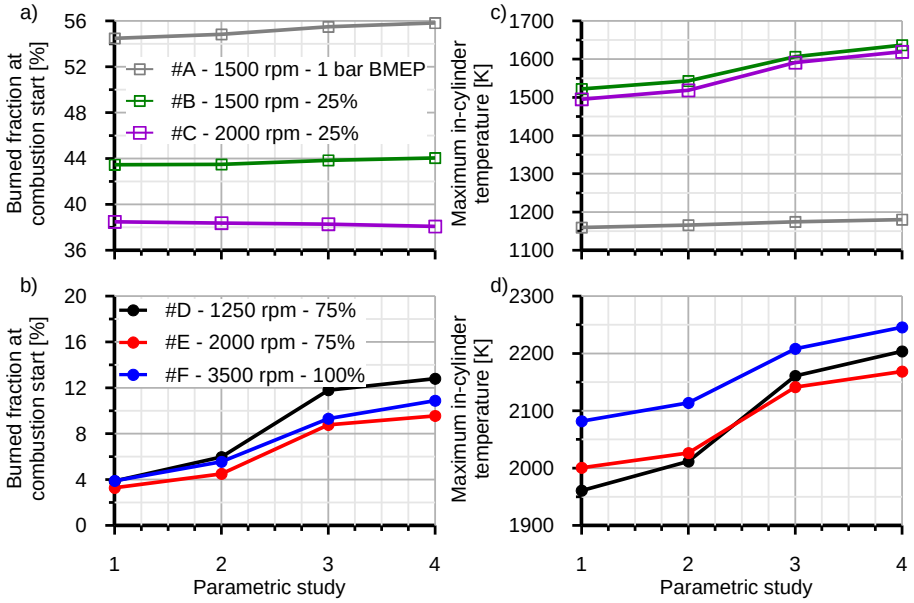

Figure 7.18 – Burned fraction at start of combustion and maximum cylinder temperature at low and high load operating points as a function of the multi-step valve opening strategy

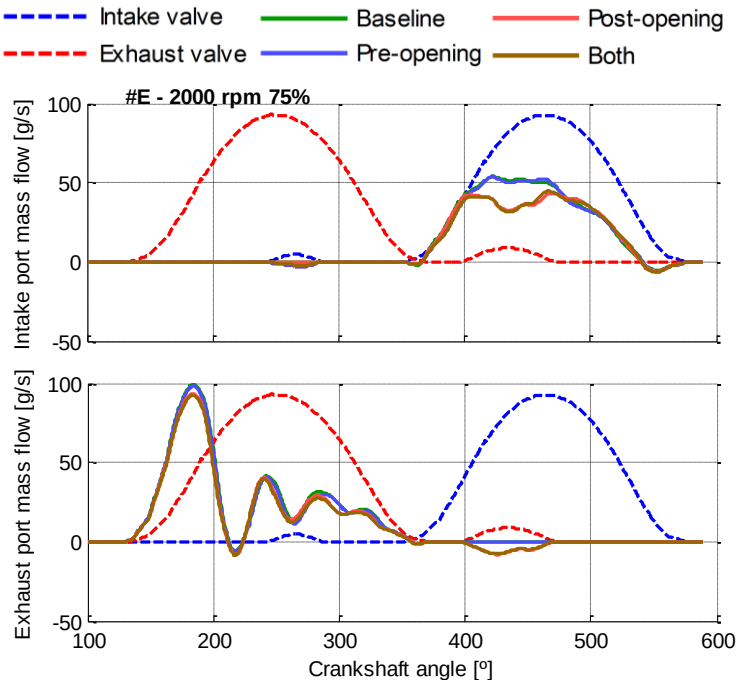

Figure 7.19 – Instantaneous mass flow in intake and exhaust ports in operating point #E as a function of the multi-step valve opening strategy.

The combination of turbine inlet temperature increase but mass flow decrease governs the final response in bsfc. An increase of the bsfc is found as main trend both in low and high load operating points. This result is shown in percentage in plots (c) and (d) of Figure 7.20 respectively. Operating points at medium speed are those most affected by fuel penalty, especially as the engine load increases. Nevertheless, benefit in T_4, which is shown in Figure 7.20 (a) and (b), reaches high magnitude when exhaust valve post-opening is considered. It ranges from 25ºC to 50ºC at low load depending on its combination with intake valve pre-opening. At high load T_4 increase is between 60ºC and 90ºC.

On the contrary, very low load operating points can get even slight benefits in bsfc but at the expense of low magnitude in T_4 increase. Similarly, high speed full load conditions (#F) show negligible influence on bsfc. Nevertheless, this operating range still keeps relevant benefits in T_4. In this operating point, the turbine inlet temperature increase offsets the mass flow decrease and gives as a result the VGT opening. Consequently a reduction in pumping losses is obtained.

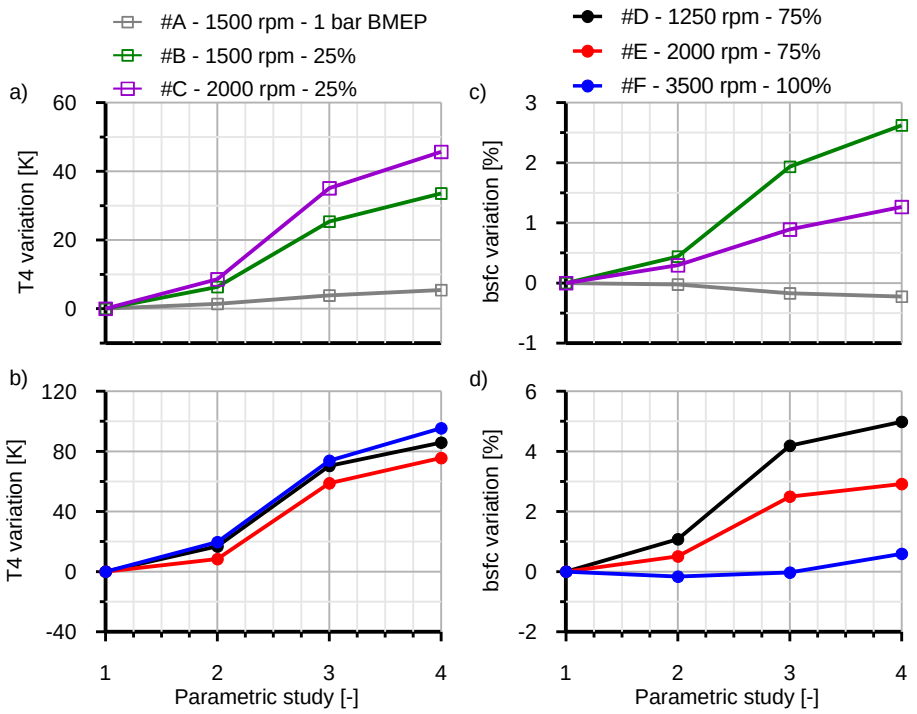

Figure 7.20 – Turbine outlet temperature and bsfc variations at low and high load operating points as a function of the multi-step valve opening strategy.

7.4 Summary and conclusions

In this chapter, the results of parametric studies to increase T_4 taking into account bsfc in a diesel turbocharged engine model in GT-Power with an advanced heat transfer and mechanical losses model have been presented. These parametric studies affected just the valves and the exhaust pipes.

The importance to increase T_4 temperature comes from the necessity to reach target conversion efficiency in catalyst reactors as well as to reduce the need of active regeneration strategies. The order of magnitude of the T_4 increase addressed by the performed studies indicates the existence of potential to widen the operating range in which catalyst reactors and passive regeneration get high performance under steady state conditions. In addition, the proposed guidelines for T_4 increase without negative effect on bsfc would have positive impact on the warm-up process reducing the time for light-off in the different exhaust aftertreatment systems."

Figure 7.21 summarizes, for all parametric studies and operation points, bsfc increase and T_4 increase with respect to baseline. The top left quadrant is where T_4 increases and bsfc decreases, i.e. the quadrant where it is always interesting to move in the engine design. There can be found exhaust length studies. The rest of the studies are in the top right quadrant, where T_4 and bsfc increases and therefore more design and operation parameters are needed to take into account.

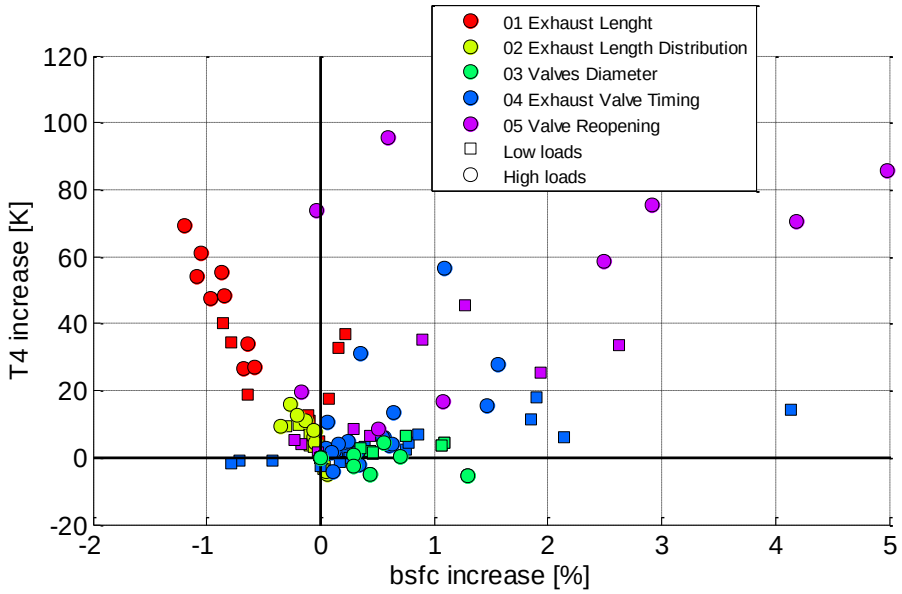

Figure 7.21 – Bsfc increase with respect to T_4 increase for all parametric studies and all operation points simulated.

Analyzing Figure 7.21 can be observed that changing the valves diameter has a very small influence in T_4 but a great influence in bsfc compared with the other studies, i.e. the slope of the points is smaller. Moreover, valve reopening and valve timing studies are mainly in top right quadrant, but the dispersion of the points is very large, having points without bsfc penalty and relevant T_4 increase and other points without T_4 increase but remarkable bsfc penalty.

Finally, exhaust length studies show a linear increase in T_4 and decrease in bsfc as exhaust length is reduced and common branch is longer. Therefore, exhaust ports have to be as short as possible and with small perimeter to reduce heat transfer losses but with large area to reduce velocity, being the best option the architecture with a large single exhaust valve. The limits of

these engine design changes are defined by other variables such as mechanical concerns.

It is worth advising that ports modification will increase also T_4 at rated power where there are already limitations due to excessive T_3. Therefore, active cooling strategies in the ports are needed at rated power. However, active control strategies to increase T_4 such as intake and exhaust valves timing, can be selective performed when higher T_4 is needed, avoiding too high T_3 temperature at rated power.

7.5 References

[1] M. Tutuianu, P. Bonnel, B. Ciuffo, T. Haniu, N. Ichikawa, A. Marotta, J. Pavlovic, H. Steven, Development of the World-wide harmonized Light duty Test Cycle (WLTC) and a possible pathway for its introduction in the European legislation, Transp. Res. Part D Transp. Environ. 40 (2015) 61–75. doi:10.1016/j.trd.2015.07.011.

[2] A. Marotta, J. Pavlovic, B. Ciuffo, S. Serra, G. Fontaras, Gaseous Emissions from Light-Duty Vehicles: Moving from NEDC to the New WLTP Test Procedure, Environ. Sci. Technol. 49 (2015) 8315–8322. doi:10.1021/acs.est.5b01364.

[3] B. Guan, R. Zhan, H. Lin, Z. Huang, Review of the state-of-the-art of exhaust particulate filter technology in internal combustion engines, J. Environ. Manage. 154 (2015) 225–258. doi:10.1016/j.jenvman.2015.02.027.

[4] M. Tutuianu, A. Marotta, H. Steven, E. Ericsson, T. Haniu, N. Ichikawa, H. Ishii, Development of a World-wide Worldwide harmonized Light duty driving Test Cycle, Tech. Rep. 3 (2014) 7–10. doi:10.3141/2503-12.

[5] A. Algieri, M. Amelio, P. Morrone, Energetic analysis of the performances of innovative aftertreatment systems, SAE Tech. Pap. 4970 (2009). doi:10.4271/2009-01-1948.

[6] J.N. Chi, Control Challenges for Optimal NOx Conversion Efficiency from SCR Aftertreatment Systems, SAE Tech. Pap. (2009). doi:10.4271/2009-01-0905.

[7] L. Stenning, Strategies for Achieving pre DPF Regeneration Temperatures using in Cylinder Post Injection on a Common Rail Diesel Engine with EGR, DOC and Intake Throttle, Sae Tech. Pap. Ser. 7 (2015) 0–8. doi:10.4271/2010-36-0306.

[8] R.P. Ranganathan, D.W. Turner, M.E. Franchett, Exhaust Manifold Gas

Temperature Predictions using System Level Data Driven Modelling, 2005 (2005). doi:10.4271/2005-01-0698.

[9] S.A.E. Technical, P. Series, Thermal Studies in the Exhaust System of a Diesel-Powered Light-Duty Vehicle, Development. (2004). doi:10.4271/2004-01-0050.

[10] J. Deng, R. Stobart, BSFC Investigation Using Variable Valve Timing in a Heavy Duty Diesel Engine, (2009). doi:10.4271/2009-01-1525.

[11] S. D'Ambrosio, A. Ferrari, E. Spessa, L. Magro, A. Vassallo, Impact on Performance, Emissions and Thermal Behavior of a New Integrated Exhaust Manifold Cylinder Head Euro 6 Diesel Engine, SAE Int. J. Engines. 6 (2013) 1814–1833. doi:10.4271/2013-24-0128.

[12] F. Payri, J.R. Serrano, P. Piqueras, O. García-Afonso, Performance analysis of a turbocharged heavy Duty diesel engine with a pre-turbo Diesel particulate filter configuration, SAE Int. J. Engines. 4 (2011) 2559–2572. doi:10.4271/2011-37-0004.

[13] GAMMA Technologies, (n.d.). http://www.gtisoft.com.

[14] OpenWAM - CMT-Motores Térmicos, Universitat Politècnica de València, (n.d.). www.openwam.org.

[15] J.R. Serrano, P. Olmeda, F.J. Arnau, A. Dombrovsky, L. Smith, Analysis and Methodology to Characterize Heat Transfer Phenomena in Automotive Turbochargers, J. Eng. Gas Turbines Power. 137 (2015) 1–11. doi:10.1115/1.4028261.

[16] J. Serrano, P. Olmeda, F.J. Arnau, A. Dombrovsky, L. Smith, Turbocharger heat transfer and mechanical losses influence in predicting engines performance by using one-dimensional simulation codes, Energy. 86 (2015) 204–218. doi:10.1016/j.energy.2015.03.130.

[17] N. Baines, K.D. Wygant, A. Dris, The Analysis of Heat Transfer in Automotive Turbochargers, J. Eng. Gas Turbines Power. 132 (2010) 42301. doi:10.1115/1.3204586.

[18] J.A. Caton, Comparisons of Thermocouple, Time-Averaged and Mass-Averaged Exhaust Gas Temperatures for a Spark-Ignited Engine, in: SAE Int. Congr. Expo., SAE International, 1982. doi:https://doi.org/10.4271/820050.

[19] J. Benajes, E. Reyes, J.M. Lujân, Modelling study of the scavenging process in a turbocharged diesel engine with modified valve operation, Proc. Inst. Mech. Eng. Part C J. Mech. Eng. Sci. 210 (1996) 383–393. doi:10.1243/PIME_PROC_1996_210_210_02.

CHAPTER 8

Conclusions and future works

Contents

8.1 Introduction

In this last Chapter, the main conclusions that can be extracted from the research tasks explained in the previous chapters will be detailed. Besides, there are some areas in the several topics treated in the present work that worth a deeper investigation and some other areas only presented, but unexplored in detail because they were out of the scope of the present work, but with a big potential for a further investigation.

8.2 Main contributions

The main contributions of this PhD thesis are summarized in the following sections. For the sake of clarity they are separated per topic.

8.2.1 Altitude simulator

In the first part of the document, an altitude simulator development is described.

The altitude simulator developed is connected to the engine intake and exhaust and generates different pressures and temperatures, simulating different altitudes. That is to say, the test cell is at room pressure and only the air that the engine is sucking is at the desired altitude. This is a big difference with respect to the hypobaric chambers usually used in the altitude test campaigns, as the altitude simulator does not need a dedicated test cell. The altitude simulator can be installed in any normal test cell, converting it into a hypobaric chamber.

The altitude simulator presents also some other advantages with respect to a hypobaric chamber. For example, a chassis-dyno inside a hypobaric chamber has to be operated by a driver inside the low pressure environment. This presents some risks in the worker health, as the body cannot withstand sudden pressure changes. However, as the altitude simulator does not modify the ambient pressure, the driver does not experiment sudden pressure changes.

With respect to the altitude simulator performance, it has shown accurate pressure stability at the engine intake connection, even during engine transient operation. The maximum peaks are lower than 20 mbar and the average mean error is lower than 2 mbar. Besides, these pressure oscillations are muffled in the engine air filter and pipes before reaching the compressor inlet. Therefore, the pressure oscillations observed at the

compressor inlet when operating with the altitude simulator and without it at sea level are very similar.

The altitude simulator has shown also enough altitude range to cover most of the automotive applications, with a maximum altitude over 5000 m. The mass flow that the system is moving is also big enough to cover most of the passenger cars applications, as the maximum mass flow at 2000 m is around 1200 kg/h.

The altitude simulator has been patented and licensed to HORIBA GmbH for its exclusive commercialization.

8.2.2 Correlation with a hypobaric chamber

After the development of the altitude simulator, a test campaign to see the differences in performance and emissions of an engine when operating inside a hypobaric chamber or connected to the altitude simulator was performed.

The results show that the engine is not affected by the use of the altitude simulator. Its performance and emissions are the same independently on the system used to generate the altitude.

However, it has been shown that some things have to be taken into account in the tests with the altitude simulator.

The blow-by pipe that connects the engine sump to the compressor inlet might be not enough permeable to evacuate all the gases in the sump. The crankshaft retainers maybe not tight enough to avoid room air leakages inside the crankcase. If any of that happens, the sump pressurizes, either with blow by from combustion gases or with the air that comes into the sump from the high pressure atmosphere through the crankshaft retainers. In this situation high quantity of oil mist is sucked by the compressor and burned in the engine with abnormal oil consumption and white smoke emissions. To avoid this problem, the engine sump has to be connected to the same vacuum generated by the altitude simulator in order to keep controlled pressure at sump.

Other element that operates different with the altitude simulator is the ECU pressure sensor. This sensor is measuring the ambient pressure and is used in the maps of the ECU. When the engine is operating with the altitude simulator, this sensor is at room pressure, i.e. does not measure the generated pressure. Therefore, the ECU has a mismatch with the compressor inlet pressure and goes to a safe mode. To solve this problem,

the ECU pressure sensor has to be connected to the same vacuum generated by the altitude simulator or recalibrated in the INCA software to be "cheated".

Finally, the last element that could present some differences in operation with the altitude simulator is the VGT. In some VGTs, the vacuum to move the actuator is generated by a vacuum pump with some extra help coming from the compressor inlet connection. The help is in form of an atmosphere were vacuum is released to control VGT actuation, and this is the compressor inlet. Since compressor inlet is at high vacuum with respect to test room ambient vacuum release valve has to open a lot to release. It means the simulated altitude helps to the vacuum pump to work less. Since this release valve position is main feedback to ECU about VGT opening, the reading from the ECU about VGT opening is wrong. This is not a big issue when VGT is generally closed loop with p_2. Actual VGT position will be the same even reading is wrong. It is advised to disconnect vacuum release from compressor inlet and let connected to test room ambient to minimize this effect. In the short term all VGTs will be actuated by wire and this issue will disappear.

8.2.3 Engine behavior when operating at high altitude

In the next chapter, a turbocharged diesel engine was tested at different altitudes with the altitude simulator.

The results showed that the emissions increase with the altitude, as the engine control strategies are focused in keeping the engine performance constant with the altitude. For example, the EGR closes with the altitude, being fully closed at 2000 m and 3000 m. This triggers NOx emissions to more than double with respect to sea level values. Also the VGT closes in the EUDC in order to keep p_2 constant, what leads to an increment of the fuel consumption caused by the increment of the pumping losses.

With respect to the turbocompressor, it tends to operate closer to surge and overspeed limits; due to respectively the lower atmospheric pressure and to the exhaust gasses backflows, which increase residuals presence in combustion chamber and decrease engine volumetric efficiency.

During transient operation, both closed and open loop operation of the turbine leads to abnormally high p_3/p_2 ratio generating exhaust backflows much higher than at sea level. As a consequence, residuals in combustion chamber are out of calibration limits and so HC, CO and soot emissions are uncontrolled since not foreseen by calibration.

With the new extended conditions that will force to homologate emissions up to 1300 meters above sea level, the control strategies have to be improved in order to reduce the emissions while keeping constant the engine performance. The decrease of the ambient pressure cannot be compensated only with active elements that increase back pressure (VGT) or reduce oxygen concentration within the cylinders (EGR), because this leads to an unacceptable increment of the emissions. More elements have to be part of the potential solution, such as the aftertreatment systems optimization, the variable valve timing (VVT) adapted to different altitudes or injection-combustion control strategies.

8.2.4 Strategies to reduce emissions

One of the ways to reduce emissions with the altitude is increasing the efficiency of the aftertreatment systems, which is very dependent with the temperature. For that reason, in the last chapter, different strategies to increase the inlet aftertreatment temperature (T_4) are studied.

An engine model was coupled to an advanced heat transfer model in the turbocharger for a better T_4 prediction. Then, different parametric studies were performed to analyze their effect in the T_4 and bsfc. The strategies studied can be divided in two different groups: those that increase T_4 while reduce the bsfc; and those that increase T_4 with a penalty in the fuel consumption.

In the first group is the reduction of the exhaust manifold length. The model showed that the exhaust manifold is the element with higher temperature losses in the exhaust line and reducing its length reduces the heat losses and therefore increments T_4, while reduces the bsfc due to the reduction of the pumping losses and increase of the turbine inlet energy.

In the same group can be classified the exhaust length distribution variation, where the exhaust manifold layout has been changed to reduce the parts with higher temperature losses, but keeping constant the total length.

This two strategies are not always easy to implement in an engine, where the geometry is many times restricted by space or material resistance. However, the good results show that maybe it worth increasing the effort in the exhaust manifold design because the temperature losses and bsfc reduction are not negligible.

The rest of the strategies simulated can be classified in the second group, where the increment of T_4 is obtained with an increment in bsfc. These

strategies are the change in the intake and exhaust valve diameter, the change in the exhaust valve timing and the valve reopening to generate internal EGR.

In this second group of strategies, the most interesting ones are those that can be applied only in some cases during the engine operation, such as the change in the exhaust valve timing or the valve reopening. For example, these strategies can be applied only during the cold engine start, to increase T_4 faster and reduce the time it takes to reach the target conversion efficiency, what would lead to an important decrease of the emissions.

8.3 Future works

Once the main conclusions have been described, some topics treated in the present work worth a deeper analysis and study, but they were out of the scope of the tasks and studies performed in this doctoral thesis.

8.3.1 New systems development

One of the main motivation of this doctoral thesis has been the extended conditions introduced by the new homologation, which will force to reduce emissions in altitude up to 1300 meters above sea level and up to -7 ºC. This doctoral thesis has focused in the study of an altitude simulator development that will be able to generate different altitudes at the engine intake and exhaust. However, the altitude simulator cannot reach -7 ºC at all the altitudes, as its temperature range is highly dependent on the simulated altitude and on the room temperature.

A very promising research path is the design and development of a system able to operate coupled with the altitude simulator that extends its temperature range. Both systems would be able to simulate a wide range of altitudes and temperatures independently on the ambient conditions. This would be a very powerful tool in research tasks, as the results obtained in a given test cell could be compared with the results obtained in another test cell in any other part of the world.

Going deeper in this, also the humidity plays a key role in the emissions, and it is highly affected by the location of the test cell, as the humidity is affected by the room pressure and temperature as well. Then, the design and development of a system able to control the humidity, working together

with the altitude simulator and the temperature extension unit, would increase even more the versatility of the system.

8.3.2 Hypobaric chamber correlations

The altitude simulator has been compared with a hypobaric chamber. The engine tested with both systems has shown the same performance and emissions at different altitudes. However, the effect of the temperature has not been analyzed. The altitude simulator can also generate lower temperature at the engine intake than the temperature at the rest of the room. Then, another interesting test campaign would the comparison of the engine emissions and performance when operating with the altitude simulator with only the engine intake and exhaust air is at low pressure and temperature, with respect to the hypobaric chamber where all the air in the test cell at low pressure and temperature.

The correlation study in the present work has been done at different steady state points in the engine. Other interesting test campaign would be a correlation study between the altitude simulator and the hypobaric chamber during different engine dynamic tests (WLTP or other driving cycles).

8.3.3 Engine altitude tests

An E4 turbocharged diesel engine has been tested at different altitudes at different steady state points and NEDC. The NEDC will be replaced by the new homologation cycle will be the WLTC. Then, it would be interesting to analyze an E6 engine when operating at different altitudes with this new WLTC cycle, and to compare the results with those shown here with the NEDC.

8.3.4 Strategies to reduce emissions in extended conditions

The new homologation will force to regulate the emissions in altitude. As has been shown, the emissions abatement in altitude cannot be fulfill only with the current strategies and the aftertreatment systems will gain importance.

For this reason, in the last chapter, the effect of different engine parameters in the inlet aftertreatment temperature is studied, trying to identify how this temperature can be increased with low bsfc penalty, in

order to improve the target conversion efficiency of the aftertreatment systems.

The results of this study is very promising, and they could be validated in a real engine.

Finally, independently the fact that the aftertreatment systems will be more important for the emissions abatement in the extended conditions, the current control strategies should be improved. Now, the control strategies are fully focused in the engine performance without taking into account the emissions. Therefore, a big area of research is the study of different control strategies of the VVT; the VGT; the EGR and the injection-combustion processes in order to reduce the emissions with the altitude and low temperature with low performance penalty.

8.4 Scientific and Technical contribution

From the studies performed during this doctoral thesis have been obtained some relevant results that helped in the information presented in this work. These results have been published in journals, presented in congress with international impact and patented.

8.4.1 Journals

- V. Bermúdez, J. R. Serrano, P. Piqueras, J. Gómez, and S. Bender. *"Analysis of the role of altitude on diesel engine performance and emissions using an atmosphere simulator"*, IJER Vol 18, Issue 1-2, 2017.
- J. R. Serrano, P. Piqueras, J. Gómez, and S. Bender. *"Der Einfluss von Höhe auf die Emissionsmessung"*, MTZ Extra, 21 (Suppl 2): 32, 2016.
- J. Galindo, J. R. Serrano, P. Piqueras, and J. Gómez. *"Description and Performance Analysis of a Flow Test Rig to Simulate Altitude Pressure Variation for Internal Combustion Engines Testing"*, SAE Int. J. Engines 7(4):1686-1696, 2014.

8.4.2 Congresses

- V. Bermúdez, J. R. Serrano, P. Piqueras, J. Gómez, and S. Bender. *"Using an altitude simulation machine to analyze emissions and*

performance of a turbocharged Diesel engine operating at a high plateau", THIESEL Conference, 2016.

- Broach, J. R. Serrano, A. Abbad, R. Tabet, S. Bender, and J. Gómez. *"Emissions and performance correlations of a turbocharged diesel engine when operating on plateaus at high altitude inside an altitude chamber or connected to an altitude simulator"*, EAEC Congress, 2017.
- J. R. Serrano, P. Piqueras, R. Navarro, J. Gómez, M. Michel, and B. Thomas *"Modelling Analysis of Aftertreatment Inlet Temperature Dependence on Exhaust Valve and Ports Design Parameters"*, SAE Technical Paper 2016-01-0670, 2016.

8.4.3 Patents

The work developed in this thesis has been patented in order to protect the altitude simulator layout and licensed in exclusive to Horiba GmbH for its commercialization in the automotive industry.

- J.M. Desantes, J.Galindo, F.Payri, et al., *Dispositivo de acondicionamiento de atmósfera para el ensayo de motores de combustión, procedimiento y uso relacionados*, ES2485618B1 (P201430071) PCT/ES23015/070037, 2014.
- J.M. Desantes, J.Galindo, F. Payri, et al., *Dispositivo para acondicionar la atmósfera en ensayos de motores de combustión interna alternativos, procedimiento y uso de dicho dispositivo*, ES2544516B1 (P201530075), WO 2015/110683 A1, 2015.

Bibliography

A. Algieri, M. Amelio, P. Morrone, Energetic analysis of the performances of innovative aftertreatment systems, SAE Tech. Pap. 4970 (2009). doi:10.4271/2009-01-1948.

A. Ashtari, E. Bibeau, S. Shahidinejad, Using Large Driving Record Samples and a Stochastic Approach for Real-World Driving Cycle Construction: Winnipeg Driving Cycle, Transp. Sci. 48 (2014) 170–183. doi:10.1287/trsc.1120.0447.

A. Bell, Modern SI Engine Control Parameter Responses and Altitude Effects with Fuels of Varying Octane Sensitivity, SAE Tech. Pap. (2010) 25. doi:10.4271/2010-01-1454.

A. Marotta, J. Pavlovic, B. Ciuffo, S. Serra, G. Fontaras, Gaseous Emissions from Light-Duty Vehicles: Moving from NEDC to the New WLTP Test Procedure, Environ. Sci. Technol. 49 (2015) 8315–8322. doi:10.1021/acs.est.5b01364.

Á. Ramos Diezma, Emisiones contaminantes diésel en condiciones transitorias de motores y vehículos empleando combustibles alternativos, Universidad de Castilla-La Mancha, 2016.

Á. Ramos, R. García-Contreras, O. Armas, Performance, combustion timing and emissions from a light duty vehicle at different altitudes fueled with animal fat biodiesel, GTL and diesel fuels, Appl. Energy. 182 (2016) 507–517. doi:10.1016/j.apenergy.2016.08.159.

A. Tirez, P. Luickx, X. He, V. Rious, Possible impact of electric cars on electricity spot prices, in: Int. Conf. Eur. Energy Mark., 2010: pp. 1–6. doi:10.1109/EEM.2010.5558730.

A. Warey, A.S. Bika, D. Long, S. Balestrino, P. Szymkowicz, Influence of water vapor condensation on exhaust gas recirculation cooler fouling, Int. J. Heat Mass Transf. 65 (2013) 807–816. doi:10.1016/j.ijheatmasstransfer.2013.06.063.

A.C. Hoffmann, L.E. Stein, Gas Cyclones and Swirl Tubes, New York. (2007)

434.

A.M. Williams, A.T. Baker, C.P. Garner, R. Vijayakumar, Turbo-discharging turbocharged internal combustion engines, Proc. Inst. Mech. Eng. Part D J. Automob. Eng. 227 (2013) 52–65. doi:10.1177/0954407012455986.

AVL, Intake Air Conditioning Consys Air, (n.d.). https://www.avl.com/-/intake-air-conditioning.

B. Bendz, M. Rostrup, K. Sevre, T.O. Andersen, P.M. Sandset, Association between acute hypobaric hypoxia and activation of coagulation in human beings., Lancet. 356 (2000) 1657–8. doi:10.1016/S0140-6736(00)03165-2.

B. Daham, H. Li, G.E. Andrews, K. Ropkins, J.E. Tate, M.C. Bell, Comparison of Real World Emissions in Urban Driving for Euro 1-4 Vehicles Using a PEMS, Mater. Eng. (2009). doi:10.4271/2009-01-0941.

B. Degraeuwe, M. Weiss, Does the New European Driving Cycle (NEDC) really fail to capture the NOXemissions of diesel cars in Europe?, Environ. Pollut. 222 (2017) 234–241. doi:10.1016/j.envpol.2016.12.050.

B. Guan, R. Zhan, H. Lin, Z. Huang, Review of the state-of-the-art of exhaust particulate filter technology in internal combustion engines, J. Environ. Manage. 154 (2015) 225–258. doi:10.1016/j.jenvman.2015.02.027.

B. Hu, J.W.G. Turner, S. Akehurst, C. Brace, C. Copeland, Observations on and potential trends for mechanically supercharging a downsized passenger car engine:a review, Proc. Inst. Mech. Eng. Part D J. Automob. Eng. 231 (2017) 435–456. doi:10.1177/0954407016636971.

B. van Wee, K. Maat, C. de Bont, Improving Sustainability in Urban Areas: Discussing the Potential for Transforming Conventional Car-based Travel into Electric Mobility, Eur. Plan. Stud. 20 (2012) 95–110. doi:10.1080/09654313.2011.638497.

Beckhoff, (n.d.). https://www.beckhoff.com/.

C. Brand, Beyond "Dieselgate": Implications of unaccounted and future air pollutant emissions and energy use for cars in the United Kingdom, Energy Policy. 97 (2016) 1–12. doi:10.1016/j.enpol.2016.06.036.

C. He, Y. Ge, C. Ma, J. Tan, Z. Liu, C. Wang, L. Yu, Y. Ding, Emission characteristics of a heavy-duty diesel engine at simulated high altitudes, Sci. Total Environ. 409 (2011) 3138–3143. doi:10.1016/j.scitotenv.2011.01.029.

C. Lin, B. Hillman, A. Williams, Performance of Slotted Metallic Membranes as Particulate Filters, (2018). doi:10.4271/2014-01-2807.Copyright.

C. Sistem, Engine Altitude Conditions Simulator, (n.d.). https://www.controlsistem.it/standard-products/eacs.html.

C.A. Chaffin, T.L. Ullman, Effects of Increased Altitude on Heavy-Duty Diesel Engine Emissions, (1994).

C.J. Bartholomew, W. Jensen, T. V Petros, F.R. Ferraro, K.M. Fire, D. Biberdorf, E. Fraley, J. Schalk, D. Blumkin, D. The, M. Levels, The Effect of Moderate Levels of Simulated Altitude on Sustained Cognitive Performance, Int. J. Aviat. Psychol. 9 (1999) 351–359. doi:10.1207/s15327108ijap0904.

C.T. Bowman, Kinetics of pollutant formation and destruction in combustion, Prog. Energy Combust. Sci. 1 (1975) 33–45. doi:10.1016/0360-1285(75)90005-2.

Car emission testing facts - What is the Real Driving Emission (RDE) test?, (n.d.). http://www.caremissionstestingfacts.eu/rde-real-driving-emissions-test/#.

Commission Regulations (EU) 2016/646, Euratom. (n.d.). doi:http://eur-lex.europa.eu/pri/en/oj/dat/2003/l_285/l_28520031101en00330037.pdf.

D. Bogdanov, S. Poniaev, Numerical simulation of turbulent flow in a cyclonic separator, J. Phys. Conf. Ser. 572 (2014). doi:10.1088/1742-6596/572/1/012056.

D. Campos Navarro, Estudio de las emisiones de escape en motores de combustión interna alternativos utilizando diferentes sistemas de control de contaminantes, (2016). doi:10.4995/Thesis/10251/64066.

D. Norse, Non-point pollution from crop production: Global, regional and national issues, Pedosphere. 15 (2005) 499–508.

D. Testa, Apparatus and method for altimetric conditioning of internal-combustion engines, 2011. https://google.com/patents/EP2295950B1?cl=ja.

D.B. Olsen, B.D. Willson, The Impact of Cylinder Pressure on Fuel Jet Penetration and Mixing, (2017) 1–7. doi:10.1115/ICEF2002-502.

D.G. Gardner, V.A. Zaccardi, P.A. Jalbert, M. Denise Bryant, Reducing the Cost of Aircraft Engine Emission Measurements, Proc. Int. Instrum. Symp. 49 (2003) 57–66.

D.M. Human, T.L. Ullman, T.M. Baines, Simulation of High Altitude Effects on Heavy-Duty Diesel Emissions, SAE Tech. Pap. 900883. (1990). doi:10.4271/900883.

D.W. Dockery, C.A. Pope, Acute Respiratory Effects of Particulate Air

Pollution, Annu. Rev. Public Health. 15 (1994) 107–132. doi:10.1146/annurev.pu.15.050194.000543.

DieselNet. Emission Test Cycles - Worldwide Harmonized Light Vehicles Test Cycle (WLTC), (n.d.). https://www.dieselnet.com/standards/cycles/wltp.php.

DieselNet. EU: Cars and Light Trucks Emissions Standards, (n.d.).

E. Commission, EU action to curb air pollution by cars : Questions and Answers, (2017).

EJ Bowman - Exhaust gas heat exchanger, (n.d.). https://www.ejbowman.co.uk/products/ExhaustGasHeatExchangers.htm

ESDU International PLC, Equations for calculation of International Standard Atmosphere and associated off-standard atmospheres, 1986.

European Commission, EU legislation on passenger car type approval and emissions standards, (2016). http://europa.eu/rapid/press-release_MEMO-16-4269_en.htm.

European Environment Agency, Air pollution at street level in European cities, 2006.

F. Payri, J. Benajes, J. Galindo, J.R. Serrano, Modelling of turbocharged diesel engines in transient operation. Part 2: Wave action models for calculating the transient operation in a high speed direct injection engine, Proc. Inst. Mech. Eng. Part D J. Automob. Eng. 216 (2002) 479–493. doi:10.1243/09544070260137507.

F. Payri, J. Benajes, M.D. Chust, Programme pour étude assistée par ordinateur de systèmes d'admission et d'échappement de moteurs, Entropie. 27 (1991) 17–23.

F. Payri, J.M. Corberan, F. Boada, Modifications to the method of characteristics for the analysis of the gas exchange process in internal combustion engines., Proc. Inst. Mech. Eng. Part D, Transp. Eng. 200 (1986) 259–266. https://www.scopus.com/inward/record.uri?eid=2-s2.0-0022877864&partnerID=40&md5=332bdd1f2512d04f22f88ec2bec7820c.

F. Payri, J.M. Desantes, J. Galindo, J.R. Serrano, P. Piqueras, Unit for simulating the pressure and temperature conditions of the air drawn in by a reciprocating internal combustion engine, ES2398095B1 Spanish Pat. Date 20/01/2014. PCT/ES2012/070010. USA Pat. No 9038578. Japan Pat. No 5788025. Eur. Pat. Appl. No. 12742066.9 - EP2672248. Chinese Pat. Appl. No 201280007012.6. (2011). [1]

F. Payri, J.M. Desantes, Motores de combustión interna alternativos, Editor.

Reverté. (2015).

F. Payri, J.R. Serrano, P. Piqueras, O. García-Afonso, Performance analysis of a turbocharged heavy Duty diesel engine with a pre-turbo Diesel particulate filter configuration, SAE Int. J. Engines. 4 (2011) 2559–2572. doi:10.4271/2011-37-0004.

F.O. Igbinovia, G. Fandi, R. Mahmoud, J. Tlustý, A Review of Electric Vehicles Emissions and its Smart Charging Techniques Influence on Power Distribution Grid, J. Eng. Sci. Technol. Rev. 9 (2016) 80–85.

F.R. Jacur, The environmental dimension of the dieselgate: A European and international legal perspective, in: Dieselgate A Leg. Perspect., 2017: pp. 171–178. doi:10.1007/978-3-319-48323-8_10.

Formation and control of nitrogen oxides, Catal. Today. 2 (1988) 369–379. doi:10.1016/0920-5861(88)80002-6.

G. Busca, L. Lietti, G. Ramis, F. Berti, Chemical and mechanistic aspects of the selective catalytic reduction of NO x by ammonia over oxide catalysts : A review, Appl. Catal. B Environ. 18 (1998) 1–36. doi:10.1016/S0926-3373(98)00040-X.

G. Fontaras, P. Dilara, The evolution of European passenger car characteristics 2000-2010 and its effects on real-world CO 2 emissions and CO 2 reduction policy, Energy Policy. 49 (2012) 719–730. doi:10.1016/j.enpol.2012.07.021.

G. Fontaras, V. Franco, P. Dilara, G. Martini, U. Manfredi, Development and review of Euro 5 passenger car emission factors based on experimental results over various driving cycles, Sci. Total Environ. 468–469 (2014) 1034–1042. doi:10.1016/j.scitotenv.2013.09.043.

G. Osculati, M. Revera, G. Branzi, A. Faini, G. Malfatto, G. Bilo, A. Giuliano, F. Gregorini, F. Ciambellotti, C. Lombardi, P. Agostoni, G. Mancia, G. Parati, Effects of hypobaric hypoxia exposure at high altitude on left ventricular twist in healthy subjects: Data from HIGHCARE study on Mount Everest, Eur. Heart J. Cardiovasc. Imaging. 17 (2016) 635–643. doi:10.1093/ehjci/jev166.

G. Wang, J.M. Ogden, D. Sperling, Comparing air quality impacts of hydrogen and gasoline, Transp. Res. Part D Transp. Environ. 13 (2008) 436–448. doi:10.1016/j.trd.2008.09.006.

G. Wang, The role of hydrogen cars in the economy of California, Int. J. Hydrogen Energy. 36 (2011) 1766–1774. doi:10.1016/j.ijhydene.2010.10.083.

G. Zhou, R. Liu, S. Dong, G. Liu, Z. Zheng, S. Hao, Experimental study on

plateau matching performance of turbocharger and vehicle diesel engine, Proc. - 2010 Int. Conf. Digit. Manuf. Autom. ICDMA 2010. 1 (2010) 710–713. doi:10.1109/ICDMA.2010.305.

G.A. Bishop, J.A. Morris, D.H. Stedman, L.H. Cohen, R.J. Countess, S.J. Countess, P. Maly, S. Scherer, The effects of altitude on heavy-duty diesel truck on-road emissions, Environ. Sci. Technol. 35 (2001) 1574–1578. doi:10.1021/es001533a.

G.H. Abd-Alla, Using exhaust gas recirculation in internal combustion engines: a review, Energy Convers. Manag. 43 (2002) 1027–1042. doi:10.1016/S0196-8904(01)00091-7.

GAMMA Technologies, (n.d.). http://www.gtisoft.com.

Global Internal Combustion Engine Market 2017-2021, (2017).

H. Hiroyasu, M. Arai, M. Tabata, Empirical Equations for the Sauter Mean Diameter of a Diesel Spray, SAE Tech. Pap. 890464. (1989). doi:10.4271/890464.

H. Li, L. Shi, K. Deng, Development of turbocharging system for diesel engines of power generation application at different altitudes, J. Energy Inst. (2015). doi:10.1016/j.joei.2015.04.001.

H. Sandquist, R. Lindgren, I. Denbratt, Sources of Hydrocarbon Emissions from a Direct Injection Stratified Charge Spark Ignition Engine, in: SAE Tech. Pap., 2000. doi:10.4271/2000-01-1906.

H. Wu, K. Nithyanandan, N. Zhou, T.H. Lee, C.F. Lee, C. Zhang, Impacts of acetone on the spray combustion of Acetone–Butanol–Ethanol (ABE)-Diesel blends under low ambient temperature, Fuel. 142 (2015) 109–116. doi:10.1016/j.fuel.2014.10.009.

H. Zhang, W. Zhuge, Y. Zhang, Study of the Control Strategy of the Plateau Self-adapted Turbocharging System for Diesel Engine, (2008). doi:10.4271/2008-01-1636.

H. Zhao, Overview of gasoline direct injection engines, in: H. Zhao (Ed.), Adv. Direct Inject. Combust. Engine Technol. Dev., Woodhead Publishing, 2010: pp. 1–19. doi:https://doi.org/10.1533/9781845697327.1.

H. Zhu, S. V. Bohac, Z. Huang, D.N. Assanis, Emissions as functions of fuel oxygen and load from a premixed low-temperature combustion mode, Int. J. Engine Res. 15 (2014) 731–740. doi:10.1177/1468087413501317.

Holset HY40V - Service Repair Manual, (2007).

ISO, Standard Atmosphere, ISO 2533:1975, Int. Stand. Organ. 2533 (1975).

ISO-16183:2002, Heavy duty engines - Measurement of gaseous emissions from raw exhaust gas and of particulate emissions using partial flow dilution systems under transient test conditions, (2002).

J. a Raub, Health effects of exposure to ambient carbon monoxide, Chemosph. Glob. Charg. Sci. 1. 1 (1999) 331–351. doi:10.1016/S1465-9972(99)00005-7.

J. Agudelo, A. Agudelo, J. Pérez, Análisis energético y exergético de un motor diesel de automoción operando en diferentes altitudes, Rev. Fac. Ing. (2009) 45–54.

J. Appel, H. Bockhorn, M. Frenklach, Kinetic modeling of soot formation with detailed chemistry and physics: Laminar premixed flames of C2 hydrocarbons, Combust. Flame. 121 (2000) 122–136. doi:10.1016/S0010-2180(99)00135-2.

J. Benajes, E. Reyes, J.M. Lujân, Modelling study of the scavenging process in a turbocharged diesel engine with modified valve operation, Proc. Inst. Mech. Eng. Part C J. Mech. Eng. Sci. 210 (1996) 383–393. doi:10.1243/PIME_PROC_1996_210_210_02.

J. Deng, R. Stobart, BSFC Investigation Using Variable Valve Timing in a Heavy Duty Diesel Engine, (2009). doi:10.4271/2009-01-1525.

J. García-Villalobos, I. Zamora, J.I. San Martín, F.J. Asensio, V. Aperribay, Plug-in electric vehicles in electric distribution networks: A review of smart charging approaches, Renew. Sustain. Energy Rev. 38 (2014) 717–731. doi:10.1016/j.rser.2014.07.040.

J. Pielecha, J. Merkisz, J. Markowski, R. Jasiński, Analysis of Passenger Car Emission Factors in RDE Tests, 73 (2016) 1–7. doi:10.1051/e3sconf/20161000073.

J. Ramón, F. José, L.M. García-cuevas, A. Dombrovsky, Development and validation of a radial turbine efficiency and mass flow model at design and off-design conditions, 128 (2016) 281–293. doi:10.1016/j.enconman.2016.09.032.

J. Serrano, P. Olmeda, F.J. Arnau, A. Dombrovsky, L. Smith, Turbocharger heat transfer and mechanical losses influence in predicting engines performance by using one-dimensional simulation codes, Energy. 86 (2015) 204–218. doi:10.1016/j.energy.2015.03.130.

J. Serras-Pereira, P.G. Aleiferis, D. Richardson, Imaging and heat flux measurements of wall impinging sprays of hydrocarbons and alcohols in a direct-injection spark-ignition engine, Fuel. 91 (2012) 264–297. doi:10.1016/j.fuel.2011.07.037.

J. Simperl, H. Erlach, Method for supplying an internal combustion engine with conditioned combustion gas, device for carrying out said method, method for determining the quantities of pollutants in the exhaust gases of an internal combustion engine, and device for carrying out, 2003. https://www.google.com/patents/WO2002042730A3?cl=en.

J. Theis, E. Gulari, A LNT+ SCR system for treating the NOx emissions from a diesel engine, SAE Tech. Pap. (2006). doi:10.4271/2006-01-0210.

J. Warnatz, U. Maas, R.W. Dibble, Combustion: Physical and chemical fundamentals, modeling and simulation, experiments, pollutant formation, 2006. doi:10.1007/978-3-540-45363-5.

J.A. Caton, Comparisons of Thermocouple, Time-Averaged and Mass-Averaged Exhaust Gas Temperatures for a Spark-Ignited Engine, in: SAE Int. Congr. Expo., SAE International, 1982. doi:https://doi.org/10.4271/820050.

J.C.G. Palencia, Y. Otsuka, M. Araki, S. Shiga, Impact of new vehicle market composition on the light-duty vehicle fleet CO2 emissions and cost, Energy Procedia. 105 (2017) 3862–3867. doi:10.1016/j.egypro.2017.03.790.

J.E. Dec, A conceptual model of DI diesel combustion based on laser sheet imaging, SAE Tech. Pap. (1997). doi:10.4271/970873.

J.H. Roberts, W.R. Beyerly, M.W. Mason, J.R. Glazier, R.H. Wiley, PW4084 engine testing in altitude & sea level test facilities, (1994). doi:10.4271/942140.

J.J. Cottrell, Altitude exposures during aircraft flight. Flying higher, Chest. 93 (1988) 81–84. doi:10.1378/chest.93.1.81.

J.J. Streicher, Automobile fuel system vapor emission following evaporation canister breakthrough, J. Environ. Sci. Heal. - Part A Toxic/Hazardous Subst. Environ. Eng. 34 (1999) 1035–1060. doi:10.1080/10934529909376880.

J.-L. Lei, Z. Tan, S. Liu, Y.-H. Bi, L.-Z. Shen, Performance of Diesel Engine Fueled with Ethanol-diesel Blends in Different Altitude Regions, 2010 Int. Conf. Digit. Manuf. Autom. (2010) 82–85. doi:10.1109/ICDMA.2010.45.

J.M. Corberan, Contribución al modelado del proceso de renovación de la carga en motores de combustión interna alternativos, Universitat Politècnica de València, 1984.

J.M. Desantes Fernández, J.G. Lucas, F. Payri González, P. Piqueras Cabrera, J.R. Serrano Cruz, Dispositivo para acondicionar la atmósfera en

ensayos de motores de combustión interna alternativos, procedimiento y uso de dicho dispositivo, ES2544516B1 (P201530075), WO 2015/110683 A1, 2015.

J.M. Desantes, J.G. Lucas, F.P. González, P. Piqueras Cabrera, J.R. Serrano Cruz, Dispositivo de acondicionamiento de atmósfera para el ensayo de motores de combustión, procedimiento y uso relacionados, ES2485618B1 (P201430071) PCT/ES23015/070037, 2014.

J.M. Desantes, M.D. Chust, J. Llorens, Análisis comparativo de métodos numéricos para la resolución del flujo no estacionario en colectores de motores de combustión interna alternativos, II Congr. Métodos Numéricos En Ing. (1996).

J.N. Chi, Control Challenges for Optimal NOx Conversion Efficiency from SCR Aftertreatment Systems, SAE Tech. Pap. (2009). doi:10.4271/2009-01-0905.

J.P. Meyers, Getting back into gear: fuel cell development after the hype, Electrochem. Soc. Interface. 17 (2008) 36–39.

J.R. Serrano, P. Olmeda, F.J. Arnau, A. Dombrovsky, L. Smith, Analysis and Methodology to Characterize Heat Transfer Phenomena in Automotive Turbochargers, J. Eng. Gas Turbines Power. 137 (2015) 1–11. doi:10.1115/1.4028261.

J.R. Serrano, P. Piqueras, E. Angiolini, C. Meano, J. De La Morena, On Cooler and Mixing Condensation Phenomena in the Long-Route Exhaust Gas Recirculation Line, (2015). doi:10.4271/2015-24-2521.

J.R. Sodré, S.M.C. Soares, Comparison of engine power correction factors for varying atmospheric conditions, J. Brazilian Soc. Mech. Sci. Eng. 25 (2003) 279–284. doi:10.1590/S1678-58782003000300010.

J.W. Dennis, Turbocharged Diesel Engine Performance at Altitude, in: Natl. Truck. Powerplant, Fuels Lubr. Meet., SAE International, 1971. doi:10.4271/710822.

K. Nakata, S. Utsumi, A. Ota, K. Kawatake, T. Kawai, T. Tsunooka, The Effect of Ethanol Fuel on a Spark Ignition Engine, (2006). doi:10.4271/2006-01-3380.

K. Young, C. Wang, L.Y. Wang, K. Strunz, Electric Vehicle Battery Technologies, 2013. doi:10.1007/978-1-4614-0134-6.

K.D. Kihm, D.P. Terracina, S.E. Payne, J.A. Caton, Synchronized Droplet Size Measurements for Coal-Water Slurry Sprays Generated from a High-Pressure Diesel Injection System, J. Inst. Energy. 67 (1994) 2–9.

L. Pelkmans, P. Debal, Comparison of on-road emissions with emissions measured on chassis dynamometer test cycles, Transp. Res. Part D Transp. Environ. 11 (2006) 233–241. doi:10.1016/j.trd.2006.04.001.

L. Shen, Y. Shen, Combustion Process of Diesel Engines At Regions With Different Altitude, SAE Tech. Pap. 950857. (1995). doi:10.4271/950857.

L. Stenning, Strategies for Achieving pre DPF Regeneration Temperatures using in Cylinder Post Injection on a Common Rail Diesel Engine with EGR, DOC and Intake Throttle, Sae Tech. Pap. Ser. 7 (2015) 0–8. doi:10.4271/2010-36-0306.

L. Yang, V. Franco, P. Mock, R. Kolke, S. Zhang, Y. Wu, J. German, Experimental Assessment of NOxEmissions from 73 Euro 6 Diesel Passenger Cars, Environ. Sci. Technol. 49 (2015) 14409–14415. doi:10.1021/acs.est.5b04242.

L. Yu, Y. Ge, J. Tan, C. He, X. Wang, H. Liu, W. Zhao, J. Guo, G. Fu, X. Feng, X. Wang, Experimental investigation of the impact of biodiesel on the combustion and emission characteristics of a heavy duty diesel engine at various altitudes, Fuel. 115 (2014) 220–226. doi:10.1016/j.fuel.2013.06.056.

Lagos de Covadonga, Asturias (Spain), (n.d.). https://www.climbbybike.com/climb.asp?Col=Lagos-de-Covadonga&qryMountainID=4590.

M. André, The ARTEMIS European driving cycles for measuring car pollutant emissions, Sci. Total Environ. 334–335 (2004) 73–84. doi:10.1016/j.scitotenv.2004.04.070.

M. Desai, R.P. Harvey, Inventory of U.S. Greenhouse Gas Emissions and Sinks: 1990-2015, Fed. Regist. 82 (2017) 10767. doi:EPA 430-R-13-001.

M. Ghazikhani, M. Ebrahim Feyz, O. Mahian, A. Sabazadeh, Effects of altitude on the soot emission and fuel consumption of a light-duty diesel engine, Transport. 28 (2013) 130–139. doi:10.3846/16484142.2013.798743.

M. Hosoya, M. Shimoda, The application of diesel oxidation catalysts to heavy duty diesel engines in Japan, Appl. Catal. B Environ. 10 (1996) 83–97. doi:10.1016/0926-3373(96)00025-2.

M. Lapuerta, O. Armas, J.R. Agudelo, A.F. Agudelo, Estudio del efecto de la altitud sobre el comportamiento de motores de combustión interna. Parte 2: Motores diesel, Inf. Tecnol. 17 (2006).

M. Lapuerta, O. Armas, J.R. Agudelo, C.A. Sánchez, Estudio del Efecto de la Altitud sobre el Comportamiento de Motores de Combustión Interna. Parte 1: Funcionamiento, Inf. Tecnológica. 17 (2006) 21–30.

doi:10.4067/S0718-07642006000500005.

M. Matti Maricq, Chemical characterization of particulate emissions from diesel engines: A review, J. Aerosol Sci. 38 (2007) 1079–1118. doi:10.1016/j.jaerosci.2007.08.001.

M. Szedlmayer, C.M. Kweon, Effect of Altitude Conditions on Combustion and Performance of a Multi-Cylinder Turbocharged Direct-Injection Diesel Engine, SAE Tech. Pap. 2016-01-0742. (2016) 4271. doi:10.4271/2016-01-0742.

M. Tutuianu, A. Marotta, H. Steven, E. Ericsson, T. Haniu, N. Ichikawa, H. Ishii, Development of a World-wide Worldwide harmonized Light duty driving Test Cycle, Tech. Rep. 3 (2014) 7–10. doi:10.3141/2503-12.

M. Tutuianu, P. Bonnel, B. Ciuffo, T. Haniu, N. Ichikawa, A. Marotta, J. Pavlovic, H. Steven, Development of the World-wide harmonized Light duty Test Cycle (WLTC) and a possible pathway for its introduction in the European legislation, Transp. Res. Part D Transp. Environ. 40 (2015) 61–75. doi:10.1016/j.trd.2015.07.011.

M. Weiss, P. Bonnel, J. Kühlwein, A. Provenza, U. Lambrecht, S. Alessandrini, M. Carriero, R. Colombo, F. Forni, G. Lanappe, P. Le Lijour, U. Manfredi, F. Montigny, M. Sculati, Will Euro 6 reduce the NOxemissions of new diesel cars? - Insights from on-road tests with Portable Emissions Measurement Systems (PEMS), Atmos. Environ. 62 (2012) 657–665. doi:10.1016/j.atmosenv.2012.08.056.

M. Weiss, P. Bonnel, R. Hummel, N. Steininger, A complementary emissions test for light-duty vehicles: Assessing the technical feasibility of candidate procedures, 2013. doi:10.2790/65654.

M. Yang, Y. Gu, K. Deng, Z. Yang, S. Liu, Influence of altitude on two-stage turbocharging system in a heavy-duty diesel engine based on analysis of available flow energy, Appl. Therm. Eng. 129 (2018) 12–21. doi:10.1016/j.applthermaleng.2017.09.138.

M. Yang, Y. Gu, K. Deng, Z. Yang, S. Liu, Influence of altitude on two-stage turbocharging system in a heavy-duty diesel engine based on analysis of available flow energy, Appl. Therm. Eng. 129 (2018) 12–21. doi:10.1016/j.applthermaleng.2017.09.138.

M. Zheng, G.T. Reader, J.G. Hawley, Diesel engine exhaust gas recirculation - A review on advanced and novel concepts, Energy Convers. Manag. 45 (2004) 883–900. doi:10.1016/S0196-8904(03)00194-8.

M.J. Hu, Optimizing Crankcase Ventilation System of Gasoline Engine, Appl. Mech. Mater. 58–60 (2011) 171–176.

doi:10.4028/www.scientific.net/AMM.58-60.171.

M.R. Heal, P. Kumar, R.M. Harrison, Particles, air quality, policy and health, Chem. Soc. Rev. 41 (2012) 6606. doi:10.1039/c2cs35076a.

N. Baines, K.D. Wygant, A. Dris, The Analysis of Heat Transfer in Automotive Turbochargers, J. Eng. Gas Turbines Power. 132 (2010) 42301. doi:10.1115/1.3204586.

N.G. Barton, The Expansion-Cycle Evaporation Turbine, J. Eng. Gas Turbines Power. 134 (2012) 51702–51707. http://dx.doi.org/10.1115/1.4004743.

N.S. Ayoub, R.D. Reitz, Multidimensional modeling of fuel composition effects on combustion and cold-starting in diesel engines, SAE Tech. Pap. (1995). doi:10.4271/952425.

National Geophysical Data Center, U.S. standard atmosphere (1976), Planet. Space Sci. 40 (1992) 553–554. doi:10.1016/0032-0633(92)90203-Z.

Number of passenger cars and commercial vehicles in use worldwide from 2006 to 2015 in (1,000 units), (2015). https://www.statista.com/statistics/281134/number-of-vehicles-in-use-worldwide/.

O.P.R. van Vliet, T. Kruithof, W.C. Turkenburg, A.P.C. Faaij, Techno-economic comparison of series hybrid, plug-in hybrid, fuel cell and regular cars, J. Power Sources. 195 (2010) 6570–6585. doi:10.1016/j.jpowsour.2010.04.077.

O.S. Azmir, A.J. Alimin, M.Y. Ismail, K.W. Hui, Performance and Emission Characteristics of Direct Injection C.I Engine Retrofitted with Mono-CNG System, Appl. Mech. Mater. 446–447 (2013) 443–447. doi:10.4028/www.scientific.net/AMM.446-447.443.

OpenWAM - CMT-Motores Térmicos, Universitat Politècnica de València, (n.d.). www.openwam.org.

P. Benjumea, J. Agudelo, A. Agudelo, Effect of altitude and palm oil biodiesel fuelling on the performance and combustion characteristics of a HSDI diesel engine, Fuel. 88 (2009) 725–731. doi:10.1016/j.fuel.2008.10.011.

P. Boffetta, N. Jourenkova, P. Gustavsson, Cancer risk from occupational and environmental exposure to polycyclic aromatic hydrocarbons., Cancer Causes Control. 8 (1997) 444–72. doi:10.1023/A:1018465507029.

P. Dimitriou, R. Burke, Q. Zhang, C. Copeland, H. Stoffels, Electric Turbocharging for Energy Regeneration and Increased Efficiency at Real Driving Conditions, Appl. Sci. 7 (2017) 25. doi:10.3390/app7040350.

P. Handsford, S. Birkett, J. Bullied, T. Caccavone, N. Earnshaw, R. Goldney, P.

Gregory, P. Kumar, F. Medda, S. Moroney, H. Pantelidou, K. Simmonds, M. Sugarman, J. Venables, Engineering Cleaner Air, (2017).

P. Leduc, B. Dubar, A. Ranini, G. Monnier, Downsizing of Gasoline Engine: an Efficient Way to Reduce CO2 Emissions, Oil Gas Sci. Technol. 58 (2003) 115–127. doi:10.2516/ogst:2003008.

P. Lu, C. Brace, B. Hu, C. Copeland, Analysis and comparison of the performance of an inverted brayton cycle and turbo-compounding with decoupled turbine and cvt driven compressor for small automotive engines, in: Proc. ASME Turbo Expo, 2016. doi:10.1115/GT2016-57675.

P.E. Morrow, Toxicological data on nox: An overview, J. Toxicol. Environ. Health. 13 (1984) 205–227. doi:10.1080/15287398409530494.

Parker AC Frequency Drive Inverter AC30 Frame H, (n.d.). http://www.parker.com/Literature/Electromechanical Europe/User Guides/HA501718U001_EN.pdf.

R. Liu, Z. Zhang, S. Dong, G. Zhou, High-Altitude Matching Characteristic of Regulated Two-Stage Turbocharger With Diesel Engine, J. Eng. Gas Turbines Power. 139 (2017) 94501. doi:10.1115/1.4036283.

R. Snyder, Leukemia and benzene., Int. J. Environ. Res. Public Health. 9 (2012) 2875–2893. doi:10.1016/S1526-0046(03)00020-7.

R.E. Smith, J. Ferrell, High-Altitude Tests of Rocket Engines in Ground Test Facilities, in: SAE Tech. Pap. 640811, 1964. doi:10.4271/640811.

R.J. Levy, Carbon monoxide pollution and neurodevelopment: A public health concern, Neurotoxicol. Teratol. 49 (2015) 31–40. doi:10.1016/j.ntt.2015.03.001.

R.P. Ranganathan, D.W. Turner, M.E. Franchett, Exhaust Manifold Gas Temperature Predictions using System Level Data Driven Modelling, 2005 (2005). doi:10.4271/2005-01-0698.

R.S. Benson, The Thermodynamics and Gas Dynamics of Internal Combustion Engines, 1 (1982).

Rotrex A/S - C38-92, (n.d.). http://www.rotrex.com/.

S. Akhter, N. Nabi, Design , Construction and Performance Testing of a Cyclonic Separator to Control Particulate Pollution from Diesel Engine Exhaust, (2005).

S. D'Ambrosio, A. Ferrari, E. Spessa, L. Magro, A. Vassallo, Impact on Performance, Emissions and Thermal Behavior of a New Integrated Exhaust Manifold Cylinder Head Euro 6 Diesel Engine, SAE Int. J. Engines. 6 (2013) 1814–1833. doi:10.4271/2013-24-0128.

S. Karstadt, J. Werner, S. Münz, R. Aymanns, Effect of Water Droplets Caused by Low Pressure EGR on Spinning compressor Wheels, in: 19th Supercharging Conf. Dresden, 24th Sept. 2014, 2014.

S. Liu, L. Shen, Y. Bi, J. Lei, Effects of altitude and fuel oxygen content on the performance of a high pressure common rail diesel engine, Fuel. 118 (2014) 243–249. doi:10.1016/j.fuel.2013.10.007.

S. Sawant, D. Prajapati, U.G. Student, N. Mumbai, A review on zero emissions vehicles, 8 (2017) 198–202.

S. Weichenthal, Selected physiological effects of ultrafine particles in acute cardiovascular morbidity, Environ. Res. 115 (2012) 26–36. doi:10.1016/j.envres.2012.03.001.

S.A.E. Technical, P. Series, Thermal Studies in the Exhaust System of a Diesel-Powered Light-Duty Vehicle, Development. (2004). doi:10.4271/2004-01-0050.

S.G. Barberá, Estudio CFD de separadores inerciales centrífugos de un simulador de altitud: estudio paramétrico de las condiciones de operación, Universitat Politècnica de València, 2015.

S.J. Harris, M.M. Maricq, Signature size distributions for diesel and gasoline engine exhaust particulate matter, J. Aerosol Sci. 32 (2001) 749–764. doi:10.1016/S0021-8502(00)00111-7.

S.J.G. Arias, Análisis CFD y optimización de un separador ciclónico, Universitat Politècnica de València, 2015.

S.M.C. Soares, J.R. Sodré, Effects of atmospheric temperature and pressure on the performance of a vehicle, Part D J Automob. Eng. 216 (2002) 473–477. doi:10.1243/09544070260137499.

Schubert & Salzer, Control Systems, Control Valve GS8021, (n.d.). http://schubertsalzerinc.com/products/gs-valves/type-8021/.

T. Li, X. Chen, Z. Yan, Comparison of fine particles emissions of light-duty gasoline vehicles from chassis dynamometer tests and on-road measurements, Atmos. Environ. 68 (2013) 82–91. doi:10.1016/j.atmosenv.2012.11.031.

T. Lucchini, G. D'Errico, A. Onorati, G. Bonandrini, L. Venturoli, R. Di Gioia, Development of a CFD Approach to Model Fuel-Air Mixing in Gasoline Direct-Injection Engines, (2012). doi:10.4271/2012-01-0146.

T.D. Sheet, Rotrex C38 Supercharger range, (n.d.) 1–7.

U. Shrinivasa, The evolution of diesel engines, Resonance. 17 (2012) 365–377. doi:10.1007/s12045-012-0038-3.

U.G. Alkemade, B. Schumann, Engines and exhaust after treatment systems for future automotive applications, 177 (2006) 2291–2296. doi:10.1016/j.ssi.2006.05.051.

V. Betageri, R. Mahesh, Effects of the Real Driving Conditions on the NOx Emission of a Medium Duty Diesel Commercial Vehicle, SAE Tech. Pap. (2017) 1–6. doi:10.4271/2017-26-0124.

V. Vestreng, L. Ntziachristos, A. Semb, S. Reis, I.S.A. Isaksen, L. Tarrason, Evolution of NOx emissions in Europe with focus on road transport control measures, Atmos. Chem. Phys. 9 (2009) 1503–1520. doi:10.5194/acp-9-1503-2009.

W. Peng, A.C. Hoffmann, H.W.A. Dries, M.A. Regelink, L.E. Stein, Experimental study of the vortex end in centrifugal separators: The nature of the vortex end, Chem. Eng. Sci. 60 (2005) 6919–6928. doi:10.1016/j.ces.2005.06.009.

W.S. Epling, L.E. Campbell, A. Yezerets, N.W. Currier, J.E. Parks, Overview of the Fundamental Reactions and Degradation Mechanisms of NOx Storage/Reduction Catalysts, Catal. Rev. 46 (2004) 163–245. doi:10.1081/CR-200031932.

Weather statistics for Sierra Nevada, Andalucía (Spain), (n.d.). https://www.yr.no/place/Spain/Andalucía/Sierra_Nevada/statistics.html.

WIKA - Piezoresistive pressure sensor S20, (n.d.). https://en-co.wika.de/s_20_en_co.WIKA.

X. Li, S. Xu, Y. Xiong, X. Liu, Effects of oxygenated fuel on diesel engine performance under the simulated condition of plateau area, Shiyou Xuebao, Shiyou Jiagong/Acta Pet. Sin. (Petroleum Process. Sect. 32 (2016) 215–220. doi:10.3969/j.issn.1001-8719.2016.01.030.

X. Shi, T. Wang, C. Ma, Simulations of the diesel engine performance with a two-stage sequential turbocharging system at different altitudes, Proc. Inst. Mech. Eng. Part D J. Automob. Eng. 228 (2014) 1718–1726. doi:10.1177/0954407014535919.

X. Wang, H. Yin, Y. Ge, L. Yu, Z. Xu, C. Yu, X. Shi, H. Liu, On-vehicle emission measurement of a light-duty diesel van at various speeds at high altitude, Atmos. Environ. 81 (2013) 263–269. doi:10.1016/j.atmosenv.2013.09.015.

X. Wang, Y. Ge, L. Yu, Combustion and Emission Characteristics of a Heavy-Duty Diesel Engine at Idle at Various Altitudes, SAE Int. J. Engines. 6 (2013) 2013-01–1516. doi:10.4271/2013-01-1516.

X. Wang, Y. Ge, L. Yu, X. Feng, Comparison of combustion characteristics and

brake thermal efficiency of a heavy-duty diesel engine fueled with diesel and biodiesel at high altitude, Fuel. 107 (2013) 852–858. doi:10.1016/j.fuel.2013.01.060.

X. Wang, Y. Ge, L. Yu, X. Feng, Effects of altitude on the thermal efficiency of a heavy-duty diesel engine, Energy. 59 (2013) 543–548. doi:10.1016/j.energy.2013.06.050.

X. Zheng, L. Jin, T. Du, B. Gan, F. Liu, H. Qian, Effect of temperature on the strength of a centrifugal compressor impeller for a turbocharger, Proc. Inst. Mech. Eng. Part C J. Mech. Eng. Sci. 227 (2013) 896–904. doi:10.1177/0954406212454966.

Y. Jun, I. Yang, C. Kim, S. Yang, D. Lee, Uncertainty Analysis and Improvement of an Altitude Test Facility for Small Jet Engines, KSAS Int. J. 5 (2004) 46–56.

Y. Ohno, K. Funato, K. Kajita, An integration approach on powertrain control system, SAE Tech. Pap. (1989). doi:10.4271/890762.

Y. Zama, W. Ochiai, T. Furuhata, M. Arai, Experimental study on spray angle and velocity distribution of diesel spray under high ambient pressure conditions, At. Sprays. 21 (2011) 989–1007. doi:10.1615/AtomizSpr.2012004722.

Z. Zhu, F. Zhang, C. Li, T. Wu, K. Han, J. Lv, Y. Li, X. Xiao, Genetic algorithm optimization applied to the fuel supply parameters of diesel engines working at plateau, Appl. Energy. 157 (2014) 789–797. doi:10.1016/j.apenergy.2015.03.126.

Z.A. Needell, J. McNerney, M.T. Chang, J.E. Trancik, Potential for widespread electrification of personal vehicle travel in the United States, Nat. Energy. 1 (2016). doi:10.1038/nenergy.2016.112.

Z.F. Tan, L.Z. Shen, D.C. Jin, Y.W. Bin Ou, A Research on the Performance of a Common Rail Diesel Engine Fueled with Different Blending Ratio of Biodiesels, Adv. Mater. Res. 860–863 (2013) 555–559. doi:10.4028/www.scientific.net/AMR.860-863.555.

Z.X. Zhu, F.J. Zhang, C.J. Li, K. Han, Calibration for Fuel Injection Parameters of the Diesel Engine Working at Plateau via Simulating, Adv. Mech. Eng. 2014 (2014). doi:10.1155/2014/621946.